Dissertation zur Erlangung des Doktorgrades

der Fakultät für Chemie und Pharmazie

der Ludwig-Maximilians-Universität München

Concepts and Syntheses towards Substrates with autocatalytic Potential in asymmetric Diorganozinc Alkylations

Simone Heitsch

aus

München, Deutschland

2023

Erklärung

Diese Dissertation wurde im Sinne von §7 der Promotionsordnung vom 28. November 2011 von Herrn **Prof. Dr. Oliver Trapp** betreut.

Eidesstattliche Versicherung

Diese Dissertation wurde eigenständig und ohne unerlaubte Hilfe erarbeitet.

München, den 26.07.2023

Simone Heitsch

(Simone Heitsch)

Dissertation eingereicht am	26.07.2023
Erstgutachter:	Prof. Dr. Oliver Trapp
Zweitgutachter:	Prof. Dr. Anja Hoffmann-Roeder
Mündliche Prüfung am	21.09.2023

Contents

Publications and Poster Presentations

Publications

S. Heitsch, L. C. Mayer, Y. L. Pignot, and O. Trapp, Synthesis and stereodynamics of intramolecular hemiacetals in biaryl aldehyde-alcohols. *Chirality* **2023**, 1-13. doi: 10.1002/chir.23560

S. Heitsch, O. Trapp, Hydrogen bond-stabilized six-membered rings in tautomerization of 2,3-bis(2-methoxyphenyl)-3-oxopropanals, in preparation.

L. C. Mayer, S. Heitsch, and O. Trapp, Nonlinear Effects in Asymmetric Catalysis by Design: Concept, Synthesis, and Applications. *Accounts of Chemical Research* **2022**, *55 (23)*, 3345-3361. doi: 10.1021/acs.accounts.2c00557

Poster Presentation

S. Heitsch, O. Trapp
Synthesis of novel dynamic ligands based on the hemiacetal mechanism of Soais autocatalysis, Chirality Conference 2022, Chicago (USA)

Abbreviations

ACN	acetonitrile
ATR	attenuated total reflection
BF_3	boron trifluoride
BINAP	(2,2-bis(diphenylphosphino)-1,1-binaphthyl)
BINOL	1,1-bi-2-naphthol
$CDCl_3$	deuterated Chloroform
DAIB	3-exo-(Dimethylamino)isoborneol
DCM	dichlormethane
DFT	density functional theory
DHPLC	dynamic high performance liquid chromatography
DIBAL-H	diisobutylaluminiumhydrid
DMAP	4-dimethylaminopyridine
DME	dimethoxyethane
DMF	dimethylforamide
DMSO	dimethylsulfoxide
DNA	deoxyribonucleic acid
ee	enantiomeric excess
EtOAc	ethyl acetate
EtOH	ethanol
FIA	flow injection analysis
FT-ICR	Fourier-transform ion cyclotron resonance
GC	gas chromatography
h	hours
HCl	hydrochloride

HPLC	high performance liquid chromatography
HV	high vacuum
IPA	isopropyl alcohol
IR	infrared
KOH	potassium hydroxide
$NaBH_4$	sodium borohydride
Na_2CO_3	sodium carbonate
$NaHCO_3$	sodium bicarbonate
NaOH	sodium hydroxide
Na_2SO_4	sodium sulphate
LDA	lithium diisopropylamide
$LiAlH_4$	lithium aluminium hydride
MeOH	methanol
MIB	3-exo-morpholinoisoborneol
min	minutes
MnO_2	manganese oxide
MS	mass spectrometry
$NaClO_3$	sodium chlorate
NBS	*N*-bromosuccinimide
NLE	non-linear effect
NMR	nuclear magnetic resonance
PE	*n*-pentane
PM3	Parametric Method 3
Q2MM	Quantum to Molecular Mechanics
RNA	ribonucleic acid
RT	retention time
SEGPHOS	5,5-Bis(diphenylphosphino)-4,4-bi-1,3-benzodioxole
S_N2	nucleophile substitution
t	time
T	temperature
TBDPS	*tert*-butyldiphenylsilyl

THF	tetrahydrofuran
TLC	thin-layer chromatography
TPS	triphenylsilane
UV	ultra violet

Abstract

Asymmetric autocatalytic processes and high asymmetric amplification due to non-linear effects (NLEs) attract great interest in enantioselective chemistry, as they are invoked as key elements to understand the origin of homochirality. The still unexplained phenomenon of the emergence of homochirality has fascinated scientists for decades and has driven them to find an explanation. In particular, strongly asymmetric amplifying and autocatalytic systems came into focus as a possible starting point for explaining an initial imbalance in enantiomeric distribution. These systems are rare and only a few examples are mechanistically understood and sufficiently investigated. These few valuable findings can help to develop new reaction systems with the same or similar properties as the original systems.

The present work is generally concerned with the development of new autocatalytic substrates on the basis of literature-known systems. The first part deals with a concept for a dynamic hemiacetal structure motif based on a published mechanism for the autocatalytic Soai reaction, whose central catalytically active compound is based on a hemiacetal motif. The investigation focused on coumestan- and classical biaryl-derived backbones. Their dynamic properties and ultimate suitability as an autocatalytic substrate were analyzed in DHPLC and NMR studies. In the course of the synthesis of the coumestan-derived compounds, hydrogen bonds were found to stabilize a six-membered ring in a tautomeric enol-form of a β-ketoaldehyde precursor, which thereby became extremely dominant in all compounds. The extraordinary stabilization was successfully confirmed in time- and temperature-dependent studies. Furthermore, a simple one-step synthesis to novel potentially dynamic biaryl ligands is described. The synthesis pathway starting from commercially available starting materials possesses great potential to further development of this ligand motif. In part, the interconversion barriers and the kinetic parameters in DHPLC investigations were successfully determined for synthesized structures. The values obtained

were found to be in agreement with those reported for the transient hemiacetal catalyst in the Soai reaction.

The work's second part adopts an approach based on literature-known good enantioselectivities of β-amino alcohols in alkylations with diorganozinc reagents. A concept towards autocatalytic β-amino aldehyde substrates was developed. In this context, a pre-selection of primary β-amino alcohol compounds, required for this purpose as precursors, were investigated experimentally. So far, the focus has been mainly on secondary and tertiary alcohol compounds in this ligand class and is often limited to the use of diethylzinc in numerous previously reported asymmetric alkylation reactions with β-amino alcohols. In the course of a larger coverage, three different alkylation reagents were tested in the present work. Synthesized *N*-methyl- and *N*-benzyl- derivatives of enantiomerically pure primary β-amino alcohols as well as commercially available β-amino alcohols were successfully applied as ligands in alkylations of benzaldehyde with dimethyl-, diethyl- and diisopropylzinc. The product enantioselectivities were rated with moderate to good selectivity. Interestingly, contrary to previously published results, the highest selectivities were achieved in alkylations with dimethyl and diisopropylzinc for the primary β-amino alcohols. For the *N*-methylated derivatives, a trend towards significantly better selectivities was obtained with diisopropylzinc in contrast to the dimethyl- and diethylzinc comparison groups. For the *N*-benzylated derivatives, the trend was observed to be reversed. A generally higher selectivity with primary prolinol-derived ligands could be achieved with diisopropylzinc than with the comparative diorganozinc reagents, irrespective of the *N*-substitution. Furthermore, studies with enantiomeric ligand pairs revealed large deviations in the obtained enantiomeric excesses of some ligands, indicating possible non-linear effects.

Kurzzusammenfassung

Asymmetrische autokatalytische Prozesse und eine hohe asymmetrische Amplifizierung aufgrund nicht-linearer Effekte (NLEs) stoßen auf großes Interesse im Bereich der enantioselektiven Chemie. Beide werden als Schlüsselelemente für das Verständnis des Ursprungs der Homochiralität angeführt. Das bislang ungeklärte Phänomen der Homochiralität fasziniert seit Jahrzehnten und beschäftigt die Welt der Wissenschaft mit einer Suche nach möglichen Erklärungen. Insbesondere stark asymmetrische amplifizierende und autokatalytische Systeme rückten dabei als möglicher Ansatzpunkt zur Erklärung einer initialen Imbalance in der Enantiomerenverteilung in den Fokus. Diese Systeme sind selten und nur wenige Beispiele sind mechanistisch ausreichend untersucht und vollständig aufgeklärt. Diese wenigen wertvollen Erkenntnisse bieten das Potential neue Reaktionssysteme mit den gleichen oder ähnlichen Eigenschaften auf Basis der urspünglichen Systeme zuentwickeln.

Die vorliegende Arbeit befasst sich im Allgemeinen mit der Entwicklung neuer autokatalytischer Substrate auf der Basis literaturbekannter Systeme. Der erste Teil befasst sich mit einem Konzept für dynamische Halbacetal-Strukturmotive, basierend auf einem publizierten Mechanismus für die autokatalytische Soai-Reaktion, deren zentrale katalytisch aktive Verbindung auf einem Halbacetal-Motiv beruht. Die Untersuchungen konzentrierten sich auf Cumestan-basierte und klassische Biaryl-Grundgerüste. Deren dynamischen Eigenschaften und die potentielle Eignung als autokatalytisches Substrat wurden in DHPLC- und NMR-Studien analysiert. Im Zuge der Synthese der Cumestan-basierten Verbindungen wurde festgestellt, dass sechsgliedrige wasserstoffbrücken- stabilisierte Ringe in einer tautomeren Enolform zu einer extremen Dominanz dieses Tautomers in untersuchten Vorstufen führten. Diese außer gewöhnliche Stabilisierung wurde in zeit- und temperaturabhängigen Studien erfolgreich analysiert und bestätigt. Darüber hinaus konnte

eine einfache einstufige Synthese zu neuen, potentiell dynamischen Biarylliganden mit großem Potential zur Erschließung weiterer Liganden dieser Klasse beschrieben werden. Teilweise konnten für die erhaltenen Strukturen die Interkonversionsbarrieren und die Aktivierungsparameter in DHPLC-Untersuchungen ermittelt werden. Die erhaltenen Werte stehen dabei im Einklang mit denen des transienten Halbacetal-Katalysators in der Soai-Reaktion.

Der zweite Teil der Arbeit verfolgt einen Ansatz, der auf literaturbekannten guten Enantioselektivitäten mit β-Aminoalkoholen in Alkylierungen mit Diorganozink-Reagenzien beruht. Neben der Darstellung des Konzepts hin zu autokatalytischen Substraten, wurde eine Vorauswahl der hierfür benötigten primären β-Aminoalkoholverbindungen experimentell untersucht. Generell gibt es bereits unzählige Veröffentlichungen zu Alkylierungen mit β-Aminoalkoholen als Liganden. Bisher lag der Fokus jedoch hauptsächlich auf sekundären und tertiären Aminoalkoholverbindungen und beschränkte sich dabei oft auf die Verwendung von Diethylzink. Um ein größeres Spektrum abzudecken, wurden alle Liganden erfolgreich in Alkylierungen mit Dimethyl-, Diethyl- und Diisopropylzink getestet. In den Alkylierungsreaktionen an Benzaldehyd wurden sowohl kommerziell erhältliche Liganden, als auch auf dem Syntheseweg hergestellte Methyl- und Benzylderivate von enantiomerenreinen primären β-Aminoalkoholen getestet. Anschließend wurden die Enantioselektivitäten mittels chiraler HPLC untersucht und Trends in den Vergleichsgruppen bewertet. Die Enantioselektivitäten der Produkte wurden mit mäßiger bis guter Selektivität bewertet. Interessanterweise wurden im Gegensatz zu bereits veröffentlichten Ergebnissen die besten Selektivitäten mit primären β-Aminoalkohole in Alkylierungen mit Dimethyl- und Diisopropylzink erzielt. Für die *N*-methylierten Derivate wurde mit Diisopropylzink im Gegensatz zu den Vergleichsgruppen Dimethyl- und Diethylzink ein Trend zu deutlich besseren Selektivitäten beobachtet. Bei den *N*-benzylierten Derivaten wurde eine Umkehrung dieses Trends beobachtet. Unabhängig von der *N*-Substitution konnte mit Diisopropylzink eine generell höhere Selektivität mit primären Prolinol-derivatisierten Liganden erreicht werden, als mit den vergleichbaren Diorganozink-Reagenzien. Darüber hinaus wurden im Zuge von Untersuchungen mit enantiomeren Ligandenpaaren Abweichungen in den erhaltenen enantiomeren Überschüssen einiger Liganden beobachtet, die mögliche nicht-lineare Effekte indizieren.

1 Introduction

A strongly disputed question of research is the origin of the selective occurrence of only one enantiomer of essential chiral biomolecular building blocks in nature. The emergence of this homochirality has so far remained unexplained.[1] One of the most prominent examples are the D-sugars of DNA and RNA, which have the same relative configuration (fig. 1.1, **1**). Also, all essential amino acids, with the exception of glycine, occur only in the L-form in nature (fig. 1.1, **2**).[2]

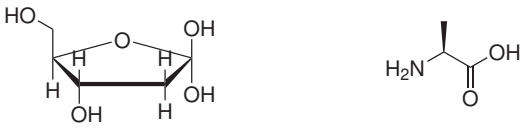

1 **2**

Figure 1.1: Enatiomerically pure building blocks: D-deoxyribose **1** and L-aminoacid **2**.

The property of homochirality is of crucial importance in molecular recognition and replication processes and therefore appears to be necessary for the evolution of life. Some mechanisms for the construction of biomolecules are known from nature, getting along with an initially low enantiomeric excess (*ee*) and without the support of enzymes or other chiral auxiliary materials, but are nevertheless able to multiply the *ee*.[1] Chiral compounds can transfer their stereo information directly to the desired product compounds through intermolecular interactions and create a chiral environment. The principle of transferred stereo information by observing nature has been applied in many ways in synthetic chemistry over the last decades.[3–5] Asymmetric catalysis and synthesis are one important possibility to synthesize enantiomerically pure compounds, for example, for pharmaceutical purposes.[6] Asymmetric synthesis is possible under various assumptions. Such processes usually require a chiral auxiliary medium to induce an *ee* in the achiral starting material.[7]

In the 1970s, *Izumi et al.* proposed a differentiation between 'diastereoselective' and 'enantioselective synthesis'.[8]

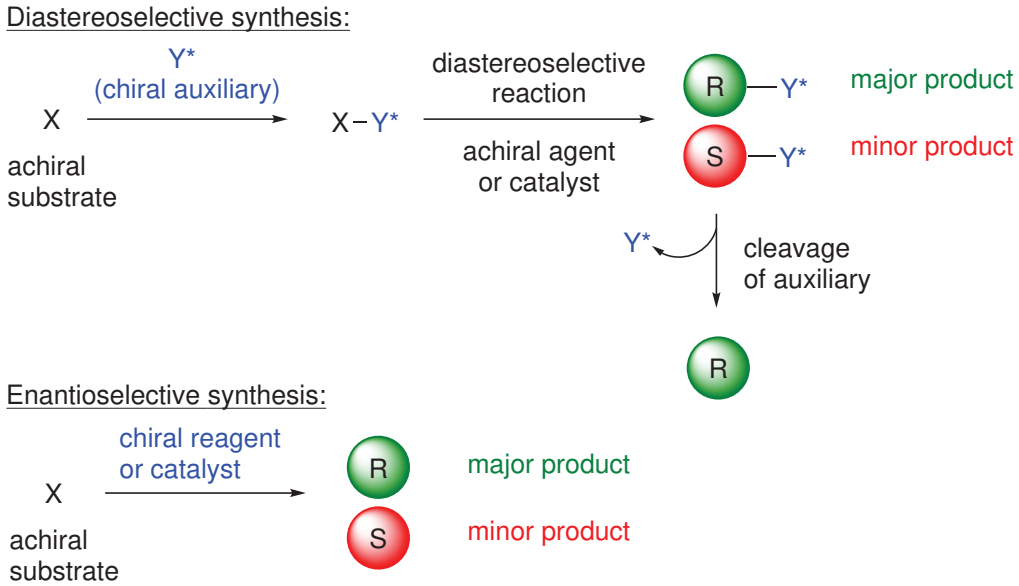

Figure 1.2: Examplary scheme for diastereoselective and enantioselective synthesis based on *Izumi*.[8]

In a 'diastereoselective synthesis', a chiral auxiliary is bound to an achiral substrate in the initial step (fig. 1.2). Afterward, the molecule contains a center of chirality and prochirality. The two faces of the prochiral center become diastereotopic and may react at different rates with an achiral reagent. In the best case, one face is thereby highly favored. In the end, a mixture of diastereomers forms, which becomes a mixture of enantiomers after removing the chiral auxiliary.[8] Prominent examples are asymmetric syntheses using chiral auxiliaries, like asymmetric alkylation with chiral oxazolidinones developed by *Evans et al.* (fig. 1.3).[9] The chiral auxiliary **3** is bound to the substrate giving diastereotopic spaces around the prochiral center. Subsequently, compound **4** is deprotonated with LDA. For the following diastereoselective alkylation to **5**, one of the two diastereotopic sides is sterically favored. After cleaving the auxiliary, the desired α-alkylated carboxylic acid derivate **6** is obtained in high enantiomeric excess.

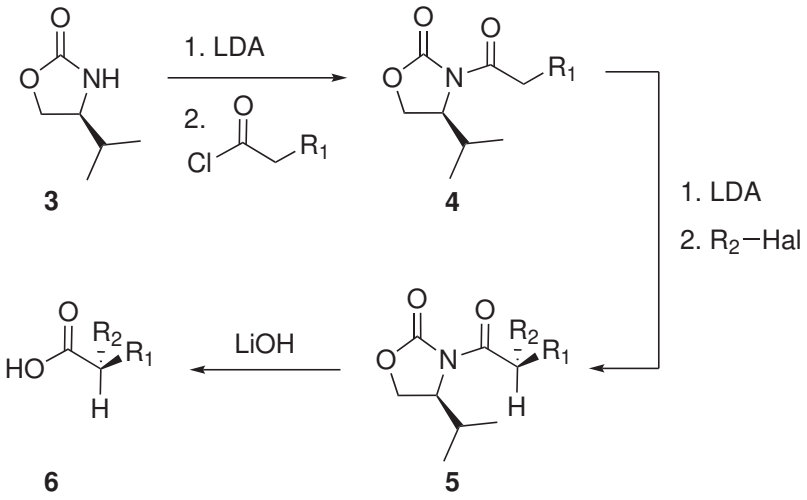

Figure 1.3: Example for diastereoselective synthesis with an oxazolidinone auxiliary developed by *Evans*.[9]

The 'enantioselective synthesis' is given through an achiral substrate containing at least one prochiral center (fig. 1.2). The two faces of the prochiral center are in enantiomeric relation to each other. In difference to the 'diastereoselective synthesis' with the help of chiral auxiliaries, an enantioselective reactant or an enantioselective catalyst can differentiate between those two enantiotopic faces of the prochiral molecule. The rate constants of the attack to both faces are different. Consequently, the *S*- and the *R*-products are formed in unequal quantities.[8] It depends on the enantioselectivity of the reagent or the catalyst, and how much the excess of one enantiomer is obtained. The most elegant method of enantioselective synthesis is enantioselective catalysis. The roots of enantioselective catalysis go back to 1912, when *Bredig et al.* prepared the first alkaloid-catalyzed cyanohydrin compound. It was the first reaction describing an organocatalysis, although the *ee* is quite low.[10] Since then, many more catalysts have been developed with great achievements in higher *ee*'s over the years. Many developed asymmetric catalysts are metal catalysts that mostly use transition metals combined with a chiral ligand for catalysis.[11] The leading work of *Noyori*, *Knowless* and *Sharpless et al.* deserves to be mentioned in particular, as they were honored with a Nobel Prize in this field.[12] Their research led to many metal-based catalysts with different ligand systems, able to be applied in various enantioselective reactions. Significant milestones were, for example, the development of asymmetric epoxidation by *Sharpless et al.*[13,14] (fig. 1.4) or the development of the BINAP ligand system

9 in the application of enantioselective hydrogenations by *Noyori et al.*[15,16] (fig. 1.5).

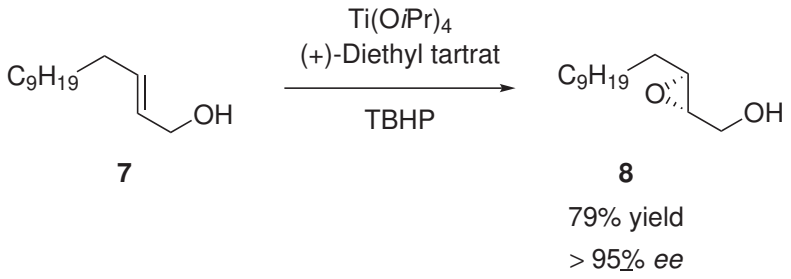

Figure 1.4: Epoxidation of an (*E*)-allylic alcohol **7** with Ti-catalysator based on on Sharpless.[14]

The applied metal catalysts can coordinatively bind the substrate and a chiral ligand that provides the chiral stereo information. The subsequently transferred stereo information determines the configuration of the final product. Both reactions can be seen as initial pioneers for further developments in the field of enantioselective synthesis.

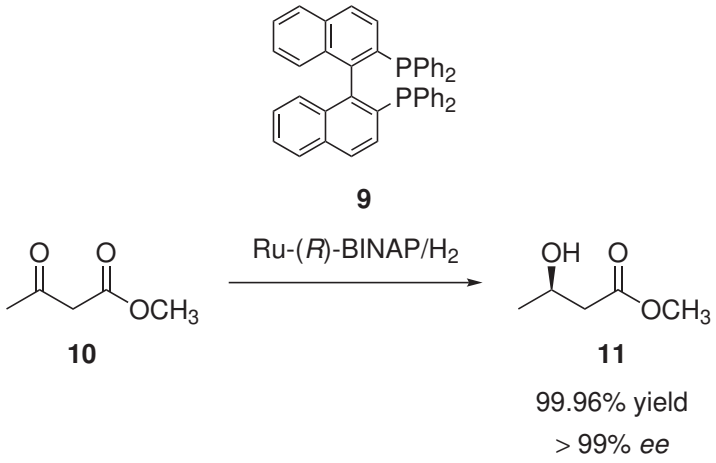

Figure 1.5: Hydrogenation of β-keto esters **10** with Ru-catalysator based on a BINAP ligand system **9** developed by Noyori.[15]

In comparison to these examples, an absolutely asymmetrical synthesis, without the aid of chiral substances, generally leads to quite low *ee*. To solve the initial question of the emergence of homochirality, an initial scenario with a low enantiomeric imbalance can be assumed. It is, therefore, necessary to take a closer look at how an initially low *ee* can be multiplied and finally results in a high *ee*.

1.1 Asymmetric Amplification

The achievement of optical purity is the key challenge in asymmetric preparations. An asymmetric synthesis is subject to an asymmetric amplification process if the *ee* of the obtained product is above the anticipated given *ee* of the chiral auxiliary or catalyst that serves the stereo information.[17,18] Such a deviation from a linear relationship (see fig. 1.6, C) between the *ee* of the catalyst and the *ee* of the product is termed a positive non-linear effect (see fig. 1.6, A, (+)-NLE). Thus, the influence of a positive non-linear effect makes a high enantiomeric purity in the final product possible at an initially low *ee*. Analog for experimental values of the product *ee* below the assumed linear values, a negative non-linear effect occurs (see fig. 1.6, B, (-)-NLE).[19–22]

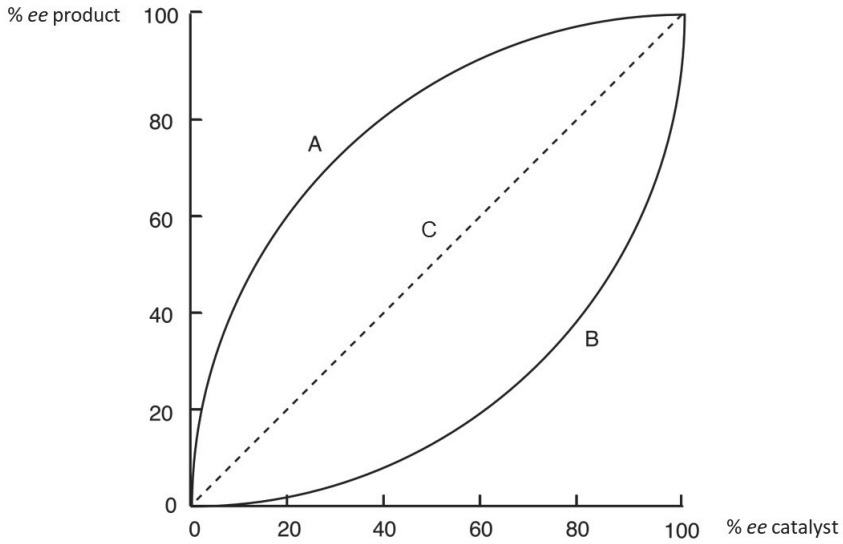

Figure 1.6: Relation between *ee* of catalytst and product; A: positive (+)-NLE; B: negative (-)-NLE; C: linear relation.

NLEs are caused by self-organization, self-assembly, and other aggregation processes.[23–26] Self-assembly and recognition play an important role in nature and the biology of our life and means the spontaneous association of at least two compound species through the formation of reversible, supramolecular, mostly non-covalent interactions to form a larger aggregate.[27] The interactions are mostly dominated by hydrogen bondings or π-cloud interactions.[27] A common example is pairing our DNA strands to form the double helix

structure. The two complementary strands recognize each other through hydrogen bonds and π-π stacking, forming the most thermodynamically stable product in a self-assembly process. Self-amplification in asymmetric catalysis is based on the idea of interaction between the received catalysis product and the catalyst itself through self-assembly, to increase and control enantioselectivity.[28] Enhanced enantioselectivity through the presence of chiral additives could be observed in several catalytical processes before. An early example of a (+)-NLE is given by the previously mentioned Sharpless epoxidation (see fig. 1.4). *Kagan et al.* observed this effect in studies with non-enantiopure auxiliaries resulting in higher *ee*'s than expected when assuming a linear correlation.[18] The deviation was explained by forming an active diastereomeric species through auto aggregation that is impossible to form under the enantiopure condition of the ligand. The enantioenrichment resulted from the removal of the racemic diethyl tartrate from the catalytic cycle due to higher stability and lower reactivity of the heterochiral species detected by kinetic and X-ray structural investigations.[29,30] However, the observed amplification in the epoxidation of geraniol is only moderate in comparison to the very strong asymmetric amplifications in the later reported addition of diethylzinc to aldehydes under the use of chiral β-amino alcohols.[17,31] In this relation, probably one of the best-known examples providing high *ee* is the alkylation of benzaldehyde using the chiral camphor derivative (-)-DAIB **13** investigated by *Noyori et al.* (fig.1.7).[31,32]

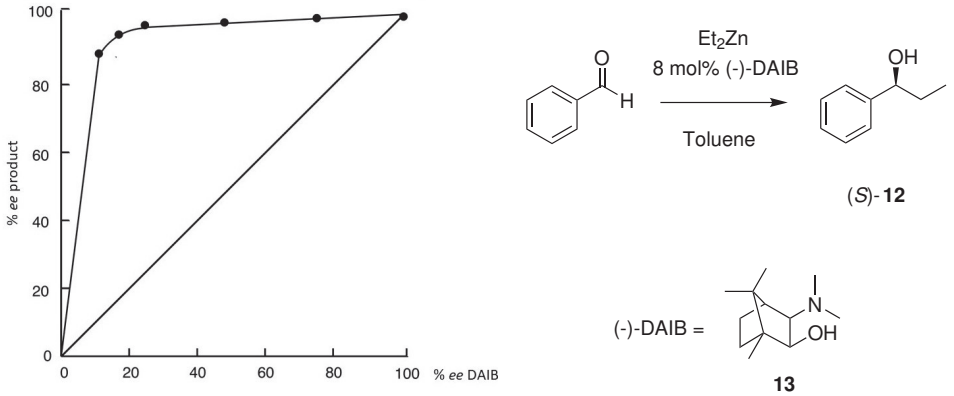

(a) (b)

Figure 1.7: (+)-NLE in the addition of Et_2Zn to benzaldehyde with the usage of 8 mol% (-)-DAIB in toluene reported by *Noyori et al.*.[31]; a) experimental data showing (+)-NLE; b) Addition of Et_2Zn to benzaldehyde with (-)-DAIB **13**.

The employed ligand (-)-DAIB **13** with 15% *ee*, yields the corresponding *S*-alcohol **12** product in optical purity up to 95% *ee* after hydrolysis.[31] The positive non-linear effect is induced by an aggregation of the dialkylzinc and the chiral ligand. An initial low *ee* comprising both enantiomers results in homo- and heterochiral dimers that are catalytically inactive (fig. 1.8). The dimers are in a dynamic equilibrium with the catalytically active monomers, which predominantly produce one enantiomer of the product alcohol.

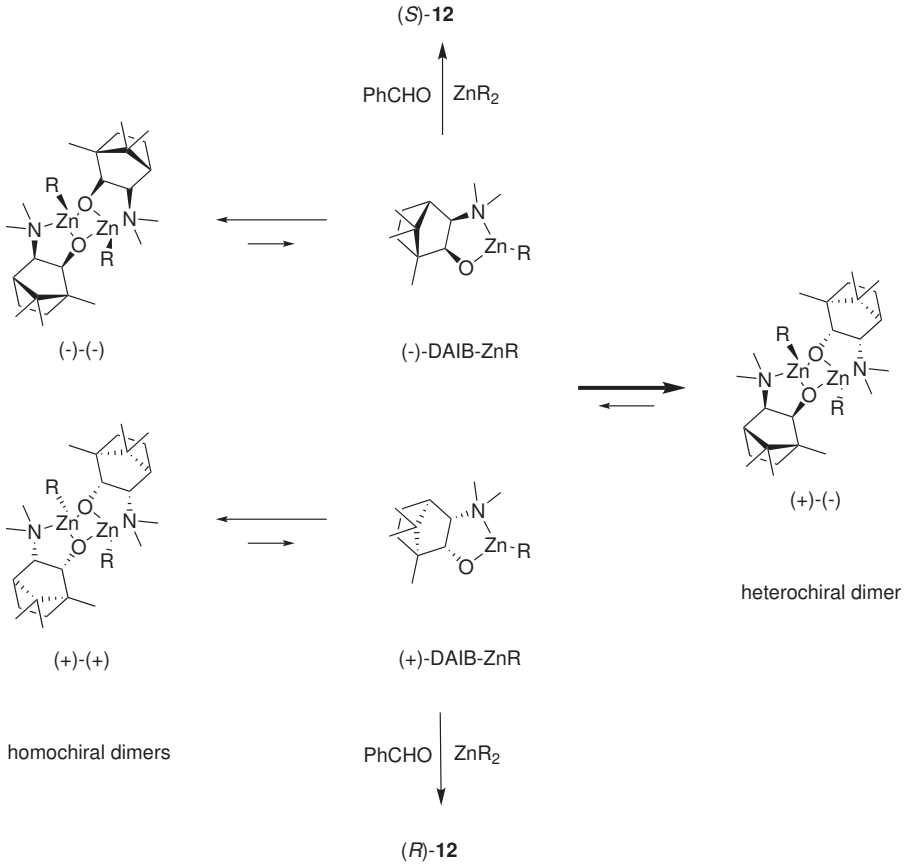

Figure 1.8: Dynamic equilibrium between dimer and monomer complexes explaining the (+)-NLE in diorganozinc additions to benzaldehyde.[22,31]

Further investigations, including X-ray diffraction, kinetic investigations, and NMR spectroscopic measurements, showed higher stability and decreased reactivity due to a *anti*-configuration between the alkyl groups for the heterodimer. The dihedral angles between the 4- and 5-membered rings were found to differ widely with 135-146° for the homochiral complex and 112-124° for the heterochiral complex. These findings in the interaction of

the dynamic equilibrium of all structures explain the enantiomeric enrichment of the dominantly present configuration and the (+)-NLE to be observed.[31,32] For more detailed explanations, mathematic models and further examples of non-linear effects in asymmetric synthesis than presented and considered relevant for this work, a series of reviews, especially by *Kagan et al.*, give deeper insights into this research field.[19,21,22] NLEs are common over various metal catalysts or ligand classes and are often investigated to gain insight into the mechanism behind a reaction.[22,33] Generally, the mechanisms behind NLEs cannot be generalized and are highly dependent on the particular reaction system. Even very small differences in the catalyst structure or in the catalyst substrate used can lead to different results or can no longer be explained by the same mechanisms. A given example is the morpholino variant MIB (see section 4.1 for more details) of the commonly known DAIB ligand developed by *Nugent et al.*.[34] Further experimental investigations of *Walsh et al.* showed a substrate dependency of the NLE in asymmetric alkylation with dialkyl zinc reagents when using electron-donating substituents to benzaldehyde.[35] The observation of more significant NLEs in these cases is not explainable within the concluded mechanism for DAIB comprising different stability and reactivity of the hetero and homo dimers.[33] To understand and explain the observations by *Walsh et al.*, substrate interactions must also be taken into account. Therefore, *Blackmond et al.* suggested an extension of the current mechanism considering weak or strong substrate binding by analyzing the reaction rates, that are able to explain the given phenomenon.[33] Even if this example shows that individual consideration of each reaction and all its components is indispensable, the elucidation of catalytically active species or molecular interactions, as well as the basic understanding of the generation of NLEs, can contribute to the design of new highly enantioselective catalytic systems. In particular, autocatalytic systems raise great attention. They usually comprise significant NLEs and are the subject of ongoing mechanistic investigations, since they do not require an initial chiral induction of an additional substance. The following section will briefly overview autocatalytic principles and the rare experimental proven asymmetric examples in organic chemistry (see section 1.2). A striking example of an extremely strong amplification of *ee* and thus a high (+)-NLE is the autocatalytic Soai reaction.[36,37] The ongoing mechanistic understanding and elucidation of this unique reaction is described in different approaches in the literature and will be discussed in the first chapter as it is crucial for parts of this work (see chapter 3).

1.2 Autocatalysis

As previously mentioned, the research on autocatalytic processes attracts great interest in the context of enantioselective synthesis. In addition, the understanding of self-amplifying and self-recognizing processes, which are invoked as a key element in the nature of the living state, represents an approach to understanding the origin of life.[38–40] The concept of autocatalysis generally originates from *Wilhelm Ostwald*, who described it for the first time in his article 'Ueber Autokatalyse' in 1890.[41] According to *Ostwald*, the description of an autocatalysis of one or multiple reactions simultaneously can be represented by a reaction equation in which the reactants and the products do not overlap. At least one reactant or one product has a catalytic effect on the entire process in the equation described.[38,41,42] The most common definition of autocatalysis today differs from *Ostwalds*. It is defined as a single- or multi-step reaction that is catalyzed by at least one of its provided final products.[38] Various different scenarios with autocatalytic behavior are known and postulated in literature, which relate to the emergence of life.[43,44] In a detailed review of autocatalytic mechanisms, *Bissette and Fletcher* described three types of scenarios that are believed to have a major role in this field of research (fig. 1.9).[39] In addition to the simplest scenario of classical autocatalysis, as just described, there are cross-catalyzes and hypercycles (fig. 1.9).

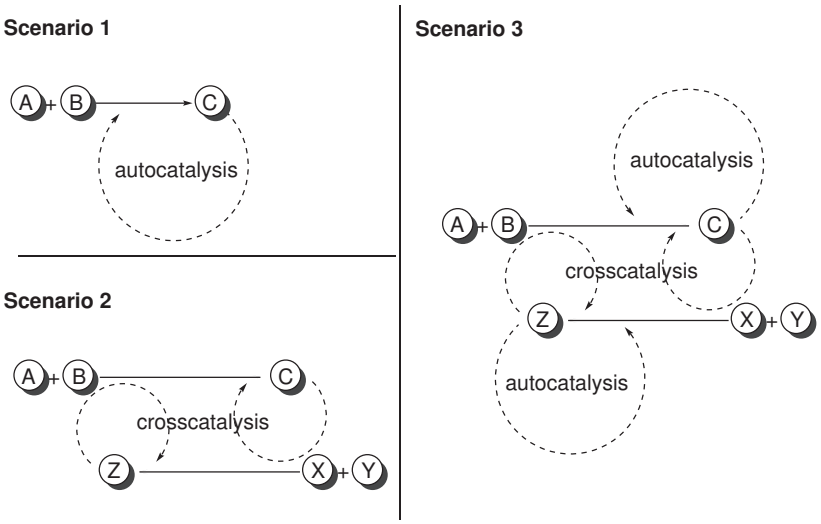

Figure 1.9: Autocatalytic related forms according to *Bisette et al.*[39]; Scenario 1: classic autocatalytic cycle; Scenario 2: cross-catalytic cycle; Scenario 3: hyper cycle.

In the latter, several reactions are involved whose products or reactants catalyze each other, also known as mutual catalysis. A hypercycle forms from two mutal catalytic autocatalysts. In addition to the three scenarios presented, entire autocatalytic networks and more complex mechanisms with short-living intermediates are also possible.[45] Probably the best-known example of this is the autocatalytic network around the formosis reaction.[46] The reaction was discovered in 1861 by *Butlerow* and provided a broad variety of over 40 different sugars and other products.[47] The reaction of aqueous formaldehyde and calcium hydroxide or calcium carbonate is non-directional and non-selective in relation to stereo information and carbon chain length.[48,49] The mechanism of the formosis reaction remains still not fully understood due to the large variety of products and its sensitivity.[49,50] An additional common feature of all autocatalytic processes worth mentioning is their kinetics. A graphical plot of concentration versus time typically shows a non-linear character appearing in a sigmoidal curve (S-shaped, fig. 1.10 (a)).[51,52] In autocatalytic reactions, sigmoidal kinetics is usually expected, since most are kinetically exponential and substrate availability is always experimentally limited.[45] The sigmoidal curve is thus an important experimental sign of autocatalysis. The sigmoidal curve is divided into three areas (fig. 1.10 (a)).[45] In the initial period, only a small part of the starting material is converted into the product, so the increase in the curve is small. The exponential phase shows the acceleration of the reaction rate due to the catalytic activity of the product previously formed. In the saturation phase (range from the bending point to the completion of the reaction), it decreases again.

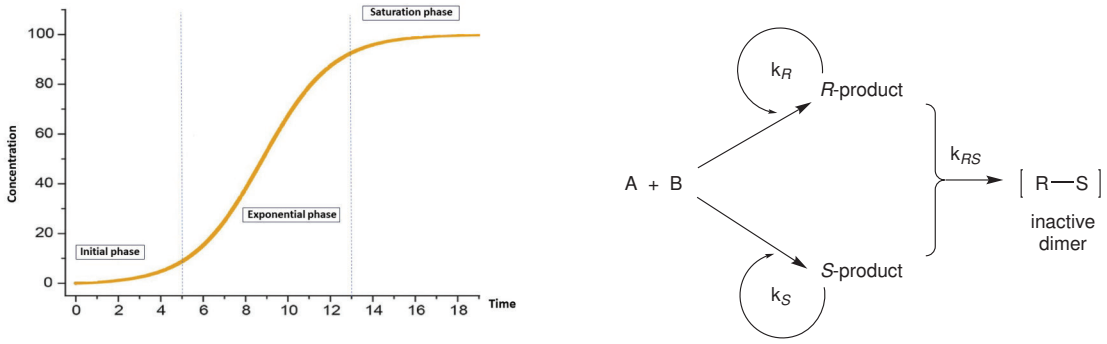

(a) (b)

Figure 1.10: (a) characteristic sigmoidal curve (S-shape) for the non-linear character of autocatalytic behavior; (b) *Frank*'s model explaining enrichment with inhibition by dimerization.[22,53]

The S-shape degree depends on the autocatalytic reaction's efficiency, which is always accompanied by direct, non-catalyzed product conversion.[45] The ratio of parallel-driven autocatalytic and non-catalyzed pathways is therefore determining.[45,51] Many other examples of autocatalysis exist in a wide variety in fields of chemistry[45], like autocatalytic acid/base reactions[54], organometallic autocatalysis[55–57], photo-autocatalysis[58,59] and asymmetric autocatalysis[25,60–62], just mentioning those in the field of organic chemistry. Asymmetric autocatalysis is one of the most challenging areas of which only very few practical examples are known.[63] Thereby, a chiral product acts as the chiral catalyst for its own production.[64] Asymmetric autocatalysis is implicated in the origin of biological homochirality.[53] In 1953, *Frank* discussed the emergence of homochirality in a mathematical model of asymmetric autocatalysis.[53] The idea behind *Frank's* model is based on a chiral chemical substance that catalyzes its own formation and at the same time acts as an inhibitor for the formation of the opposite enantiomer by the formation of an inactive dimer (fig. 1.10 (b)).[53,65] The mechanistic requirements for asymmetric autocatalysis are large and controversial. There is currently no mechanistic solution based on one of the few examples on which the published literature seems to be in complete agreement (see Introduction 3). *Frank's* assessment of autocatalysis seemed justified at the time: 'A laboratory demonstration may not be impossible'.[53] Research of the past decades up until today is therefore intensively engaged in the mechanistic elucidation and the discovery and development of new autocatalytic systems. The rarely known systems are presented in more detail in the following part.

Asymmetric autocatalysis

An asymmetric autocatalytic process was experimentally described by *Soai et al.* in 1990 for the first time.[66] *Soai et al.* reported an asymmetric autocatalytic behavior in the reaction of pyridine-3-carbaldehyde and diisopropylzinc. Initial studies of this reaction used the product-catalyst, containing an amino alcohol-moiety in high *ee*'s, resulting in lower product *ee*'s (47%*ee*).[66] The results were investigated intensively in the following years, leading to another breakthrough in 1995.[25] The further developed system now included a pyrimidine unit instead of a pyridine one. The *ee* could be increased by up to 95% using almost enantiomerically pure catalysts. Inspired by the results of the system, *Soai et al.* tried to test the autocatalytic activity of the system with an initial catalyst of

very low *ee*. After several reaction cycles, the *ee* could be significantly increased (fig. 1.11).

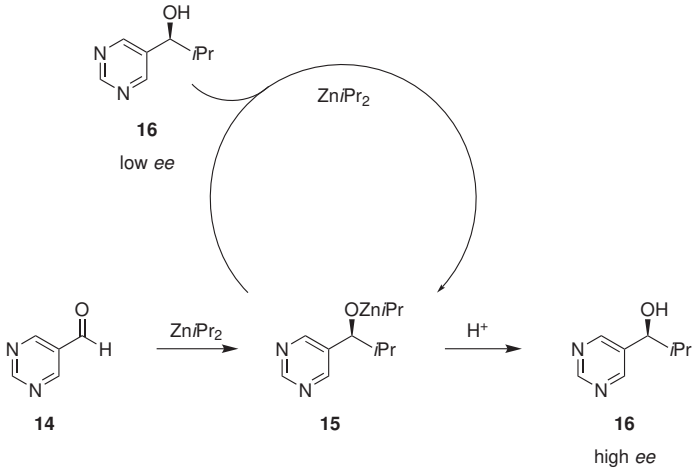

Figure 1.11: Postulated asymmetric autocatalysis cycle for the Soai reaction.[25]

The obtained product of each previous catalytic cycle serves again as a catalyst in the following turnover. Each cycle generates a higher *ee* than the previous one and the *ee* finally reaches a value of 89% in the fourth cycle, beginning with 10% *ee* after the first turnover.[25] This publication is still one of the most relevant of the last 50 years according to the renowned journal *Nature* and still fascinates the science community in different fields.[67] It was the initiator for intensive further development and findings of this asymmetric autocatalytic active system. In the following years, extensive investigations were made regarding the further optimization of the system to reach the limits of the best possible. In particular, the structural requirements for the starting material and the reaction conditions were investigated. Various basic scaffolds with a rigid γ-amino alcohol unit were investigated for their autocatalytic abilities.[37,68,69] The best results for a spontaneous symmetry breaking were achieved with a 2'-trimethylsilylethynyl residue for the pyrimidine system in toluene (74%*ee*). Further investigations included the influence of various reaction parameters such as the initial catalyst amount and enantiopurity, chiral additives, solvent[70], and temperature dependence[69]. The autocatalytic system reacts sensitively to changes in those various parameters. The influence of the amount of catalyst was studied with enantiopure and low *ee* catalysts by the groups of Soai[37,71], and Gehring[69]. An almost enantiomerically pure catalyst with a loading of 20 mol% could achieve >99.5%

ee in the obtained product **18** with a 2'-substituted pyrimidine aldehyde with *tert*-butyl ethinyl residue **17** (fig. 1.12).[37] By using an almost racemic catalyst mixture (0.00005% *ee*) the alcohol **18** could also be obtained with >99.5% *ee*, but within three additional consecutive catalytic cycles.[71] Studies with a 2'-adamantylethynyl-residue showed the highest *ee* adding a low *ee* (7.2%*ee*) catalyst at the beginning (95.8%*ee*).[69] In the same study, no significant influence of the catalyst loading on the *ee* of the formed product could be found in a range between 0.2 to 20 mol%. For higher catalyst loadings, the amplification of the *ee* is decreasing. Smaller catalyst concentrations below 0.01 mol% give different non-reproducible results, which indicate static effects or very sensitive behavior to the smallest changes.[67,69,71]

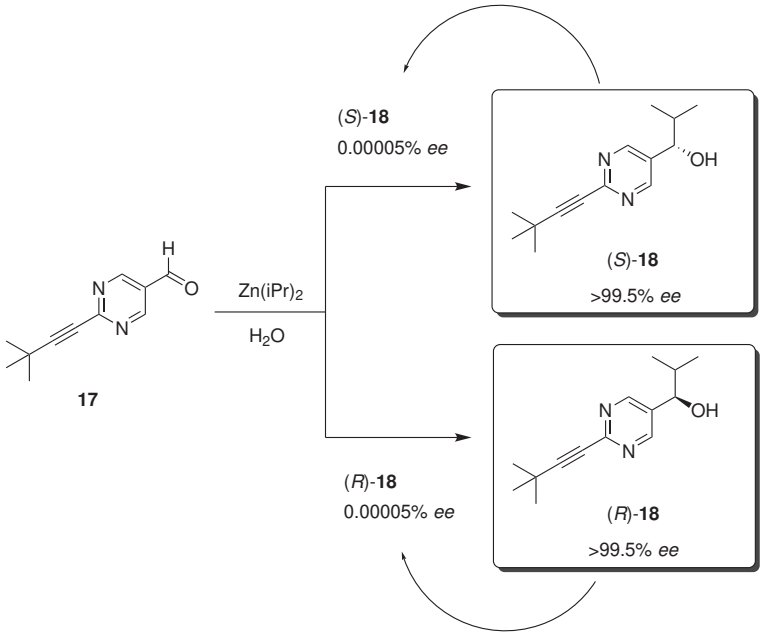

Figure 1.12: Asymmetric autocatalysis for the developed Soai reaction in 1999.[37,71]

In further research it was observed that not only the product leads to an enantioselective amplification by autocatalysis, but also other sources of chirality can generate very high *ee* values. Various compounds with one or more chirality centers, planes, or axes, were able to create a chiral environment in their presence and thus cause an increase in enantioselectivity.[72] For example, enantiomorphic crystals like quartz or $NaClO_3$ and circularly polarized UV light could be used to induce significant high *ee* values.[2]

In 2011, *Carreira et al.* reported a reaction with autocatalytic behavior in the synthesis of the antiretroviral drug Efavirenz.[61] In this first reported autocatalysis for a pharmaceutical-relevant synthesis, an enantioselective process is described in which the combination of the chiral ligand (1*R*,2*S*)-N-pyrrolidinyl norephedrine and sub-stoichiometric amounts of the (*S*)-product **19** (R_1) are used as autocatalyst at the beginning of the reaction (fig. 1.13, R_1). The product-ligand combination could achieve higher *ee* values in the diethylzinc-mediated addition of an alkyne to a ketone than the chiral ligand exclusively. However, without adding the external chiral ligand by purely product-controlled selectivity, the product could only be obtained racemically. According to the definition of *Albert and Wyneberg*, the term autoinduction is therefore suitable.[60,73] It is defined as the product influencing the further course of the reaction by modifying the nature of the reagent or the catalyst.

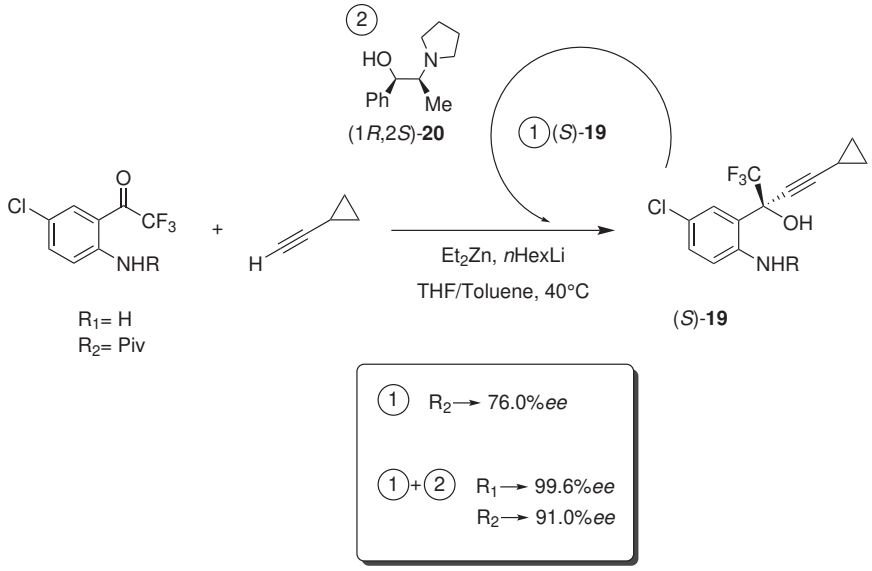

Figure 1.13: Asymmetric autocatalysis in course of the development of a synthesis route towards Efavirenz investigated by *Carreira et al.*.[61]

In further investigations, *Carreira et al.* were able to display an autocatalytic behavior for an *N*-pivaloyl-protected derivative of the above described (fig. 1.13, R_2).[61] Test reactions were carried out with either exclusively chiral ligand (results in 20%*ee*) or product (results in 76%*ee*) as control group wherein significantly higher enantioselectivity by the product was observed. Subsequently, the reaction was also carried out in the presence of both con-

trol groups (chiral ligand and product), giving the best results (94%*ee*). Besides the solely autocatalytic effect of the product of the protected N-pivaloyl derivative, the synergistic effect between the product and the chiral ligand thus reinforces the existing autocatalytic effect with an additional autoinduction in this case. A few years earlier, another asymmetric autocatalysis was discovered, representing the third and last experimentally proven example in this field. In contrast to the previous examples, which both describe autocatalytic reactions with organozinc reagents, *Mauksch et al.* demonstrated an organocatalytic example in a Mannich reaction.[62] The best *ee* values were reached with very high catalyst loadings of 30-50 mol% (up to 96%*ee* for the *R*-product). The group proposes product-substrate interactions based on hydrogen bonds with the prochiral substrate as indicator for the autocatalytic behavior.[62]

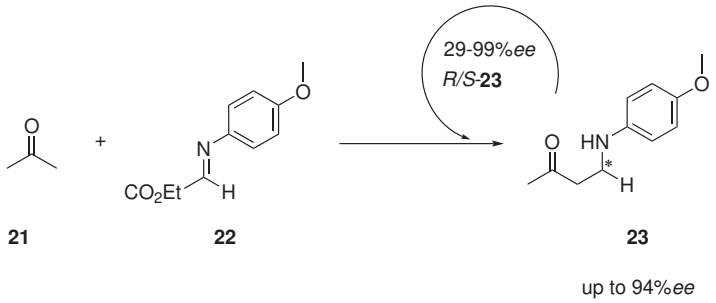

Figure 1.14: Asymmetric autocatalysis reported in a Mannich reaction by *Mauksch et al.*.[62]

The only three examples discovered to date illustrate the rarity of asymmetric autocatalysis in experimental implementation. Each system is unique in itself and can follow different mechanistic principles. A complete mechanistic elucidation is often complex and challenging due to parallel-driven reaction scenarios. However, an understanding of the specific processes involved in symmetry breaking and amplification allows the conceptualization of new ideas and structural design for potential novel autocatalytic systems. The term symmetry breaking is to be understood as the spontaneous generation of an imbalance of the enantiomeric ratio, favoring one enantiomer in the absence of a chiral external source.[65] An initial symmetry breaking is crucial to initiate a subsequent amplification process and can therefore be seen as a key element of an autocatalytic process. There is yet no explanation based on theoretical or experimental findings for the phenomenon of symmetry breaking. The subject of discussion is a tiny energy difference between two

enantiomers due to parity violation that could make a possible difference in the emergence of the imbalance.[74]

The Soai reaction was the first and still unique to obtain the highest chiral amplification through autocatalysis and a positive NLE. In addition, it is probably the most intensively studied asymmetric autocatalysis due to great interest in its mechanistic elucidation. It thus represents the most important point of reference for a possible explanation of enantioselective amplification and autocatalytic activity in one system.

2 General Research Objective

The general target of the present work is to develop new potential autocatalytic substrates and to make them accessible *via* a synthesis route. As stated in the introduction, exact prediction of an autocatalytic activity or the presence of NLEs is almost impossible, no matter which approach one chooses. However, in order to increase the chances for potentially conceived results, it is very beneficial to study literature on known systems with the same properties. The following thesis presents two different structural concepts based on literature-known results. This work is divided into two main parts. The first chapter comprises a substrate design based on the mechanistic results of the autocatalytic Soai reaction by *Trapp et al.*.[75,76] The structural motif focuses on a dynamic hemiacetal which is assumed to be potentially catalytically active in dioragnozinc mediated alkylations. The second part is based on various highly enantioselective results with ligands that are β-amino alcohol based. Of initial importance are the results of *Oguni et al.*.[17,77] The focus for structural design is on primary β-amino-alcohols. These structures exhibit the possibility of oxidation to an aldehyde, which can be selectively reduced to a catalytically active product in an alkylation with diorganozinc reagents, thus enabling an autocatalytic cycle. For both approaches, the initial conceptualization is followed by the implementation on the synthesis path, which should be as simple as possible to ensure easy availability. After successful realization, the structures are analyzed in detail in order to obtain indications of suitability or to preclude non-suitable structures. If the designed and synthesized structures are in accordance with the conceived properties, the last step is to catalytically test alkylations using diorganozinc reagents and afterward evaluate the results. Individual concepts and related background information are formulated in more detail at the beginning of each chapter.

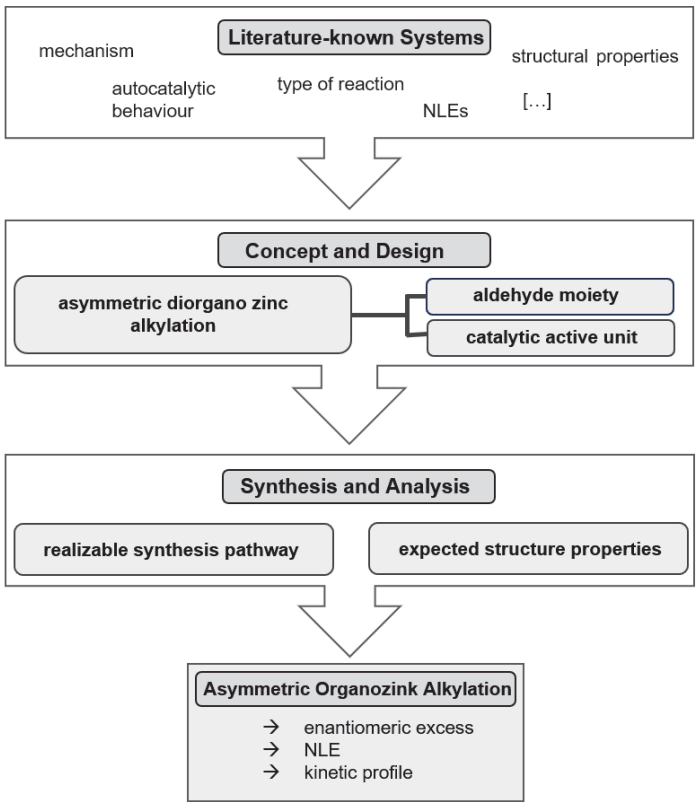

Figure 2.1: Flow-chart for the general process of developments during this work.

3 Chapter 1 - Autocatalytic Substrate Design based on the transient catalytically active Hemiacetal in the Soai Reaction

3.1 Introduction

The discovery of the Soai reaction led to countless attempts at theoretical and experimental explanations of the mechanism. Through the elucidation, it is hoped to gain knowledge about the function of self-amplifying autocatalytic processes and possibly pave the way toward similar systems. In the following, the most important and plausible models to explain the mechanism of the Soai reaction are presented, including the hemiacetal model proposed by *O. Trapp et al.*[76], which provided a final explanation and evidence of the mechanism.

Soai-model

In 2001, *Soai et al.* could propose an autocatalytic mechanism. The basis was formed by kinetic studies between the reaction time and the yields of the product in the enantioselective addition of diisopropylzinc to pyrimidine-5-carbaldehyde using different amounts of enantiomeric catalyst. Therefore, two different possibilities for autocatalytic models were suggested, that could describe the reaction process.[78] The first path (fig. 3.1) resembles the mechanism assumed on the basis of a dimer model almost simultaneously proposed by *Blackmond et al.* in 2001, which is described in detail in the next chapter (section 3.1).[79] The second path (fig. 3.1) is also a way to explain *Soai's* kinetic observations.

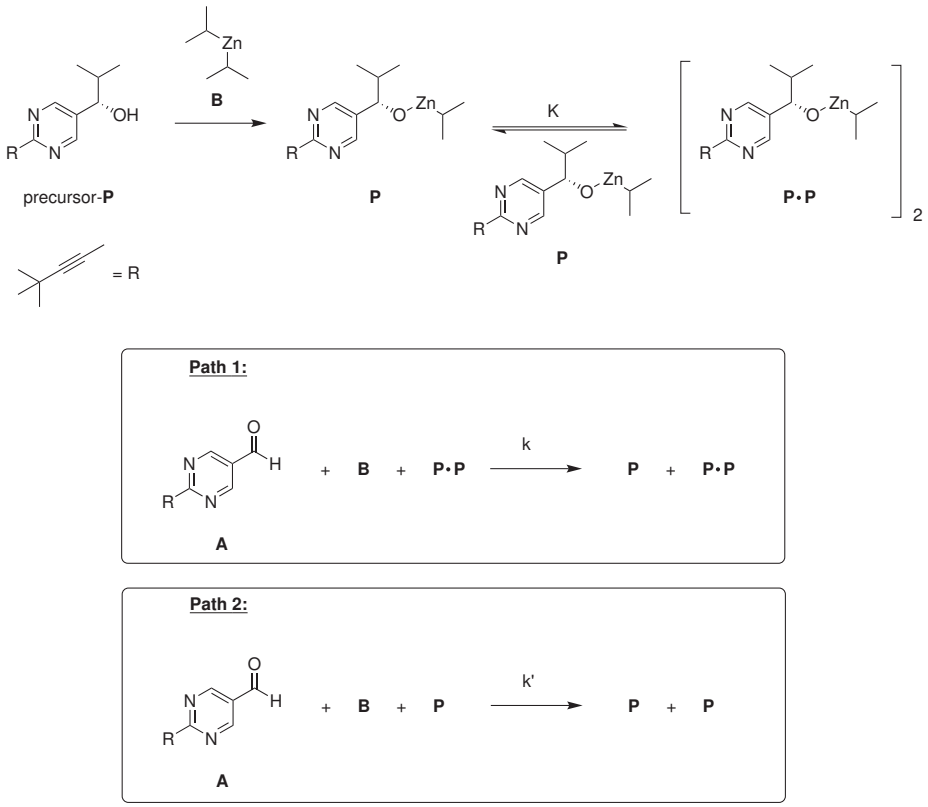

Figure 3.1: Possible autocatalytic pathways according to *Soai et al.*; modified figure, originally published in *Tetrahedron: Asymmetry, 12*, **2001**, 19651969.[78]

The reaction proceeds rapidly in the middle stage after an initial incubation time and gets slow in the final stage, which is characteristic of an autocatalytic reaction. A complex formation between monomeric product alcohol and catalyst is assumed (fig. 3.2). Supported by the experimental findings, *Soai et al.* suggested a second-order kinetic model with the following rate law.[78] Even if the reaction progress is well displayed in simulating the reaction speed of the model, the large excess of enantiomers remains unclear. In the proposed mechanism, each enantiomer would catalyze its own formation in the same way and thus no excess of a single enantiomer is able to arise.

$$v{=}k'[AP][BP] = k'KK'[A][B][P]^2 \tag{3.1}$$

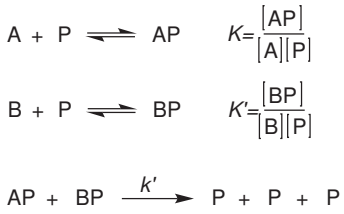

Figure 3.2: Equilibria under the presumption of a complex formation between reactant and catalyst (fig. 3.1, pathway 2).[78]

Two years later, *Soai et al.* published an extended theory on their mechanistic model due to further kinetic investigations based on previous findings. In the novel model, the self-amplification of enantiomers is explained next to an autocatalytic process by the participation of product inhibition *via* the formation of trimers (fig.3.3).[80] It was observed, that the *ee* increases if the complex of autocatalyst and product $P_S{\cdot}P_S{\cdot}P_R$ would have higher stability than the complex of autocatalyst and product $P_S{\cdot}P_S{\cdot}P_S$. Thus, heterochiral trimer complexes are assumed to be more stable than the homochiral trimer complexes, and the active dimer complexes $P_S{\cdot}P_S$, $P_R{\cdot}P_R$ and $P_R{\cdot}P_S$.

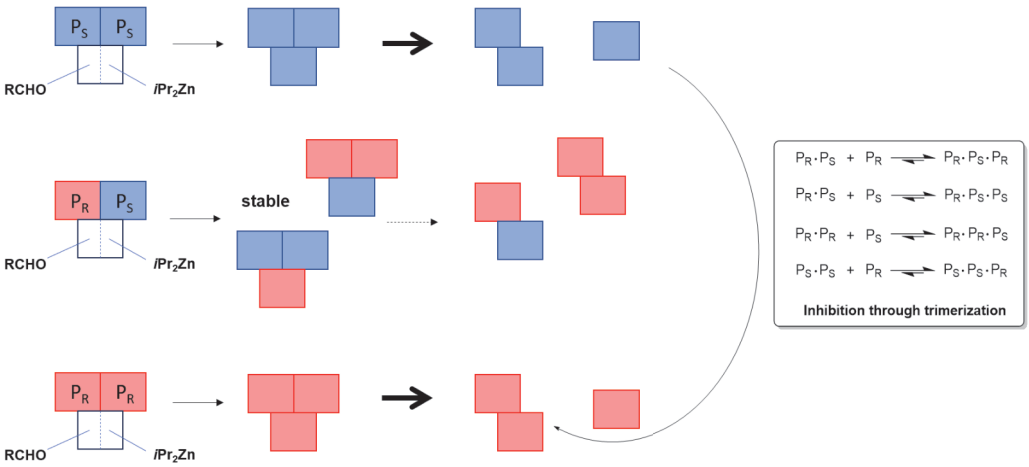

Figure 3.3: Extended model of *Soai et al.*, showing the catalytic self-amplification through product inhibition by trimer formation; modified figure originally published in *Tetrahedron: Asymmetry, 14 (8)*, **2003**, 975-979.[80]

The hetero-dimeric complexes thus disappear from the equilibrium, while the dimer of the non-favored enantiomer is inhibited by the amplified monomeric product enantiomer

(fig. 3.3). Although the model could be well supported by the experimental data, since it predicts good reaction rates and *ee*, no experimental evidence could be provided for the catalytic role of trimeric structures.

Several years later *Soai and Co-workers* reported enantiopure and racemic alkoxide tetramer structures and higher oligomeric structures determined by X-ray structure analysis that are regarded as potential key intermediates.[81] Coordinative tetrameric structures based on these findings and further investigations came back into focus a few years later through a proposed mechanism by *Denmark's* group to explain the extraordinary amplification as well as the symmetry breaking in the Soai reaction.[26] A separate section is devoted to this part (see 3.1).

Dimer-model according to *Blackmond et al.*

The model of *Blackmond et al.* is based on a combination of computer calculations of possible species, NMR, and kinetic studies assuming the presence of statistically distributed homo- and heterochiral dimers. The heat flow profile obtained in microcalorimetry measurements provides a direct measurement of the rate of reaction as a function of time and thus of the overall progress of the reaction.[79] A comparison between the use of a racemic catalyst and an enantiomerically pure catalyst by kinetic investigations of *Blackmond et al.* showed that the conversion of the Soai reaction under the use of a racemic catalyst proceeds in half of the velocity obtained with the enantiopure catalyst. The displayed time-resolved course of the Soai reaction and thus the determination of the rate law could prove an autocatalytic process.[79] The experimental observation suggests a dependence of the concentration of the active catalyst on the *ee* of the initial catalyst based on theoretical assumptions of *Kagan's* reservoir model introduced in 1994.[82] *Kagan's* model proposes hetero- and homo-dimers as key roles in the Soai reaction and attributes active catalytic activity to them (fig. 3.4, left). The modified variant of *Blackmond et al.* assumes stochastically formed hetero- and homochiral dimers with approximately equal stability, whereby the increased chirality results from the inactivity of the heterochiral dimers (fig. 3.4, right).[79,83]

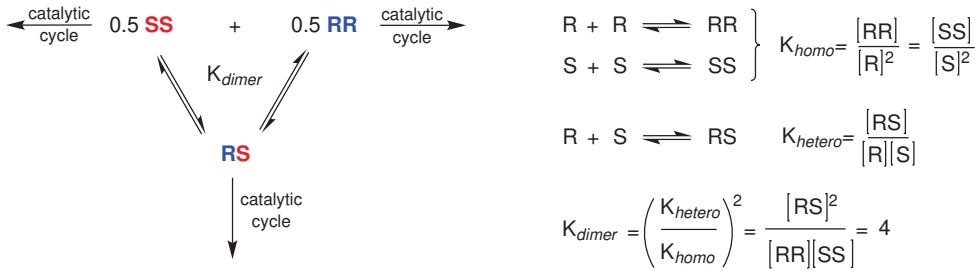

Figure 3.4: Dimer-model for the Soai reaction, including thereon-based equilibriums and reactions.[79,84]

The suggested value K_{dimer}=4[84], predicted by the model, was later confirmed by ^{1}H NMR studies of *Brown et al.*.[85] It revealed that solutions of enantiopure alcohols only form homochiral dimers, while solutions of racemic alcohols show quite similar ratios of both hetero- and homochiral dimers. Thus, the assumption of the stochastic distribution and the same stability of the dimers as of the value K_{dimer} can be confirmed. The NMR analyses proposed a structure with central square $[ZnO]_2$-unit, which could be also confirmed by DFT calculations (fig.3.5).[85]

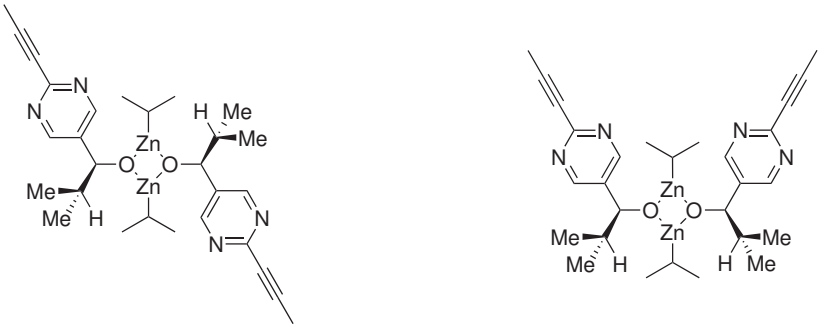

Figure 3.5: NMR spectroscopically confirmed homochiral **24** and heterochiral dimer **24** structures in the Soai reaction.[85]

Blackmond et al. postulated the derived reaction rate on the basis of experimental investigations to describe the autocatalytic system of the Soai reaction, assuming homochiral dimers as the catalytic active species.[83] In this case the selectivity is a pure kinetic process. In further kinetic studies of *Blackmond* and *Buono*, it turned out, that the equation is only valid for the description of the rate law for an equal ratio between aldehyde and zinc organyl.[83] By increasing the concentration of the zinc organyl, the experimental

data did not agree with the model. For that purpose, a renewed rate law was introduced, which is independent of the zinc organyl concentration and based on the assumption of the formation of a complex between the aldehyde and the zinc organyl.

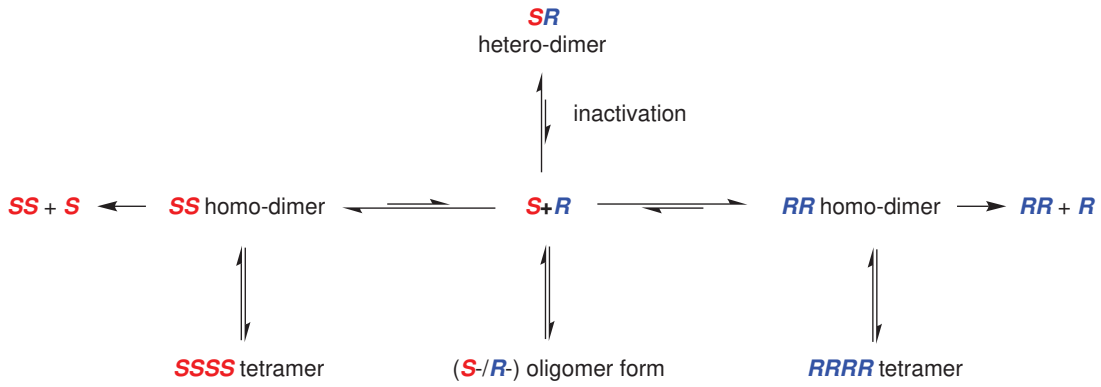

Figure 3.6: Overview over mechanistic examinations according to *Blackmond et al.*.[83–86]

In this context *Blackmond* and *Buono* suggested the interaction of two molecules with the dimeric catalyst in the presumption of the formation of a tetrameric transition state, consisting of two zinc complexed aldehyde molecules and the dimer.[83,84] *Klankermayer* and *Brown* were able to determine a tetramer complex, as well as oligomeric species, by NMR analysis and DFT calculations (fig. 3.6).[86,87] Later on *Soai et al.* confirmed these structures in X-ray structure analysis as mentioned in the previous section.[81] Nevertheless, the self-replicating system of the Soai reaction with its ideal autocatalytic behavior speaks rather against a role in the catalytic mechanism of such a transition state. By the work of *Noyori* and *Yamakawa*, tetrameric intermediates from reactions of amino alcohols with zinc organylene were already known.[32] The tetrameric structures could be regarded as a side reaction because they do not actively participate in the catalysis cycle and are independent of the catalytic dimer species. Such non-catalyzed side reactions could possibly lead to a reduction of autocatalytic activity.[32] A little later, *Gridnev* and *Vorobiev* proposed homochiral brandy glass tetramer macrocycles on the basis of DFT calculations as a key role for the Soai reaction in solution. However, they also confirmed reduced catalytic activity due to competition between dimers, tetramers, and other oligomeric forms in the catalysis cycles.[88] In 2012 *Blackmond* and *Brown* made an interesting discovery of hemiacetal intermediates, which provides direct indications of the model by *Trapp et al.*

presented below (section 3.1). The species could be detected by 2D NMR spectroscopy at -40°C (fig. 3.7). Their concentration increases during the reaction and decreases towards the end.[89] *Blackmond* and *Brown* did not consider these hemiacetals as potential catalytically active.[89]

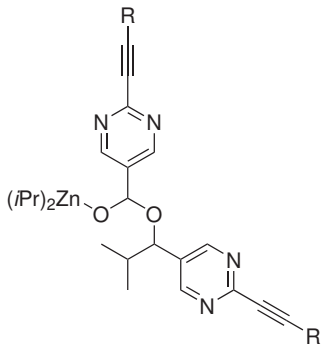

Figure 3.7: Hemiacetal intermediate in the Soai reaction.[89]

The latest mechanistic proposals were published in 2020 by the groups of *Denmark et al.* and *Trapp et al.* resulting in different conclusions.[26,76] Both approaches are based on earlier observations of the main catalytically active species. In the following, both mechanistic approaches will be presented, since both claim, in different ways, a complete mechanistic explanation. The hemiacetal-based approach is the essential reference point for the objectives of the first chapter of this work. In this context, it is also worth mentioning the comparison of *Y. Geiger*, who recently discussed both mechanisms in a review paper.[90]

Floor-to-floor (SMS-tetramer) model according to *Denmark et al.*

The catalytic key structure in the mechanistic approach is a homo tetramer in a square-macrocycle-square (SMS) conformation, according to *Demark et al.*[26] The mechanistic studies are based on a pyridine system with the same substituent in the 2'-position, in contrast to a pyrimidine system as used for the Soai reaction. The group observed auto-catalytic behavior within this system, unexpected to prior findings for the bare pyridine that were unsuccessful. As described in previous sections, tetramers have already been the subject of mechanistic considerations based on DFT calculations and as an extension in an active dimeric species scenario.[78–80,86,88]

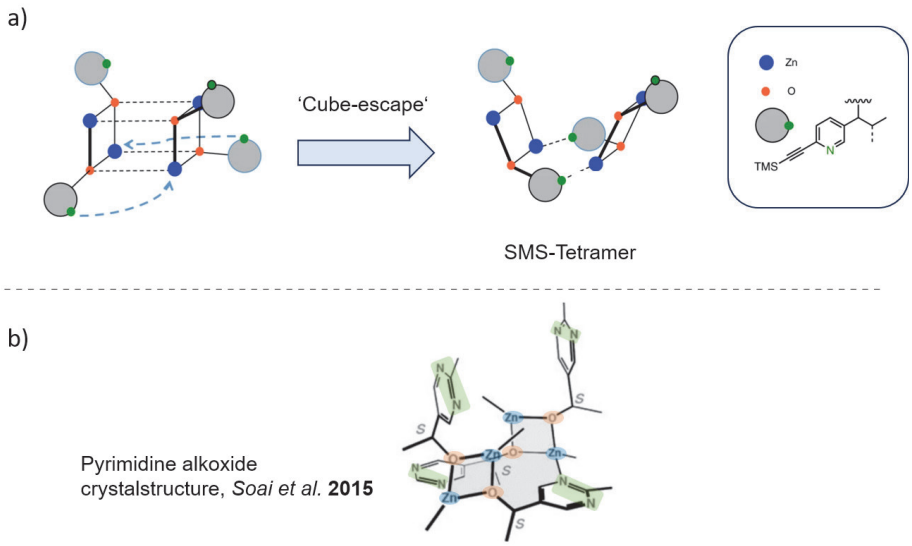

Figure 3.8: Catalytic active assume tetrameric SMS-structure; a) cube-escape model; b) crystal structure of the pyrimidine alkoxide SMS-tetramer reported to in the Soai reaction.[26,81,91]

Experimentally, tetramers and oligomers could also be detected later in the Soai reaction by *Soai and Co-workers*.[81] The SMS-tetramer composed of two N-coordinated Zn-O square dimers, described by the cube escape model, is therefore not novel (fig.3.8) .[26,79,88] Based on experimental and computational studies, *Denmark et al.* developed a new model based on an autocatalytic pyridine system deviating from the used pyrimidine system in the Soai reaction. In context to the claim of the demystifying of the asymmetric amplification of the autocatalytic Soai reaction, the group showed the negligible role of the second N-atom in various catalyst-substrate experiments.[26] According to *Denmark et al.*, the new pyridine system is in great agreement with the Soai system, comprising a sigmoidal reaction profile, an increased catalytic rate for the homochiral autocatalyst, autocatalytic absence with diethylzinc or the missing tri isopropyl silyl substituent and an inversed rate profile regarding temperature.[26] In further investigation, the group suggested a floor-to-floor binding model of the transition state of the addition of $i\mathrm{Pr}_2\mathrm{Zn}$ and the homochiral tetramer **26** based on DFT calculations. As a catalytically active species, a Zn-O tetramer **26** is proposed in which two bonds are replaced by an aromatic pyridine linker (fig. 3.9). This allows a two-point bonding of the aldehyde substrate in spatially defined floor-to-floor spacing to unsaturated Zn atoms (see transition state **27**). The resulting spatially

restricted complex allows only selective alkyl transfer, yielding homochiral product alkoxide (fig. 3.9). The large asymmetric amplification arises due to a thermodynamic favoring and a kinetic inhibition of the homochiral tetramer over the meso tetramer **26**. The catalytic cycle completes with the dissociation of the alkoxide **25** and a resembling into the tetramer.[26,91]

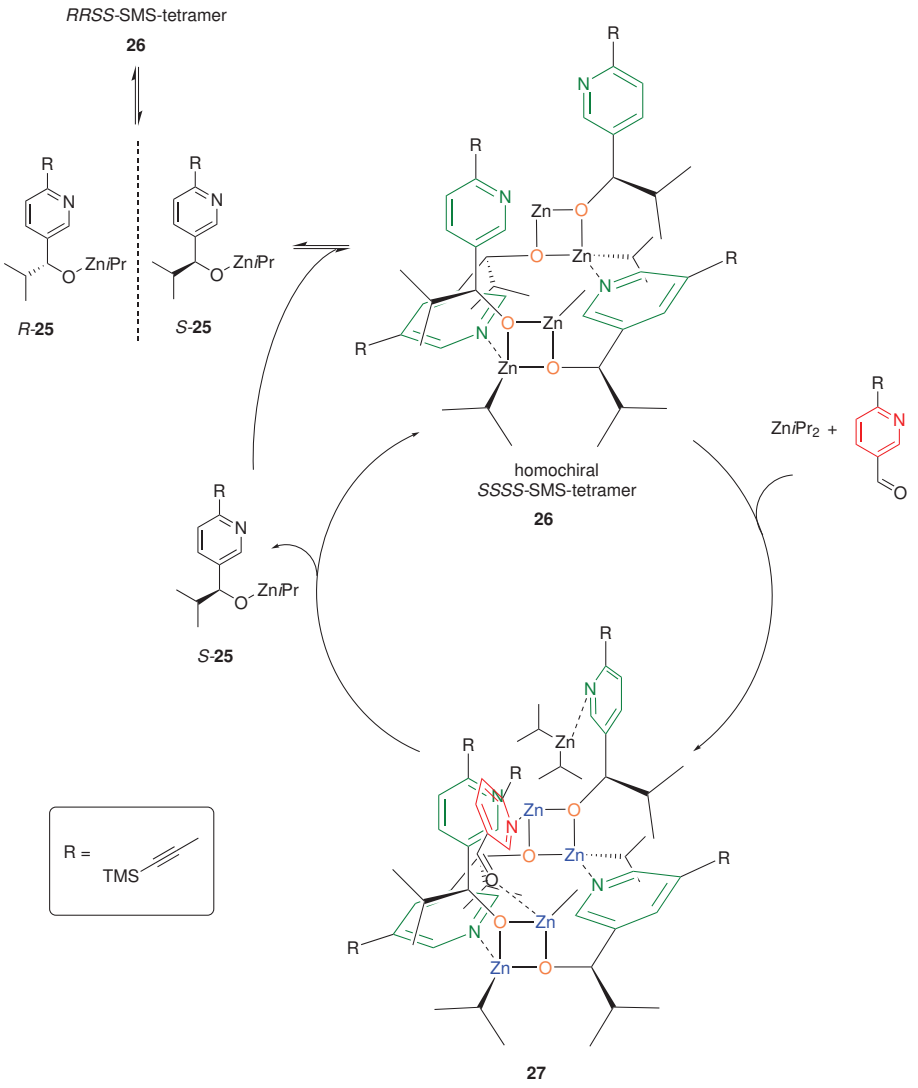

Figure 3.9: Catalytic cycle comprising catalytic active homochiral tetramer **26** according to Denmark et al. displaying exemplary the formation of the *S*-enantiomer.[26,90]

In a following research report, *Denmark et al.* presented consistent structural insight into

the assumed floor-to-floor model in additional mixed catalyst-substrate experiments as well as kinetic simulations.[91] Accordingly, the solubility of the alkynyl substituent, for example, plays a role in catalyst formation and selective reactivity. In comparative studies with a fluorine-substituted nicotinaldehyde derivative, dependencies between catalyst performance and Lewis basicity were found. A lower Lewis basicity thus eliminates inhibition effects and is suggested to explain the superior performance in the Soai reaction due to the low Lewis basicity of the pyrimidine nitrogen.[91] In the same year, the research group around *O. Trapp* published a completely different mechanistic approach which also presents a valid solution in kinetic calculations and mass spectroscopic investigations on the original reactions system that is consistent with all phenomenons of the Soai reaction.[76]

Hemiacetal-model according to *O. Trapp et al.*

As previously mentioned *Trapp and Co-workers* were also involved in mechanistic investigations to elucidate the mechanism behind the Soai reaction. A flow-injection method with a multiplexing HPLC[92,93] was chosen to study the reactions kinetic.[76] This method allows the monitoring of the reaction course by flow-injection analysis in which the reactant and product enantiomers are separated from each other (fig. 3.10).[76,94] By changing the solvent of the mobile phase from THF to IPA, isopropyl hemiacetals could be characterized during the separation of the reaction mixture.[76] Additional, to experimental investigations with FIA-HPLC-MS, simulations for the Blackmond-model and the Soai-model were performed with special computer software using the Runge-Kutta algorithm simultaneously. The simulation tool is able to calculate the temporal concentration and selectivity profiles of the Soai reaction and the dependence of product selectivity and maximum reaction rate on the *ee* of the catalyst based on experimental investigations of the addition of $Zn(i\mathrm{Pr})_2$ to pyrimidine. The results of the simulations for the literature-known models lead in part to strongly deviating values, compared with the values determined experimentally, and suggest vulnerabilities of the postulated mechanisms by *Blackmond* and *Soai*.[95] Furthermore, the prolonged induction phase or the temperature dependence[65] with respect to the kinetics remained unexplained by the previously described mechanisms.[75,76]

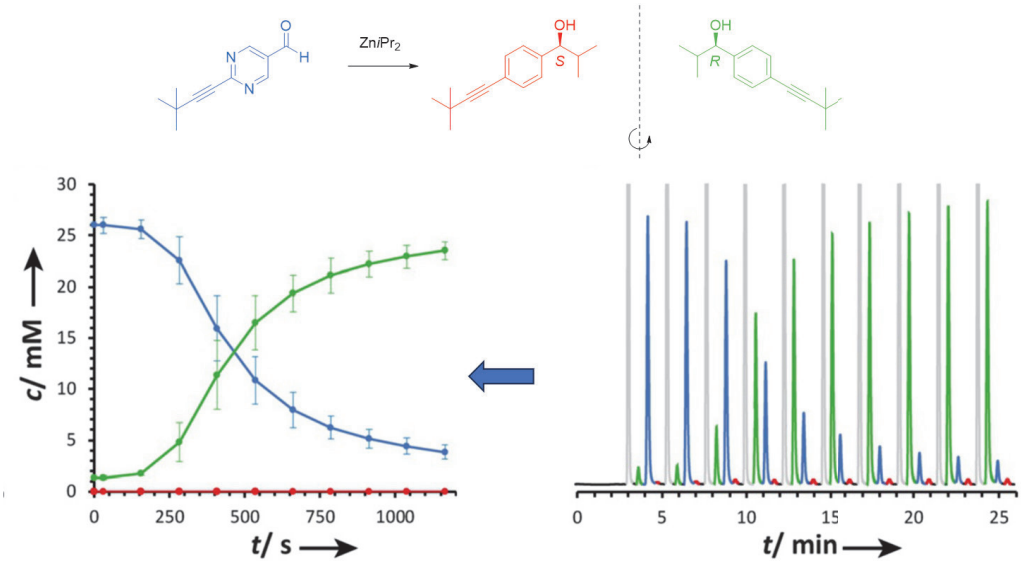

Figure 3.10: Separation of educt (blue) and product enantiomers (red,green) *via* flow-injection by chiral HPLC resulting in the concentration vs. time plot displaying the reaction course; modified figure published in O. Trapp et al., *Chem. Eur. J.* **2020**, *26*, 15871.[76]

Even the simultaneous mechanism proposed by *Denmark et al.* which offers an explanation, is not based on the original system so a transfer of the mechanism to the original Soai system does not necessarily apply.[26,90,91] Due to the demand for further mechanistic studies, the research continued and placed the observed hemiacetal species in the focus of interest. Thermodynamic and kinetic data obtained from DHPLC and temperature dependent ^{1}H NMR spectroscopic studies suggest a favoring of hemiacetal formation at low temperatures, which is related to the observed acceleration in the Soai reaction at a decreased temperature.[76] The kinetics obtained in the formation of the hemiacetals is also consistent with the observed induction phase.[76] *Trapp et al.*, therefore, assume that a catalytically active Zn-hemiacetal complex transient catalyst is responsible for the autocatalytic conversion of the pyrimidine aldehyde derivative in the Soai reaction. As in previously presented models, a statistically distributed homo- and hetero-dimer formation of the zinc alkoxylate molecules is also assumed, but in addition to the formation of the catalytic active hemiacetal, resulting from pyrimidine aldehyde and zinc organyl (fig. 3.11). First simulations of a simplified hemiacetal model were able to predict the experimentally obtained *ee* and is close to the experimentally obtained values, concerning the maximum reaction rate.[95] The final proof of a sophisticated mechanism succeeded in subsequent

studies of *Trapp et al.*. Based on the previous observation, the kinetic studies using FIA-HPLC were optimized with regard to undesired side reactions, and it was possible to make qualitative statements about the influence of different reaction components. An increase in the reaction rate at high initial concentrations of aldehyde and in an attenuated form, the same for the catalytic amounts of alcohol was observed.

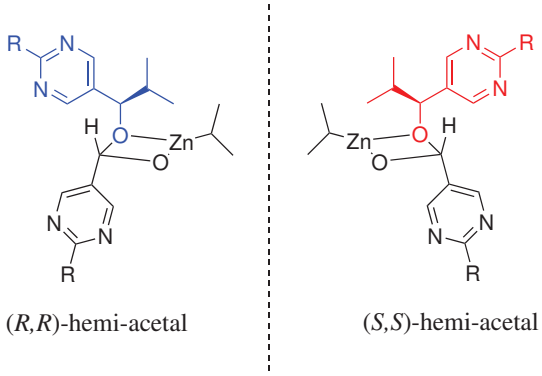

Figure 3.11: Catalytically active substrate attached hemiacetal intermediate in the postulated mechanism elucidated by *Trapp et al.*[76].

As a breakthrough success, the ZnO_2 dimers, as well as the postulated hemiacetals, various intermediate modifications, and the educts, could be detected by in situ high-resolution mass spectroscopic reaction tracking at the Orbitrap MS whereby the missing puzzle pieces of the participating intermediates in the catalytic cycle were identified.[76] The new insights supported by DFT calculations led to the elaboration of the mechanism for the Soai reaction based on the formation of hemiacetal structures, according to which homo- and heterochiral dimers are initially formed by the formation of zinc alcoholate (fig. 3.12).[76] In addition to this formation, a simultaneous reaction between the zinc alcoholate and the aldehyde is also possible, resulting in the zinc complexed catalytically active hemiacetals (fig. 3.11). In further progress, another aldehyde is bound, and the alkyl is transferred. This formation leads to the creation of new stereo centers, which in turn creates a distinct chiral environment and a specific deposition of the substrate molecules used. Thus, increased enantioselectivity can be observed in the following catalytic cycles (fig. 3.12).[76] The experimentally obtained kinetic profiles for the postulated mechanism were evaluated by different kinetic models that are implemented in a software program capable of calculating kinetic reaction profiles by solving the corresponding differential

equations by a Runge-Kutta algorithm. The calculated kinetics were compared to the experimental data sets and are found to be in agreement.[76]

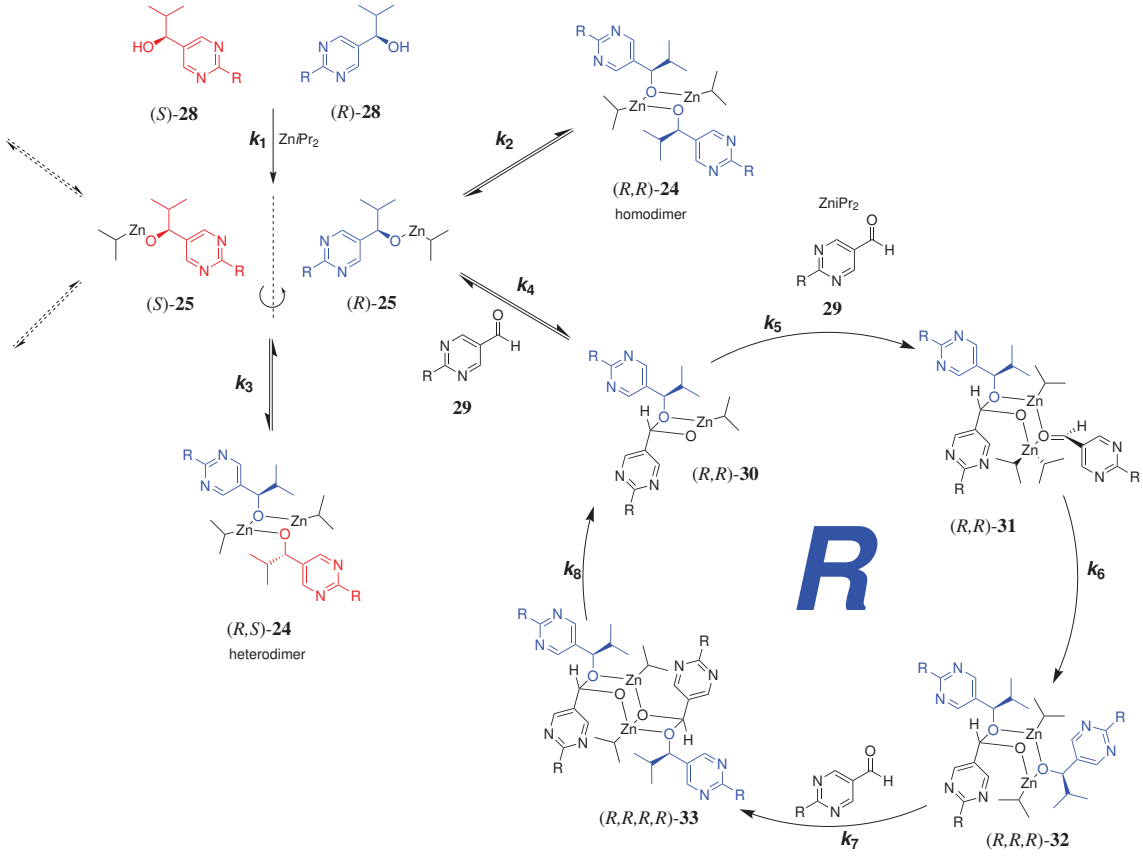

Figure 3.12: Postulated hemiacetal mechanism according to *Trapp et al.*[76]

Further simulation experiments based on the suggested mechanism were also consistent with the observed prolonged induction period achieving correct predictions. In addition to that, *Trapp et al.* proved that correlation experimentally in doping experiments with the predicted transient hemiacetal catalyst. The induction period thus was observed to be decreased by 55 s in a monitored reaction doped with transient catalyst (fig. 3.13). The elucidation of the mechanism of the Soai reaction leads to new perspectives on applying acquired knowledge. Since the system of the Soai reaction with its both autocatalytic and self-amplifying properties is still unique, it is of great interest to develop similar systems. The following work will deal with the synthesis of potential novel systems comprising

autocatalytic behavior based on the recently proven hemiacetal mechanism by *Trapp et al.*.[76]

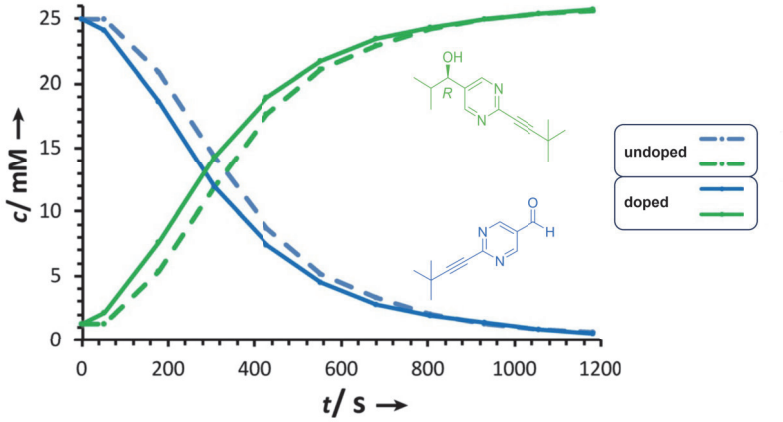

Figure 3.13: Decreased induction period in doping experiments with transient catalyst in a monitored reaction course; modified figure published in O. Trapp et al., *Chem. Eur. J.* **2020**, *26*, 15871.[76].

3.2 Research Objective

The understanding of the mechanism behind the Soai reaction opens up the possibility for new catalyst designs based on the structural insights of the catalytically active hemiacetal species observed as a transient catalyst. In dynamic covalent chemistry, the use of a hemiacetal formation between aldehydes and alcohols is known. The reversible formation and possible thermodynamic stabilization by metal complexation or the kinetic effect of neighbor group participation is a useful and regularly applied tool in this field of chemistry.[96,97] Especially, regulated dual reactivity controlled by ring-chain tautomerism attracted attention regarding this work. Ring chain-tautomerism is a commonly known phenomenon for compounds comprising one or more carbonyl groups together with an alcohol moiety in organic chemistry. The intramolecular forming of dynamic covalent bonds results in an equilibrium between an open carbonyl moiety and a cyclic hemiacetal.[97]

On the basis of these given prerequisites, this chapter is directed towards the synthesis and characterization of potentially novel dynamic biaryl ligands for the Soai reaction. The target structures are atropisomers bearing chiral information and possessing an aldehyde group within spatial distance to an alcohol moiety that allows cyclic hemiacetal formation. In summary, a structure is described that exists in a dynamic equilibrium between an open-chain aldehyde and cyclic hemiacetal and thus provides the prerequisites to serve as a substrate as well as a potential ligand in a Soai-like reaction (see 3.14, grey box). The ring closure to the hemiacetal motif leads to the formation of a newly formed stereocenter at the α-carbon atom. A system capable of reversible dynamic conversion of an aldehyde to a hemiacetal, providing stereo information, could comprise catalytic activity immediately at the beginning of a Zn-mediated alkylation reaction. An induction period, which would occur in autocatalysis due to the initial progress of the formation of the catalytically active product, as in the case of the Soai reaction, would thus be bypassed. The presence of a shifted equilibrium towards the open aldehyde form is an important requirement for the realization of such a concept since the cyclic closed hemiacetal itself can not participate in the reaction, due to a lack of the aldehyde moiety. The following chapter is divided into two parts dealing with the synthesis and subsequent analysis of potential dynamic structures with the structural motif described above. The first part deals with coumestan-based systems and the second part with classical biaryl structures. The analysis of the

structures with regard to their equilibrium and ligating properties decide on their suitable use in catalytic test reactions, which are subsequently discussed with regard to the obtained results.

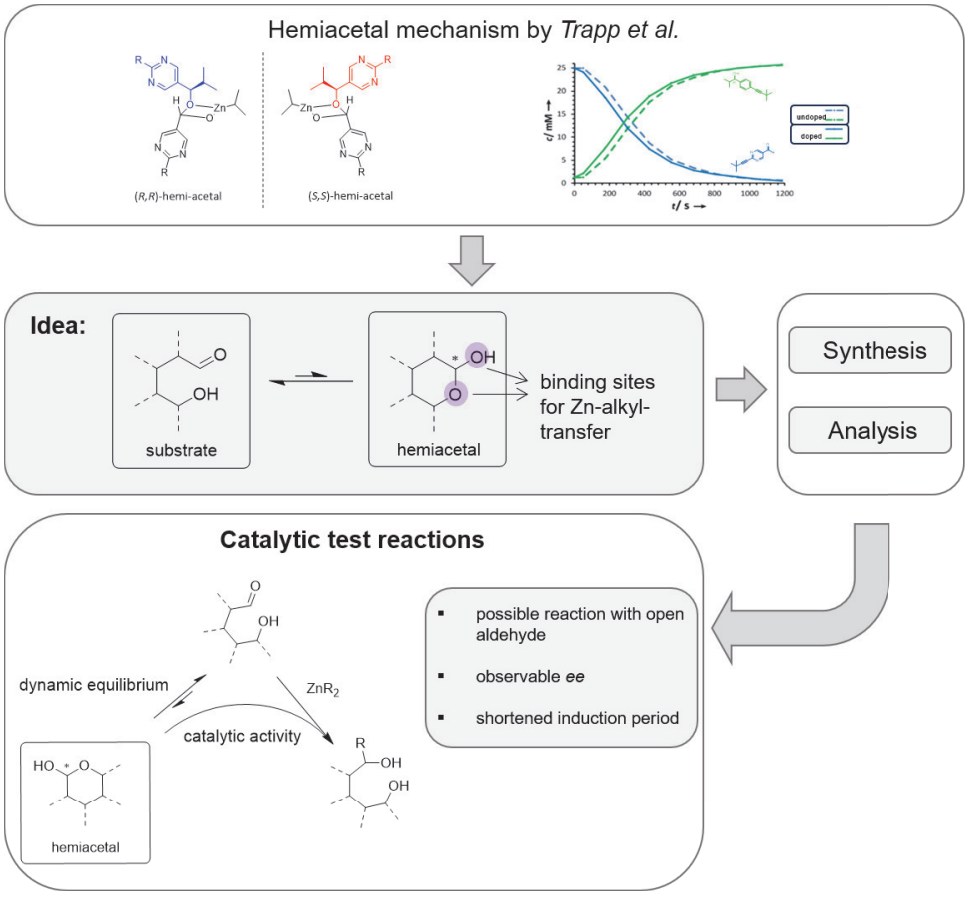

Figure 3.14: Schematic concept towards autocatalytic aldehyde substrates in dynamic equilibrium to a hemiacetal in context to the elucidated hemiacetal mechanism in the Soai reaction by *Trapp et al.*[76]

3.3 Results and Discussion

3.3.1 Coumestan-based Hemiacetal Ligands

In 2016, *Tang et al.* made an interesting discovery when investigating a new synthetic pathway to coumestan structures that are known to provide a broad range of biological activity.[98] Coumestans belong to the natural substance class of coumarins and consist of a pyrone ring that is attached to a benzene ring and a benzofurane ring on the other side.[99] Depending on the derivative, they can exhibit antibacterial, antiviral, antifungal, or estrogen activity.[100–103] *Tang and Co-workers* described a two-step reaction process *via* 2,3-bis(2-methoxyphenyl)-3-oxopropanals to the coumestan end products, in which a ring-chain tautomerization of an intermediate was observed. The intermediate was reported to be arylbenzo[b]furans, which exists in a temperature-dependent equilibrium between the open-chain aldehyde and the closed lactol form. Reported NMR studies revealed that by heating the system to >50°C, only the opened aldehyde form is present (see fig. 3.15).[98]

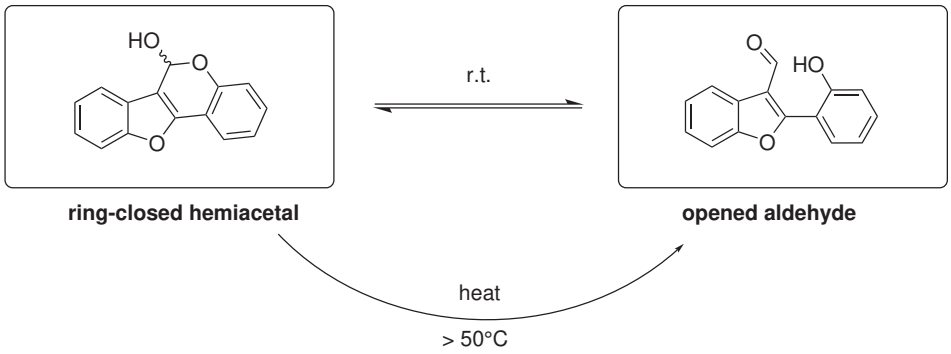

Figure 3.15: Structure motif for arylbenzo[b]furans; modified figure according to *Tang et al.*.[98]

In regard to the hemiacetal-based catalytic mechanism in the Soai reaction described above, various derivatives of this structural motif should be synthesized on the basis of the reported synthesis procedure to study the equilibrium and find a potential substrate that is suitable for an autocatalytic application. Especially, the possibility of controlling the equilibrium *via* temperature changes promised a good starting point.
The first part of the synthesis pathway was the preparation of α, β-epoxyketones in accordance with *Ruan et al.*[104] with varying residues at the 4'-position of the phenyl units resulting in eight different compounds. The commercially available starting materi-

als were converted in an aldol condensation reaction followed by epoxidation to obtain α, β-epoxyketones in moderate to good yields (see tab. 3.1).

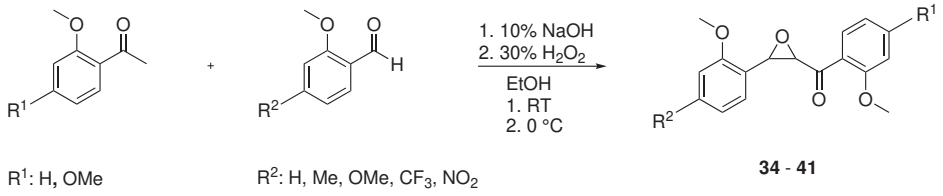

Figure 3.16: Synthesis of α, β-epoxyketones according to *Ruan et al.*.[104]

Compound	R^1	R^2	Yield [%]
34	H	H	80
35	H	Me	33
36	H	OMe	67
37	H	CF_3	77
38	H	NO_2	28
39	OMe	H	73
40	OMe	Me	11
41	OMe	OMe	46

Table 3.1: Summarized yields of the synthesis of α, β-epoxyketones.

In the second synthesis step, the α, β-epoxyketones **34-40** were converted to β-ketoaldehydes, which serve as precursors for the target compounds. The optimized synthesis according to *Mathew et al.*[105] and *Ruan et al.*[104] proceeds in a Meinwald rearrangement induced by the ring opening of the epoxide by the Lewis acid BF_3. The synthesis products **42-49** could be obtained mainly in the enol form, which is in a strongly shifted equilibrium to the minor β-ketoaldehyde product tautomer. Due to a large number of structurally extremely similar by-products, proper column chromatographic purification was not possible for the products **47**, **48**, and **49**. The significant signal for the predominant enol species was nevertheless evident and confirmed the successful synthesis of these attempts. All other products were obtained in moderate to satisfactory yields after successful purification (tab. 3.2).

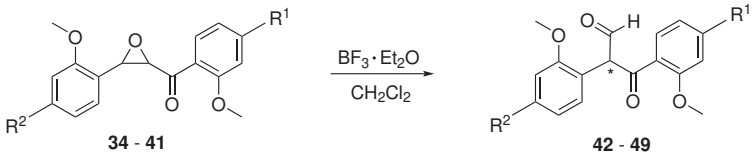

R1: H, OMe
R2: H, Me, OMe, CF_3, NO_2

Figure 3.17: Synthesis of β-ketoaldehydes in an optimized way in accordance with *Ruan et al.* and *Mathew et al.*.[104,105]

Compound	R^1	R^2	Yield [%]
42	H	H	61
43	H	Me	33
44	H	OMe	47
45	H	CF_3	41
46	H	NO_2	28
47	OMe	H	58[a]
48	OMe	Me	42[a]
49	OMe	OMe	38[a]

Table 3.2: Summarized yields of the synthesis of β-ketoaldehydes; [a] referes to crude product.

Bicarbonyls, like β-ketoaldehydes in this case, are generally known to exist in equilibrium with their enol form.[106] The discussed coumestan precursor structures are 1,3-dicarbonyls with substituted aryl residues in the 2'- and 3'- positions. This results in nine possible tautomeric forms in equilibrium with each other. If the structure contains a ketone and an aldehyde moiety (fig. 3.18; keto form I, green), the bonds around the C2 atom are freely rotatable and a chiral center is present, but its enantiomers cannot be distinguished by NMR spectroscopy without additional additives. The situation is different for the various enol forms, which can be formed either by a new double bond between C1 and C2 (fig. 3.18; *cis*-enol $II^{(**)}$, red) or one between C2 and C3 (fig. 3.18; *cis*-enol $III^{(*)}$, blue) and subsequent proton transfer. The bonds are now no longer freely rotatable, but a distinction can be reached between *cis*- and *trans*-isomers. Depending on the orientation of the substituted aryl residues, four different isomers per different enol form (fig. 3.18; enol $II^{(**)}$ and

enol III$^{(*)}$, red and blue) are possible. With the presence of all nine ^{1}H NMR spectroscopically distinguishable forms, characterization would be extremely challenging. Contrary to the presented β-ketoaldehyde products described in the literature[98,104] an extremely shifted equilibrium towards the *cis*-enols III* and II** was found. NMR analyses revealed almost exclusive evidence for this *cis*-enol form, which is easily distinguished from the other tautomers by its extremely downfield shifted signals. Depending on the substituent, the conversion between the two *cis*-enol forms III* and II** is faster or slower so that a broad signal or a signal split is seen (fig. 3.19). The dominant enol signal is also clearly visible for substances for which purification and NMR spectroscopic full characterization were not possible (fig. 3.20). The enolic proton is surrounded by two carbonyls and thus assumed to be hydrogen bond stabilized. Significant downfield shifted signal values, like 15.28 ppm for **47** up to 15.55 ppm for **47** are also known in the literature for this type of enols.[107] In 1989, *Gilli et al.* proposed a resonance-assisted hydrogen bonding model in the enol form of β-diketones related to acetylacetone (acac) based on quantum mechanical calculations, crystal structure analysis, NMR and IR spectroscopic results.[107] A remarkably strong hydrogen bonding of the enols was found, which according to the results is correlated with the delocalized π-system of the six-membered ring fragment (acacH). The NMR spectroscopic study of the β-ketoaldehyde coumestan precursors **42**-**49**, confirms the stability of this fragment through the dominance of the hydrogen bond-stabilized enol forms. However, in the case of complete electron delocalization and resonance in the six-membered ring, no signal splittings would be visible, since the protons of II and III* would not be distinguishable. The discussed observation is therefore only partially consistent with the model postulated by *Gilli et al.*, which is not at least due to asymmetry caused by the different residues in the substances **42**-**49** compared to the symmetrical acacH fragment. Especially compounds **44** and **45** with substituents providing a strong inductive electron-withdrawing effect show a clear splitting of the enol signal. Electron withdrawing groups lower the electron density in the phenyl unit and increase the asymmetry around the 1,3-dicarbonyl motif. In this case, as revealed by crystal structures for symmetric β-dicarbonyls, the enolic proton is not centered between the two carbonyls.[108] The stability of the hydrogen bond-stabilized enols in the tautomeric equilibrium was further studied in a time-dependent manner.

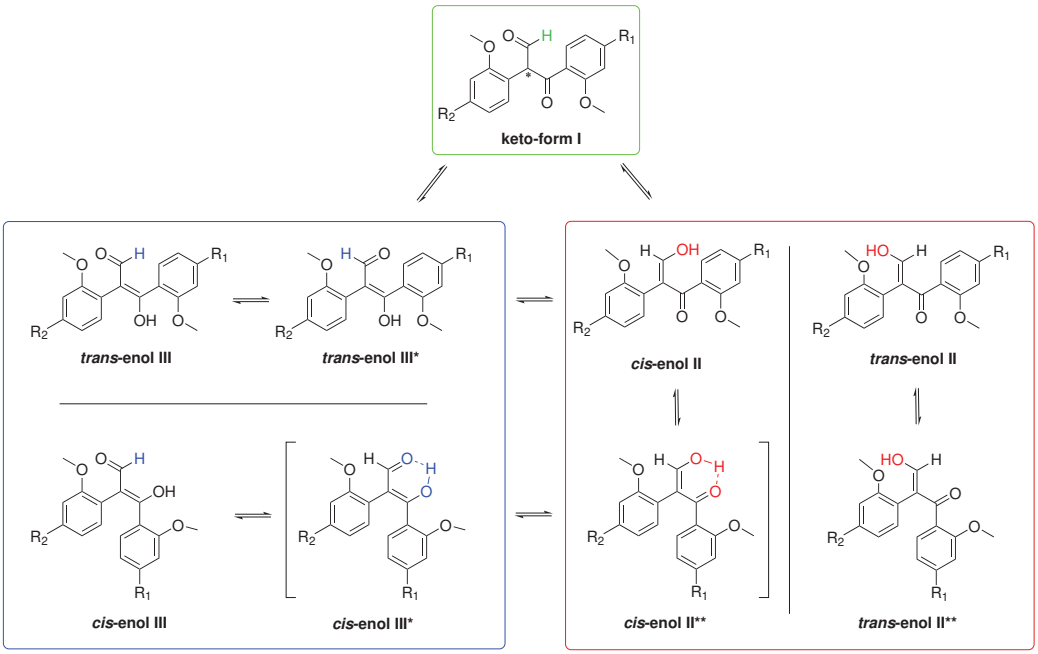

Figure 3.18: Potential structures caused by tautomerism and *cis-* /*trans-* isomerization: keto-form I (green), enol-aldehyde III (blue), enol-ketone II (red).

Compound	Ratio 1d	Ratio 3d	Ratio 5d	Ratio 7d
42	100[a] : 13 : 3 : 2	100[a] : 6 : 9	100[a] : 6 : 2[*]	100[a] : 5 : 1
43	100[a] : 8 : 11	100[a] : 7 : 3	100[a] : 7 : 6	100[a] : 6 : 3
45	100[a] : 7 : 20 : 10	100[a] : 6 : 14 : 2	100[a] : 4 : 3 : 1	100[a] : 4 : 3 : 1[*]
46	100[a] : 6 : 10 : 4	100[a] : 3 : 1[*]	-[**]	-[**]
47	100[a] : 21	100[a] : 1 : 15 : 2	100[a] : 1 : 13 : 4	100[a] : 14 : 2

Table 3.3: Summarized ratios of the tautomeric equilibrium in time-dependent ^{1}H NMR studies in 2 d cycles, wherein the enol signal is set 100% compared to further observed dominant signals in the aldehyde range; [a] integrated enol signal set 100%; [*] multiple further signals in aldehyde range (integrated $\leq$ 1%);[**] assumed decomposition occured.

The analysis only includes all purified β-ketoaldehydes **42**, **47**, **45**, **43** and **46**, since the enol stability of II** and III* was measured on the basis of their relative proportion to the significant signals of the other tautomeric forms. The proportion was determined in ^{1}H NMR spectroscopic measurements *via* integral determination of the enol and aldehyde signals (tab. 3.3; see Appendix 7.1.1 for ^{1}H NMR spectra).

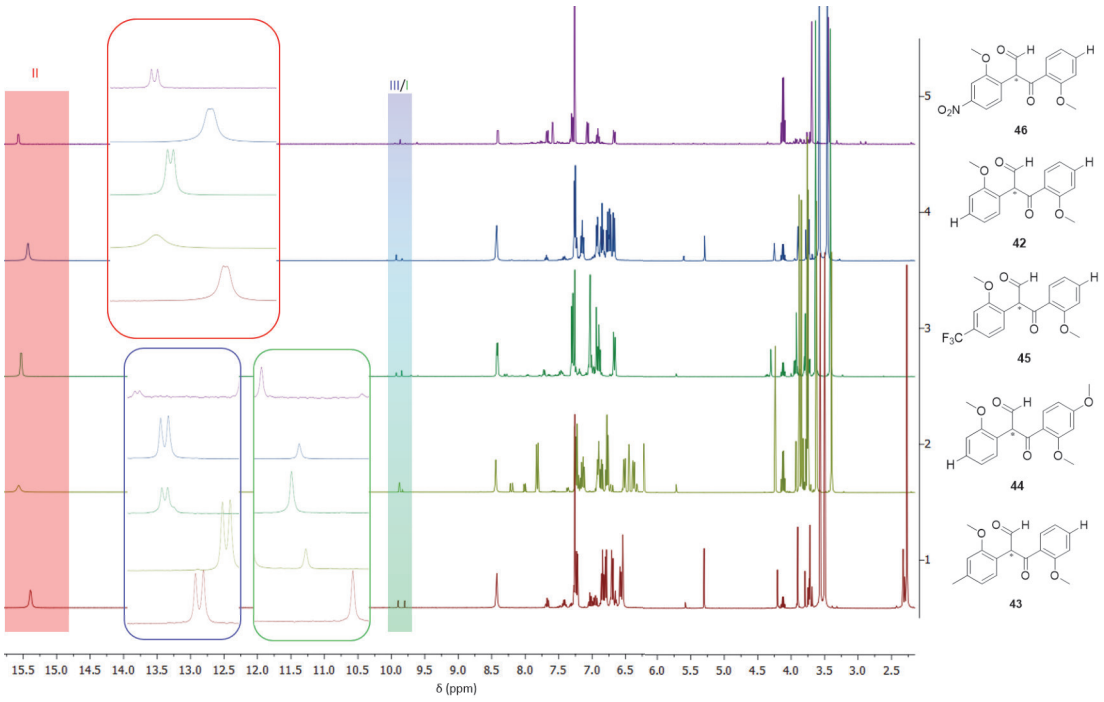

Figure 3.19: Overview of ^{1}H-NMR spectra of purified β-ketoaldehydes **42**-**46**; stabilized enol main species II**/III* (red); aldehyde enol form III (blue, except *cis*-enol III*); keto form I (green); remark: zoomed views of specific signals are not proportional.

All five compounds were measured in two-day cycles with a maximum of seven days after which the equilibrium remains in equal ratios. Due to the comparatively low intensities of the different side species I and III, only the stabilized enol form *cis*-II** or respectively *cis*-III* could be clearly assigned and characterized (fig. 3.19, 3.20; red). For all five substances, two signals in the aldehyde range are still clearly recognizable and can be integrated (fig. 3.19, 3.20; green and blue). One signal splits and is therefore assigned to enol III (blue). The keto form I (green) is assumed for the remaining predominant single aldehyde signal. In some measurements, additional signals are present which were also integrated partly into the summarized table 3.3 if integration was possible due to their low intensity. An exception is the substance **46** which shows clearly more signals in the aldehyde region from the beginning. Although stabilization of the enol with respect to the integral ratios can be observed on day three, decomposition in the NMR was observed on day five. In compounds **42** and **47**, an additional non-assignable aldehyde signal is observed on day one that vanishes in the measurements afterward (tab. 3.3). The signal

is suggested for structure *trans*-III$^{(*)}$. For the compounds **43** and **45** no remarkable additional signals are observable. The trends of the ratios for these two compounds imply a conversion from species I over III to II. In summary, all of the structures showed an extraordinary stabilization of the enol tautomer II** and III* over time at room temperature.

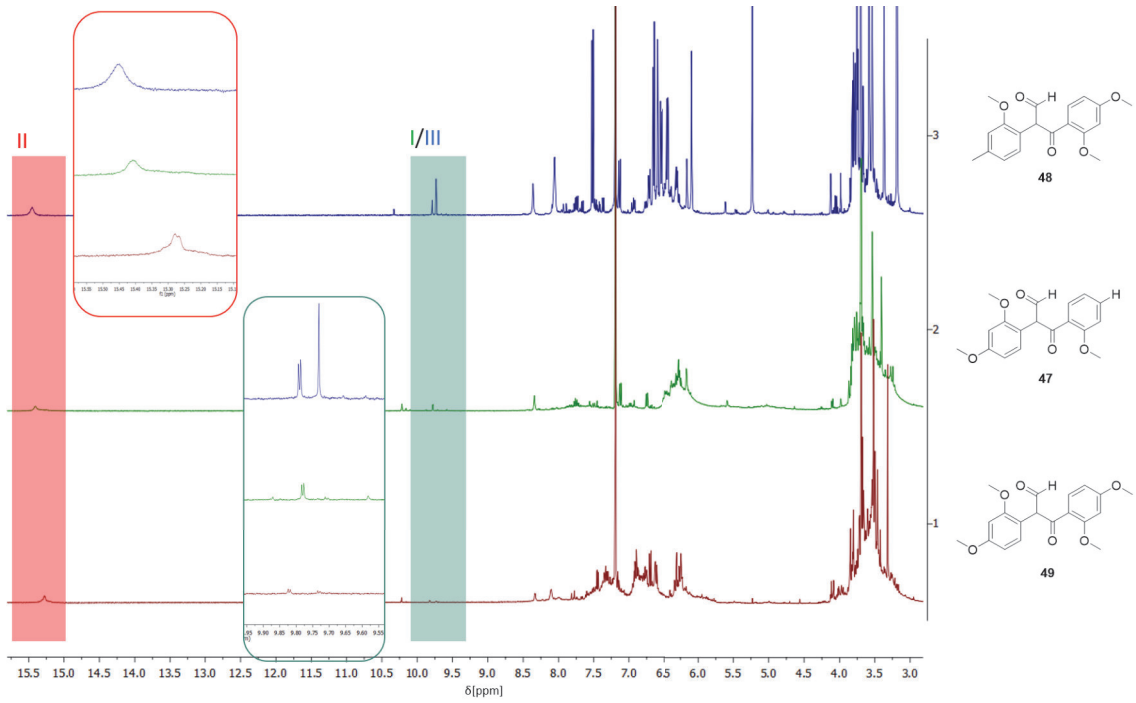

Figure 3.20: Overview of ^{1}H-NMR spectra of unpurified β-ketoaldehydes **47-49**; stabilized enol-ketone main species II (red); enol-aldehyde form III (blue); keto form I (green); remark: zoomed views of specific signals are not proportional.

The two compounds with the highest (**42**) and lowest enol proportions (**47**) after reaching an equilibrium were subjected to exemplary temperature experiments (fig. 3.22, 3.21). Thereby, compound **42** was heated up to 40°C and tracked *via* NMR spectroscopy in eight cycles over 15 minutes while remaining at this temperature (3.21). The analysis did not reveal any changes in the existing ratios of enol or aldehyde signals. Furthermore, no new signals were detected that would have provided an indication of further equilibrium components that had not been detected at room temperature so far. The only minor noticeable change is the decreasing signal splitting of the stabilized enol during increasing time. The higher temperature accelerates the interconversion between the six-membered

ring enol forms *cis*-**42** III* and *cis*-**42** II**. In a second study, compound **47** was observed in an increasing temperature profile from 0°C up to 30°C. The temperature was increased by 5°C in every hour. Again, no changes in aldehyde or enol ratios could be detected. An extremely clear splitting of the enol signal was achieved by lowering the temperature, which was not recognizable at previous room temperature measurements.

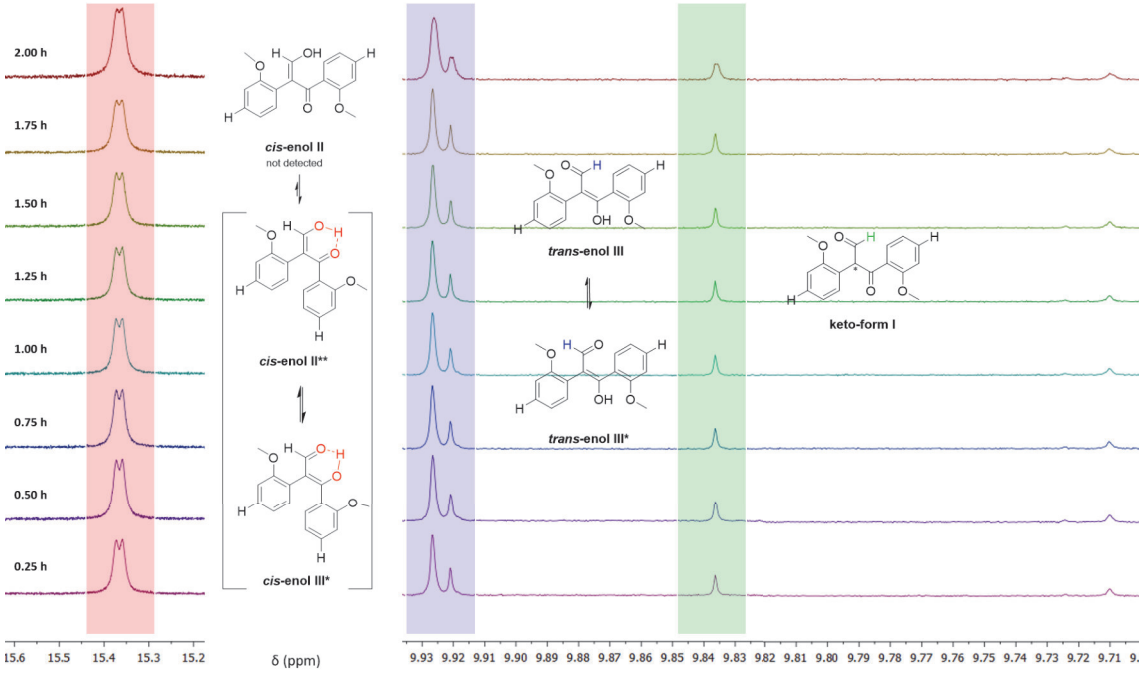

Figure 3.21: Temperature-dependant ^{1}H-NMR spectra of **42** at 40°C in eight 15-minute intervals showing time shifts of enol and aldehyde regions; remark: zoomed signals are not proportional.

Contrary to expectations, the signal splitting also remained after reaching room temperature and values above it. The observed 'memory effect' in **47** probably results from the fixation by means of the formed hydrogen bonds in cis-**47** II** and cis-**47** III*. The interconversion of the two enol forms thus seems to be less temperature-related than following a temporal component. In subsequent longer time-delayed measurements at room temperature, the splitting disappeared again. In addition, a shift of the enol signal towards downfield at lower temperatures was well observable. These expected shifts appear characteristically for hydrogen-bonded protons.[109]

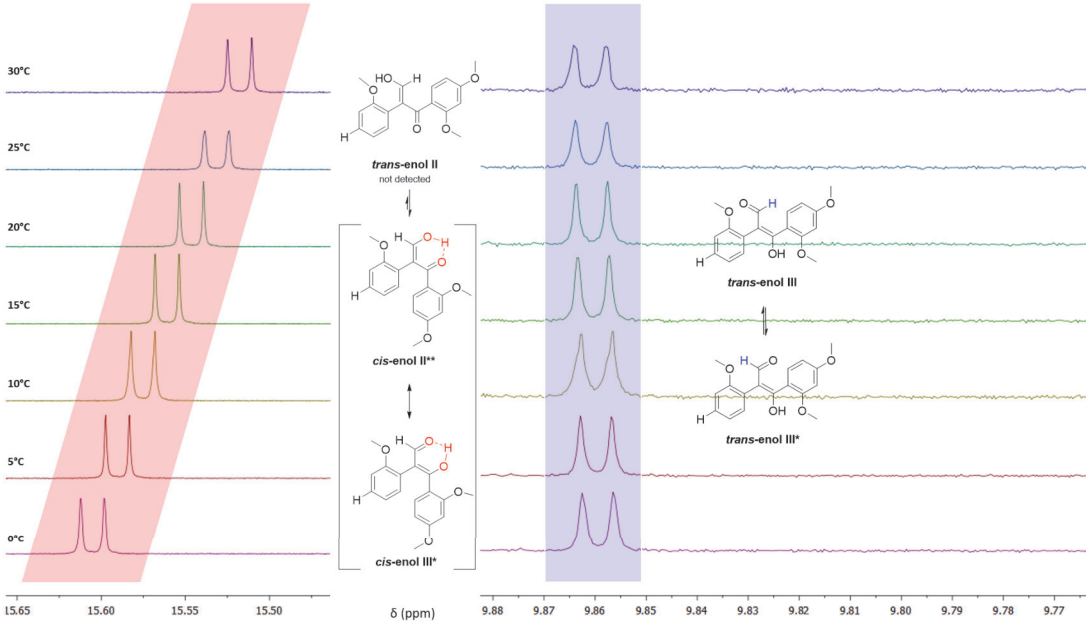

Figure 3.22: Temperature-dependant ^{1}H-NMR spectra of **47** with increasing temperature of 5°C in eight intervals (1 h), showing time shifts of enol and aldehyde regions; remark: zoomed signals are not proportional.

With a longer time frame, at some point, a decomposition process is ongoing for all structures similar to the early decomposition observation for **46** according to NMR analyses. The lack of mention of the dominating enol structures for synthesized coumestan precursors in the literature[98,104] is barely explicable in the context of the presented findings. In the synthesis procedure described by *Mathew et al.*[105] and *Ruan et al.*[104], the methoxy groups in the β-ketoaldehydes are demethylated by the use of BBr_3 and can be cyclized by subsequent attack on the carbonyl groups in an annealing reaction. However, a necessary prerequisite for a reaction according to this mechanism would be the presence of the keto form I of the β-ketoaldehydes used or at least a dynamic equilibrium between the tautomeric forms. Due to the fixation of the proton between the two carbonyl functions and the associated stabilization, it appears difficult to carry out the process according to the previously postulated mechanism. The exemplary attempt to convert **42** to **50** supports this theory. The final product **50** of the reduced coumestan structure could be obtained but in extremely reduced yields of a maximum of 3%, which required enormous amounts of educt to further proceed. ^{1}H NMR measurements in $CDCl_3$ at room temperature revealed that only the ring-opened aldehyde form was present. These findings are again in contrast

to the reported results by *Tang et al.* who described a completely shifted equilibrium only at temperatures above 50°C.[98]

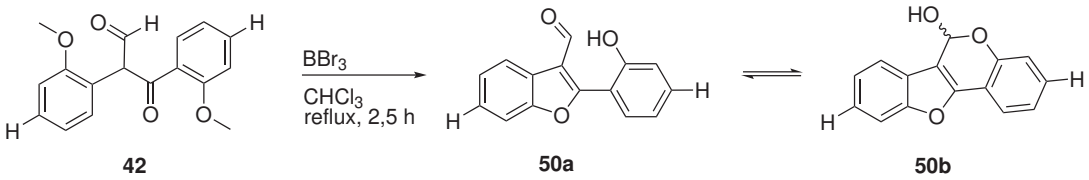

42 **50a** **50b**

Figure 3.23: Synthesis of coumestan-based hemiacetal **50** in an optimized way in accordance to *J. Tang et al.*.[98]

Due to the interrupted synthesis path caused by the unfavorable tautomeric equilibrium and the unfavorable properties of the target structure exemplarily synthesized, this approach will not be pursued further.

3.3.2 Biaryl Hemiacetal Ligands

The second approach for a system in a state of equilibrium between aldehyde and hemiacetal uses a structural motif that is similar in its functionalities. 2-Hydroxy-2-biarylcarbaldehydes with both chemical functionalities in close proximity have the ability to a ring-chain-tautomerism, an intramolecular six-membered ring closure to their respective lactol. Probably the most famous example of ring-chain tautomerism is found in monosaccharides, among a number of other tautomer-forming structural motifs that have been discovered.[110] 2-Hydroxy-2-biarylcarbaldehydes also provide, in addition to the structural possibility of ring closure, just like the reduced coumestan form, a chiral axis. The biarly structure offers in general a wide variety of possibilities that were stated in literature. In the open-chain aldehyde form, the biaryls can be *tropos* or *atropos*, depending on the substituents that affect the rotation around the central σ-bond.[111–113] In addition, the biaryl structure enables the formation of naphthyl moieties or cyclic bridging structures.[114,115] As in the previous section, the combination of alcohol and aldehyde units allows a potential intramolecular ring closure in the formation of a new stereocenter. *Bringmann and Co-workers* gained insight into these 2-hydroxy-2-biarylcarbaldehyde compounds as precursor structures while finding a way to an *atrop*-selective preparation of axially chiral biaryls.[116] They earlier suggested them as key intermediates in the *atrop*-selective ring-opening of lactones.[117,118]

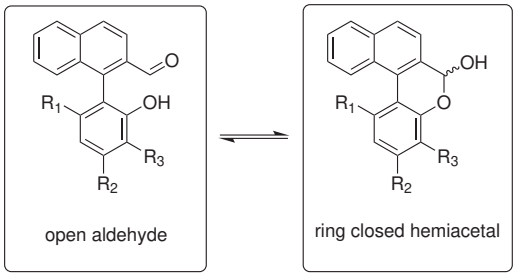

Figure 3.24: Reported dynamic structure motif according to *Bringmann and Co-workers*.[119]

The described equilibria between opened aldehyde and closed lactol hemiacetal of substituted 1-(2-hydroxyphenyl)naphthalene-2-carbaldehydes were reported as strongly dependent on their attached substituents.[118,119] A complete shift of equilibrium to the open-chain aldehyde was found in the case of an *ortho*-aligned substituent (fig.3.24; R_1) to the chiral axis. In the absence of an *ortho*-substituent (R_1) and thus unhindered axis alignment, the lactol form was predominant.[119] This section describes the path to the synthesis of 2-hydroxy-2-biarylcarbaldehydes with the aim of studying equilibrium influences between the possible *atrop*-isomers and their corresponding intramolecular ring closed hemiacetal enantiomers. The motif should be adapted with further substituents and also include heterocycles (fig. 3.25). Large parts of the following summary of results have already been published by *S. Heitsch, L. C. Mayer, Y. L. Pignot, O. Trapp* in 'Synthesis and stereodynamics of intramolecular hemiacetals in biaryl aldehyde-alcohols', *Chirality*, **2023**; 1-13.[120]

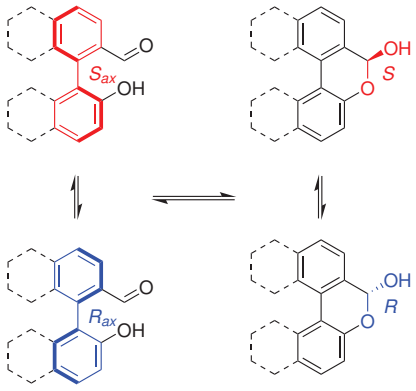

Figure 3.25: Structure motif for biaryl derivatives with potential ring closing undergoing hemiacetal formation.[120]

The simplest obvious structure based on the motif is a simple unsubstituted biaryl backbone. Syntheses by reduction of the corresponding lactone to the shown hemiacetal structure motif can be found in the literature.[121–123] Since the commercial availability of various lactones is relatively large, which would provide easy access to many substrates with this motif in a one-step synthesis, this synthetic route was the first to be considered and investigated. To access the most simple structure of the dynamic motif, 6*H*-benzo[c]chromen-6-one **58** was reduced in a literature-known procedure for lactones to its corresponding lactols.[121,123] The reduction experiments were based on reported procedures and were further optimized to gain access to the reduced lactol form **59b** (tab. 3.4). Since other lactone structures were used as substrates in the literature, the specifications were only used as a reference point and were further optimized.

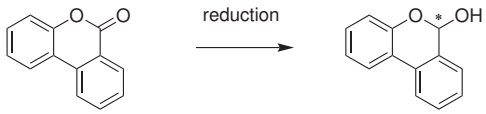

58 **59b**

Figure 3.26: Reduction attempt of unsubstituted biaryl lactone.

Reducing Agent	**Solvent**	**Time**	**Temperature [°C]**	**Product**
DIBAL-H	Toluene	20 min	-20	diol
DIBAL-H	THF	10 min	-20	diol
DIBAL-H	THF	20 min	-60	diol
DIBAL-H	Toluene	20 min	-70	diol
DIBAL-H	Toluene	10 min	-70	diol
$NaBH_4$	THF	1 h	-20	educt
$NaBH_4$	THF	3 h	-20	educt
$NaBH_4$	EtOH	3 h	-10	educt
$NaBH_4$	MeOH	1 d	r.t.	educt
$NaBH_4$	THF	1 d	r.t.	educt

Table 3.4: Reduction attemps of 6*H*-benzo[c]chromen-6-one **58** to corresponding potential dynamic lactol 6*H*-dibenzo[b,d]pyran-6-ol **59**.

In common practice, many reductions of lactones using DIBAL-H to corresponding lactols are successfully described.[121] Unfortunately, this could not be confirmed for the desired biaryl structure **59b** in various trials. A shortened reaction time, temperature reduction, and solvent variation all resulted in the further reduced diol form, where a ring opening occurs at the heterocycle. In this case, the milder reducing agent $NaBH_4$ was used in order to capture the product at the first reduction stage. In further various trials, the desired product could not be obtained in this way either. In contrast to the first attempts with DIBAL-H, $NaBH_4$ appeared to be too weak as a reducing agent for the biaryl lactone. After increasing the temperature and the reaction time, only the educt was detected in five different reaction approaches in THF and MeOH. After the initially failed reduction attempts, a second route was developed using C-C Suzuki couplings, which also offers commercially available starting materials and thus makes substrates achievable in a one-step synthesis (fig.3.27). As a standard, the cross-coupling was tested and optimized under various conditions, after which the first test in THF was successful with a moderate yield. The best results were obtained in a solvent mixture of THF, MeOH, and water at 70°C, with a yield of 65% (tab. 3.5, Entry 6).

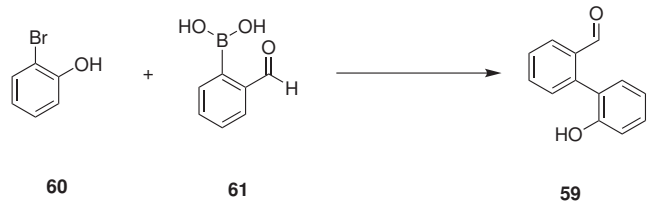

60 **61** **59**

Figure 3.27: Synthesis pathway for **59**.

Entry	**Solvent**	**Catalyst**	**Base**	**Yield** [%]
1	THF:EtOH	$Pd(PPh_3)_4$	K_2CO_3	33
2	THF	$Pd(PPh_3)_4$	Na_2CO_3	40
3	THF	$PdCl_2((PPh)_3)_2$	Na_2CO_3	47
4	THF:MeOH	$PdCl_2((PPh)_3)_2$	Na_2CO_3	53
5	THF:H_2O	$PdCl_2((PPh)_3)_2$	Na_2CO_3	58
6	THF: MeOH:H_2O	$PdCl_2((PPh)_3)_2$	Na_2CO_3	65

Table 3.5: Optimization of Suzuki coupling reaction towards **59**

Since the structural motif is generally not described in detail in literature and only a few publications exist that report an equilibrium, the initial observations by *Bringmann et al.*[119] were used as a reference point for further investigations. However, the synthesis pathway was adapted in a different more simple way from *Bringmann et al.*[119] and achieved also *via* a Suzuki coupling yielding **66**. The aldehyde halogenide precursor **64** to be coupled was prepared in a two-step literature-known synthesis process, starting from α-tetralone (fig. 3.28).[124,125] The same synthesis parameters that gave the best results for the unsubstituted biaryl structure resulted in only 35% yield for the *Bringmann* structure (see 3.5, entry 7). By varying the reaction parameters analogous exemplary shown for **59** (see tab.3.5), the yield could be increased to 54% (fig. 3.28). The aldehyde halide precursor **64** was again used for a 2'-position Cl-substituted derivative **65** of the *Bringmann* lactol which was obtained in 81% yield after optimization of the reactions conditions (fig. 3.28).

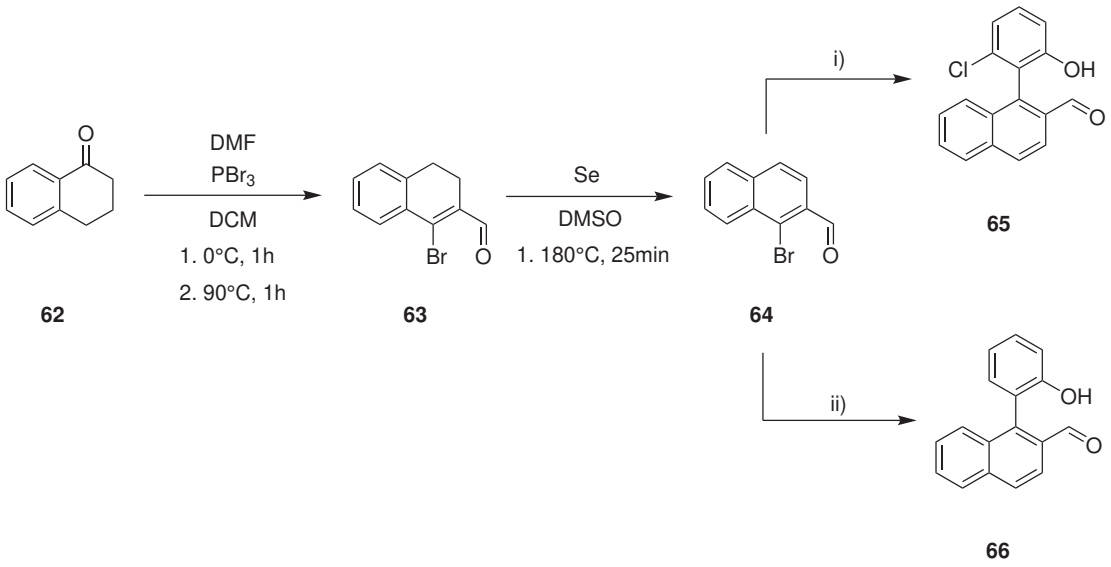

Figure 3.28: Synthesis pathway for **65** and **66**; i) (2-chloro-6-hydroxyphenyl)boronic acid, Na_2CO_3, $Pd(PPh_3)_4$, DME/H_2O, 80°C, 24h; ii) (2-hydroxyphenyl)boronic acid, Na_2CO_3, $Pd(PPh_3)_2Cl_2$, $THF/MeOH/H_2O$, 70°C, 24h;

To compare the dynamically unsubstituted biaryl **59** and the single naphthyl-based backbone structures **66** and **65**, a sterically demanding binaphthalene scaffold **69** as well as a Cl-substituted biaryl **72** should still be realized synthetically. A synthesis route for the binaphthyl derivative **69** is described by *Martinez et al.*.[126]

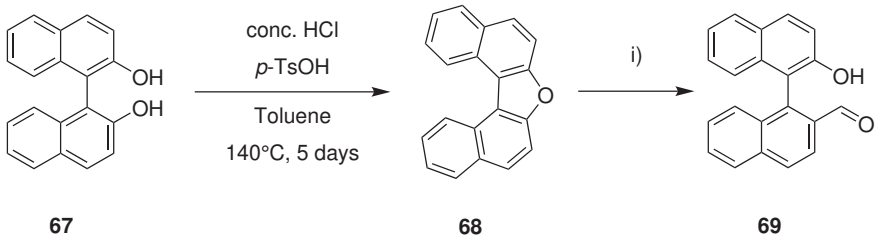

Figure 3.29: Synthesis pathway for **69** according to *Martinez et al.*; i) 1. Et_2O, toluene, Li, 0°C, 24h; 2. DMF, -78°C, 2h; 3. r.t., 15h.[126]

However, there are no references in the publication to an investigation of the dynamics of the hydroxy aldehyde structural motif. The synthesis approach starts from commercially available BINOL **67** that is transferred in a ring-closed furane intermediate **68**. Subsequently, the aldehyde function was introduced by a lithium-mediated ring-opening using dimethylformamide (fig. 3.29). The final product **69** was obtained in satisfactory yields analogous to *Martinez et al.*.[126] NMR spectroscopic analysis in chloroform showed no visible dynamics at room temperature for all four synthesized structures **59**, **66**, **65** and **69**. In the spectrum, either only the open aldehyde or the closed hemiacetal form was present (tab. 3.6; fig. 3.30). Closed hemiacetal form and opened aldehyde form can be easily distinguished by their characteristic signals of the lactol or aldehyde proton in the NMR spectrum (fig. 3.30).

Structure	Aldehyde	Hemiacetal	Ratio Main Specie [%]
59	-	✓	100
66	-	✓	100
65	✓	-	100
69	✓	-	100

Table 3.6: Present species detected *via* NMR spectroscopy in $CDCl_3$ at room temperature.

Bringmann's observation and prediction of a dominant lactol form for the unsubstituted mono naphthalene scaffold **66** could be confirmed ^{1}H NMR spectroscopically in deuterated chloroform.[119] More than that, this form was observed exclusively in the present measurements. For the two synthesis products with sterically more demanding residues and hindered axis rotation **69** and **65**, only the opened aldehyde form was detected. The

unsubstituted biaryl structure **59** with the most freely rotatable axis was present as expected in the form of a hemiacetal. It is interesting to note that the 2'-substitution with Cl in the case of mono-naphthalene structure **65** impairs the rotation around the axis to such an extent that only the aldehyde can be detected compared to the unsubstituted hemiacetal **66**. Equilibrium shifts associated with structural change are typically often strongly dependent on the solvent chosen, as these can stabilize different structural properties in different ways.

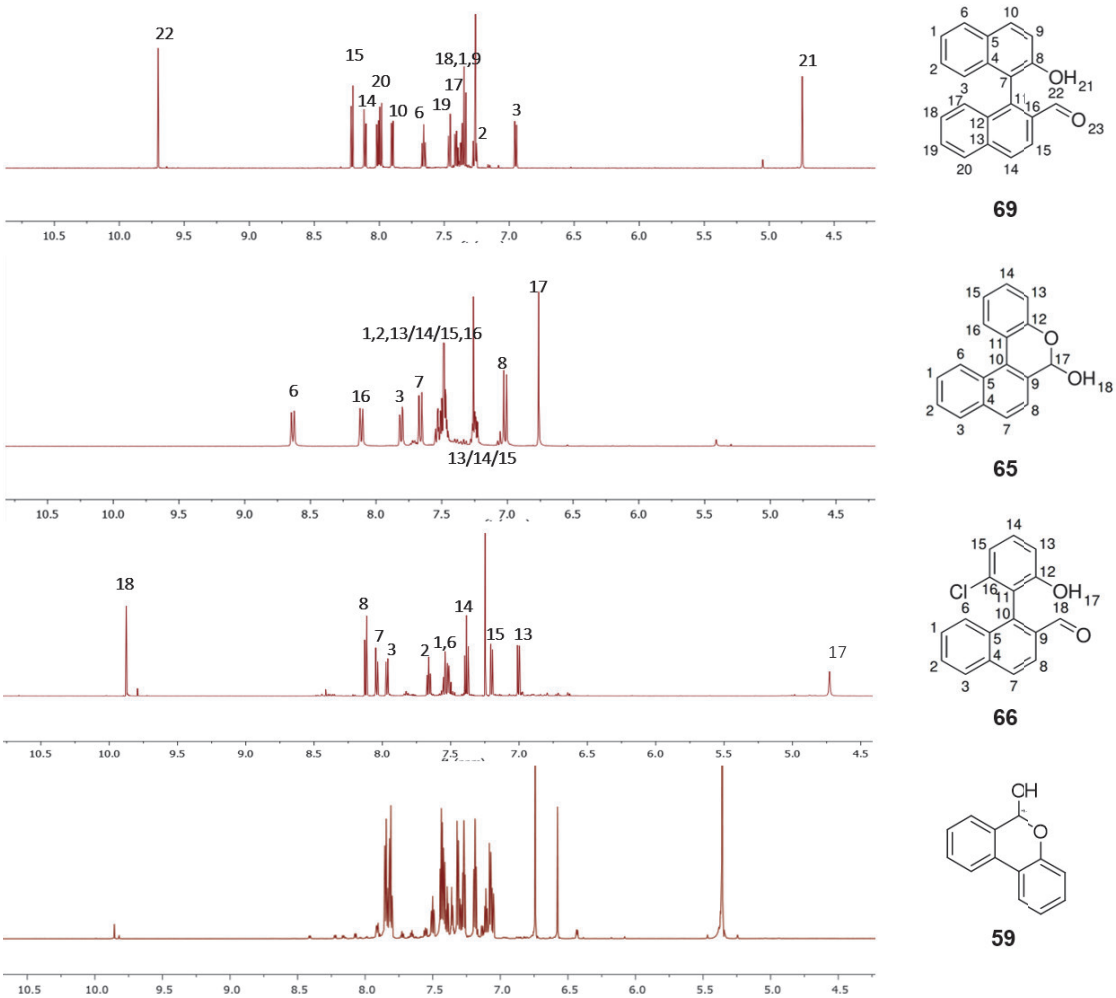

Figure 3.30: ^{1}H-NMR spectra in $CDCl_3$ of **59** to **65** at room temperature; remark: signals for compound **59** are not assigned due to remaining impurities after column chromatography, signals in the aldehyde range are associated with aldehyde educt of **59**.

The solubility and acidity of the solvent can also be decisive for the equilibrium distribution.[119] For this reason, ^{1}H-NMR spectra were recorded for all four compounds **69**, **66**, **65**, and **59** in five additional solvents at room temperature. Potential ratios between open aldehyde (A) and closed hemiacetal (H) were determined by the characteristic proton signals for these functionalities (tab. 3.7). All compounds remained exclusively stable in their favored form as previously detected in $CDCl_3$ independent of the chosen solvent. The result is surprising since some of the deuterated solvents selected show significant differences in their polarity and acidity.

Solvent/Substance	**69**	**66**	**65**	**59**
Acetone-d_6	A	H	A	H
DMSO-d_6	A	H	A	H
THF-d_8	A	H	A	H
DCM-d_2	A	H	A	H
Toluene-d_8	A	H	A	H

Table 3.7: ^{1}H-NMR spectroscopic detected aldehyde (A) and hemiacetal (H) proton signals for synthesized compounds, solely favoring one formation.

Supplementary to the synthesized structures **59**-**69**, it would be interesting to investigate the Cl-substituted biaryl structure to be present exclusively in open aldehyde form or potentially detectable in an equilibrium. Several attempts have been made to access the Cl-substituted biaryl **72** *via* Suzuki coupling. Surprisingly, the coupling did not succeed in various implementations (fig. 3.31, tab. 3.8), since the biaryl **72** was supposed to be sterically less demanding than the corresponding mono naphthalene backbone **65**, which could be synthesized well *via* a Suzuki coupling after optimization. A side reaction of the boronic acid halide with itself, which prevents a successful coupling, would be possible but rather unlikely as the Cl- reactivity is estimated to be lower in comparison to the Br-site. However, since the reaction to the mono naphthalene-based structure was also carried out with the latter and no interfering side reaction was observed, a different reactivity of the halide derivative to be coupled is assumed.

The enantiomers of the four successfully synthesized structures were subsequently analyzed by HPLC-MS and characterized by mass trace (fig. 3.32). All enantiomers could be visibly separated by analytical HPLC. In the course of screening for columns with different chiral selectors and solvent ratios, **69** could also be separated semi-preparatively. The retention

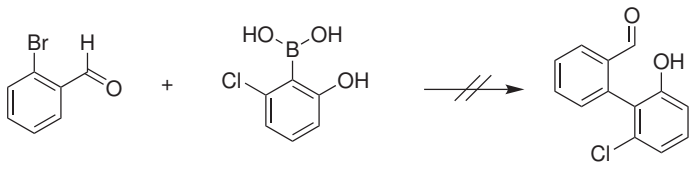

70 **71** **72**

Figure 3.31: Synthesis attempt for compound **72**.

Entry	Solvent	Catalyst	Base	Yield [%]
1	THF:MeOH	$PdCl_2((PPh)_3)_2$	K_2CO_3	-
2	DMF	$Pd(PPh_3)_4$	Na_2CO_3	-
3	THF:EtOH	$PdCl_2((PPh)_3)_2$	CsOH	-
4	THF:EtOH:H_2O	$PdCl_2((PPh)_3)_2$	NEt_3	-
5	THF:EtOH:H_2O	$Pd(PPh_3)_4$	NEt_3	-
5	THF:EtOH:H_2O	$Pd(PPh_3)_4$	NaOH	-
6	DMF	$PdCl_2((PPh)_3)_2$	NEt_3	-
7	THF: MeOH:H_2O	$PdCl_2((PPh)_3)_2$	Na_2CO_3	-
8	THF: MeOH:H_2O	$Pd(PPh_3)_4$	NEt_3	-
9	THF: MeOH:H_2O	$Pd(PPh_3)_4$	NaOH	-
10	DME: MeOH:H_2O	$PdCl_2((PPh)_3)_2$	NaOH	-

Table 3.8: Optimization of Suzuki coupling reaction towards **72**

times of the other enantiomers measured were too close in time on the available semi-preparative columns, so that no preparative separation was possible. Since all compounds are biaryls, the rotation barriers were investigated by dynamic HPLC measurements. At room temperature, no plateau formation was observed for any compound, implying no conversion of one enantiomer into the other. The given set allows measurements up to 80°C depending on the solvent and the respective column used. Even temperatures up to this limit did not result in any observable plateau formation. The barriers for synthesized structures **69**, **66**, **65**, and **59** are thus above what can be determined in the applied setup and can therefore be classified as relatively high. The relatively high barrier for **59** is surprising because of the completely free axis due to no existing substitutes. For the remaining compounds, higher barrier values were rather expected, as the backbone around the axis is sterically quite demanding.

Even though the synthesized structures do not meet the requirement of a dynamically

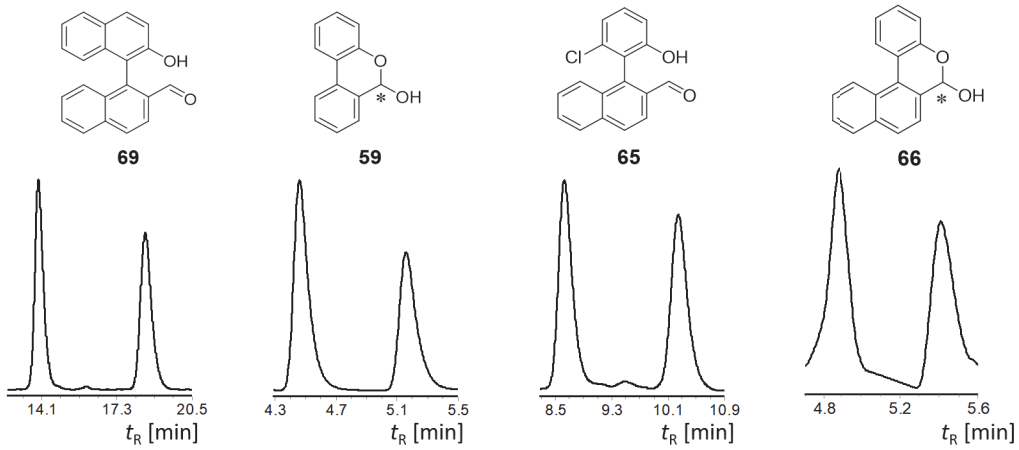

Figure 3.32: Overview of enantiomer separation at room temperature using HPLC (left to right); **69** (CHIRALPAK IC, *n*-hexanes 90: IPA 10); **59** (CHIRALPAK IA, *n*-hexanes 80: IPA 20); **65** (CHIRALPAK IC, *n*-hexanes 80: IPA 20); **66** (CHIRALPAK IC, *n*-hexanes 80: IPA 20) .

distributed equilibrium between hemiacetal and aldehyde, but are completely shifted to one of the two sides, initial catalytic tests are being carried out. The aim is to determine whether the aldehydes of the structural motifs are suitable alkylation substrates without a catalyst at all. An alkylation of benzaldehyde with diethylzinc at room temperature, for example, is not possible without a catalyst.[127] The absence of an initial catalyst is, of course, a prerequisite for an autocatalytic substrate, which would make such a scenario an exclusion criterion for further investigations of this initial structure motif. In order to investigate the alkylation properties of the two open-chain aldehyde structures, test reactions were carried out with three different diorganozinc reagents each in slight excess (1.20 equiv.) in toluene at room temperature. Samples of the test reactions were taken from the reaction solution, quenched, and then prepared in a mini-workup in GC vials for subsequent analysis by HPLC-MS (fig. 3.33). The solvent toluene must be removed after the mini workup, as its UV absorption maximum is at 210 nm which corresponds to the same UV absorption range as the alkylated product. Due to the high signal intensity of toluene, the alkylated product would no longer be detectable or only detectable to a very small extent. The first samples were taken after a reaction time of 6 h and after no product was detectable, extended to 12 h and 24 h (tab. 3.9). By means of HPLC-MS, no conversion was detectable in all cases with the various diorganozinc reagents for any of the aldehyde structures **69** and **65**.

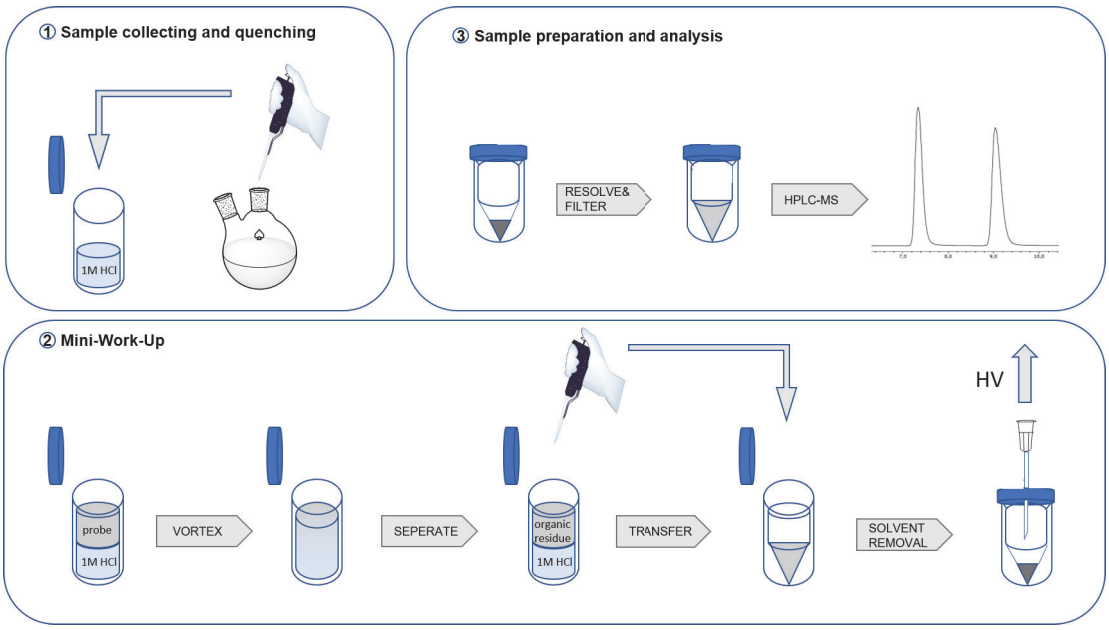

Figure 3.33: Sample preparation of catalytic test reactions with diorganozinc reagents for HPLC-MS analysis.

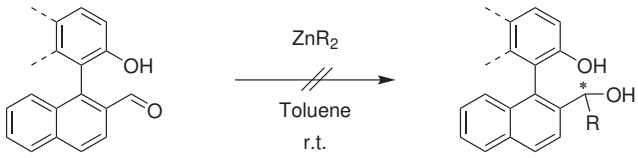

Figure 3.34: Diorganozink alkylation reaction scheme for **69** and **65**

However, traces of the respective products could be detected in the samples taken after 12 h as well as 24 h in a high-resolution mass spectrometer. The reactivity with respect to zinc alkylation reactions thus appears to be too low for those two synthesized structures. The remaining compounds possessing the equilibrium on the hemiacetal side, are not suitable as an alkylation substrate due to lack of an aldehyde moiety. However, the ligand properties of the hemiacetal motifs can be investigated. The fact that benzaldehyde, as already mentioned, does not show an alkylation reaction with diorganozinc reagents at room temperature in toluene and that it is only possible with the aid of a suitable catalyst, makes the substrate an ideal test candidate for the hemiacetal ligands. *Oguni et al.* were able to record the first successes in the alkylation of benzaldehyde with diethylzinc using *L*-leucinol.[17] Since the choice of the zinc reagent is significantly influenced by the substrate and, as in the case of the Soai reaction for example, is limited to only one specific one, tests

Structure	Time	Dimethylzinc	Diethylzinc	Diisopropylzinc
	6h	×	×	×
69	12h	×	×	×
	24h	×	×	×
	6h	×	×	×
65	12h	×	×	×
	24h	×	×	×

Table 3.9: Diorganozink alkylation attempts of **69** and **65**; x = no product detection in HPLC-MS analysis.

should again be carried out with different alkyl residues. Stock solutions of the hemiacetal compounds **66** and **59** were prepared in degassed toluene, which were then added to the reaction vessel charged with degassed toluene and organozinc reagent (1.20 equiv.). The reaction was then started by adding the substrate benzaldehyde. Aliquots were then taken from the test reactions and analyzed by HPLC-MS. Since the enantiomers of the two hemiacetals **66** and **59** could not be separated preparatively with the given resources, they were applied racemically. Spontaneous alignment causing potential enantioselectivity is also not possible due to the high energy barrier at room temperature, as shown by the previous temperature measurements. The focus is therefore rather on observing a successful reaction that can be mediated by the hemiacetal ligand. An enantioselectivity is not expected.

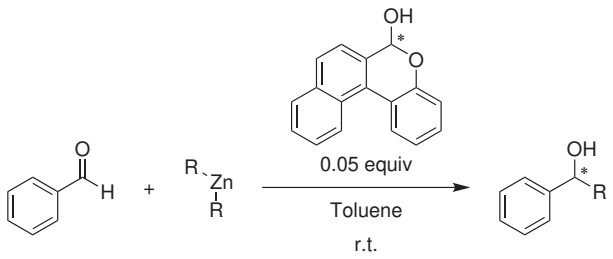

R	Yield [%]	Enantiomeric Ratio
Me	61	50:50
Et	89	49:51
*i*Pr	72	49:51

Table 3.10: Alkylation test reactions with the substrate benzaldehyde for the ligand system **66**.

As expected, the product alcohol was obtained racemic in moderate for dimethylzinc

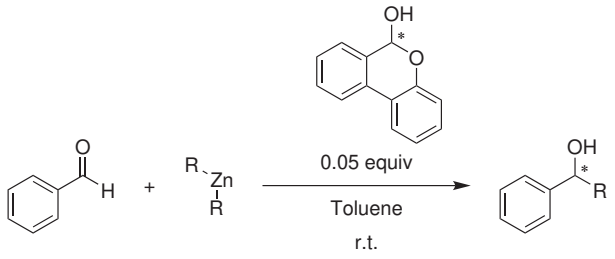

R	Yield [%]	Enantiomeric Ratio
Me	42	52:48
Et	82	49:51
*i*Pr	79	50:50

Table 3.11: Alkylation test reactions with the substrate benzaldehyde for the ligand system **59**.

and good yields for diethylzinc and diisopropylzinc (tab. 3.10 and 3.11). The obtained hemiacetal structures are therefore particularly suitable for the addition of diethylzinc or diisopropylzinc to carbonyl groups with good ligating properties, which can be assumed from the obtained yield.

After the first spectroscopic observations of the presented structures **69**, **66**, **65** and **59**, the idea of forced steric proximity of the aldehyde and alcohol moiety by a modified backbone was pursued in the case of the binaphthyl scaffold **69**. In order to facilitate the equilibrium to a hemiacetal structure and change the reactivity, this approach relies on an electron-repelling backbone to reduce the angle between the functional groups. The phenomenon of dihedral angular narrowing between the aromatic faces is already known for the phosphorus ligand SEGPHOS, which opened up a whole ligand class for transition metal catalysts.[128,129] The initiator for the angle modification are two electron-rich benzodioxole moieties which are part of the biaryl backbone. For the realization of such a system, as successfully implemented for **69**, the methodology of *Martinez et al.*[126] was considered for the decisive step to the final product **77**. The furan **76** required for this purpose was obtained in good yield in a three-step synthesis pathway based on literature-known synthesis procedures starting from sesamol **73** (fig. 3.35).[130,131] The final step after a previously successful method could not be realized for the SEGPHOS-related ligand system **77**.

Due to the low reactivity of the synthesized aldehydes **69** and **65** in initial test reactions

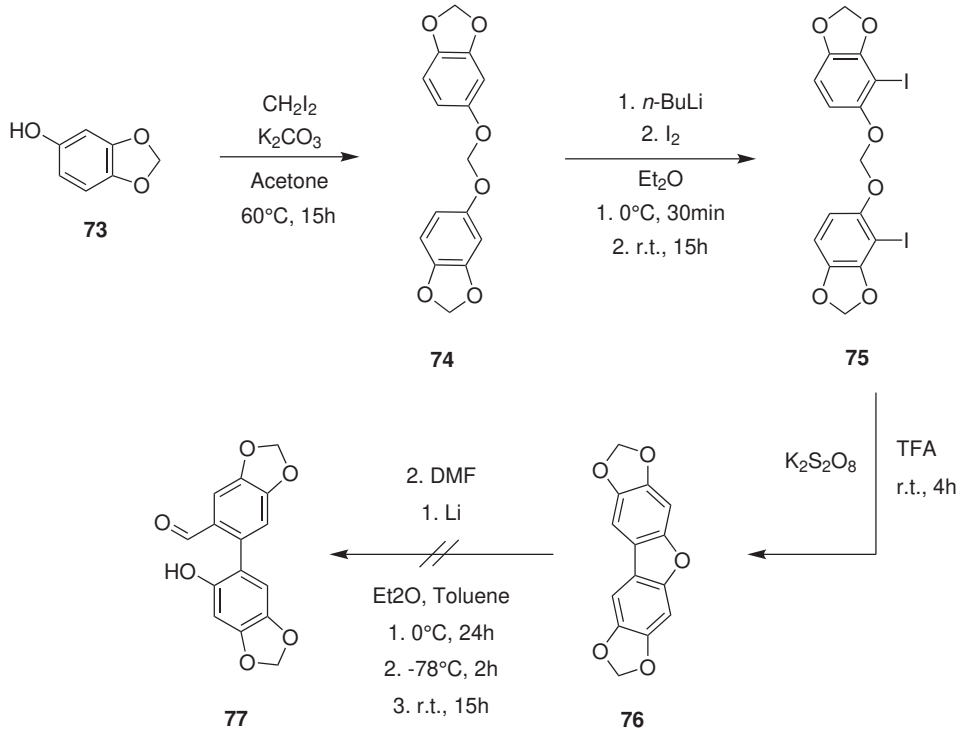

Figure 3.35: Synthesis pathway towards 2-hydroxy-2-biarylcarbaldehyde **77**, with the idea of a SEGPHOS derived backbone[128,129] in partial synthesis procedures according to *Martinez et al.*[126], *Delogu et al.*[131] and *Jeganmohan et al.*[130].

similar to benzaldehyde, the focus of further work will be on heterocyclic compounds with the same structural motif. Compared to benzaldehyde alkylations, a much higher reactivity is known from alkylations with pyridines and pyrimidine derivatives, as shown for the Soai reaction.[26,66] In addition, the comparison of the energetic rotational barrier discovered for the Soai hemiacetal intermediates is thematically relevant and will be investigated. Due to easy accessibility, an attempt was made to prepare four biaryl compounds with a pyridine heterocycle included in the system. The position of the nitrogen atom should be in the *meta* position as known from successful pyridine aldehyde alkylations and unusual in the *ortho* position.

The compounds **78** and **79** were successfully obtained by the proven method of Suzuki coupling. Optimization and adjustment of the synthesis parameters resulted in a maximum yield of 36% for **78** and 68% for **79** (fig. 3.36). In particular, changing the solvent to a mixture of DME, EtOH, and water (2:1:1) resulted in a significant increase of the yields.

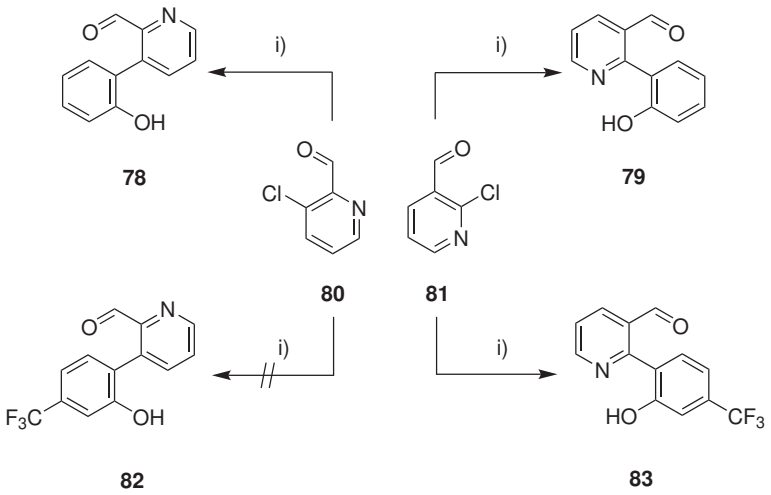

Figure 3.36: Synthesis pathway for **78**, **79** and **83**; i) Na_2CO_3, (2-formylphenyl)boronic acid, $Pd(PPh_3)_2Cl_2$, THF, MeOH, 70°C, 24h.

Compound **78** was for example not realizable in a classic THF/MeOH solvent mixture at all. Under identical reaction conditions, the yields for the nicotinaldehyde-based ligand **79** with the nitrogen at the 4'-position (*meta*-position) in the heterocycle are significantly higher compared to the ligand **78**. In addition to the influence of the position of the hetero atom on the halogen leaving group, a slightly poorer solubility of the halogen educt **80** could also be observed, which is a possible reason for the lower yield. The findings persisted in the further syntheses of both heterocycles with a strongly electron-withdrawing substituent in the *para*-position on the lower alcohol-substituted ring. The synthesis of **83** was carried out with the same parameters as used before resulting in 61% yield. The picoline aldehyde derivative **82**, on the other hand, could not be detected by mass spectroscopy or NMR spectroscopy under the same conditions. Further attempts were performed to obtain the desired structure. In particular, the base, solvent, and catalyst loading were varied. With the bases LiCl and CsOH in DMF, the product could be detected in HR-mass spectrometry but was not detectable NMR spectroscopically after workup and purification. No discernible reason for the failure is apparent, but the reactivity difference between the picolinaldehyde and nicotinaldehyde derivatives is obviously remarkable.

The three successfully synthesized compounds **78**, **79**, and **83** were investigated by ^{1}H NMR spectroscopy, as previously for the other compounds. Different deuterated solvents are also used to study their dependence on a potential equilibrium. In the first measure-

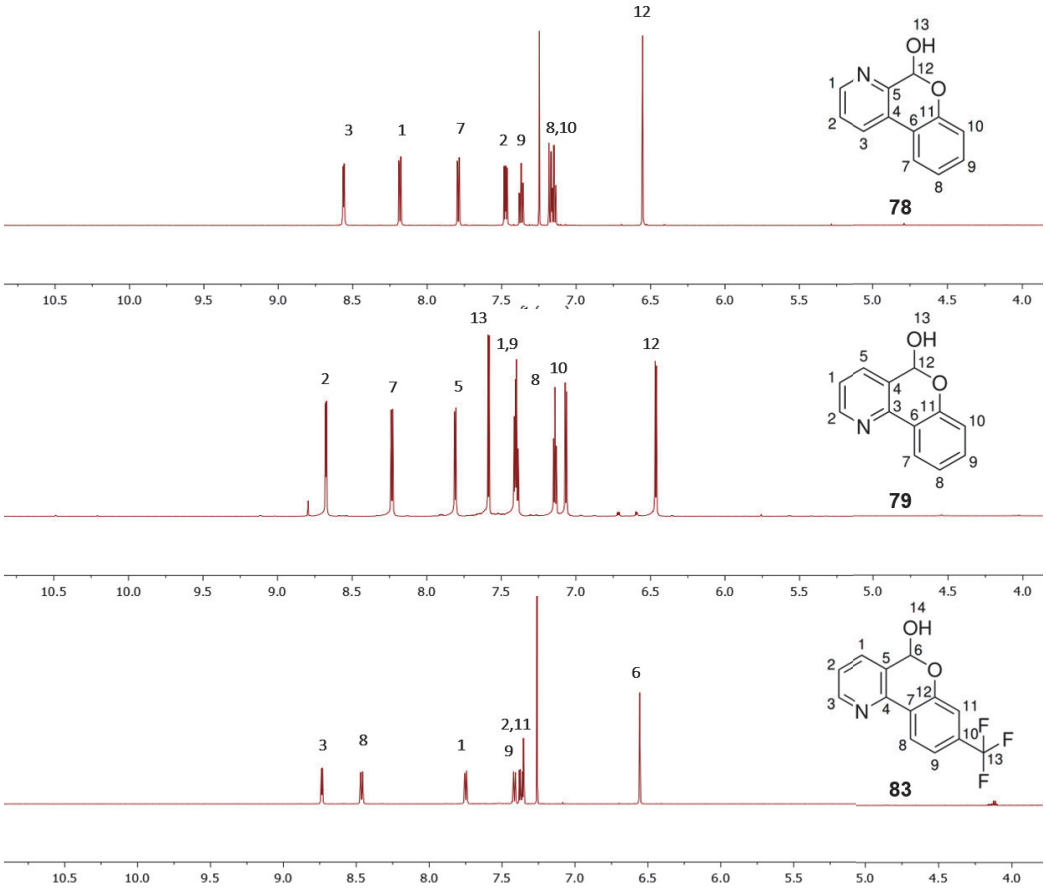

Figure 3.37: ^{1}H-NMR spectra in $CDCl_3$ at room temperature of **66** to **83**.

ments with $CDCl_3$, only the hemiacetal form was observed for all three compounds (fig. 3.37). As before, this trend continued for measurements in other deuterated solvents. The hemiacetal of **78**, **79**, and **83** remained stable and no interconversion to the aldehyde could be detected independent to the used solvent (tab. 3.12).

The nicotinaldehyde derivatives **79** and **83** were separated by analytical HPLC-MS at room temperature (fig. 3.38). In both cases, a plateau formation can be recognized, which demonstrates a conversion at room temperature. The plateau formation of the compound with the trifluoromethyl residue in *para*-position to the axis at the lower ring is more intense. For the picolinaldehyde derivative **78**, only a broad signal can be detected at room temperature. It was immediately apparent that the enantiomeric signals merge into each

Solvent/Substance	78	79	83
$CDCl_3$	H	H	H
Acetone-d_6	H	H	H
DMSO-d_6	H	H	H
THF-d_8	H	H	H
DCM-d_2	H	H	H
Toluene-d_8	H	H	H

Table 3.12: ^{1}H-NMR spectroscopic detected aldehyde (A) and hemiacetal (H) proton signals for synthesized compounds **78**, **79**, and **83**.

other through rapid interconversion[132], since the product could be clearly characterized by NMR analyis. By lowering the temperature in the setup used to a minimum of 0°C, the enantiomeric pair could be visualized without a complete peak coalescence (fig. 3.38). The interconversion at 0°C is nevertheless still remarkably high. The rate constant k_1 was determined to be $4.9{\cdot}10^{-3}$ s^{-1} for compound **78** with a barrier of $\Delta G^{\ddagger} = 78.8$ kJ·mol^{-1}.

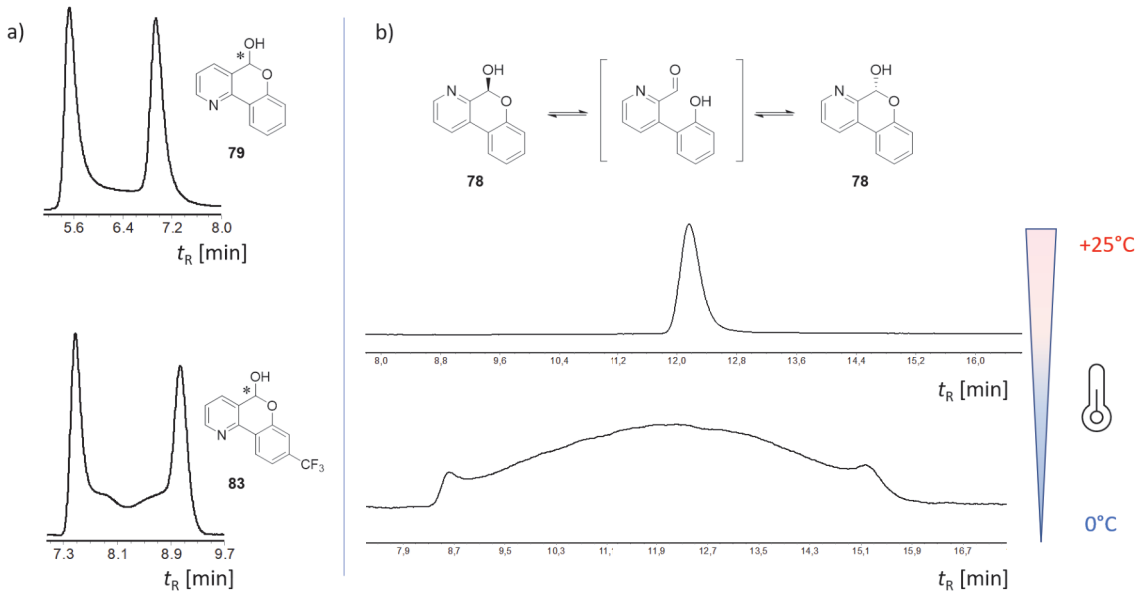

Figure 3.38: Overview of enantiomer separation at room temperature using HPLC; a) room temperature analysis for **79** (CHIRALPAK IA, *n*-hexanes 80 : IPA 20) and **83** (CHIRALPAK IA, *n*-hexanes 95 : IPA 5) ; b) fast interconverting **78** at room temperature and possible visual separation at 0°C (Chiralpak IA, *n*-hexanes 80 : IPA 20)

The setup for dynamic HPLC measurements allows temperature-dependent measurements in a range from 0-80°C. The nicotinaldehyde derivatives **79** and **83** showed conversion at

room temperature and fit perfectly in the feasible range to determine their rotational barrier $\Delta G^{\ddagger}$ and the activation parameters $\Delta H^{\ddagger}$ and $\Delta S^{\ddagger}$ by Eyring-Plot analysis. The temperature measurement series of **79** and **83** show an increase in the plateau between the two enantiomeric peaks during the course of the temperature rise, which converges to a broad peak since at this individual temperature point the interconversion is occurring at such a rapid rate that it is no longer possible to distinguish between the individual enantiomers. The data of these chromatographic peak profiles (fig. 3.39 and 3.40) are applied to the unified equation for dynamic chromatography[133] to produce the enantiomerization rate constants k_1 under usage of the software DCXplorer.[134]

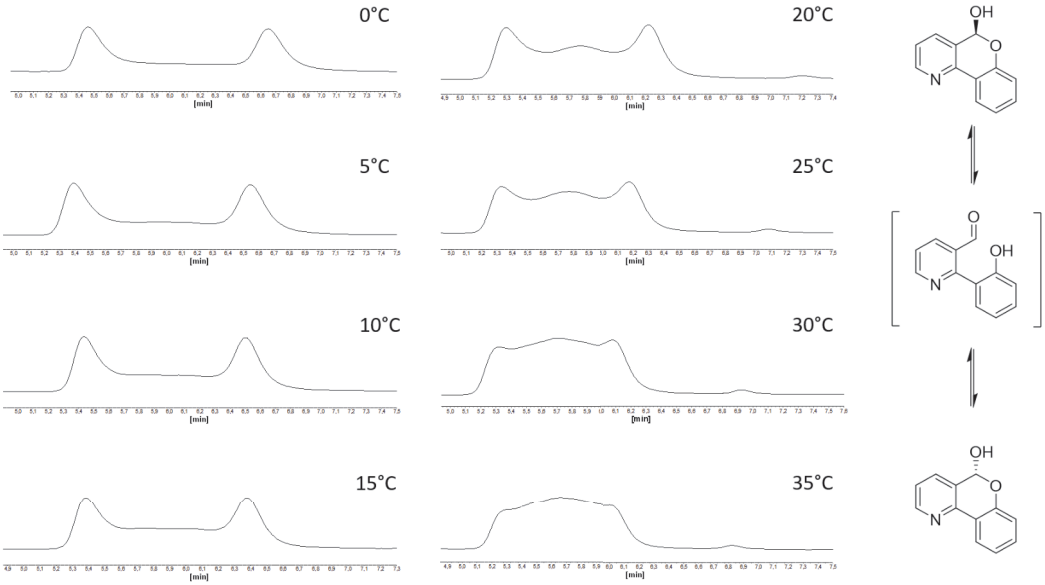

Figure 3.39: Temperature-dependant DHPLC measurement of **79** between 0-35°C; CHIRALPAK IA, *n*-hexanes 75 : IPA 25.

The obtained values for the rate constant k_1 now allow the Eyring plot. With the linear regression of the plot, the interconversion barrier $\Delta G^{\ddagger}$ and the activation parameters $\Delta H^{\ddagger}$, and $\Delta S^{\ddagger}$ were determined (fig. 3.41). For the linear regression, three data sets of each temperature were considered. The Eyring plot of compound **83** resulted in $\Delta G^{\ddagger} = 85.0$ kJ·mol^{-1} for the barrier energy and $\Delta H^{\ddagger} = 33.2 \pm 3$ kJ·mol^{-1} and $\Delta S^{\ddagger} = -174 \pm 96$ kJ·mol^{-1} for the activation parameters in a temperature range between 4 - 40°C. For compound **79** the enantiomerization barrier was determined to be $\Delta G^{\ddagger} = 86.4$ kJ·mol^{-1} and the activation parameters $\Delta H^{\ddagger} = 47.2 \pm 3$ kJ·mol^{-1} and $\Delta S^{\ddagger} = -132 \pm 22$ kJ·mol^{-1} in a temperature range

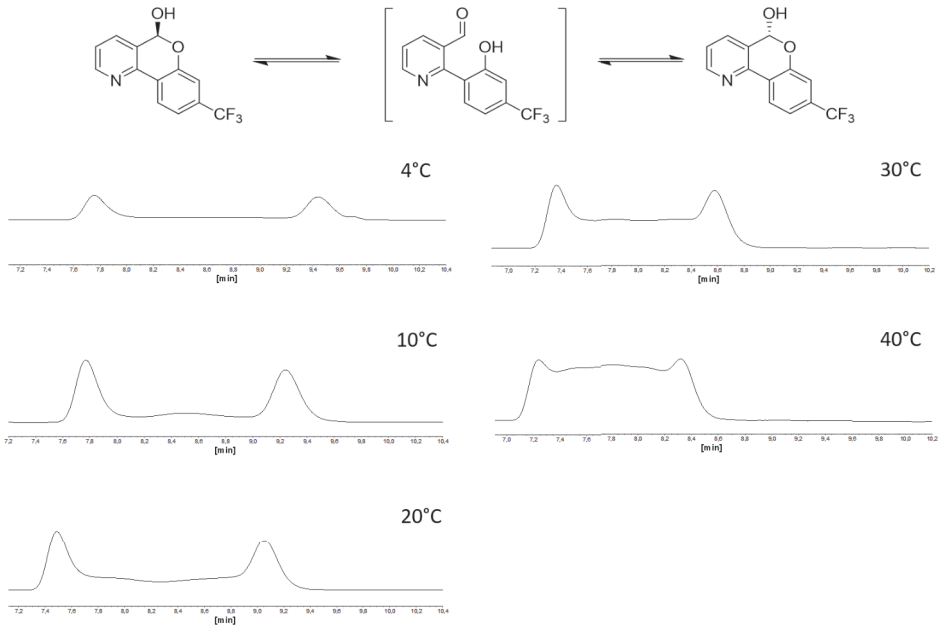

Figure 3.40: Temperature-dependant DHPLC measurement of **83** between 4-40°C; CHIRALPAK IA, *n*-hexanes 90 : IPA 10.

between 0 - 35°C. In comparison to **78** the enantiomerization barrier of **79** is significantly increased with a difference of 4.3 kJ·mol^{-1}. The observation suggests a destabilization of the hemiacetal in the case of N-atom in the *ortho*-position of the corresponding pyridine ring.

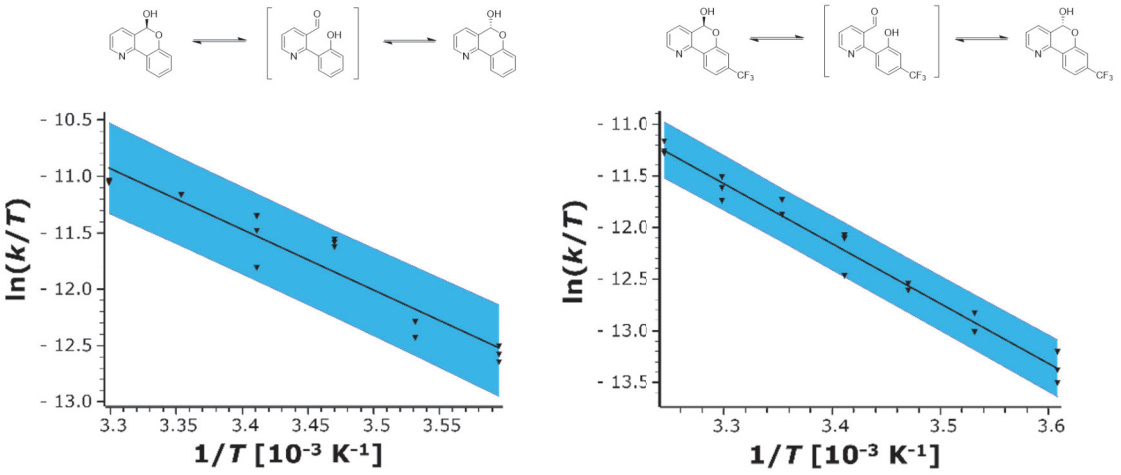

Figure 3.41: Eyring-Plots for compounds **79** (left) and **83** (right).

The measured values for the interconversion barriers of the nicotinaldehyde derivatives **79** and **83** are in agreement with the predicted values of the interconversion-barriers and formation of the transient hemiacetal catalyst in relation to the hemiacetal based mechanism in the Soai reaction proposed by *Trapp et al.*.[75,76]

As previously already described, only the function as a ligand can be tested in catalytic test reactions, since the synthesized structures repeatedly exclusively appeared in the hemiacetal form. For this purpose, alkylation on benzaldehydes with three different alkyl substituents is tested in the same manner. The alkylation reactions proceeded with all three ligands **78**-**83** and tested alkyl substituents to the corresponding alcohol. This time, the interconversion barriers at room temperature for all hemiacetals were low enough for interconversions to take place, and thus a potential alignment in case of favored coordination would have been possible. In the case of the presented heterocyclic hemiacetal ligands, the obtained product is indicative of catalytic activity, but not in a selective manner (tab. 3.13).

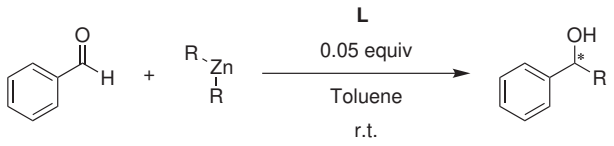

L	R	Yield [%]	Enantiomeric Ratio
	Me	72	48:52
78	Et	76	50:50
	*i*Pr	68	49:51
	Me	55	50:50
79	Et	79	50:50
	*i*Pr	72	48:52
	Me	69	50:50
83	Et	85	50:50
	*i*Pr	61	51:49

Table 3.13: Alkylation testreactions with the substrate benzaldehyde for the ligand systems **78**-**83**.

Moreover, the use of enantiomerically pure ligands, if the separation was possible, is also not an option since the rotational barriers are too low at room temperature and the enantiomers would be converted back into a racemic mixture. Compounds comprising the presented structure motif with higher enantiomeric barriers and possible chiral separation could thus be promising.

All the structures obtained (**59**, **65**, **66**, **78**, **79**, and **83**) show a pattern of difficult accessibility to a substrate which fulfills the conditions for the initially described idea of a dominantly aldehydic structure in dynamic equilibrium to a cyclic hemiacetal form. It is possible that there are structures that exhibit these properties, but the task of finding them is a lengthy process of wandering on the narrow burr of sensitive equilibrium, depending on substituents, solvents, temperature differences, or other components. In addition, the aldehydic substrates did not convert to the desired product, suggesting that this type of substrate would not be suitable for the intended purpose even under the desired properties of the concept idea. Possibly, the spatial limitation due to the proximity of the alcohol moiety is disadvantageous for alkylation on corresponding aldehydes.

3.4 Summary and Outlook - dynamic hemiacetal approach

The synthesis and investigation of dynamic substrate-ligand compounds based on an aldehyde-alcohol motif were pursued in two different approaches. The potential dynamics of the structure motif chosen are based on the possibility of an intramolecular ring closure between aldehyde and alcohol function to form a hemiacetal and a new stereogenic center. The structures could thus act both as a substrate (open-chain aldehyde form) and as a potential catalytic ligand (ring-closed hemiacetal). The first synthesis approach was based on published results of a precursor structure of coumestan compounds. *Tang et al.* reported a temperature-dependent equilibrium for those compounds (fig. 3.42).

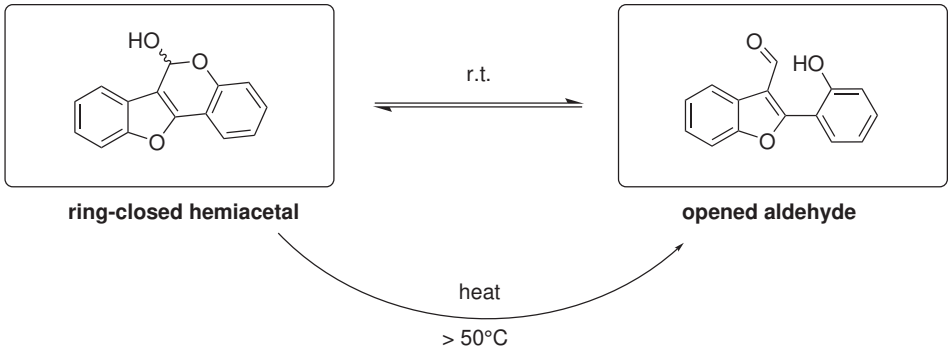

Figure 3.42: Structure motif for arylbenzo[b]furans; modified figure according to *Tang et al.*.[98]

The reported equilibrium was to be investigated in seven novel variations with different substituents compared to the reported reference structure **50** to study their influences. All approaches were feasible in the 3-step synthesis process in good yields only to the second β-keto aldehyde stages. By closer investigation of these 2,3-bis(2-methoxyphenyl)-3-oxopropanals precursors with electron withdrawing and electron donating groups, an extreme stabilization of a single tautomer in the overall keto-enol equilibrium was found. In time dependant ^{1}H-NMR measurements the stabilization increased over seven days independent of the substituents, which was determined *via* the ratio of significant proton signals of the different tautomers present in the equilibrium. The extraordinary stabilization of the *cis*-enol tautomers results from a hydrogen-bonded proton in a six-membered ring, that is electronically stabilized between the two carbonyl groups (fig. 3.43). The hydrogen-bonded proton between the carbonyl groups is for all investigated compounds

characteristically shifted downfield in the NMR spectra (∼15 ppm). Time and temperature dependant ^{1}H-NMR studies reveal a slow conversion rate that is independent of temperature influences in exemplary investigations of the compounds **42** and **47**. Most noteworthy is the conformational memory effect in the hydrogen-bonded six-membered ring at low temperatures that lead to a complete fixation, even if subsequently elevated temperatures are applied.

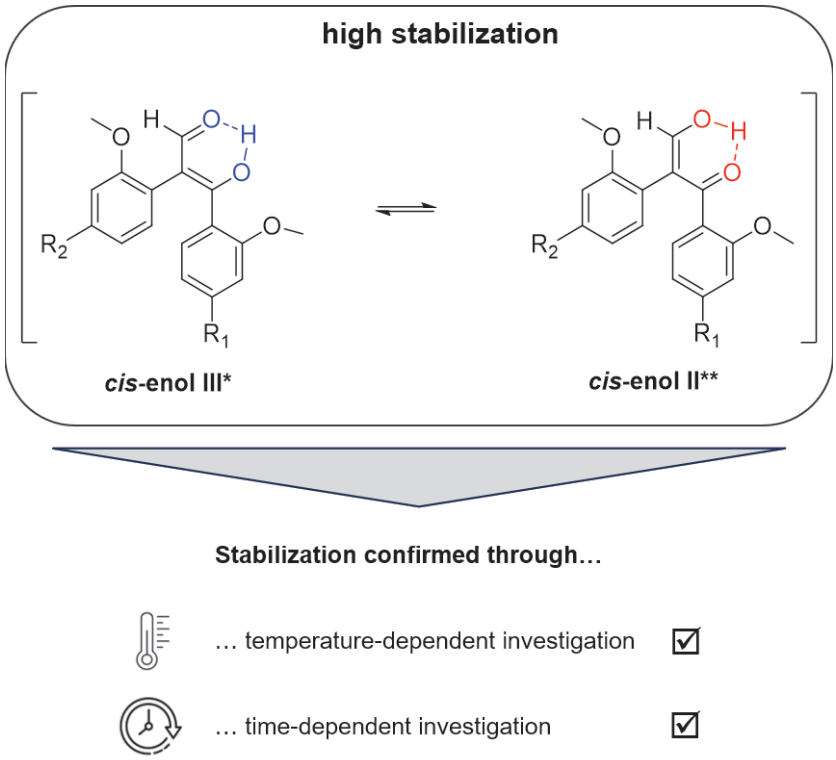

Figure 3.43: Hydrogen-bond stabilized dominating tautomers in coumestan precursor β-ketoalehydes **42**-**49**.

The final step towards the target structure **50** was exemplarly realized for reference structure **50** with R_1, R_2=H, yielding only 3%. Due to the exceptional shift of the equilibrium towards the hydrogen stabilized enol, the low yield is not surprising, since the concerned synthesis step is mediated *via* a different minor tautomer of **42**. Since the stabilization prevents or extremely complicates the further reaction to the desired target compounds, this approach was not pursued further in the following. It should be noted that the publication of the synthetic route towards **50**[98] does not mention the strongly shifted equilibrium of

the β-keto aldehyde intermediate **42**. The further reaction to the final aldehyde-alcohol product **50** which was used as a reference point, is not in agreement with the results obtained in this work.

The second approach to access dynamic aldehyde-alcohol compounds was based on simpler axial biaryl structures. A total of seven structures with the selected aldehyde-alcohol motif, based on a biaryl optionally containing a naphthyl unit or a binaphthyl backbone, were successfully synthesized (fig. 3.44).

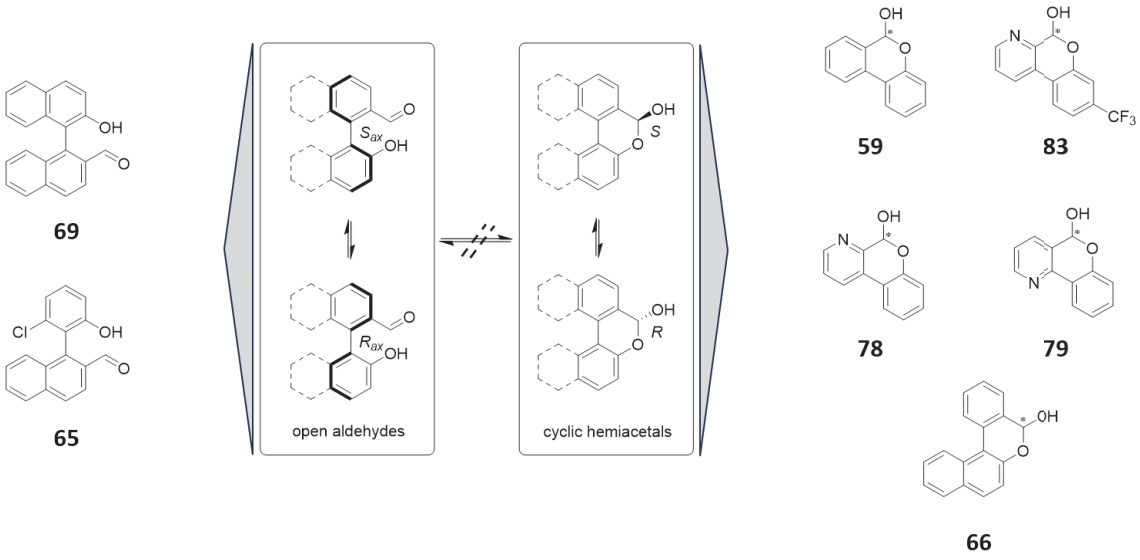

Figure 3.44: Summary of synthesized potentially dynamic structures, solely detected either open-chain aldehyde (left) or ring-closed hemiacetal formation (right).

The compounds **69**[126] and **66**[119] were already literature-known and dynamics had already been reported for structure **66** and substituted derivatives.[119] Apart from these references, which often require several steps to the final product, the structural motif is not described in detail in the literature. With the exception of **69**, an easily accessible synthesis route *via* Suzuki-coupling reactions starting from commercially available materials was presented for the remaining six potentially dynamic aldehyde-alcohol compounds **59**, **66**, **65**, **78**, **79**, and **83**. The synthesized compounds were all investigated NMR spectroscopically as well as by HPLC-MS with respect to their dynamics. For all

seven compounds, the equilibrium was exclusively found to be either on the open-chain aldehyde side or in closed hemiacetal form. Compounds **69** and **65** with the most sterically demanding residues around the rotation axis favored the aldehyde form. The remaining compounds **59**, **66**, **78**, **79**, and **83** were present in the hemiacetal form. In ^{1}H-NMR studies, all structures were stable and unaffected in their favored formation independent of the chosen solvent (tested in $CDCl_3$, DCM-d_2, THF-d_8, Acetone-d_6, Toulene-d_8, and DMSO-d_6). Both the enantiomers of the axial chiral compounds and those formed by ring closure could be visibly separated on analytical HPLC using immobilized chiral stationary polysaccharide phases[135] with subsequent mass detection. In subsequent DHPLC investigations, the rotational barriers and the activation parameters of the heterocyclic biaryl derivatives **79** and **83** could be determined *via* Eyring-plot analysis. The values were found in agreement with the transient hemiacetal catalyst in the Soai reaction as proposed by *Trapp et al.*[75,76] The rotational barrier for picolinaldehyde derivative **78** could also be determined at 0°C and has a large decrease of the enantiomerization barrier compared to nicotinaldehyde derivative **79**, due to a destabilizing N-position in the heterocycle. Finally, all structures were tested for their catalytic activity, even if they did not correspond to the ideal basic idea of the developed concept. The open-chain aldehydes **69** and **65** could not be alkylated in toluene at room temperature. In this course, the three organozinc reagents dimethyl-, diethyl-, and diisopropylzinc were tested. A similar phenomenon is known for benzaldehyde, which can only be alkylated in the presence of a catalytically active ligand.[127] This opens up the prospect for future investigations of testing the reactivity of the synthesized aldehydes **69** and **65** in the presence of a chiral catalyst. However, this possibility was not pursued further, since the use of external catalysts would not achieve the desired objective of autocatalysis. The same applies to the hemiacetal structures **59**, **66**, **78**, **79**, and **83**, since the motif provides no aldehyde function for alkylation. The use of a hemiacetal motif as a ligand in a zinc-mediated alkylation was nevertheless of interest with regard to the reported catalytically active hemiacetal in the Soai reaction.[76] Since the enantiomers of the hemiacetal compounds could not be separated preparatively, the focus in alkylation reactions with benzaldehyde was on the ligating property of the hemiacetal moiety and no enantioselectivity was aimed for. Since alkylations with benzaldehydes, as mentioned above, do not occur at room temperature without a capable ligand, this substrate was ideally suited for this purpose. Benzaldehyde was successfully alkylated by the residues R=Me, Et, *i*Pr using all prepared hemiacetals

as racemic ligands with corresponding diorganozinc reagents. The ligating properties of the hemiacetal moieties were confirmed in good yields of the alkylated benzaldehyde products. The use of enantiomerically pure compounds of hemiacetal structural motifs could thus be promising for metal-mediated asymmetric catalyzes and provides incentives for deeper research. The simple synthesis route described opens up the possibility of generating further compounds with this structural motif and investigating the ligating properties in more detail. Compounds with higher interconversion barriers and possible enantiomeric separation could be promising ligands and should be tested for their enantioselectivity.

4 Chapter 2 - Autocatalytic Substrate Design based on β-Amino Alcohol Derivatives

4.1 Introduction

Many naturally occurring, biologically or pharmaceutically active compounds are based on enantiomerically pure secondary alcohols. Enantioselective addition of alkyl residues mediated by diorganozinc reagents to aldehydes provides important access to these optically active compounds, unlike the conventional organolithium or organomagnesium reagents.[136] In the 1980s, *Oguni* and *Omi* were the first who made the discovery that *S*-Leucinol and other chiral 2-amino-1-alcohols catalyze the otherwise hardly proceeding addition of diethylzinc to benzaldehyde in moderate enantioselectivities.[77] It is noteworthy that *Oguni et al.* obtained the corresponding 1-phenyl-propan-1-ol in *R*-configuration for the applied ligands in *S*-configuration. The breakthrough to very high enantioselectivities was achieved shortly afterward by *Noyori et al.* with the tertiary amino alcohol (-)-DAIB, a camphor derivative.[137] At the latest, a new generation of enantioselective catalyst systems based on amino-alcohol structure motifs begins with this discovery. The addition of diethylzinc to benzaldehyde under usage of the ligand (-)-DAIB yields *S*-l-phenylpropanol with 99% *ee*. The reaction occurs enantioselective in the presence of the ligand in high as well as low optical purity due to a non-linear effect as described at the beginning of the general introduction (see chapter 1). The optical purity of the product obtained exceeds the initial values of the chiral catalyst used. In the presence of only 2 mol% and initial *ee* of 14%, the addition product could be obtained with up to 98% *ee*.[31,137] This extraordinary nonlinear effect can be attributed to the fact that the diastereomeric dimeric complexes

formed between the dialkylzinc compound and the auxiliary DAIB, differ greatly in their chemical properties, as previously discussed in the general introduction section (see 1). A (+)-NLE was also observed when dimethylzinc was used for the alkylation, but in a less pronounced manner than for diethylzinc.[31] *Noyori et al.* and several other research groups were able to gain a mechanistic understanding of this important reaction in the following years considering kinetic considerations, alkyl scrambling experiments, single-crystal X-ray analysis, ^{1}H NMR investigations and molecular weight determination of certain key intermediates[31,32,138], modeling by a Q2MM force field[139,140] and PM3 transition state modeling[141,142]. Thereby, the amino alcohol **13** reacts with one equivalent of the zinc reagent to form **84**. The remaining alkyl group cannot be transferred to the aldehyde. Only the coordination of a further equivalent of zinc reagent to the alkoxy zinc group **85** leads to activation, so that addition to the aldehyde is possible, resulting in complex **86**. During this process, the transition state **87** leads to complex **88**. The chiral product **89** is released under regeneration of **84**, which can undergo a further catalytic cycle (fig. 4.1).

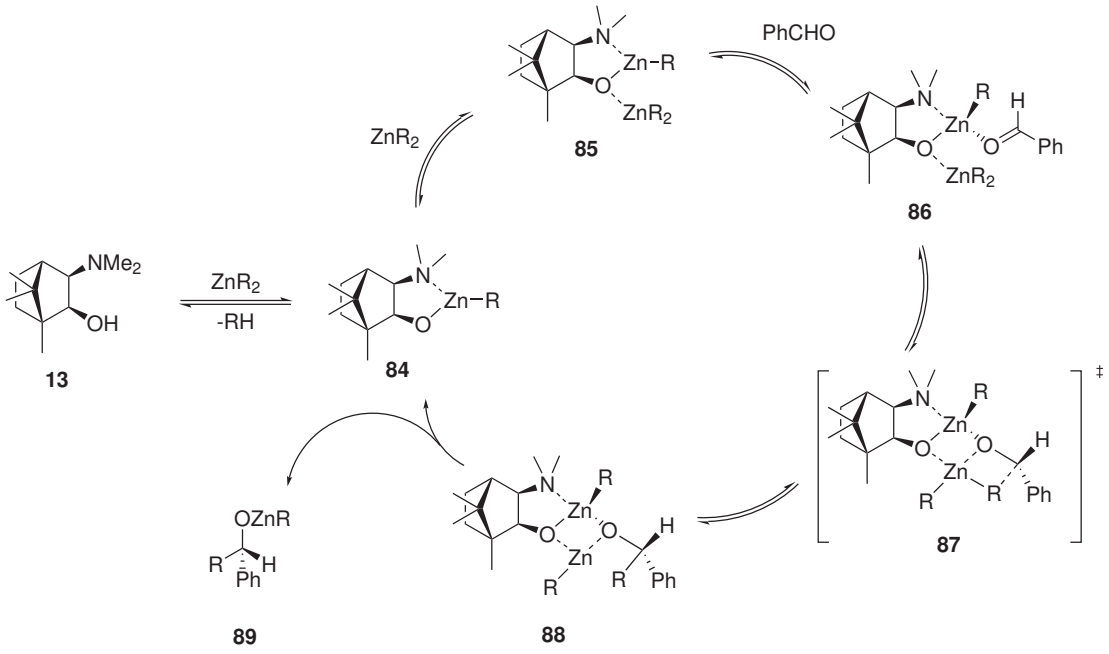

Figure 4.1: Catalytic cycle in the Zn-alkylation of benzaldehyde with DAIB according to Noyori et al..[31,32,138]

Since then, a growing library of chiral catalysts has been developed whose potential has been tested in the asymmetric alkylation of benzaldehyde and other aldehyde substrates

using diorganozinc reagents. For a more detailed overview than presented below, the review paper by *Soai et al.* on the 'enantioselective addition of organozinc reagents to aldehydes' is recommended.[143] The first catalysts that did not preexist and were specially designed for enantioselective addition of dialkylzinc reagents were based on secondary pyrrolidinylmethanols derived from the basic structure of the amino acid proline.[144–146] The proline-derived amino alcohols providing high enantioselectivities asymmetric alkylation reactions of benzaldehyde, showed a modification at the N-atom as well as at the carbon atom bearing the alcohol group (fig. 4.2).

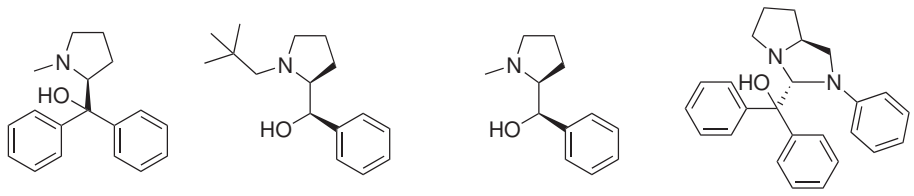

90 97% *ee, S*-config. **91** 100% *ee, R*-config. **92** 72% *ee, R*-config. **93** 96% *ee, S*-config.

Figure 4.2: Prolinol-based catalysts with high enantioselectivities in asymmetric ethylation of benzaldehyde.[144,147]

The initial success with the prolinol derivatives sparked the search for other suitable ligands. The naturally available pool of amino acids provided easy access to a wide variety of possibilities and the essential prerequisites for such catalytic systems. The good commercial availability and often simple and known synthesis routes quickly made various ligand designs based on amino acids accessible. In the following years, a number of catalysts were developed from this pool. The figure below shows selected examples of valine[148], leucine[149] and tyrosine-derived[150] catalysts in the asymmetric ethylation of benzaldehyde (fig. 4.3). The examples demonstrate the large influences of the different attached substituents and their positions within the same basic structure. Just as *Oguni et al.* initially reported, the selectivities for the alkylation products using the derivatized 2-amino-1-alcohols on amino acid basis presented below are all reversed (fig. 4.3).[148–150] In addition to the standard substrate benzaldehyde, research was also expanded to include aliphatic or substituted aldehyde substrates providing good enantioselectivities.[143,148,150]

In addition to the natural amino acid pool, as in the case of DAIB, a large variety of natural substance derivatives are structurally possible ligands for asymmetric zinc alkylations and

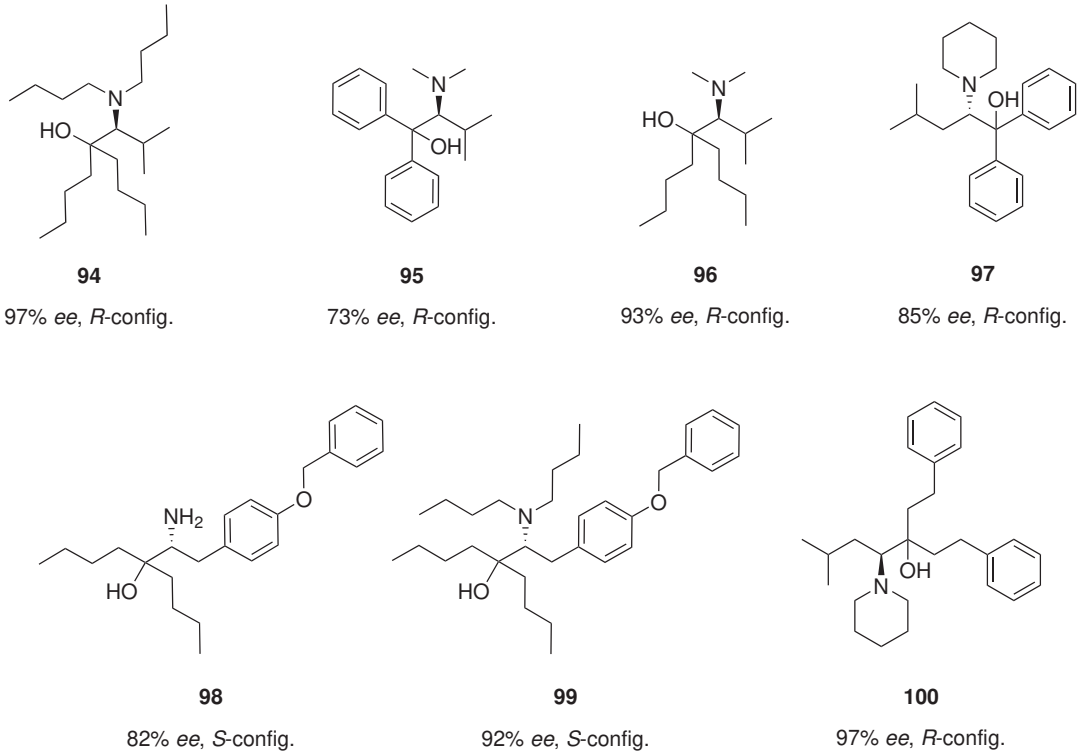

94 97% *ee*, *R*-config.

95 73% *ee*, *R*-config.

96 93% *ee*, *R*-config.

97 85% *ee*, *R*-config.

98 82% *ee*, *S*-config.

99 92% *ee*, *S*-config.

100 97% *ee*, *R*-config.

Figure 4.3: Different amino acid derivative based catalysts; Valine-derived **94**-**96**[148], Leucine-derived **97** and **98**[149], Tyrosine-derived **99** and **100**[150] with high enantioselectivities in asymmetric ethylation of benzaldehyde.

have also been investigated. An investigated group of these included epherine[151–153] and norepherin[154,155] derivatives. These naturally occurring substances contain two stereo centers located at the alcohol-bound and amine-bound carbon atoms. Experiments with the lithium salt of (1*R*,2*S*)-*N*-[2-(dimethylamino)ethyl]ephedrine **101** in the ethylation of benzaldehyde showed good enantioselectivities (90% *ee*, *R*-configuration) as usual with previous β-amino alcohols reversed to the stereo configuration of the carbon atom adjacent to the amine moiety (see fig. 4.3).[153] Interestingly, the same reaction with the catalyst (1*S*, 2*S*)-pseudoephedrine **101** resulted in opposite *S*-enantiomer (91% *ee*). This reverse selectivity indicates that the configuration of the alcohol-bound carbon atom is prioritized in determining the product configuration (fig. 4.4).[153]

This selective dependence was also found independently for previously described proline derivatives **91** and **92** exhibiting two stereocenters (fig. 4.2).[144] Existing ligands were also further developed and optimized with regard to the substitutes, diorganozinc reagent or

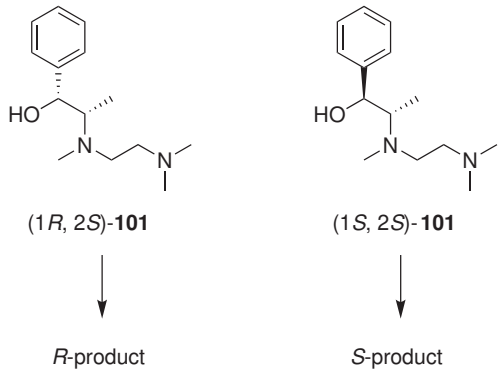

Figure 4.4: Determined product configuration prioritized controlled by configuration at the alcohol located stereo center reported by *Corey et al.*.[153]

the substrate used. A notable example is the ligand 3-exo-morpholinoisoborneol **103** (MIB) with a modified substituent compared to known DAIB at the amine position, which also showed very high enantioselectivities and a positive non-linear effect.[34] The ligand was developed by *Nugent et al.* and showed better enantioselectivities for several α-branched aliphatic aldehydes compared to pioneering ligand DAIB.[34,35] MIB **103** was also effective in the enantioselective addition of dimethylzinc to various aldehydes. A selectivity with 95% *ee* was achieved with *m*-tolualdehyde **102** (fig. 4.5).[34]

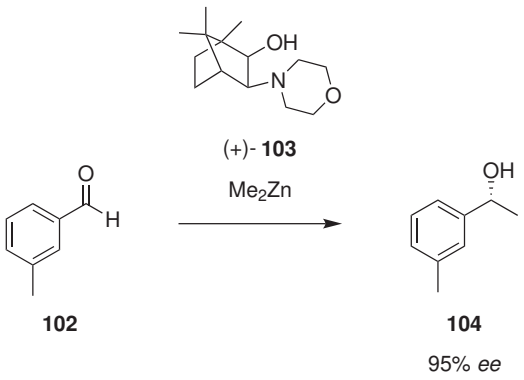

Figure 4.5: Enantioselective addition of dimethylzinc to *m*-tolualdehyde **102** using the ligand (+)-MIB **103**.[34,35]

The structural variations of the catalyst concept around amino alcohols are broad. There is no structural subunit that generally works optimally. The increasing interest in asymmetric diorganozinc alkylation, in particular, has resulted in a huge library of suitable catalysts. From amino alcohol-related compounds with electron-withdrawing substituents[156–158],

alkyl or aryl substituents[144,147–150,159], to sterically demanding or rigid[157,160–162] structures, there are many examples with good selectivities that differ enormously in their structure. Very small structural changes or substituent changes are enough to have an enormous impact on the effectiveness of the catalyst in terms of its selectivity. Most of the structures reported in the literature associated with high enantioselectivities comprise secondary or tertiary alcohols such as amines. Bulky and rigid structures often prove successful as substituents. In addition, regarding the reaction parameters, an increased selectivity was also found in the excess use of diorganozinc reagent and was proved in various independent literature reports.[34,143,163] The most commonly used reagent is by far diethylzinc, with which better selectivities were usually achieved than with corresponding dialkyl zinc reagents tested in parallel, such as dimethyl, dibutyl, and diisopropylzinc.[143] Further developments included even more challenging highly enantioselective phenyl transfer reactions, as shown by *Bolm et al.*[164] and *Pu et al.*[165] using a planar chiral hydroxy ferrocenyl oxazoline and a 3',3-disubstituted naphthol ligand in the reaction with a *para*-Chlorobenzaldehyde substrate. The β-amino alcohol motif in enantioselective catalysts is not exclusively limited to diorganozinc alkylations. They are used as universally applicable catalyst motifs or as chiral selectors in reduction reactions[166], asymmetric hydrations[167], chiral selectors, and catalysts at immobilized stationary phases[168], organo catalysis[169] and several further implementations. The wide range of applications and diversity of accessible research results in this field make the β-amino alcohol structural motif an ideal starting point for a design concept for the new development of substrates with potential autocatalytic behavior.

4.2 Research Objective

Based on the good results known from the literature with amino alcohols as ligands in enantioselective alkylation with diorganzinc reagents mainly researched on diethylzinc with various aldehyde substrates, β-amino aldehydes are considered as potential substrates that can be able to undergo autocatalysis. The basic structure should be similar to that of amino alcohol with the difference that an aldehyde group, capable of alkylation, is used instead of an alcohol. Thus, the target compounds comprise a catalytic active subunit and an aldehyde moiety that can be reduced by alkylation. During alkylation, a secondary β-amino alcohol with a new residue at the carbon atom approximated to the formed alcohol moiety would be formed. The β-amino alcohol generated in this way should serve as an enantioselective ligand in the Zn-mediated alkylation to catalyze the formation of itself. For this purpose, various steps are being considered to realize this project (fig. 4.6).

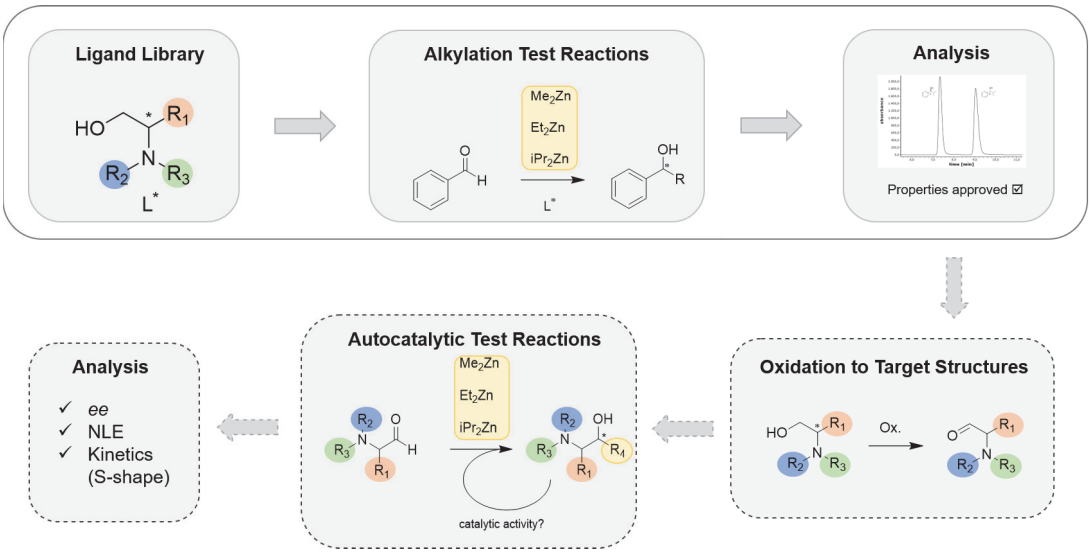

Figure 4.6: Schematic concept towards autocatalytic substrates on the basis of β-amino aldehydes; solid boxes: this work; dashed boxes: further steps.

The aim of this chapter and the first step towards the autocatalytic substrate is the preparation of a catalyst pool based on primary β-amino alcohols modified at the amino group and comprising a primary alcohol group, oxidizable to an aldehyde. As mentioned in the brief introduction, most literature reported β-amino alcohols that provide good ligand and selectivity properties include secondary or tertiary alcohol moieties. On this occasion, the

primary β-amino alcohols obtained by synthesis or accessed commercially will be tested with the standard substrate benzaldehyde for their ligand abilities and enantioselectivities with different diorganozinc reagents in advance. The catalytic tests will provide a first insight into the properties of the ligands' influence of different substituents, mainly at the N-site and different Zn-alkylating agents on the enantioselectivity. This initial assessment should help in the selection of potential target structures and will finally decide whether further oxidation to the aldehyde species can be considered or not. In the second part, the β-amino alcohols obtained, which have shown good catalytic potential, are to be oxidized to the corresponding aldehyde species. These can be tested in alkylations with various diorganozinc reagents subsequently. The choice of the alkyl chain can be very important for the catalytic activity of the final product, as it influences the structure of the resulting reaction product acting as a ligating catalyst.
As part of a collaborative project, the first part of the presented concept is discussed in the following section (fig. 4.6, solid lined upper box). The catalysis pool developed in this context focuses on *N*-benzylated and *N*-methylated primary β-amino alcohol derivatives of several amino acids. The presented ligands were subsequently tested in diorganozinc alkylations of the standard substrate benzaldehyde with dimethyl-, diethyl-, and diisopropylzinc and subsequently analyzed in context to their enantioselectivity.

4.3 Results and Discussion

4.3.1 Catalyst Pool

Commercially available β-amino alcohol derivatives

Commercially, some amino alcohol derivatives are meanwhile available in optical purity at reasonable prices, as they represent important building blocks in many areas of synthetic chemistry. Due to their functional groups, they exhibit excellent inter- and intramolecular binding properties and are suitable for stereo information transfer due to their provided configuration. They are often used in asymmetric synthesis and catalysis as selectors on larger ligands or as ligands themselves. From the commercially available catalyst pool, mainly prolinol derivatives were chosen alongside a morpholine compound **107** (fig. 4.7). Four out of seven compounds have a free oxidizable alcohol function (**106**, **109**, **107**, and **110**), which is necessary for the previously presented idea concept. The other compounds contain attached residues at the C atom of the alcohol group in the case of compounds **105** and **108**. These three non-oxidizable compounds serve as comparators to the remaining available catalyst pool, including the compounds synthesized in the following sections. Compound **108** is, for example, already known to yield high *ee*'s with diethylzinc in addition to fluorinated aldehydes.[170] Compound **105** in the reversed *S*-configuration is also literature known for the alkylation with diethylzinc to yield the *S*-product in 92% *ee*.[146]

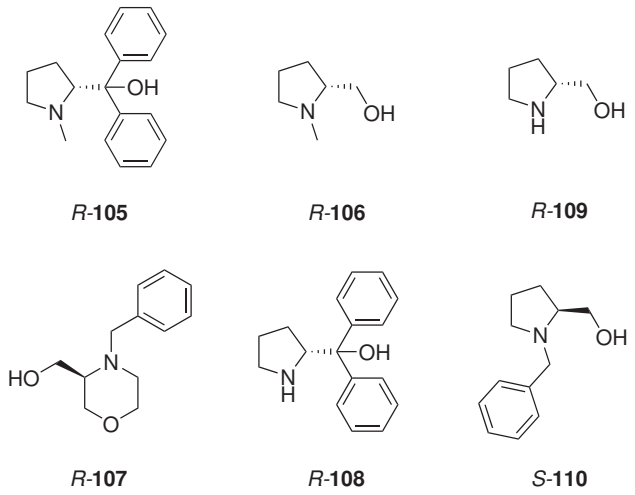

Figure 4.7: Enantiomeres of commercial available β-amino alcohol derivatives.

Methylated β-amino alcohols

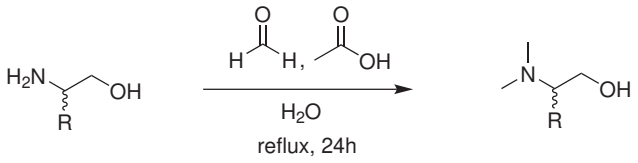

R/S- **111**-**113**

Entry	Methylated Product	Configuration	Yield [%]
1	**111**	*R*	82
2	**111**	*S*	86
3	**112**	*R*	84
4	**112**	*S*	81
5	**113**	*R*	90
6	**113**	*S*	86

Table 4.1: Summarized results of the Eschweiler-Clarke methylation to *N*-methylated β-amino alcohol derivatives.

The methylation of the amino groups was carried out according to the standard procedure of an Eschweiler-Clark reaction.[171] The commercially available enantiomerically pure alcohol derivatives of the amino acids leucine, valine, and phenylalanine were selected as starting materials because of their solubility with the attached residues present in toluene. The solubility is important for later alkylation reactions as they will be carried out in toluene. The methylating agent formaldehyde is used in excess together with excess formic acid. In the first reaction step, the nitrogen of the amine nucleophilically attacks the carbonyl carbon of the formaldehyde. The desired methylated amine is formed after the cleavage of a water molecule and hydride transfer to form carbon dioxide leaving the reaction. The methylated products subsequently required no purification and were NMR spectroscopically of high purity. The preservation of the stereo information was subsequently verified by HPLC-MS. All methylated amines were obtained in excellent yields in *R*- and *S*-configuration (tab. 4.1, fig. 4.8).

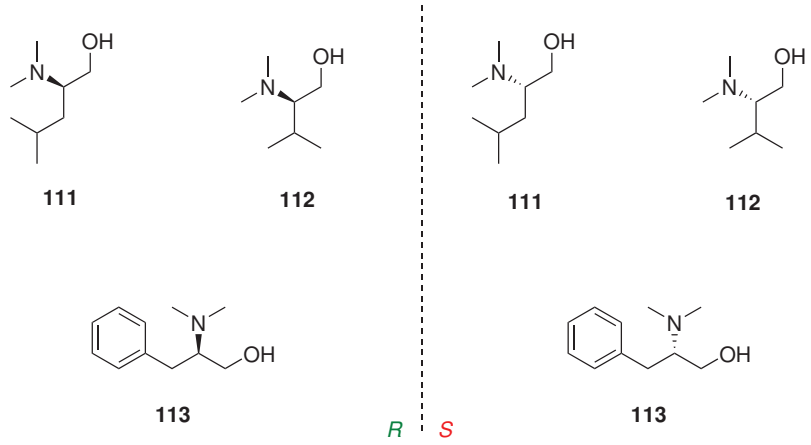

Figure 4.8: Enantiomeres of *N*-methylated Leucinol, Valinol, and Phenylalaninol.

Benzylated β-amino alcohols

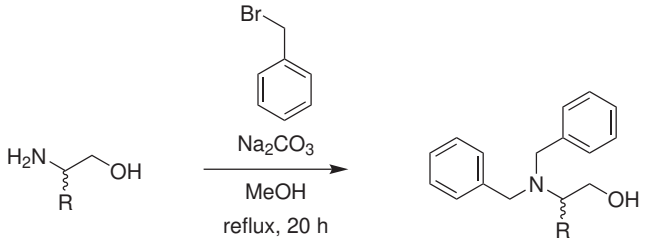

R/S- **114-118**

Entry	Benzylated Product	Configuration	Yield [%]
1	**115**	*S*	73
2	**115**	*R*	73
3	**114**	*R*	64
4	**114**	*S*	58
5	**116**	*S*	78
6	**110**	*R*	83
7	**117**	*S*	67
8	**118**	*S*	58

Table 4.2: Summarized results of the benzylation to *N*-benzylated β-amino alcohol derivatives.

The derivatization of the β-amino alcohols at the nitrogen atom was carried out in a standard S_N2 reaction with benzyl halides and the milde base Na_2CO_3. The benzyl residue was especially chosen because it is bulky, which is assumed to enhance the enantioselectivity

according to findings of *Noyori et al.*.[31] In addition, the nucleophilicity of the nitrogen atom is increased by the electron-donating properties of the benzyl substituent, which positively affects the coordinating abilities at the N-atom. As starting compounds, the optical pure β-amino alcohols leucinol, valinol, phenylalaninol were used as previously for the methylated derivatives. For the benzyl derivatives, the optical pure precursors *tert*-leucinol, prolinol, and phenylglycinol were included, as the benzyl residue is considered to have a greater potential due to the reasons given above. In summary, all derivatives containing a primary amine were twice benzylated with double the amount of benzyl halide. The products were obtained in good to excellent yields after flash column purification, remaining in their enantiomeric configuration determined by subsequent HPLC-MS analysis.

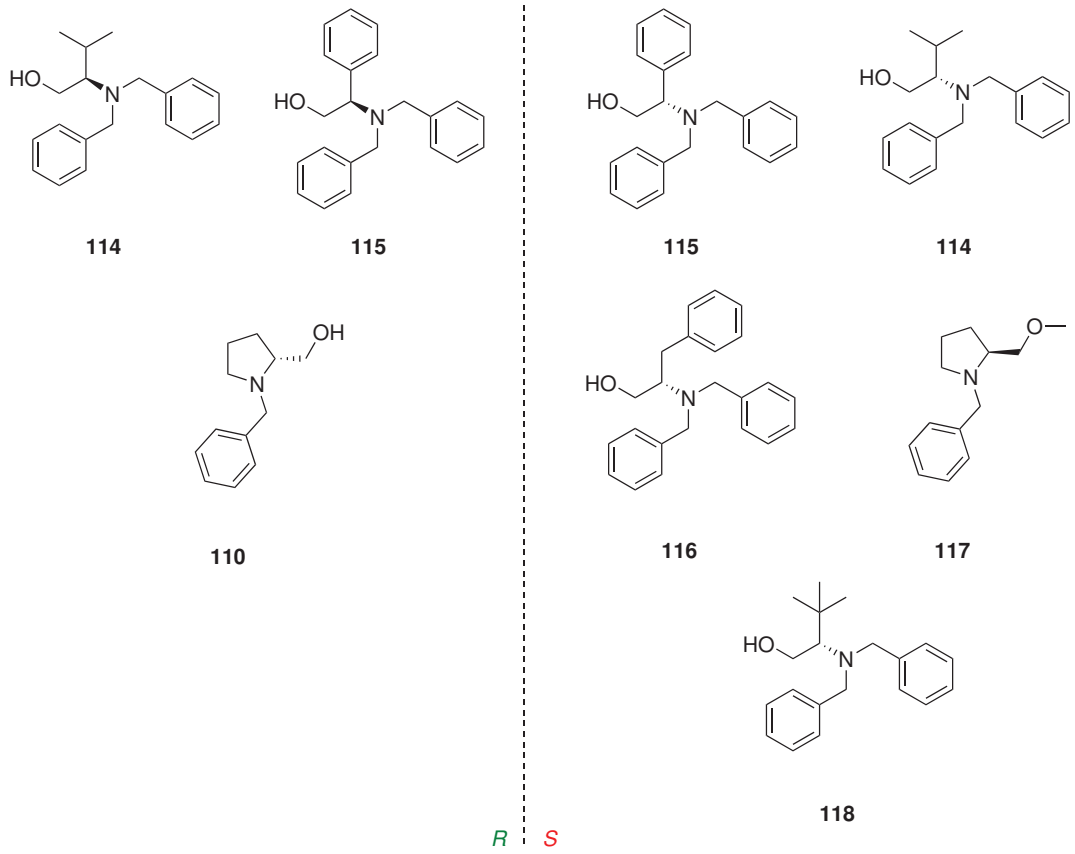

Figure 4.9: Enantiomeres of *N*-benzylated β-amino alcohols.

4.3.2 Catalyzed asymmetric Alkylations with different Diorgano-Zn Reagents

The following section presents the results of the alkylations of benzaldehyde at room temperature in toluene using the ligands of the previously presented catalyst pool. To ensure comparability, all reactions were carried out with the same parameters using 5 mol% enantio-pure catalyst. Toluene was chosen as the solvent because it does not have any coordinating properties, such as THF that could distort the results of ligand-mediated catalysis. Alkylations with diorganzinc reagents often result in poorer yields and enantioselectivities at low temperatures.[163,170] Hence all test procedures were carried out at room temperature. Benzaldehyde was chosen, because it is used as a standard substrate in asymmetric diorganozinc alkylation, usually providing a higher selectivity compared to aliphatic aldehydes.[143] For the analysis of the catalytic test reactions with benzaldehyde, aliquots were taken after 24h. The zinc reagent contained in the aliquots was quenched, and the sample was prepared in a mini work-up. The solvent toluene was then removed since its high UV absorption at 210 nm interferes with product detection on the HPLC. A detailed schematic workflow of the sample collection and preparation for the catalytic test approaches has already been explained and presented in Chapter 1 for the hemi acetal structures (Section 3.3.2, fig. 3.33). The enantiomeric product ratios were determined *via* analytical HPLC-MS separation on the CHIRALPAK column OD-H from DAICEL CORPORATION, usually using a mixture of *n*-hexanes and isopropanol as eluent (if not stated differently; see Appendix 7.2). The integrated peak areas of the individual enantiomers served as a guide for the determination of the enantiomeric ratio and the subsequent calculation of the *ee*. For the purpose of transparency, the individual chromatograms with integrated peak areas and associated data can be found in the appendix in the same order as presented in the tables (see Appendix 7.2). The listed yield results were obtained by linear regression of a dilution series of the corresponding alkylation products. For this purpose, the commercially available products were measured at different concentrations under identical conditions on the HPLC. More detailed information can be found in the experimental part (see Experimental 6.4.3).

Alkylation of Benzaldehyde with Dimethylzinc

The *ee* in Zn-mediated methylation reactions of aldehydes is typically lower in similar catalytic systems compared to alkylations with the diethylzinc species.[34,170,172,173] Due to the reduced reactivity of dimethylzinc compared to diethylzinc, which was already found in early experimental results with β-amino alcohols, there has been less reporting on the use of this organo-zinc species in the further course.[31,138] Even if diethylzinc yields slightly better enantioselectivities in the comparisons given, the ones for dimethylzinc are still worth mentioning and are in some cases above 90% *ee*.[31,34,138,170,172,173] There are also reported individual cases where the selectivity for dimethylzinc is inversely higher than for the diethyl reagent. In 2005 *Pedro et al.*[174] catalyzed the enantioselective addition of dimethylzinc to various aromatic aldehydes with *ee*'s up to 90% using amide derivatives from *S*-mandelic acid in the presence of titanium isopropoxide. Corresponding reactions with the diethylzinc specie turned out unusually less successful.[174] Another outstanding example was provided shortly afterward by *Ando et al.*, who achieved very good enantioselectivities (96% *ee*) in methylation with dimethylzinc using a fluorine ligand in this context.[175] Even if the examples mentioned with reversed enantioselectivities are exceptional cases and use other ligand classes or additional complex-forming additives, unusual selectivity in ligand dependence cannot be precluded, and the alkylation with dimethylzinc is therefore of interest.

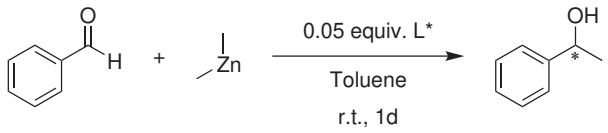

Figure 4.10: Methylation of Benzaldehyde with 1.20 equiv. Dimethylzinc in toluene at room temperature testing different β-amino alcohol ligands.

All ligands in the table showed good conversion to methylated product with yields in the range of 75-95%. However, the enantioselectivities varied widely, ranging from near racemic to moderate reverse selectivity in the final product. As *Oguni et al.*[17] initially observed with diethylzinc, the selectivities usually appear reversed for methylation with dimethylzinc. The poorest values were observed for the prolinol and the *tert*-valinol derivatives (Entry 2,3, and 18). Compound *S*-**118** is maybe too bulky with two *N*-benzyl residues and an additional *tert*-butyl group that coordination and subsequent stereocontrol is hin-

Entry	Ligand L*	e.r.[a]	*ee* [%][b]	Yield [%]
1	*S*-**116**	77 : 23	53.5 (*R*)	89
2	*S*-**117**	52 : 48	3.2 (*R*)	95
3	*S*-**118**	54 : 46	8.2 (*R*)	79
4	*S*-**115**	82 : 18	63.6 (*R*)	81
5	*R*-**115**	16 : 84	67.8 (*S*)	83
6	*S*-**114**	67 : 33	34.2 (*R*)	92
7	*R*-**114**	33 : 67	33.3 (*S*)	89
8	*S*-**111**	72 : 28	43.3 (*R*)	76
9	*R*-**112**	32 : 68	36.5 (*S*)	88
10	*S*-**112**	69 : 31	37.5 (*R*)	94
11	*S*-**113**	57 : 43	13.2 (*R*)	85
12	*R*-**113**	41 : 59	17.3 (*S*)	81
13	*R*-**108**	32 : 68	35.4 (*S*)	89
14	*R*-**111**	37 : 63	25.5 (*S*)	78
15	*R*-**107**	37 : 63	25.6 (*S*)	91
16	*S*-**110**	37 : 63	26.2 (*S*)	93
17	*R*-**106**	37 : 63	26.4 (*S*)	79
18	*R*-**110**	44 : 56	11.6 (*S*)	75

Table 4.3: Summarized results of the methylation of benzaldehyde with dimethylzinc in toluene at room temperature. [a] approximated values of integrated peak area ratio of HPLC analysis; [b] determined *via* peak area of HPLC anaysis using exact values.

dered (Entry 3). The methoxy-protected prolinol derivative *S*-**117** gave nearly racemic values as expected and confirmed the importance of the free alcohol group for coordination. The prolinol derivative with methylated amine function *R*-**106** performs slightly better with an *ee* of 26.4% (Entry 17), but is still weakly selective.

Considering the enantiomers of the benzylated prolinol derivative *R*-**110** and *S*-**110**, a huge difference appears in the enantioselectivity. The *S*-enantiomer **110** reached a value of 26.2% *ee* compared to only 11.6%*ee* for the respective *R*-enantiomer **110**, both unexpected favoring the *S*-configuration in the formed alcohol product (Entry 16 and 18). Even though the selectivities are not good in both cases, the unusual favoring of the *S*-selectivity can be highlighted and indicate a non-linear dependency.

A deviation can also be observed for the methylated leucinol derivatives *R/S*-**111** (Entry 8 and 14). The enantioselectivities correspond to the respective reverse configurations given by the ligands but are clearly more selective in the test reaction with the *S*-enantiomer **111**, for which 43% *ee* is achieved compared to 25% *ee* for the *R*-enantiomer **111**.

The literature-known ligand **108** considering alkylations with diethylzinc could only obtain moderate enantioselectivity in the alkylation with dimethylzinc (Entry 13). The morpholine derivate *R*-**107** was found to be less selective (Entry 15). Even lower enantioselectivities were achieved with the methylated phenylalanine derivatives, which, however, were approximately equal for both enantiomers *R*-**113** and *S*-**113** (Entry 11 and 12).
The benzylated phenylalanine derivate **116** gave better results with 53.5%*ee* (Entry 1). The methylated valinol derivatives *R*-**112** and *S*-**112** gave moderate enantioselectivities with 36-38% *ee* (Entry 9 and 10). The selectivities for the corresponding benzylated valinol derivatives *R*-**114** and *S*-**114** were in the same range with 33-35% *ee* (Entry 6 and 7). Both in methylated and benzylated valinol derivatives, the *S*-conformer is slightly dominating. The best selectivities in the test approaches were obtained using the benzylated phenylglycinol derivatives *R*-**115** and *S*-**115** with good *ee*'s up to 67.8% (Entry 4 and 5). The slight dominance of the *S*-enantiomer was repeatedly observed in this case, as also detected for all other enantiomeric pairs tested.

Alkylation of Benzaldehyde with Diethylzinc

The alkylation of benzaldehyde with diethylzinc is the standard setup for a catalytic test reaction in this field. Prominent examples such as those mentioned at the beginning of the introduction have achieved groundbreaking results with the use of diethylzinc reagent. One of the most prominent of these is probably the enantioselective addition of an ethyl substituent to benzaldehydes catalyzed by DAIB, reported by the later Nobel laureate *R. Noyori*.[31] Due to the increased reactivity compared to other organozinc reagents such as dimethylzinc and the generally better enantioselectivities, as shown by a large number of ligands investigated, test reactions are carried out using this reagent.[170,172,173] Furthermore, they offer good comparative values to the other alkylation reagents.

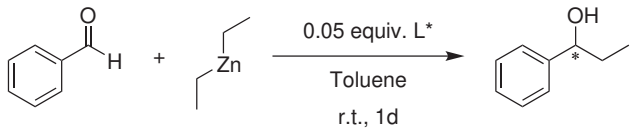

Figure 4.11: Ethylation of Benzaldehyde with 1.20 equiv. diethylzinc in toluene at room temperature testing different β-amino alcohol ligands.

At first glance, the average enantioselectivities are higher than for the corresponding methy-

Entry	Ligand L*	e.r.[a]	*ee* [%][b]	Yield [%]
1	*R*-**110**	34 : 66	32.0 (*S*)	87
2	*R*-**115**	29 : 70	41.6 (*S*)	77
3	*R*-**112**	32 : 68	36.1 (*S*)	90
4	*R*-**113**	37 : 63	25.7 (*S*)	96
5	*S*-**112**	69 : 31	38.7 (*R*)	73
6	*S*-**113**	57 : 43	14.8 (*R*)	91
7	*S*-**114**	60 : 40	20.6 (*R*)	74
8	*R*-**114**	35 : 65	29.1 (*S*)	85
9	*S*-**115**	74 : 26	48.9 (*R*)	88
10	*R*-**111**	38 : 62	24.6 (*S*)	91
11	*S*-**116**	79 : 21	58.0 (*R*)	82
12	*S*-**111**	64 : 36	28.2 (*R*)	78
13	*R*-**105**	78 : 22	57.0 (*R*)	70
14	*R*-**106**	46 : 54	7.9 (*S*)	83
15	*R*-**109**	28 : 72	43.7 (*S*)	79
16	*S*-**110**	72 : 28	44.1 (*R*)	83
17	*R*-**107**	46 : 54	7.1 (*S*)	80

Table 4.4: Summarized results of the ethylation of benzaldehyde with diethylzinc in toluene at room temperature. [a] approximated values of integrated peak area ratio of HPLC analysis; [b] determined *via* peak area of HPLC analysis using exact values.

lations with dimethylzinc, although the peak values are unexpectedly lower for the diethylzinc test reactions. The yields are approximately in the same range with good values between 73-96% as previously for the methylations. The lowest selectivity was recorded with the *N*-methylated prolinol derivative **106** with 7.9% *ee* (Entry 14). To this context a testreaction with the derivative containing a methoxy group **117** instead of the alcohol moiety was excluded based on previous results in advance.

In comparison, the selectivity for the unsubstituted *R*-prolinol performs better (43.7% *ee*, Entry 15). The literature-known prolinol derivatized ligand *R*-**105** was able to achieve quite good enantioselectivities in the diethylzinc ethylations yielding unexpected the *R*-product in 57.0% *ee* as the selectivities for β-amino alcohols usually leading to reversed enantioselectivities[17] (Entry 13). The catalyst has already been tested in an ethylation reaction on benzaldehydes and reported with 97% *ee* for the catalytically used *S*-derivative[146], which does not agree with the values obtained for the corresponding *R*-enantiomer (Entry 13). The reversed selectivity and the large deviations between the obtained and reported enantioselectivity for both enantiomers indicates a non-linearity

that may explain the differing values.
The direct comparison of the benzylated prolinol enantiomers is more positive for the *S*-enantiomer **110** with 44.1% *ee* compared to 32.0% *ee* (Entry 16 and 1). Interestingly, the unsubstituted *R*-prolinol **109** performed significantly better than the *N*-substituted *R*-derivatives. The selectivities for the methylated leucinol derivatives *R/S*-**111** are equally low in the range of 24-29% *ee* with a slight preference for the *S*-enantiomer (Entry 10 and 12). The benzylated phenylalaninol derivative **116** achieved the best enantioselectivities in this test group with diethylzinc with a comparatively good *ee* of 58% (Entry 11). In contrast, the selectivities for corresponding methylated phenylalaninol derivatives *R/S*-**113** were much lower (Entry 4 and 6). The values of the enantioselectivities differ from each other and show a higher selectivity for the *S*-enantiomer to the corresponding reverse *R*-product. The methylated valinol derivates *R/S*-**112** showed equal moderate enantioselectivities with a slightly increased selectivity for *S*-**112** (36-39% *ee*, Entry 3 and 5). Decreased values were obtained for the benzylated valinol derivatives *R/S*-**114** (Entry 7 and 8). In deviation to that observation was the higher selectivity for the *R*-enantiomer **114** with 29.1% *ee* compared to 20.6% *ee* for the test reaction with the corresponding *S*-enantiomer **114**. The enantioselectivities for the *N*-benzylated phenylglycinols *R/S*-**115** were better, albeit moderate, and were again consistent with previous observations slightly more selective in the application of the *S*-enantiomer (Entry 2 and 9).
This test group also includes some deviations in direct enantiomeric pair comparison as described. Interestingly, the ligand pairs with very large deviations in the enantiomeric excess do not match those in the methylated test reactions previously presented. Furthermore, no increased preference in selectivity for a particular enantiomer was found in all ligands as before in methylating approaches.

Alkylation of Benzaldehyde with Diisopropylylzinc

The use of diisopropylzinc is probably best known for the enantioselective as well as autocatalytic Soai reaction, which is also exclusively successful with this reagent.[36,67] Due to the sterically more demanding residues, a more selective orientation in spatial terms is assumed compared to straight-line alkyl chains such as diethylzinc.[67,86,176] The library of alkylations with diisopropylzinc using various ligands is also quite extensive, although in the case of β-amino alcohols, it is not investigated with the same frequency as the

use of diethylzinc. Here, too, some outstanding enantioselectivities were achieved with structurally related compounds.[177] In some cases, even higher enantioselectivities could be achieved than with the use of diethylzinc. In 2003, *Soai et al.* reported dendritic catalysts with chiral β-amino alcohol sites that enantioselectively catalyzed alkylations with various dialkylzinc reagents.[178] The alkylations with diisopropylzinc were more selective compared to those with diethylzinc in published results on benzaldehyde.[178] With the use of diisopropylzinc, a third promising dialkylzinc reagent is thus being tested on the ligand pool.

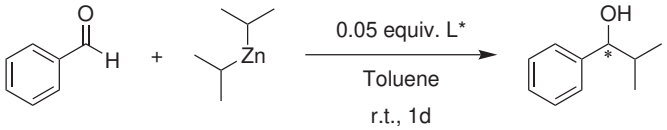

Figure 4.12: Diisopropylation of Benzaldehyde with 1.20 equiv. diisopropylzinc in toluene at room temperature testing different β-amino alcohol ligands.

Entry	**Ligand L***	**e.r.**[a]	***ee*** [%][b]	**Yield [%]**
1	*R*-**107**	26 : 74	48.5 (*R*)	85
2	*S*-**110**	21 : 79	58.6 (*R*)	81
3	*R*-**108**	67 : 33	33.4 (*S*)	76
4	*R*-**111**	62 : 38	23.5 (*S*)	84
5	*S*-**114**	-**	-**	-**
6	*R*-**114**	53:47	12.0 (*S*)	88
7	*R*-**112**	84 : 16	68.6 (*S*)	90
8	*S*-**112**	14 : 86	72.3 (*R*)	91
9	*S*-**113**	25 : 75	49.9 (*R*)	86
10	*R*-**113**	79 : 21	57.1 (*S*)	85
11	*S*-**111**	25 : 75	50.1 (*R*)	74
12	*R*-**110**	80 : 20	59.3 (*S*)	85
13	*S*-**116**	57 : 43	14.1 (*S*)	73
14	*S*-**117**	51 : 49	1.5 (*S*)	79
15	*S*-**118**	49 : 51	2.2 (*R*)	76
16	*S*-**115**	48 : 52	3.9 (*R*)	81
17	*R*-**106**	28 : 72	44.9 (*R*)	82

Table 4.5: Summarized results of the isopropylation of benzaldehyde with diisopropylzinc in toluene at room temperature. ** excluded due to overlay with second specie in HPLC 2D-spectra.

The alkylations with diisopropylzinc also showed consistently good conversions to the alkylated product. As in the methylation reactions, the enantioselectivities ranged from close

to racemic product to relatively good *ee* values up to >70%. Nearly racemic conversion is observed for the ligands **117**, **118**, and **115** (Entry 14-16). Very low enantioselectivities were found for the benzylated *S*-phenylalaninol **116** as well as for the benzylated valinol enantiomers *R/S*-**114** (Entry 13, 5, and 6). Interestingly the obtained product configuration of **116** and **117** is not inverted as expected (Entry 13 and 14). A possible non-linear effect may be considered in these cases.

The comparison of the enantiomers *R/S*-**114** showed, at first sight, a preference for the *R*-configuration resulting in a difference of 6% *ee* towards the corresponding product with the same configuration (Entry 5 and 6). The 2D spectra of the measurement with *S*-**114** revealed an overlap with a second compound that distorts the integration of the signal. However, since the selectivity for the corresponding *R*-enantiomer **114** was negligibly low and no high selectivity was to be expected for the *S*-enantiomer **114** either, no further efforts were made to find a suitable method for an exact determination of the *ee* values.

Moderate to good enantioselectivities were obtained by the methylated phenylalaninols *R/S*-**113** with a deviation between the two enantiomers (Entry 9 and 10). *R*-**113** yielded the *S*-product with 57.1% *ee* in contrast to the corresponding *S*-**113** with 49.9% *ee* for the *R*-product.

The best selectivities were provided by the methylated valinol derivatives *R/S*-**112** exhibiting a slight preference in selectivity for the *S*-enantiomer with 72.3% *ee* (Entry 7 and 8). The benzylated prolinol derivatives *R/S*-**110** gave equally quite good enantioselectivities of 58-60% *ee* (Entry 2 and 12). The *N*-methylated prolinol selectivity was compared lower in a moderate range with 44.9% *ee* (Entry 17) Literature-known ligand **108** in context to ethylation with diethylzinc gave low enantioselectivities of 33.4% *ee*.

A larger deviation can be observed for the selectivities with the methylated leucinol derivatives *R/S*-**111**, which are low for the *R*-enantiomer to the corresponding *S*-product and moderate for the reverse case with the *S*-enantiomer (Entry 4 and 11). The selectivity for the *S*-enantiomer is more than twice that of the *R*-enantiomer to their corresponding products each (23.5% *ee* compared to 50.1% *ee*). The difference is again remarkable.

The *R*-morpholine derivative **107** was found to be moderately selective with 48.5% *ee* towards the corresponding *R*-product. The configuration here is also unexpectedly inverse indicating again a NLE (Entry 17).

The tested pool was able to record the greatest deviations with diisopropylzinc. As mentioned, several inverse selectivities were observed. In the direct enantiomer pair compar-

isons, deviations are also repeatedly observed, which, as with diethylzinc, individually prefer a configuration depending on the ligand.

Comparison and Conclusion of the different Zn-alkylation Agents

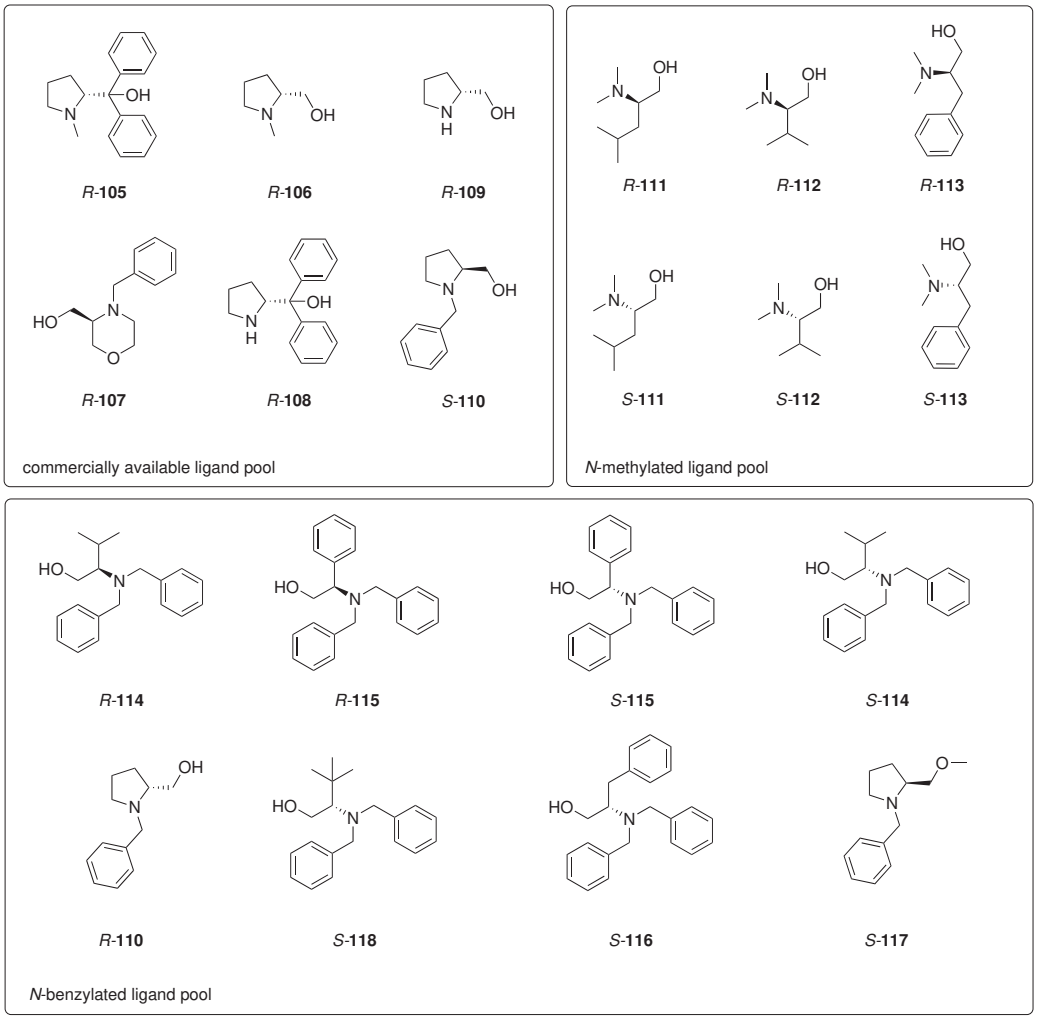

Figure 4.13: Overview over ligand pool tested in asymmetric diorganozinc alkylations with benzaldehyde.

The overview shows all *ee*'s obtained with the ligand pool using three different dialkylzinc reagents in alkylations to benzaldehydes. Overall, the primary β-amino alcohols did not achieve outstanding enantioselectivities, although there is potential in some structures. The choice of the alkyl substituent of the diorganozinc reagent plays a very decisive role

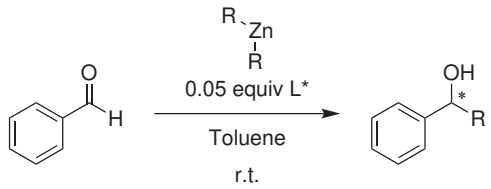

Figure 4.14: General reaction scheme for alkylations of benzaldehyde using diorganozinc reagents under standard conditions.

in the selectivity and leads to sometimes strongly deviating results with the use of the same ligand. For the *N*-methylated derivatives, significantly higher enantioselectivities were observed with diisopropylzinc used compared to dimethyl- and diethylzinc (Entries 1, 2, 6, 7, 9, and 13). An exception is the *R*-enantiomer of methylated leucinol **111**, which yields for all three dialkylzinc reagents approximately the same enantioselectivities (Entry 10), surprisingly opposite to the corresponding *S*-enantiomer (Entry 9). Repeated measurements showed the same pattern. Using *N*-methylated ligands is, therefore, most suitable for alkylations with diisopropylzinc. Best selectivities were obtained with the methylated valinol derivatives **112** (Entry 1 and 2).

Interestingly, the opposite is observed for the benzylated derivatives, where the selectivities for alkylations with diisopropylzinc are generally lower (Entries 3, 4, 5, 8, 11, and 12,). An exception is the group of prolinol derivatives and the single morpholine derivative **107** (Entries 16, 17, and 20). In these two cases, a higher selectivity for diisopropylzinc is to be expected. The differences here probably result from spatial differences in the catalytic space. The amine group of the proline and the morpholine derivative are both integrated in a 5- and 6-membered heterocycle, respectively and can thus only be benzylated once. In the case of the other reduced amino acid derivatives, primary amino moieties are provided that have been benzylated twice. In the catalysis reactions of these groups, a comparatively higher selectivity for dimethyl and diethylzinc was observed (Entries 3, 4, 5, 8, 11, and 12). Surprisingly, the selectivity is mostly better for the alkylations with dimethylzinc (Entries 3, 4, 11, and 12) which has mostly led to less selective product formations than diethylzinc according to several reporting literature, as already mentioned before. The best selectivities are provided by the benzylated phenylglycinol derivatives **115** (Entry 11 and 12).

General low enantioselectivities are observed for the *tert*-Valinol derivative **118** and for the prolinol derivative comprising a methylated alcohol moiety **117** (Entry 5 and 14). The

Entry	Ligand L*	*ee* [%], R=Me	*ee* [%], R=Et	*ee* [%], R=*i*Pr
1	*S*-**112**	37.5 (*R*)	38.7 (*R*)	72.3 (*R*)
2	*R*-**112**	36.5 (*S*)	36.1 (*S*)	68.6 (*S*)
3	*S*-**114**	34.2 (*R*)	20.6 (*R*)	-**
4	*R*-**114**	33.3 (*S*)	29.1 (*S*)	12.0 (*S*)
5	*S*-**118**	8.2 (*R*)	-	2.2 (*R*)
6	*S*-**113**	13.2 (*R*)	14.8 (*R*)	49.9 (*R*)
7	*R*-**113**	17.3 (*S*)	25.7 (*S*)	57.1 (*S*)
8	*S*-**116**	53.5 (*R*)	58.0 (*R*)	14.1 (*S*)
9	*S*-**111**	43.3 (*R*)	28.2 (*R*)	50.1 (*R*)
10	*R*-**111**	25.5 (*S*)	24.6 (*S*)	23.5 (*S*)
11	*S*-**115**	67.8 (*R*)	48.9 (*R*)	3.9 (*R*)
12	*R*-**115**	63.6 (*S*)	41.6 (*S*)	-*
13	*R*-**106**	26.4 (*S*)	7.9 (*S*)	44.9 (*R*)
14	*S*-**117**	3.2 (*R*)	-*	1.5 (*S*)
15	*R*-**109**	-	43.7 (*S*)	-
16	*R*-**110**	11.6 (*S*)	32.0 (*S*)	59.3 (*S*)
17	*S*-**110**	26.2 (*S*)	44.1 (*R*)	58.6 (*R*)
18	*R*-**108**	35.4 (*S*)	-	33.4 (*S*)
19	*R*-**105**	-	57.0 (*R*)	-
20	*R*-**107**	25.6(*S*)	7.1 (*S*)	48.5 (*R*)

Table 4.6: Summarized *ee* values of the alkylations of benzaldehyde in toluene at room temperature. * excluded from tests due to very low selectivities in previous correlating attempts.** excluded due to overlay with second specie in HPLC 2D-spectra.

test reactions with the prolinol derivative including a protected alcohol function (Entry 14) were carried out more for reasons of comparison since this class of ligands does not meet the prerequisites for the basic target compounds towards possible oxidation to an aldehyde anyway. The same applies to the literature-known prolinol derivatives bearing two benzyl substituents on the α-carbon atom with and without substitution on the *N*-side (Entry 18 and 19). Moderate selectivities were observed for the non-*N*-substituted variant **108** with dimethyl- and diisopropylzinc. The *N*-methylated variant **105** performed slightly better in alkylations with diethylzinc, but in poor selectivity compared to the reporting for the reversed enantiomer in the corresponding literature, as previously discussed in the section for the diethylzinc ethylations.

4.4 Summary and Outlook - β-amino alcohol approach

This chapter presented an approach and concept for the development of new autocatalytic substrates based on various literature-known results with β-amino alcohols in alkylation reactions, especially with diethylzinc. The present results are part of a collaboration and present the first part of the concept dealing with a pre-selection of different primary β-amino alcohols with *N*-substitution. The second, not included part deals subsequently with the transfer into the corresponding aldehydes by oxidation and the subsequent test as substrates in a potential autocatalysis. For the purpose of pre-selection, a catalyst pool of 20 β-amino alcohols was tested in alkylation reactions with diorganozinc reagents and benzaldehyde in an identical setup concerning the reaction parameters. Six of the 20 test ligands were commercially available, the remaining 14 compounds were successfully synthesized in benzylation and methylation reactions of the free amine groups of the primary amino acid alcohol derivatives in good to very good yields. The known use of β-amino alcohols as ligands in the literature has mostly focused on secondary or tertiary alcohols. Only in a few cases, different alkyl residues were tested beyond the use of diethylzinc. In contrast, alkylations with three different diorganozinc reagents were carried out with each ligand in the present work to ensure greater coverage of possible enantioselectivities. The choice of *N*-substituents to be investigated included methyl- and benzyl- residues, as both are sterically very different and, therefore, good comparison groups. Overall, the primary β-amino alcohols did not achieve peak enantioselectivities. However, good results were obtained in some cases. Contrary and unexpected to the usual results reported in publications, the best enantioselectivities were not obtained in alkylations with diethylzinc. For the *N*-methylated derivatives, a trend towards significantly better enantioselectivities with a sterically more demanding branched alkyl residue in the diorganozinc reagent used was observed. In the case of the presented investigations, this means a clear favoring of diisopropylzinc over dimethyl- and diethylzinc concerning the enantioselectivity. The best selectivities were obtained by *N*-methylated valinol derivatives *R*- and *S*-**112** with good *ee* up to 72%. The general size of the alkyl chain is not primarily decisive, as the selectivities with the *N*-methylated ligands were not necessarily better with diethylzinc than with dimethylzinc. For the *N*-benzylated derivatives with open-chain amine, the pattern was reversed. These appeared clearly more selective with the unbranched diorganozinc reagents, dimethylzinc and diethylzinc. Unusually, the majority of the higher enantioselectivities

were in favour of the reactions with the dimethyl species. The highest enantioselectivities were obtained by benzylated phenylglycinol derivatives *R*- and *S*-**115** with up to 68% *ee* using dimethylzinc. The derivatives with cyclically embedded amino groups, concerning the prolinol derivatives and the morpholino derivative, have a distinct pattern. For this group, a favoring of diisopropylzinc can be observed in both methylated and benzylated derivatives. The derivatives with cyclically embedded amino groups, concerning the prolinol derivatives and the morpholino derivative, have a distinct pattern. For this group, a favoring of diisopropylzinc can be observed in both methylated and benzylated derivatives. However, the differences in selectivity are not quite as pronounced as in the case of derivatives with open-chain amino groups. The present results show that an extension of the diorganozinc reagents applied is worthwhile. The enantioselectivity of the ligand used is significantly influenced by the interaction of its substituents at the *N*-side and the selection of the alkyl chain of the Zn reagent to be transferred. Furthermore, it is worth mentioning that the selectivities in direct enantiomeric comparisons of the ligands vary greatly in some cases. An example to be cited would be the prolinol derivatized ligand *R*-**105**, which was actually tested for comparative purposes. This ligand has already been tested in an ethylation reaction on benzaldehydes and reported with 97% *ee* of the *S*-product for the catalytically used *S*-derivative **105**[146], which does not agree with the values obtained for the corresponding *R*-enantiomer of 57% *ee*. The irregularities do not follow a pattern and, in some cases, seem to be dependent on the diorganozinc reagent used. Racemization in the ligands can be excluded, as all ligand stock solutions were first checked for optical purity. These irregularities may indicate NLEs and thus offer great potential. A more intensive investigation of these enantiomeric pairs in the future could offer new perspectives and makes those compounds interesting candidates for enhanced asymmetry. In the group of cyclic bounded amines, further anomalies in connection with a dependence on the diorganozinc reagent used are accumulating. In particular, the group of alkylations with diisopropylzinc shows deviations in the product configuration in four cases compared to dimethyl and diethylzinc. The products of the diisopropylation of prolinol derivatives *R*-**106**, *S*-**117**, and morpholine derivative **107** were obtained in the same configuration as given by the ligand, thus reversed to the alkylations with dimethyl- and diethylzinc. The same is observed for the benzylated phenylalaninol derivative *S*-**116**. For the methylation reactions, benzylated prolinol derivative *S*-**110** results in the *S*-product deviating form the other two alkylations. As previously mentioned and reported in the

literature, the ligand **105** also appears reversed for ethylations.[146]

The chapter successfully identified promising anomalies in certain ligand selectivities and trends in *N*-methylated and *N*-benzylated derivatives of primary β -amino alcohols that laid a foundation for further work. The spectrum of this structural motif is far from exhausted by the catalyst pool presented. A variety of further substitution patterns on the N-side and the β-carbon atom are possible and offer limitless perspectives for discovering further candidates with good enantioselectivities and finally converting them to the β-amino aldehyde target structures.

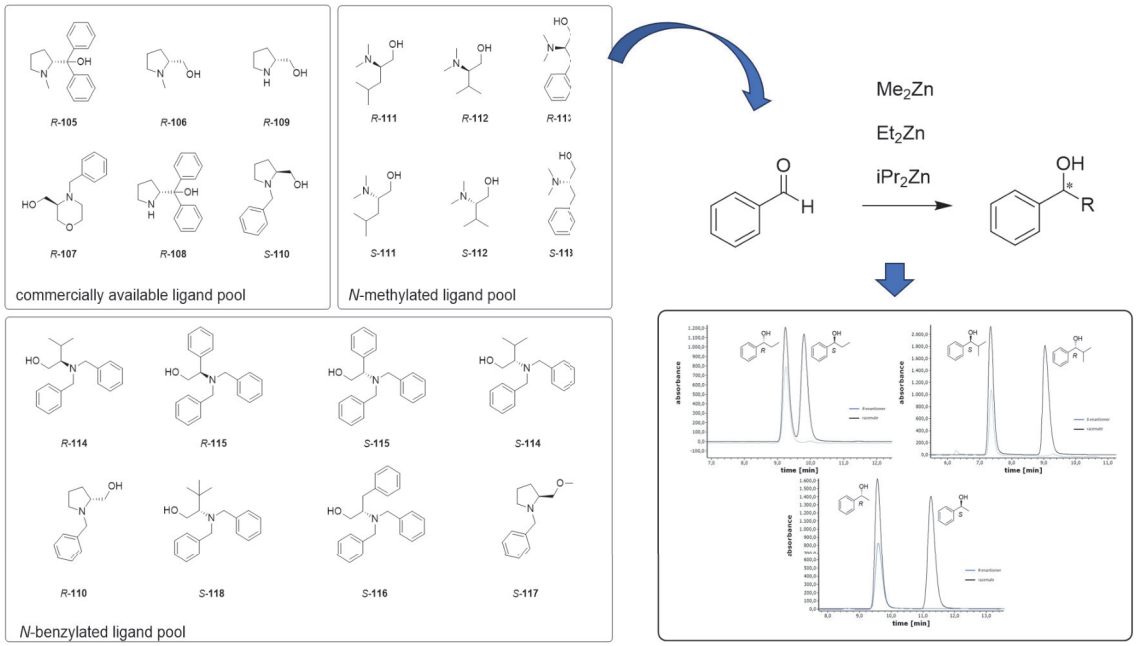

Figure 4.15: Overview of primary β-amino alkohol ligands tested in asymmetric alyklations with benzaldehyde.

5 Overview and Outlook

The present work, which is generally concerned with the development of substrates with autocatalytic potential in alkylations with diorganozinc reagents, followed two different approaches based on literature-reported results. The first chapter was directed towards the synthesis and characterization of potential new dynamic ligands based on the transient hemiacetal species that was found to be the catalytically active structure in the autocatalytic Soai reaction.[76] The target structures were atropisomers bearing chiral information and possessing an aldehyde group within spatial distance to an alcohol moiety that allows cyclic hemiacetal formation under the formation of a new stereocenter. Literature-reported equilibria in these structure motifs thus provide the prerequisites to serve as a substrate as well as a potential ligand in a Soai-like reaction.

The first approach was based on a reported temperature-dependent equilibrium for coumestan-derived compounds, including the target structure motif by *Tang et al.*. The results, including a temperature-dependent equilibrium in these structures, could not be confirmed. In addition, a precursor in the synthesis pathway to the target compounds turned out to be present in a dominant unfavorable tautomeric conformation interrupting the further synthesis process. The shifted tautomeric equilibrium of these β-ketoaldehyde precursors (compounds **42**-**49**), which was not reported in the literature, was examined in more detail. In summary, seven novel 2,3-Bis(2-methoxyphenyl)-3-oxopropanals (compounds **42**-**49**) with electron withdrawing and electron donating groups were investigated in context to their tautomeric equilibria including temperature and time-dependent experiments. An extreme stabilization of a single enol-tautomer in the overall keto-enol equilibrium was successfully identified, resulting from a hydrogen-bonded proton in a six-membered ring, that is electronically stabilized between the two carbonyl groups. Most noteworthy is the discovery of a conformational 'memory effect' in the hydrogen-bonded six-membered ring at low temperatures that lead to a complete fixation, even if subsequently elevated tem-

peratures are applied.
The further approach to access compounds, comprising a dynamic aldehyde-alcohol motif, was based on simpler axial biaryl structures. A total of seven structures with the selected aldehyde-alcohol motif, based on a biaryl optionally containing a naphthyl unit or a binaphthyl backbone, could be accessed (compounds **59**, **65**, **66**, **69**, **78**, **79**, **83**). Six of them were successfully synthesized in an optimized, simple one-step Suzuki-coupling reaction, which could provide a new, very easy access to this kind of structure motif compared to the synthesis pathway of the two reference compounds **66** and **69** described in the literature. Solvent-dependent ^{1}H NMR and temperature-dependent DHPLC investigations revealed that the equilibria were exclusively found to be either on the open-chain aldehyde side or in the cyclic-closed hemiacetal form for all seven compounds. The task of finding a structure in a suitable state of equilibrium quickly turned out to be a narrow burr walk in the substitution patterns around the biaryl axis. The subsequent unsuccessful alkylation test reactions with the open-chain aldehyde structures (compounds **65** and **69**) present, confirmed the structure motif as unsuitable for the proposed research objective. The synthesized hemiacetals were nevertheless able to show good ligand properties in alkylations on benzaldehyde. The simple and short synthetic pathway presented, starting from commercially available reactants, provides numerous structural perspectives for this novel type of ligand. An enantiomerically pure application could therefore be promising in metal-mediated asymmetric catalyses. Other structural motifs that possess the ability to form an intramolecular ring closure in the proximity of a carbonyl function, such as thiols or amine functions, are also conceivable. In addition, the interconversion barriers and activation parameters of three novel hemiacetal compounds (**78**, **79**, and **83**) could be determined in DHPLC studies. Thereby, a correspondence between the determined interconversion barriers of nicotinaldehydes (**79** and **83**) and the postulated catalytically active hemiacetal species in the Soai reaction could be successfully confirmed.
The second main part of this work presented a concept for the development of new autocatalytic substrates based on various literature-known results with β-amino alcohols in alkylation reactions. As part of an internal collaboration project, primary β-amino alcohols that possess the possibility to be oxidized to β-amino aldehydes were investigated for their enantioselectivity and catalytic activity. The focus has been on previously successfully synthesized *N*-methylated and *N*-benzylated derivatives that were used as ligands in the alkylation of benzaldehyde. In complete, the catalyst pool contained 20 different

ligands also comprising six commercially available ligands. In test reactions with three different diorganozinc reagents, trends related to the substitution pattern were observed. For *N*-methylated primary β-amino alcohol derivatives, increased selectivities (up to 72% *ee*) were observed with diisopropylzinc, whereas the benzylated derivatives were more selective with dimethylzinc and diethylzinc in the case of an open-chain amine function. In particular, the predominance of higher selectivities obtained with dimethylzinc (up to 68% *ee*) compared to the use of diethylzinc (up to 58% *ee*) was remarkable compared to published results in the literature. In the case of cyclically bound amines such as prolinol or morpholine derivatives, the trend for both benzylated and methylated derivatives tends towards increased selectivities in the presence of diisopropyl. Furthermore, in a comparative study with several enantiomeric pairs, sometimes large deviations were found that could indicate a non-linear correlation. In some cases, unexpectedly reversed enantioselectivities could be observed depending on the transferred alkyl chain. These effects occurred increased for prolinol derivatives and in alkylations with diisopropylzinc in the present test pool. These examples indicate non-linear effects, which makes these structures particularly interesting as these effects are usually accompanied by the inhibition or amplification of a single enantiomer.

Since the selectivity also depends to a large extent on the product used, no clear prediction can be made about the final outcome of the alkylations with the final β-amino aldehyde target structures. The present study shows that pre-screening with regard to the alkyl chain to be transferred is a useful tool in order to avoid an unnecessary enlargement of the test series with different diorganozinc reagents. Since structural possibilities go far beyond the tested ligand pool, this approach offers a wide range of possibilities for a potential target structure, but it makes it more difficult to limit the pool to the structures with the highest potential. The coherent dependencies between the substrate, the transferred alkyl chain, and the substitution pattern at the β-amino alcohol that always allow only small insights into possible reactivity patterns make the development quite challenging. The potential of β-amino alcohols in asymmetric catalyses is undisputed by countless literature references and makes the further development towards β-amino aldehydes very promising candidates for the realization of the discovery of new autocatalytically active substrates. Even if intensive field research and pre-screening is probably necessary, the effort could be worthwhile.

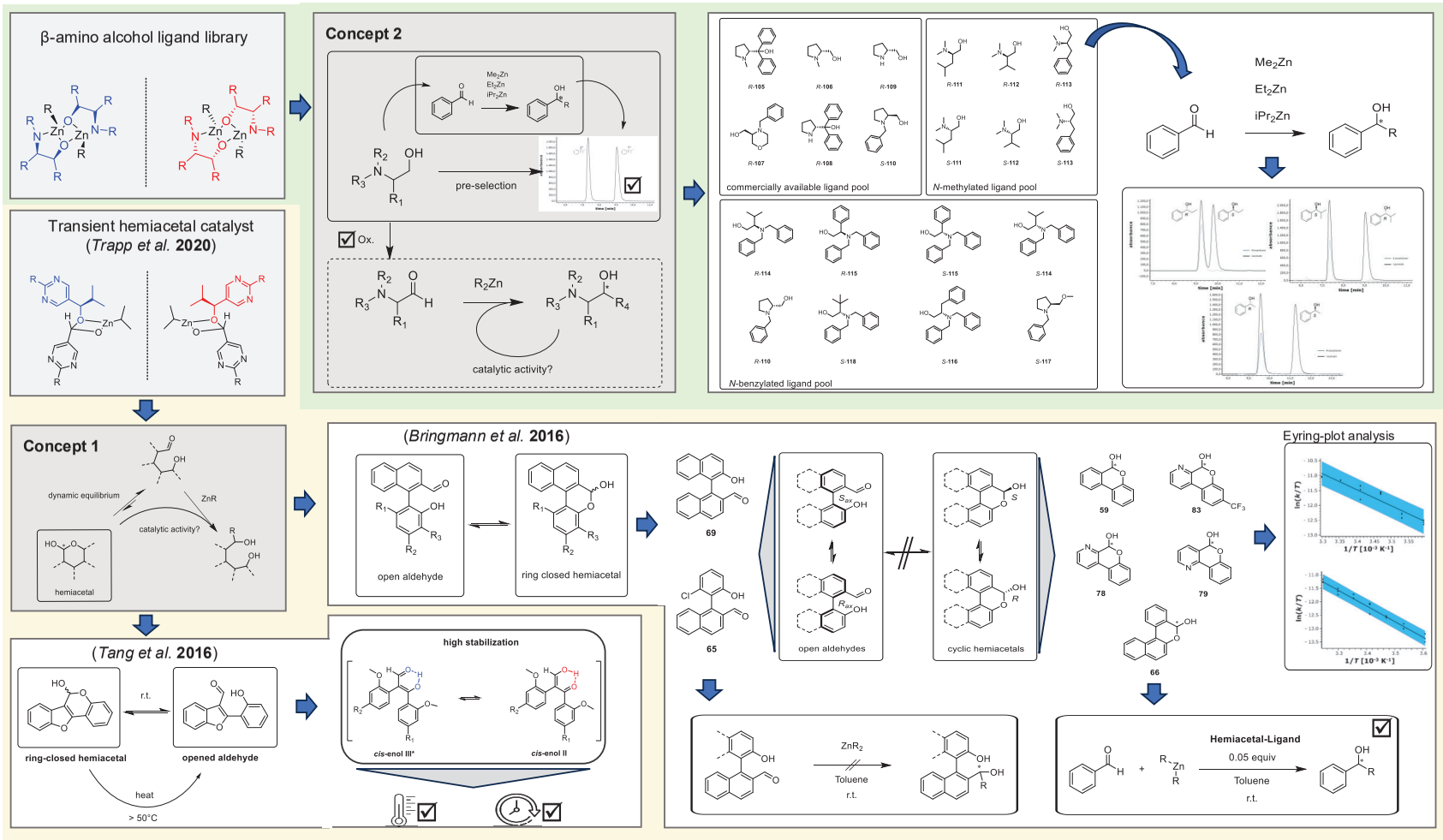

Figure 5.1: Summarized overview of the thesis topics dealing with concepts and synthesis towards substrates with autocatalytic potential; yellow: hemiacetal approach in accordance with reported transient hemiacetal catalyst in the Soai reaction by *Trapp et al*[76]; green: an approach based on enantioselective β-amino alcohols towards β-amino aldehydes, including the pre-screening of primary β-amino alcohols for this purpose presented in the present work.

6 Experimental

6.1 Work methods

6.1.1 Preliminary Remarks

General Procedures

Air and moisture-sensitive syntheses were carried out within an argon atmosphere under the exclusion of air and moisture. The argon gas was dried by silica gel and molecular sieve (4 Å). All glassware was flame-dried prior to use and standard Schlenk techniques were applied. The given yields refer to isolated and purified products.

Solvents and Reagents

Solvents (DCM, Et_2O, *n*-pentane, THF, and toluene) were dried in a MB SPS-800 system and stored under nitrogen. All other anhydrous solvents used were bought and directly used or stored under the exclusion of air and moisture. Degassing was accomplished by at least three Freeze-Pump-Thaw cycles. The anhydrous and degassed solvents were stored under argon over a molecular sieve (3 Å). Argon gas (Ar 5.0) was purchased from Air Liquide Deutschland GmbH and purified as described above. All other solvents and chemicals were purchased from manufacturing and trading companies (abcr GmbH, Acros Organics b.v.b.a., Sigma-Aldrich Co. LLC, Strem Chemicals Inc., and TCI Europe N.V.) and stored according to the respective instructions. Isolated compounds were stored under argon and, if needed, at 5 or -20°C, respectively.

6.1.2 Analytical Methods

NMR Spectroscopy

NMR spectra were recorded on a 400 MHz Bruker Advance III HD spectrometer and a 400 MHz Bruker Avance III HD spectrometer with a CyroProbe Prodigy. NMR spectra of air and moisture-sensitive compounds were measured using J. Young NMR tubes. The solvent residual signals were used for internal calibration.[179] Chemical shifts δ are reported in ppm and coupling constants J in Hz. The different multiplicities are defined by s (singlet), d (doublet), t (triplet) or m (multiplet). The assignments in ^{13}C NMR spectra refer to proton-decoupled experiments. The assignment of all signals was realized by two-dimensional NMR spectroscopy (^{1}H-^{1}H-COSY, ^{1}H-^{13}C-HSQC-ME and ^{1}H-^{13}C-HMBC experiments). Atom numbering for NMR assignments is not based on IUPAC nomenclature.

Mass Spectrometry

Mass spectrometric measurements were performed on a Thermo Finnigan LTQ Ultra FT-ICR or on a Thermo Scientific Q Exactive Plus mass spectrometer. The mode (positive/negative) of the experiment and the solvents used to solve the sample are listed. The m/z value of the most abundant or characteristic peak is given in comparison to the calculated m/z value. In the case of characteristic peaks, the abundance is given in percent. If isotopic patterns are pronounced, the most intensive peak is indicated. Molecular ions are abbreviated as M.

Vibrational Spectroscopy

IR spectra were recorded on a Thermo Scientific Nicolet 700 ATR-FT-IR spectrometer using the purified products without further modification. The background transmission was measured before the sample measurement and subtracted. Wave numbers $\tilde{v}$ are given in cm^{-1}.

High-performance liquid Chromatography (HPLC)

HPLC measurements were performed on an Agilent 1200 series high-performance liquid chromatograph from Agilent technologies (Santa Clara, CA, United States). All relevant measurements were performed with the chiralpak columns from Daicel Corporation (Osaka/Tokyo, Japan). The injection volume was 1.0 μL, the flow was 1.0 ml·min^{-1}, and the temperature varied depending on the measurement and is indicated by T. The standard injection volume was set to 1.0 μL. A mixture of *n*-hexane and isopropanol was used as eluent. The standard wavelength λ of the UV detector was usually set to 210 nm if not stated otherwise.

6.2 Chapter 1.1

6.2.1 General Procedure for the Synthesis of α, β-Epoxy ketones (WI1)

The optimized synthesis of all α, β-epoxy ketones **34-41** was carried out in accordance to *L. Ruan et al.*.[104]

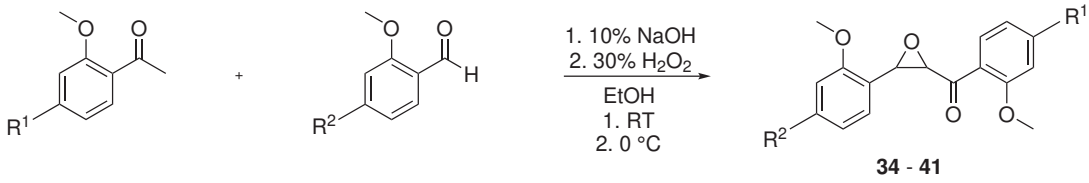

R^1: H (**51**), OMe (**52**)

R^2: H (**53**), Me (**54**), OMe (**55**), CF_3 (**56**), NO_2 (**57**)

2-Methoxybenzaldehyde **53-57** was solved in EtOH (95%) followed by the addition of 2-Methoxyacetophenone **51-52**. Subsequently, the solution was slowly added NaOH (10%), and the resulting mixture was stirred for 1 h at room temperature. The reaction process was monitored by using TLC. After completion, the reaction mixture was cooled, and H_2O_2 (30%) was added dropwise. The mixture was stirred again for 1 h at room temperature. The resulting precipitate was filtered off and washed three times with H_2O (dest.) and three times with EtOH (95%). The solvent was removed *in vacuo* to yield α, β-epoxy ketones **34-41** as colorless to yellow solids.

(2-Methoxyphenyl)(3-(2-methoxyphenyl)oxiran-2-yl)methanon 34

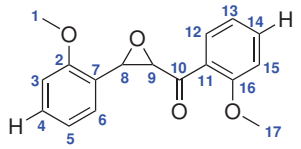

34

2-Methoxybenzaldehyde **53** (2.72 g, 20.0 mmol, 1.00 equiv.), EtOH (95%, 40 ml), 1-(2-Methoxyphenyl)ethan-1-one **51**(2.76 ml, 20.0 mmol, 1.00 equiv.), NaOH (10%, 10.0 ml, 25.0 mmol, 1.25 equiv.), H_2O_2 (30%, 6.60 ml, 64.0 mmol, 3.20 equiv.). Compound **34** (4.57 g, 16.1 mmol, 80%) was obtained as white-yellow solid.

^{1}H NMR ($CDCl_3$, 600 MHz, 295 K): δ(ppm) = 7.83 (d_d, ^{3}J = 7.7 Hz, ^{4}J = 1.8 Hz, 1H, H^{12}), 7.51(t_d, ^{3}J = 7.7 Hz, ^{4}J = 1.8 Hz, 1H, H^{14}), 7.31 (t_d, ^{3}J = 8.1 Hz, ^{4}J = 1.8 Hz, 1H, H^{4}), 7.27 (d_d, ^{3}J = 7.6 Hz, ^{4}J = 1.8 Hz, 1H, H^{6}), 7.05 (t_d, ^{3}J = 7.6 Hz, ^{4}J = 0.9 Hz, 1H, H^{13}, 6.98 (t_d, ^{3}J = 8.0 Hz, ^{4}J = 1.4 Hz, 1H, H^{5}), 6.94 (d, ^{3}J = 8.4 Hz, 1H, H^{15}), 6.91 (d,^{3}J = 8.3 Hz, 1H, H^{3}), 4.26 (d, ^{3}J = 1.9 Hz, 1H, H^{8}), 4.38 (d, ^{3}J = 1.9 Hz, 1H, H^{9}), 3.84 (s, 3H, H^{1}), 4.38 (s, H^{17}).

^{13}C{^{1}H} NMR ($CDCl_3$, 151 MHz, 295 K): δ(ppm) = 195.7 (C^{10}), 159.9 (C^{16}), 158.8 (C^{2}), 135.0 (C^{14}), 131.0 (C^{12}), 129.8 (C^{4}), 126.6 (C^{11}), 125.6 (C^{6}), 125.3 (C^{7}), 121.3 (C^{13}), 121.1 (C^{5}), 111.9 (C^{15}), 110.6 (C^{3}), 64.2 (C^{8}), 56.1 (C^{9}), 56.0 (C^{17}), 55.9 (C^{1}).

IR: $\tilde{v}$ = 3065, 3000, 2926, 2839, 1674, 1595, 1495, 1484, 1463, 1436, 1285, 1247, 1210, 1160, 1111, 1101, 1025, 1013, 897, 842, 766, 756, 746, 730 cm^{-1}.

MS (EI^{+}, acetone): $[M+H]^{+}$: $C_{17}H_{16}O_4$+H^{+}, calculated *m/z* 284.1049, found *m/z* 284.1053.

(3-(2-Methoxy-4-methylphenyl)oxiran-2-yl)(2-methoxyphenyl)methanon 35

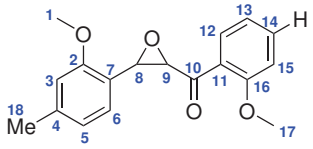

35

2-Methoxy-4-methylbenzaldehyde **54** (1.50 g, 10.0 mmol, 1.00 equiv.), EtOH (95%, 20 ml), 1-(2-Methoxyphenyl)ethan-1-one **51** (1.38 ml, 10.0 mmol, 1.00 equiv.), NaOH (10%, 12.0 ml, 30.0 mmol, 3.00 equiv.), H_2O_2 (30%, 4.10 ml, 40.0 mmol, 4.00 equiv.). Compound **35** (0.970 g, 3.25 mmol, 33%) was obtained as pale yellow solid.

^{1}H NMR ($CDCl_3$, 600 MHz, 295 K): δ(ppm) = 7.80 (d_d, ^{3}J = 7.7 Hz, ^{4}J = 1.8 Hz, 1H, H^{12}), 7.49 (t_d, ^{3}J = 8.4 Hz, ^{4}J = 1.8 Hz, 1H, H^{14}), 7.12 (d, ^{3}J = 7.7 Hz, 1H, H^{6}), 7.02 (t_d,

^{3}J = 7.6 Hz, ^{4}J = 1.0 Hz, 1H, H^{13}), 6.92 (d, ^{3}J = 8.5 Hz, 1H, H^{15}), 6.77 (d_d, ^{3}J = 7.7 Hz, ^{4}J = 1.5 Hz, 1H, H^{5}), 6.70 (s, 1H, H^{3}), 4.31 (d,^{3}J = 1.9 Hz, 1H, H^{8}), 4.24 (d, ^{3}J = 2.0 Hz, 1H, H^{9}), 3.80 (s, 3H, H^{1}), 3.66 (s, 3H, H^{17}), 2.35 (s, 3H, H^{18}).

$^{13}C\{^{1}H\}$ NMR ($CDCl_3$, 151 MHz, 295 K): δ(ppm) = 195.8 (C^{10}), 159.7 (C^{16}), 158.6 (C^{2}), 139.9 (C^{4}), 134.8 (C^{14}), 130.9 (C^{12}), 126.8 (C^{11}), 125.5 (C^{6}), 122.1 (C^{7}), 121.6 (C^{5}), 121.1 (C^{13}), 111.8 (C^{15}), 111.5 (C^{3}), 63.9 (C^{9}), 56.1 (C^{8}), 55.8 (C^{17}), 55.6 (C^{1}), 21.9 (C^{18}).

IR: $\tilde{\nu}$ = 2938, 2843, 1678, 1614, 1596, 1578, 1486, 1465, 1440, 1406, 1307, 1288, 1274, 1253, 1186, 1164, 1117, 1072, 1037, 1027, 1017, 965, 927, 895, 850, 834, 821, 770, 716, 685, 651 cm^{-1}.

MS (EI^+, acetone): $[M+H]^+$: $C_{18}H_{18}O_4$+H^+, calculated *m/z* 298.1205, found *m/z* 298.1201.

(3-(2,4-Dimethoxyphenyl)oxiran-2-yl)(2-methoxyphenyl)methanon 36

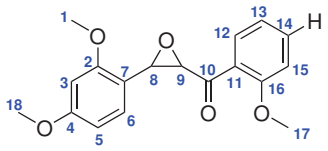

36

2,4-Dimethoxybenzaldehyde **55** (1.66 g, 10.0 mmol, 1.00 equiv.), EtOH (95%, 20 ml), 1-(2-Methoxyphenyl)ethan-1-one **51** (1.38 ml, 10.0 mmol, 1.00 equiv.), NaOH (10%, 14.0 ml, 35.0 mmol, 3.50 equiv.), H_2O_2 (30%, 4.60 ml, 45.0 mmol, 4.50 equiv.). Compound **36** (2.11 g, 6.71 mmol, 67%) was obtained as yellow solid.

^{1}H NMR ($CDCl_3$, 600 MHz, 295 K): δ(ppm) = 7.82 (d_d, ^{3}J = 7.7 Hz, ^{4}J = 1.8 Hz, 1H, H^{12}), 7.51 (t_d, ^{3}J = 8.5 Hz, ^{4}J = 1.9 Hz, 1H, H^{14}), 7.17 (d, ^{3}J = 8.4 Hz, 1H, H^{6}), 7.04 (t_d, ^{3}J = 7.5 Hz, ^{4}J = 0.9 Hz, 1H, H^{13}), 6.94 (d, ^{3}J = 8.3 Hz, 1H, H^{15}), 6.50 (d_d, ^{3}J = 8.4 Hz, ^{4}J = 2.4 Hz, 1H, H^{5}), 6.47 (s, 1H, H^{3}), 4.29 (d,^{3}J = 1.9 Hz, 1H, H^{9}), 4.27 (d, ^{3}J = 1.9 Hz, 1H, H^{8}), 3.82 (s, 3H, H^{18}), 3.81 (s, 3H, H^{1}), 3.69 (s, 3H, H^{17}).

$^{13}C\{^{1}H\}$ NMR ($CDCl_3$, 151 MHz, 295 K): δ(ppm) = 195.7 (C^{10}), 161.2 (C^{4}), 159.7 (C^{2}), 159.6 (C^{16}), 134.8 (C^{14}), 130.8 (C^{12}), 126.5 ($C^{6/11}$), 126.5 ($C^{6/11}$), 125.5 (C^{6}), 121.0 (C^{13}), 117.5 (C^{7}), 111.7 (C^{15}), 104.6 (C^{5}), 98.4 (C^{3}), 63.9 (C^{8}), 56.0 (C^{9}), 55.7 (C^{17}), 55.6 ($C^{1/18}$), 55.6 ($C^{1/18}$).

IR: $\tilde{v}$ = 2988, 2963, 2940, 2835, 1673, 1617, 1595, 1577, 1508, 1465, 1454, 1437, 1344, 1309, 1288, 1254, 1205, 1159, 1116, 1070, 1047, 1024, 1015, 963, 925, 864, 833, 810, 771, 685, 652 cm^{-1}.

MS (EI^+, acetone): $[M+H]^+$: $C_{18}H_{18}O_5$+H^+, calculated m/z 314.1154, found m/z 314.1147.

(3-(2-Methoxy-4-(trifluoromethyl)phenyl)oxiran-2-yl)(2-methoxyphenyl)methanon 37

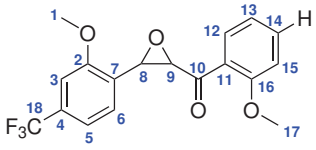

37

2-Methoxy-4-(trifluoromethyl)benzaldehyde **56** (1.01 g, 4.49 mmol, 1.00 equiv.), EtOH (95%, 20 ml), 1-(2-Methoxyphenyl)ethan-1-one **51** (1.00 ml, 4.49 mmol, 1.00 equiv.), NaOH (10%, 2.5 ml, 6.18 mmol, 1.25 equiv.), H_2O_2 (30%, 1.60 ml, 15.8 mmol, 3.20 equiv.). Compound **37** (1.34 g, 3.80 mmol, 77%) was obtained as colorless solid.

^{1}H NMR ($CDCl_3$, 600 MHz, 295 K): δ(ppm) = 7.84 (d_d, ^{3}J = 7.7 Hz, ^{4}J = 1.8 Hz, 1H, H^{12}), 7.53 (t_d, ^{3}J = 8.3 Hz, ^{4}J = 1.8 Hz, 1H, H^{14}), 7.39 (d, ^{3}J = 7.9 Hz, 1H, H^{6}), 7.26-7.25 (m, 1H, H^{5}), 7.11 (s, 1H, H^{3}), 7.06 (t_d, ^{3}J = 7.6 Hz, ^{4}J = 1.0 Hz, 1H, H^{13}), 6.96 (d, ^{3}J = 8.4 Hz, 1H, H^{15}), 4.38 (d,^{3}J = 2.0 Hz, 1H, H^{9}), 4.22 (d, ^{3}J = 1.9 Hz, 1H, H^{8}), 3.90 (s, 3H, H^{1}), 3.67 (s, 3H, H^{17}).

$^{13}C\{^{1}H\}$ NMR ($CDCl_3$, 151 MHz, 295 K): δ(ppm) = 194.9 (C^{10}), 159.7 (C^{16}), 158.4

(C^2), 135.2 (C^{14}), 132.0-131.3 (q, $^3J_{C\text{-}F}$ = 32.3, C^{14}), 130.9 (C^{12}), 129.3 (C^7), 126.8-131.3 (q, $^1J_{C\text{-}F}$ = 270.8, C^{18}) , 126.2 (C^{11}), 125.9 (C^6), 121.2 (C^{13}), 117.9-117.8 (q, $^3J_{C\text{-}F}$ = 3.7, C^5), 111.9 (C^{15}), 107.1-107.0 (q, $^3J_{C\text{-}F}$ = 3.8, C^3), 63.8 (C^8), 55.9 (C^1), 55.7 (C^{17}), 55.2 (C^9).

IR: $\tilde{v}$ = 2937, 2846, 1683, 1616, 1597, 1577, 1486, 1462, 1412, 1346, 1321, 1289, 1254, 1247, 1213, 1163, 1118, 1078, 1028, 1017, 917, 958, 895, 861, 832, 799, 771, 739 cm^{-1}.

MS (EI^+, acetone): $[M+H]^+$: $C_{18}H_{15}F_3O_4$+H^+, calculated *m/z* 352.0922, found *m/z* 352.0914.

(3-(2-Methoxy-4-nitrophenyl)oxiran-2-yl)(2-methoxyphenyl)methanon 38

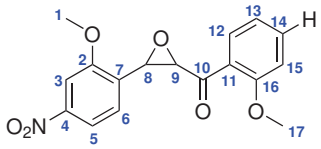

38

2-Methoxy-4-nitrobenzaldehyde **57** (1.09 g, 6.00 mmol, 1.00 equiv.), EtOH (95%, 15 ml), 1-(2-Methoxyphenyl)ethan-1-one **51** (830 μl, 6.00 mmol, 1.00 equiv.), NaOH (10%, 3.00 ml, 7.50 mmol, 1.25 equiv.), H_2O_2 (30%, 2.00 ml, 19.6 mmol, 3.27 equiv.). Compound **38** (0.571 g, 1.70 mmol, 28%) was obtained as pale yellow solid.

^{1}H NMR ($CDCl_3$, 600 MHz, 295 K): δ(ppm) = 7.86 (d, ^3J = 8.4 Hz, 1H, H^6), 7.82 (d_d, ^3J = 7.8 Hz, ^4J = 1.8 Hz, 1H, H^{12}), 7.74 (s, 1H, H^3), 7.52 (t_d, ^3J = 7.6 Hz, ^4J = 1.0 Hz, 1H, H^{14}), 7.41 (d, ^3J = 8.4 Hz, 1H, H^5), 7.05 (t, ^3J = , 1H, H^{13}), 6.94 (d, ^3J = 8.4 Hz, 1H, H^3), 4.37 (d,^3J = 1.9 Hz, 1H, H^9), 4.20 (d, ^3J = 1.7 Hz, 1H, H^8), 3.94 (s, 3H, H^1), 3.65 (s, 3H, H^{17}).

$^{13}C\{^1H\}$ NMR ($CDCl_3$, 151 MHz, 295 K): δ(ppm) = 194.4 (C^{10}), 159.8 (C^{16}), 158.6 (C^2), 149.0 (C^4), 135.2 (C^{14}), 132.9 (C^7), 131.0 (C^{12}), 126.2 (C^{11}), 126.1 (C^6), 121.4 (C^{13}), 116.4 (C^5), 111.8 (C^{15}), 105.4 (C^3), 63.9 (C^8), 56.3 (C^1), 55.8 (C^{17}), 55.0 (C^9).

IR: $\tilde{\upsilon}$ = 3119, 2949, 2875, 1657, 1615, 1598, 1579, 1519, 1485, 1466, 1406, 1340, 1310, 1283, 1254, 1243, 1214, 1162, 1117, 1055, 1021, 1010, 957, 906, 865, 840, 810, 760, 736, 687, 654 cm^{-1}.

HR-MS (ESI^-, acetone): $[M-H]^-$: $C_{17}H_{14}NO_6$-H^+, calculated *m/z* 328.0821, found *m/z* 328.0827.

(3-(2,4-Dimethoxyphenyl)oxiran-2-yl)(2-methoxyphenyl)methanon 39

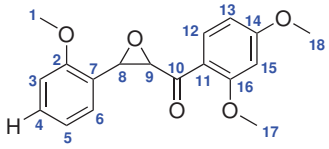

39

2-Methoxybenzaldehyde **53** (1.36 g, 10.0 mmol, 1.00 equiv.), EtOH (95%, 20 ml), 1-(2,4-Dimethoxyphenyl)ethan-1-one **52** (1.80 g, 10.0 mmol, 1.00 equiv.), NaOH (10%, 10.0 ml, 25.0 mmol, 2.50 equiv.), H_2O_2 (30%, 4.00 ml, 38.8 mmol, 3.88 equiv.). Compound **39** (2.28 g, 7.26 mmol, 73%) was obtained as colorless solid.

^{1}H NMR ($CDCl_3$, 600 MHz, 295 K): δ(ppm) = 7.88 (d, ^3J = 8.7 Hz, 1H, H^{12}), 7.28 (t_d, ^3J = 8.2 Hz, ^4J = 1.8 Hz, 1H, H^4), 7.26 (d_d, ^3J = 7.7 Hz, ^4J = 1.8 Hz, 1H, H^6), 6.96 (t, ^3J = 8.1 Hz, 1H, H^5), 6.88 (d_d, ^3J = 8.2 Hz, ^4J = 1.0 Hz, 1H, H^3), 6.55 (d_d, ^3J = 8.7 Hz, ^4J = 2.3 Hz, 1H, H^{13}), 6.39 (s, 1H, H^{15}), 4.33 (d,^3J = 2.0 Hz, 1H, H^9), 4.24 (d, ^3J = 1.9 Hz, 1H, H^8), 3.84 (s, 3H, H^{18}), 3.81 (s, 3H, H^1), 3.60 (s, 3H, H^{17}).

^{13}C{^{1}H} NMR ($CDCl_3$, 151 MHz, 295 K): δ(ppm) = 193.4 (C^{10}), 165.5 (C^{14}), 161.8 (C^{16}), 159.8 (C^2), 133.1 (C^{12}), 129.5 (C^4), 125.5 (C^6), 125.4 (C^7), 120.9 (C^5), 119.7 (C^{11}), 110.5 (C^3), 105.9 (C^{13}), 98.4 (C^{15}), 64.1 (C^8), 55.8 (C^{18}), 55.8 (C^{17}), 55.7 (C^1), 55.6 (C^9).

IR: $\tilde{\upsilon}$ = 2994, 2975, 2944, 2834, 1654, 1602, 1578, 1496, 1467, 1427, 1339, 1283, 1257,

1251, 1213, 1188, 1176, 1104, 1064, 1047, 1022, 939, 904, 875, 836, 819, 768, 742, 688 cm^{-1}.

MS (EI^+, acetone): $[M+H]^+$: $C_{18}H_{18}O_5$+H^+, calculated m/z 314.1154, found m/z 314.1149.

(2,4-Dimethoxyphenyl)(3-(2-methoxyphenyl)oxiran-2-yl) methanon 40

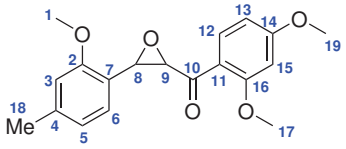

40

2-Methoxy-4-methylbenzaldehyde **54** (1.50 g, 10.0 mmol, 1.00 equiv.), EtOH (95%, 20 ml), 1-(2,4-Dimethoxyphenyl)ethan-1-one **52** (1.80 g, 10.0 mmol, 1.00 equiv.), NaOH (10%, 10.0 ml, 25.0 mmol, 2.50 equiv.), H_2O_2 (30%, 4.00 ml, 39.0 mmol, 3.9 equiv.). Compound **40** (376 mg, 1.15 mmol, 11%) was obtained as light yellow solid.

^{1}H NMR ($CDCl_3$, 600 MHz, 295 K): δ(ppm) = 7.87 (d, ^3J = 8.7 Hz, 1H, H^{12}), 7.12 (d, ^3J = 7.7 Hz, 1H, H^6), 6.77 (s, 1H, H^5), 6.69 (s, 1H, H^3), 6.54 (d_d, ^3J = 8.8 Hz, ^4J = 2.3 Hz, 1H, H^{13}), 6.39 (s_d, ^4J = 2.3 Hz, 1H, H^{15}), 4.28 (d, ^3J = 2.0 Hz, 1H, H^9), 4.25 (d,^3J = 2.0 Hz, 1H, H^8), 3.84 (s, 3H, H^{19}), 3.79 (s, 3H, H^1), 3.61 (s, 3H, H^{17}), 2.35 (s, 3H, H^{18}).

^{13}C{^{1}H} NMR ($CDCl_3$, 151 MHz, 295 K): δ(ppm) = 193.6 (C^{10}), 165.5 (C^{14}), 161.8 (C^2), 158.6 (C^{16}), 139.7 (C^4), 133.1 (C^{12}), 125.5 (C^6), 122.3 (C^7), 121.5 (C^3), 119.8 (C^{11}), 111.5 (C^3), 105.8 (C^{13}), 98.4 (C^{15}), 64.0 (C^8), 55.8 ($C^{1/9/17/19}$), 55.7 ($C^{1/9/17/19}$), 55.6 ($C^{1/9/17/19}$), 21.9 (C^{18}).

IR: $\tilde{\nu}$ = 2938, 2843, 1677, 1653, 1598, 1578, 1509, 1463, 1439, 1425, 1406, 1284, 1255, 1214, 1191, 1115, 1073, 1021, 1010, 943, 928, 897, 843, 832, 821, 807, 771, 716, 660, 652 cm^{-1}.

MS (EI^+, acetone): $[M+H]^+$: $C_{19}H_{20}O_5$+H^+, calculated m/z 328.1311, found m/z 328.1307.

(2,4-Dimethoxyphenyl)(3-(2,4-dimethoxyphenyl)oxiran-2-yl) methanon 41

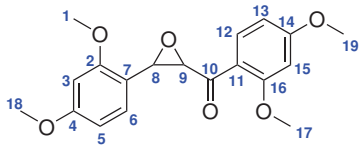

41

2-Methoxy-4-methylbenzaldehyde **55** (1.66 g, 10.0 mmol, 1.00 equiv.), EtOH (95%, 20 ml), 1-(2,4-Dimethoxyphenyl)ethan-1-one **52** (1.80 g, 10.0 mmol, 1.00 equiv.), NaOH (10%, 10.0 ml, 25.0 mmol, 2.50 equiv.), H_2O_2 (30%, 4.00 ml, 39.0 mmol, 3.9 equiv.). Compound **41** (1.59 g, 4.62 mmol, 46%) was obtained as colorless solid.

^{1}H NMR ($CDCl_3$, 600 MHz, 295 K): δ(ppm) = 7.88 (d, ^3J = 8.8 Hz, 1H, H^{12}), 7.16 (d, ^3J = 8.5 Hz, 1H, H^6), 6.55 (d_d, ^3J = 8.8 Hz, ^4J = 2.3 Hz, 1H, H^{13}), 6.48 (d, ^3J = 8.7 Hz, 1H, H^3), 6.40 (s, 1H, H^{15}), 4.26 (d, ^3J = 2.1 Hz, 1H, H^8), 4.24 (d,^3J = 2.2 Hz, 1H, H^9), 3.84 (s, 3H, H^{19}), 3.81 (s, 3H, H^{18}), 3.79 (s, 3H, H^1), 3.63 (s, 3H, H^{17}).

^{13}C{^{1}H} NMR ($CDCl_3$, 151 MHz, 295 K): δ(ppm) = 193.6 (C^{10}), 165.5 (C^{14}), 161.9 (C^{16}), 161.2 (C^4), 159.8 (C^2), 133.0 (C^{12}), 126.5 (C^6), 119.8 (C^{11}), 117.8 (C^7), 105.8 (C^{13}), 104.7 (C^6), 98.5 (2C, $C^{3/15}$), 64.0 (C^8), 55.8 (C^{19}), 55.7 (3C, $C^{1,17,18}$), 55.6 (C^9).

IR: $\tilde{v}$ = 2967, 2943, 2909, 1654, 1618, 1599, 1571, 1561, 1508, 1468, 1463, 1427, 1336, 1295, 1254, 1205, 1158, 1119, 1105, 1081, 1040, 1017, 936, 922, 906, 884, 845, 829, 826, 781, 729, 683, 669 cm^{-1}.

MS (EI^+, acetone): $[M+H]^+$: $C_{19}H_{20}O_6$+H^+, calculated m/z 344.1260, found m/z 344.1257.

6.2.2 General Procedure for the Synthesis of β-Ketoaldehydes 42-48 (WI2)

The optimized synthesis of all β-ketoaldehydes **42-48** was carried out in accordance to *L. Ruan et al.* and *P. Mathew et al.*.[104,105]

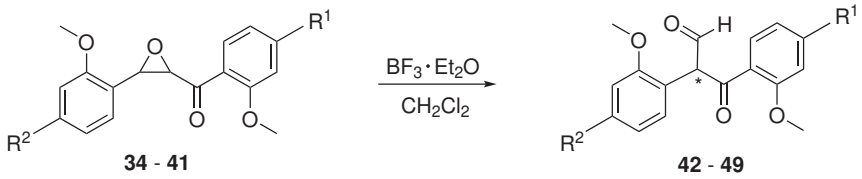

R^1: H, OMe
R^2: H, Me, OMe, CF_3, NO_2

A Schlenk-flask was charged with the corresponding α, β-epoxy ketone **34-41** solved in DCM and subsequently cooled to 0°C. $BF_3{\cdot}OEt_2$ was added to the colorless solution over 10 min., resulting in a red-brown color change. After the reaction mixture was stirred for a minimum of 2 h (time of reaction = tor), it was quenched by $NaHCO_3$ (5%). The now orange mixture was subsequently extracted three times with DCM or $CHCl_3$ and washed three times with H_2O (dest.). The combined organic layers were dried over Na_2SO_4 and the solvent was removed *in vacuo*. The purification was carried out by flash column chromatography (Silica, PE: EtOAc) to yield β-ketoaldehydes **42-48** in equilibrium to their corresponding tautomers.

2,3-Bis(2-methoxyphenyl)-3-oxopropanal 42

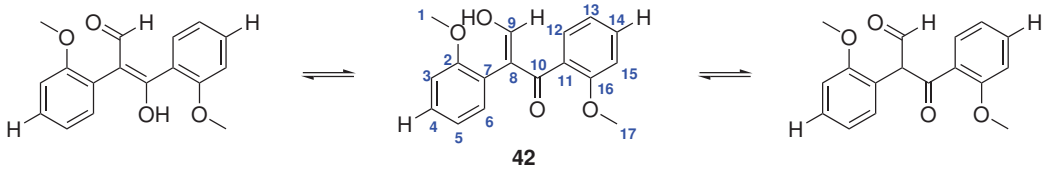

α, β-epoxy ketone **34** (2.84 g, 10.0 mmol, 1.00 equiv.), anhydrous DCM (30 ml), $BF_3{\cdot}OEt_2$ (1.023 ml, 10.0 mmol, 1.00 equiv.). Compound **42** (1.72 g, 6.06 mmol, 61%) was obtained as yellow oil, after purification *via* column chromatography (Silica, PE 20: EtOAc 1).

^{1}H NMR ($CDCl_3$, 600 MHz, 295 K): δ(ppm) = 15.35 (s_d, ^{1}J = 5.7 Hz, 1H, HO), 8.41 (s_d, ^{1}J = 4.0 Hz, 1H, H^{9}), 7.25-7.21 (m, 2H, $H^{6,4}$), 7.13 (t_d, ^{3}J = 8.0 Hz, ^{4}J = 1.8 Hz, 1H, H^{14}), 6.91 (d_d, ^{3}J = 7.4 Hz, ^{4}J = 1.8 Hz, 1H, H^{12}), 6.83 (t_d, ^{3}J = 7.5 Hz, ^{4}J = 0.9 Hz, 1H, H^{5}), 6.75 (t_d,^{3}J = 7.5 Hz,^{4}J = 1.1 Hz, 1H, H^{13}), 6.71 (d, ^{3}J = 8.2 Hz, 1H, H^{16}), 6.66 (d, ^{3}J = 8.5 Hz, 1H, H^{3}), 3.56 (s, 3H, H^{17}), 3.44 (s, 3H, H^{1}).

^{13}C{^{1}H} NMR ($CDCl_3$, 151 MHz, 295 K): δ(ppm) = 187.6 (C^{8}), 182.6 (C^{9}), 157.2 (C^{16}), 156.3 (C^{2}), 131.7 (C^{12}), 131.5 (C^{4}), 129.6 (C^{6}), 128.9 (C^{14}), 126.6 (C^{7}), 124.3 (C^{11}), 120.3 (C^{13}), 120.1 (C^{5}), 114.2 (C^{10}), 111.0 (C^{3}), 110.5 (C^{15}), 55.3 (C^{1}), 55.2 (C^{17}).

HR-MS (EI^{+}, acetone): [M+Na]$^{+}$: $C_{17}H_{16}O_4$+Na^{+}, calculated *m/z* 307.0941, found *m/z* 307.0942.

2-(2-Methoxy-4-methylphenyl)-3-(2-methoxyphenyl)-3-oxopropanal 43

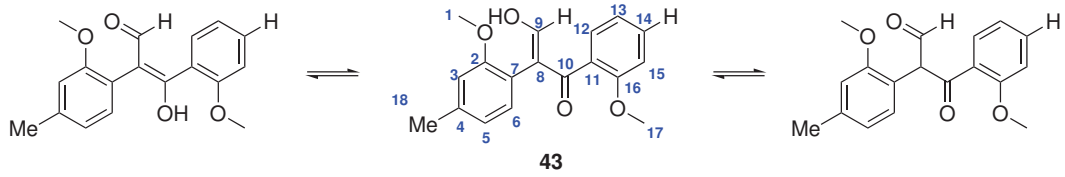

43

α, β-epoxy ketone **35** (896 mg, 3.00 mmol, 1.00 equiv.), anhydrous DCM (12 ml), $BF_3{\cdot}OEt_2$ (800 μl, 3.00 mmol, 1.00 equiv.). Compound **43** (297 mg, 996 μmol, 33%) was obtained as yellow oil, after purification *via* column chromatography (Silica, PE 15: EtOAc 1).

^{1}H NMR ($CDCl_3$, 600 MHz, 295 K): δ(ppm) = 15.37 (s_d, ^{1}J = 3.5 Hz, 1H, HO), 8.42 (s_d, ^{1}J = 5.7 Hz, 1H, H^{9}), 7.21 (d, ^{3}J = 8.5 Hz, 1H, H^{6}), 7.13 (t_d, ^{3}J = 8.9 Hz, ^{4}J = 1.4 Hz, 1H, H^{14}), 6.89 (d_d, ^{3}J = 7.5 Hz, ^{4}J = 1.5 Hz, 1H, H^{12}), 6.78-6.73 (m, 2H, $H^{13,15}$), 6.36 (d_d, ^{3}J = 8.4 Hz, ^{4}J = 1.0 Hz, 1H, H^{5}), 6.18 (s_d, ^{3}J = 2.0 Hz, 1H, H^{3}), 3.74 (s, 3H, H^{18}), 3.60 (s, 3H, H^{17}), 3.60 (s, 3H, H^{1}).

^{13}C{^{1}H} NMR ($CDCl_3$, 151 MHz, 295 K): δ(ppm) = 186.7 (C^{8}), 183.1 (C^{9}), 162.8 (C^{4}), 158.1 (C^{2}), 157.2 (C^{16}), 131.5 (C^{12}), 131.2 (C^{6}), 128.6 (C^{14}), 125.5 (C^{11}), 120.5 (C^{13}),

119.6 (C^7), 113.8 (C^{10}), 110.7 (C^{15}), 104.5 (C^5), 98.4 (C^3), 55.6 (C^{18}), 55.3 (C^{17}), 55.2 (C^1).

HR-MS (ESI$^+$, acetone): $[M+Na]^+$: $C_{18}H_{18}O_4$+Na^+, calculated *m/z* 321.1097, found *m/z* 321.1100.

2-(2-Methoxy-4-(trifluormethyl)phenyl))-3-(2-methoxyphenyl)-3-oxopropanal 45

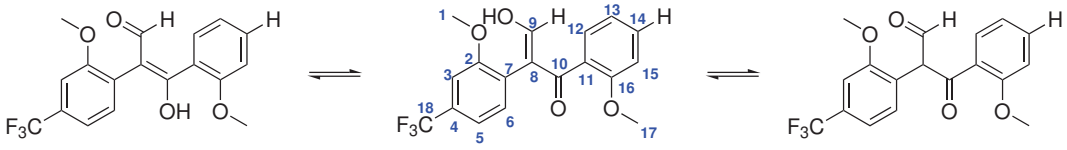

45

α, β-epoxy ketone **37** (881 mg, 2.50 mmol, 1.00 equiv.), anhydrous DCM (10 ml), $BF_3{\cdot}OEt_2$ (301 μl, 2.50 mmol, 1.00 equiv.). Compound **45** (393 mg, 1.32 mmol, 41%) was obtained as a light yellow oil, after purification *via* column chromatography (Silica, PE 10: EtOAc 1).

^{1}H NMR ($CDCl_3$, 600 MHz, 295 K): δ(ppm) = 15.51 (s_d, ^2J = 6.0 Hz, 1H, HO), 8.40 (s_d, ^1J = 4.2 Hz, 1H, H^9), 7.29-7.25 (m, 2H, $H^{12,13}$), 7.03-7.00 (m, 2H, $H^{5,6}$), 6.92 (s, 1H, H^3), 6.88 (t_d, ^3J = 7.5 Hz, ^4J = 1.0 Hz, 1H, H^{14}), 6.65 (d, ^3J = 8.4 Hz, 1H, H^{15}), 3.61 (s, 3H, H^1), 3.40 (s, 3H, H^{17}).

$^{13}C\{^1H\}$ NMR ($CDCl_3$, 151 MHz, 295 K): δ(ppm) = 186.1 (C^8), 182.4 (C^9), 162.8 (C^4), 157.3 (C^2), 156.1 (C^{16}), 132.2 (C^{13}), 131.8 (C^5), 129.7 (C^{12}), 128.9 (C^4), 126.2 (C^{15}), 122.5 (C^7), 120.5 (C^{14}), 117.9 (C^6), 111.0 (C^{16}), 55.5 (C^1), 55.1 (C^{17}), C^{10} and C^{18} could not be assigned.

HR-MS (ESI$^+$, acetone): $[M+H]^+$: $C_{18}H_{15}O_4F_3$+H^+, calculated *m/z* 353.0995, found *m/z* 353.0997.

3-(2,4-Dimethoxyphenyl)-2-(2-methoxyphenyl)-3-oxopropanal 47

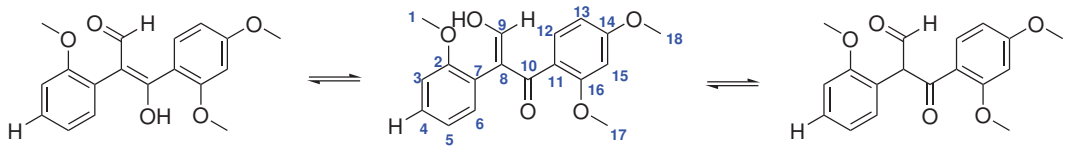

47

α, β-epoxy ketone **39** (1.89 g, 6.00 mmol, 1.00 equiv.), anhydrous DCM (18 ml), $BF_3{\cdot}OEt_2$ (741 μl, 6.00 mmol, 1.00 equiv.). Compound **47** (1.05 g, 3.34 mmol, 56%) was obtained as yellow oil, after purification *via* column chromatography (Silica, PE 5: EtOAc 1).

^{1}H NMR ($CDCl_3$, 600 MHz, 295 K): δ(ppm) = 15.50 (s, 1H, HO), 8.40 (s_d, ^1J = 5.3 Hz, 1H, H^9), 7.24-7.19 (m, 2H, $H^{4,\,5}$), 6.83 (d, ^3J = 7.6 Hz, 1H, H^6), 6.77 (d, ^3J = 7.7 Hz, 1H, H^{12}), 6.68 (d, ^3J = 8.4 Hz, 1H, H^3), 6.56 (d, ^3J = 7.7 Hz, 1H, H^{13}), 6.52 (s_d, ^3J = 1.5 Hz, 1H, H^{16}), 3.55 (s, 3H, H^{17}), 3.48 (s, 3H, H^1), 2.25 (s, 3H, H^{18}).

^{13}C{^{1}H} NMR ($CDCl_3$, 151 MHz, 295 K): δ(ppm) = 187.2 (C^8), 183.0 (C^9), 157.1 (C^{16}), 156.4 (C^2), 138.8 (C^{14}), 131.5 (C^4), 131.4 (C^{12}), 129.6 (C^5), 126.7 (C^7), 121.8 (C^{11}), 121.0 (C^{13}), 120.1 (C^6), 114.0 (C^{10}), 111.5 (C^{15}), 111.0 (C^3), 55.3 (C^1), 55.1 (C^{18}), 21.8 (C^{10}).

HR-MS (ESI$^+$, acetone): $[M+Na]^+$: $C_{18}H_{18}O_5$+Na^+, calculated *m/z* 337.1046, found *m/z* 337.1050.

2-(2,4-Dimethoxyphenyl)-3-(2-methoxyphenyl)-3-oxopropanal 44

*

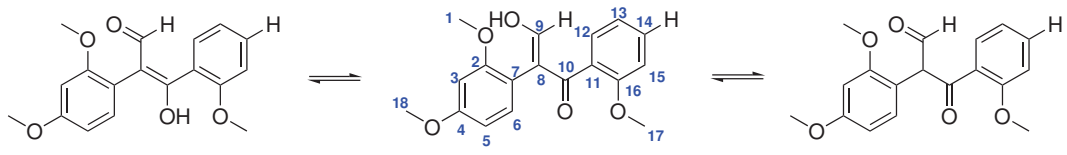

44

α, β-epoxy ketone **36** (1.89 g, 6.00 mmol, 1.00 equiv.), anhydrous DCM (18 ml), $BF_3{\cdot}OEt_2$

(741 μl, 6.00 mmol, 1.00 equiv.). The crude product **44** (893 mg, 2.84 mmol, 47%) was obtained as a green-brown oil.

^{1}H NMR ($CDCl_3$, 600 MHz, 295 K): δ(ppm) = 15.35 (s, 1H, HO), 8.17*, 7.52*, 7.42*, 7.40*, 7.38*, 6.99*, 6.97*, 6.78*, 6.76*, 6.70*, 6.68*, 6.37*, 6.32*, 3.76 (s, 3H, $H^{1/18}$), 3.59 (s, 3H, $H^{1/18}$), 3.39 (s, 3H, H^{17}).

HR-MS (ESI$^+$, acetone): $[M+H]^+$: $C_{18}H_{18}O_5$+H^+, calculated *m/z* 314.1154, found *m/z* 314.1147.

*no assigned or integrated NMR-data in the aromatic range due to remaining impurities/unidentified side species (see ^{1}H NMR discussed in section 3.3.1

2-(2-Methoxy-4-nitrophenyl)-3-(2-methoxyphenyl)-3-oxopropanal 46

*

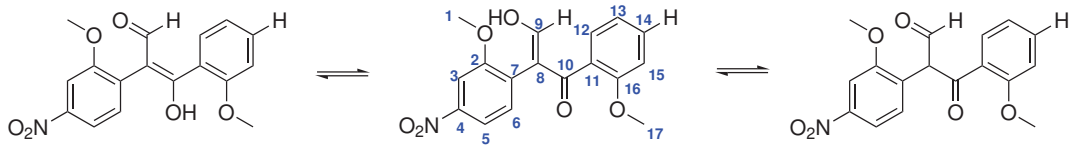

46

α, β-epoxy ketone **38** (330 mg, 1.00 mmol, 1.00 equiv.), anhydrous DCM (5 ml), $BF_3{\cdot}OEt_2$ (270 μl, 1.00 mmol, 1.00 equiv.). The crude product **46** (92.0 mg, 280 μmol, 28%) was obtained as a brown oil.

^{1}H NMR ($CDCl_3$, 600 MHz, 295 K): δ(ppm) = 15.57 (s_d, ^2J = 6.8 Hz, 1H, OH), 8.41*, 7.69*, 7.62*, 7.47*, 7.31*, 7.06*, 6.91*, 6.67*, 3.75*, 3.69 (s, 3H, H^1), 3.44 (s, 3H, H^{17}), 3.31*.

HR-MS (ESI$^+$, acetone): $[M+H]^+$: $C_{17}H_{15}O_5$+H^+, calculated *m/z* 330.0972, found *m/z*

330,0974.

*no assigned NMR-data due to initial decomposition (see ^{1}H NMR discussed in section 3.3.1)

3-(2,4-Dimethoxyphenyl)-2-(2-methoxy-4-methylphenyl)-3-oxopropanal 48

*

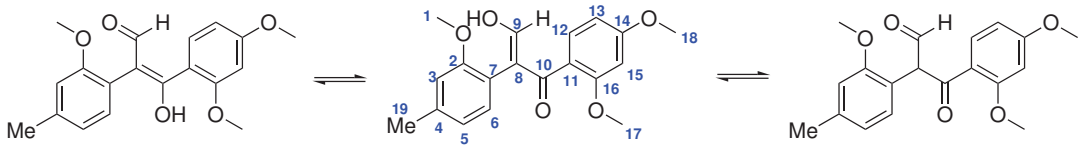

48

α, β-epoxy ketone **40** (296 mg, 900 μmol, 1.00 equiv.), anhydrous DCM (4.5 ml), $BF_3{\cdot}OEt_2$ (240 μl, 900 μmol, 1.00 equiv.). The crude product **48** (113 mg, 378 μmol, 42%) was obtained as an orange oil.

^{1}H NMR ($CDCl_3$, 600 MHz, 295 K): δ(ppm) = 15.52 (s, 1H, OH), 8.43*, 8.13*, 7.59*, 6.78*, 6.72*, 6.66*, 6.61*, 6.50*, 6.22*, 6.16*, 3.82*, 3.76 (s, 3H, $H^{17/18}$), 3.65*, 3.61 (s, 3H, $H^{17/18}$), 3.44 (s, 3H, H^1), 3.25*.

HR-MS (ESI$^+$, acetone): $[M+H]^+$: $C_{19}H_{20}O_5$+H^+, calculated m/z 329.1384, found m/z 329.1388.

*no assigned or integrated NMR-data due to impurities/ unidentified side species (see ^{1}H NMR discussed in section 3.3.1)

3-(2,4-Dimethoxyphenyl)-2-(2-methoxy-4-methylphenyl)-3-oxopropanal 49

*

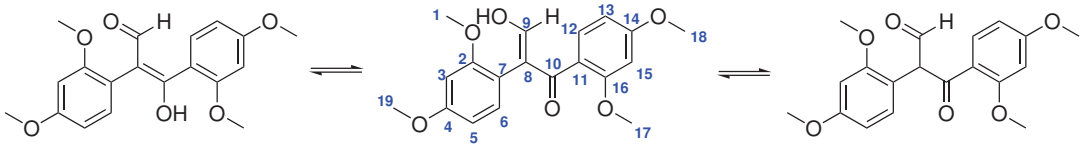

49

α, β-epoxy ketone **41** (1.03 g, 3.00 mmol, 1.00 equiv.), anhydrous DCM (17 ml), $BF_3{\cdot}OEt_2$ (340 μl, 2.76 mmol, 0.92 equiv.). The crude product **49** (392 mg, 1.14 mmol, 38%) was obtained as an orange oil.

^{1}H NMR ($CDCl_3$, 600 MHz, 295 K): δ(ppm) = 15.41 (s, 1H, OH), 8.34*, 7.76*, 7.74*, 7.14*, 7.11*, 6.76*, 6.74*, 6.50-6.10**, 3.90-3.20**, 3.70 (s, 3H, $H^{1/17/18/19}$), 3.69 (s, 3H, $H^{1/17/18/19}$), 3.54 (s, 3H, $H^{1/17/18/19}$), 3.41 (ss, 3H, $H^{1/17/18/19}$).

HR-MS (ESI$^+$, acetone): $[M+H]^+$: $C_{19}H_{20}O_6$+H^+, calculated *m/z* 344.1260, found *m/z* 344.1260.

*no assigned or integrated NMR data due to impurities/ unidentified side species (see ^{1}H NMR discussed in section 3.3.1; ** multiple merged signal groups.

6.2.3 2-(2-Hydroxyphenyl)benzofuran-3-carbaldehyde / 6*H*-Benzofuro[3,2-*c*]chromen-6-ol 50

50a **50b**

The synthesis was conducted according to *J. Tang et al.*.[98] A flame-dried SChlenk flask with a reflux condenser under Ar-atmosphere was charged with β-ketoaldehyde **42** (1.06 g, 3.70 mmol, 1.00 equiv.) and solved in $CHCl_3$ (64 ml). Subsequently, a solution of BBr_3 (1M, 9.25 ml, 9.25 mmol, 2.50 equiv.) was added. The resulting orange solution was refluxed for 2.5 h at 62°C. The color changed from orange over green to dark red. The solution was quenched with an ice-cooled saturated solution of $NaHSO_4$. The resulting mixture was extracted with $CHCl_3$ (3·50 ml) and the combined organic layers were dried over Na_2SO_4. Subsequently, the solvent was removed *in vacuo*. The crude product was purified by column chromatography (Silica, PE 25: EtOAc 1). Compound **50** (25.4 mg, 107 μmol, 3%) was obtained as a colorless oil, stored under Ar-atmosphere.

^{1}H NMR ($CDCl_3$, 600 MHz, 295 K): δ(ppm) = 11.87 (s, 1H, H^{16}), 8.14 (s, 1H, OH), 8.07-8.03 (m, 1H, H^2), 7.87 (d_d, ^3J = 8.0 Hz, ^4J = 1.7 Hz, 1H, H^{12}), 7.59-7.56 (m, 2H, H^5), 7.53 (t_d, ^3J = 8.8 Hz, ^4J = 1.7 Hz, 1H, H^{10}), 7.45-7.35 (m, 2H, $H^{3,4}$), 7.08 (d_d, ^3J = 8.4 Hz, ^4J = 1.1 Hz, 1H, H^9), 6.95 (t_d, ^3J = 8.2 Hz, ^4J = 1.2 Hz, 1H, H^{11}).

^{13}C{^{1}H} NMR ($CDCl_3$, 151 MHz, 295 K): δ(ppm) = 162.7 (C^7), 150.56 (C^{13}), 136.5 (C^{10}), 131.6 (C^{12}), 126.2 ($C^{3/4}$), 124.8 ($C^{3/4}$), 122.7 (C^2), 120.7 (C^8), 119.7 (C^{11}), 118.8 (C^9), 111.92 (C^5), $C^{1,6,14}$ and C^{16} could not be precisely assigned.

HR-MS (ESI^-, acetone): $[M-H]^-$: $C_{15}H_9O_3$-H^+, calculated *m/z* 237.0552, found *m/z* 237.0556.

6.3 Chapter 1.2

6.3.1 Synthesis of dinaphto[2,1-b:1',2'-d]furan 68

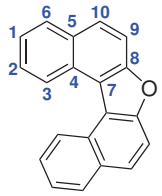

68

The synthesis was conducted according to *A. Martinez et al.*.[126]
1,1-Binaphtol (10.0 g, 35.0 mmol, 1.00 equiv.) and *p*-TsOH (6.64 g, 35.0 mmol, 1.00 equiv.) were dissloved in toluene (550 ml) and hydrochloric acid (conc., 2 ml) was added. The reaction mixture was refluxed at 140°C for 5 days. The crude product was purified *via* column chromatography (silica, PE 20: EtOAc 1, R_f= 0.59). Compound **68** (0.734 g, 2.74 mmol, 8%) was obtained as a colorless solid.

NMR spectroscopic data assorted well with the literature.[126]

HR-MS (ESI$^+$, acetonitrile): $[M+H]^+$: $C_{20}H_{12}O+H^+$, calculated *m/z* 269.0957, found *m/z* 269.0957.

6.3.2 Synthesis of 2'-hydroxy-[1,1'-binaphthalene]-2-carbaldehyde 69

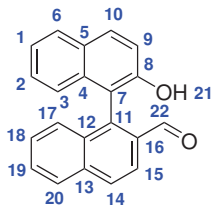

69

The synthesis was conducted according to *A. Martinez et al.*.[126]

A flame-dried round bottom Schlenk flask was charged with **68** (1.40 g, 5.22 mmol, 1.00 equiv.) and dissolved in anhydrous diethyl ether (50 ml) and toluene (16 ml) under argon atmosphere. Subsequently, lithium (79.7 mg, 11.5 mmol, 2.20 equiv.) was added at 0°C and the reaction mixture was stirred for 24 h at room temperature. The resulting mixture was cooled to -78°C and DMF (323 μl, 4.17 mmol, 0.80 equiv.) was added. The suspension was stirred at -78°C for a further 2 h, afterward, it was stirred at room temperature for an additional 15 h. The reaction was quenched with HCl (3M, 30 ml). The organic layer was filtered off, washed with HCl (3·30 ml), and dried over Na_2SO_4. The solvent was removed *in vacuo* and the crude product was purified *via* column chromatography (silica, PE 5: EtOAc 1, R_f= 0.22). Compound **69** (0.797 g, 2.67 mmol, 51%) was obtained as a light brown solid.

NMR spectroscopic data assorted well with the literature.[126]

HR-MS (EI$^+$, acetonitrile): $[M+H]^+$: $C_{21}H_{14}O_2$+H^+, calculated *m/z* 299.1067, found *m/z* 299.1060.

6.3.3 Synthesis of 1-bromo-3,4-dihydronaphthalene-2-carbaldehyde 63

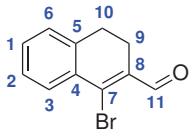

63

The synthesis was conducted according to *C. B. de Koning et al.*.[180]
A flame-dried round bottom Schlenk flask was charged with anhydrous DMF (8.02 ml, 103 mmol, 1.00 equiv.) and DCM (50 ml). The mixture was was cooled to 0°C and phosphorous tribromide (8.00 ml, 84.2 mmol, 0.87 equiv.) was added dropwise. The reaction stirred at 0°C for 1 h. In a second flame-dried Schlenk flask, α-tetralone (4.58 ml, 34.5 mmol, 0.33 equiv.) was dissolved in anhydrous DCM (90 ml) at room temperature and slowly added to the mixture in the first flask. The resulting solution was refluxed at

90°C for 1 h. The reaction mixture was quenched with $NaHCO_3$ at 0°C. The aqueous layer was extracted with DCM (3·100 ml) and the combined organic layers were dried over $MgSO_4$. After filtration over Celite®, the solvent was removed *in vacuo*. The crude product was purified *via* column chromatography (silica, *iso*-Hex 7: EtOAc 3, R_f= 0.75). Compound **63** (0.260 g, 0.905 mmol, 11%) was obtained as a brown solid.

NMR spectroscopic data assorted well with the literature.[180]

HR-MS (ESI⁺, EtOAc): $[M+H]^+$: $C_{11}H_9BrO+H^+$, calculated *m/z* 236.9910, found *m/z* 236.9911.

6.3.4 Synthesis of 1-bromo-naphthalene-2-carbaldehyde 64

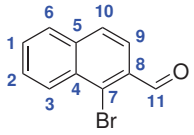

64

The synthesis was conducted according to *S. L. Ioffe et al.*.[181]
1-Bromo-3,4-dihydronaphthalene-2-carbaldehyde **64** (0.900 g, 3.78 mmol, 1.00 equiv.), selenium powder (0.600 g, 11.39 mmol, 3.00 equiv.) and DMSO (1.00 ml) were heated to 180°C. The residue was allowed to cool down to about 40°C, then water (18 ml) and EtOAc (25 ml) were added. The biphasic system was filtered through Celite®. The organic layer was separated, afterward the aqueous layer was extracted with EtOAc (3·30 ml). The combined organic layers were washed with brine (25 ml) and dried over Na_2SO_4. Subsequently, the solvent was removed *in vacuo*. The residue was filtered and purified *via* column chromatography (silica, EtOAc 1: Hex 10, R_f= 0.51) to give **64** (661 mg, 2.90 mmol, 77%) as yellow plates.

NMR spectroscopic data assorted well with the literature.[181]

HR-MS (ESI$^+$, EtOAc): $[M+H]^+$: $C_{11}H_7BrO+H^+$, calculated *m/z* 233.9680, found *m/z* 233.9678.

6.3.5 Synthesis of bis(benzo[*d*][1,3]dioxol-5-yloxy)methane 74

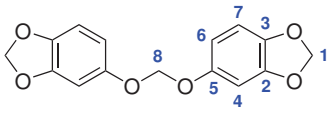

74

The synthesis was conducted according to *G. Delogu et al.*.[131]
Sesamol (10.0 g, 72.4 mmol, 1.00 equiv.) was dissloved in acetone (110 ml) and potassium carbonate (13.0 g, 94.1 mmol, 1.30 equiv.) was added while stirring. The suspension was stirred at room temperature for 30 min. Subsequently, diiodomethane (3.03 ml, 36.2 mmol, 0.50 equiv.) was added and the suspension was refluxed at 60°C for 15 h. Afterwards, the solvent was removed *in vacuo* and the brown solid was purificated *via* column chromatography (silica, DCM 1: *iso*-Hex 1, R_f= 0.48). Compound **74** (5.00 g, 17.3 mmol, 24%) was obtained as a colorless solid.

NMR spectroscopic data assorted well with the literature.[131]

HR-MS (EI$^+$, acetone): $[M+H]^+$: $C_{15}H_{13}O_6+H^+$, calculated *m/z* 288.0634, found *m/z* 288.0629.

6.3.6 Synthesis of bis((4-iodobenzo[*d*][1,3]dioxol-5-yl)oxy)methane 75

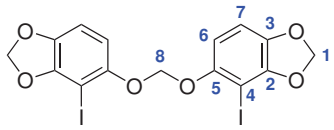

75

The synthesis was conducted according to *G. Delogu et al.*.[131]
A flame-dried Schlenk flask was charged with compound **74** (5.00 g, 17.4 mmol, 1.00 equiv.) which was dissolved in anhydrous diethyl ether (100 ml). Subsequently, *n*-BuLi (10.0 ml, 2.40M in THF, 43.2 mmol, 2.49 equiv.) was added dropwise at 0°C. The resulting suspension was stirred at 0°C for 30 min. Iodine (11.0 g, 43.2 mmol, 2.49 equiv.) was added and the suspension was stirred for 15 h at room temperature. The reaction was quenched with water (25 ml) and the aqueous layer was extracted with diethyl ether (3·75 ml). The combined organic layers were dried over Na_2SO_4 and the solvent was removed *in vacuo*. The crude product was purified *via* column chromatography (silica, PE 2: EtOAc 1, R_f= 0.84) to yield compound **75** (0.756 g, 1.40 mmol, 8%) as a light brown solid.

NMR spectroscopic data assorted well with the literature.[131]

HR-MS (EI^+, acetone): $[M+H]^+$: $C_{15}H_{11}I_2O_6$+H^+, calculated *m/z* 540.8640, found *m/z* 540.8572.

6.3.7 Synthesis of furo[2,3-f:4,5]bis[1,3]benzodioxole 76

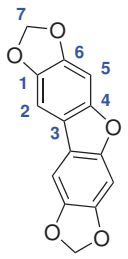

76

The synthesis was conducted according to *M. Jeganmohan et al.*.[130]
Sesamol (5.00 g, 36.2 mmol, 1.00 equiv.) and potassium peroxydisulfate (19.6 g, 72.4 mmol, 2.00 equiv.) were dissolved in TFA (50 ml) and the reaction mixture was stirred at room temperature for 4 h. After the reaction mixture was diluted with DCM, the suspension was filtered and the solvent was removed *in vacuo*. The crude product was purified *via* column chromatography (silica, PE 10: EtOAc 1, R_f= 0.46). Compound **76** (1.50 g, 5.85 mmol, 16%) was obtained as a brown solid.

NMR spectroscopic data assorted well with the literature.[130]

HR-MS (ESI$^-$, acetonitrile): $[M-C_2H_4]^-$: $C_{14}H_8O_5$-$C_2H_4^-$, calculated *m/z* 233.0455, found *m/z* 233.0461.

6.3.8 General Procedure for Suzuki-Coupling A (WI3)

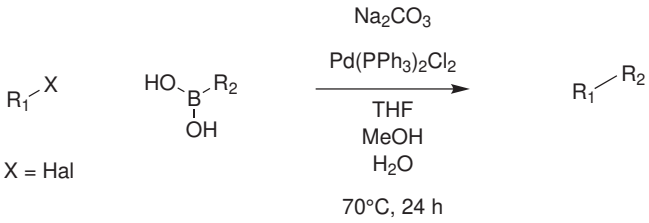

A flame-dried round bottom flask was charged with halogen derivative (1.00 equiv.), boronic acid (1.50 equiv.), and sodium carbonate (2.30 equiv.). The educts were dissolved in degassed THF, MeOH, and water. Afterward, bis(triphenyl-phosphine)palladium(II) dichloride (0.11 equiv.) was added and the mixture was refluxed at 70°C overnight. Subsequently, the reaction mixture was diluted with water and EtOAc (1:2). The layers were separated and extracted three times with EtOAc. The combined organic layers were dried over Na_2SO_4. The solvent was removed *in vacuo* and the crude product was purified *via* column chromatography.

6*H*-Naphtho[2,1-*c*]chromen-6-ol 66

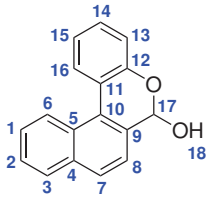

66

The reaction followed synthesis procedure A. 1-Bromo-2-naphthaldehyde **64** (1.00 g, 4.25 mmol), (2-hydroxyphenyl)boronic acid (880 mg, 6.38 mmol), sodium carbonate (1.04 g, 9.78 mmol) and bis(triphenyl-phosphine)palladium(II) dichloride (328 mg, 468 μmol) were dissolved in THF (15 ml), MeOH (10 ml) and water (7 ml). Purification *via* column chromatography (silica, cyclo-Hex 3 : EtOAc 1, R_f = 0.81) served 6*H*-naphtho[2,1-*c*]chromen-6-ol **66**(568 mg, 2.29 mmol, 54%) as a light brown solid.

^{1}H NMR ($CDCl_3$, 600 MHz, 295 K): δ(ppm) = 8.63 (d, ^{3}J= 8.4 Hz, 1H, H^{6}), 8.11 (d, ^{3}J= 8.3 Hz, 1H, H^{16}), 7.81 (d_d, ^{3}J= 7.8 Hz, ^{4}J= 1.8 Hz, 1H, H^{3}), 7.67 (s, 1H, H^{7}), 7.55-7.45 (m, 4H, $H^{1,2,13/14/15,\ 13/14/15)}$, 7.26-7.22 (m, 1H, $H^{13/14/15}$), 7.02 (d, ^{3}J= 8.3 Hz, 1H, H^{8}), 6.76 (s, 1H, H^{17}).

$^{13}C\{^{1}H\}$ NMR ($CDCl_3$, 151 MHz, 295 K): δ(ppm) = 151.6 (C^{12}), 135.0 (C^{4}), 130.2 ($C^{5/11}$), 129.7 (C^{9}), 129.0 ($C^{1/2/3/13/14/15}$), 128.9 ($C^{1/2/3/13/14/15}$), 128.63 ($C^{7/16}$), 128.59 ($C^{7/16}$), 126.9 ($C^{1/2/13/14/15}$), 126.5 (C^{10}), 126.3 ($C^{1/2/3/13/14/15}$), 125.7 (C^{6}), 123.4 (C^{8}), 122.9 ($C^{5/11}$), 122.7 ($C^{13/14/15}$), 118.8 ($C^{1/2/13/14/15}$), 93.80 (C^{17}).

IR: $\tilde{v}$ = 3098, 1597, 1483, 1451, 1393, 1234, 1196, 1103, 1050, 1037, 997, 963, 916, 804, 782, 752, 686 cm^{-1}.

HR-MS (ESI^-, chloroform): $[M-H_2O]^+$: $C_{17}H_{12}O_2$–H_2O^+, calculated *m/z* 231.0804, found *m/z* 231.0807.

6*H*-benzo[c]chromen-6-ol 59

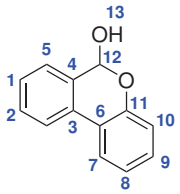

59

The reaction followed synthesis procedure A. 2-Bromophenol (1.00 g, 5.78 mmol), (2-formylphenyl)boronic acid (1.30 g, 8.67 mmol), sodium carbonate (1.41 g, 13.30 mmol) and bis(triphenyl-phosphine)palladium(II) dichloride (328 mg, 468 μmol) were dissolved in THF (15 ml), MeOH (10 ml) and water (7 ml). Purification *via* column chromatography (silica, PE 4: EtOAc 1, R_f= 0.74) served 6*H*-naphtho[2,1-*c*]chromen-6-ol **59** (748 mg, 3.77 mmol, 65%) as a light brown solid.

NMR spectroscopic data could not be assigned due to remaining impurities after column chromatography. Identification was achieved with HPLC-MS, CHIRALPAK IA (DAICEL CORPORATION), *n*-Hex 80: IPA 20, $RT_{enantiomer\ 1}$= 4.3 min, $RT_{enantiomer\ 2}$= 5.1 min.

HR-MS (ESI$^+$, EtOAc): $[M-H_2O]^+$: $C_{13}H_9O+H^+$, calculated *m/z* 181.0648, found *m/z* 181.0650.

6.3.9 General Procedure for Suzuki-Coupling B (WI4)

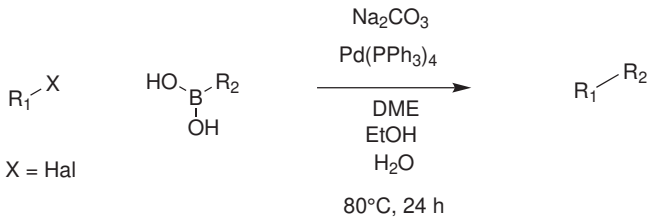

A flame-dried round bottom flask was charged with halogen aldehyde (1.00 equiv.), boronic acid (1.36 equiv.), and sodium carbonate (3.90 equiv.). The educts were dissolved in DME, EtOH, and/or degassed water. The mixed solution was subsequently degassed by passing argon through a cannula for 1 h. Afterward, tetrakis(triphenyl-phosphine)palladium(0) (0.10 equiv.) was added and the mixture was refluxed at 80°C overnight. Subsequently, the reaction mixture was diluted with water. The layers were separated and extracted three times with diethyl ether. The combined organic layers were dried over Na_2SO_4. The solvent was removed *in vacuo* and the crude product was purified *via* column chromatography.

1-(2-Chloro-6-hydroxyphenyl)-2-naphthaldehyde 65

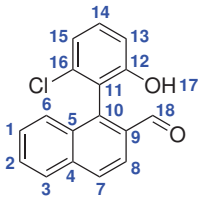

65

1-Bromo-2-naphthaldehyde **64** (1.00 g, 4.25 mmol), (2-chloro-6-hydroxyphenyl)boronic acid (1.03 g, 5.80 mmol) and sodium carbonate (1.76 g, 16.6 mmol) were added to a flame dried round bottom flask and dissolved in DME (120 ml) and degassed water (30 ml). Tetrakis(triphenylphosphine)palladium(0) was added (12.3 mg, 10.6 μmol, 0.05 equiv.) and the suspension was refluxed for 24 h at 80°C. Water (50 ml) was added, the layers were separated and the aqueous layer was extracted with diethyl ether (3·50 ml). The crude product was purified *via* column chromatography (silica, PE:EtOAc, 10:1 to 3:1,

R_f(3:1)= 0.56). 1-(2-Chloro-6-hydroxyphenyl)-2-naphthaldehyde **65** (978 mg, 3.46 mmol, 81%) was obtained as a yellow solid.

^{1}H NMR ($CDCl_3$, 600 MHz, 295 K): δ(ppm) = 9.89 (s, 1H, H^{18}), 8.13 (d, ^3J= 8.6 Hz, 1H, H^8), 8.05 (d, ^3J= 8.6 Hz, 1H, H^7), 7.98 (d, ^3J= 8.1 Hz, 1H, H^3), 7.71-7.65 (m, 1H, H^2), 7.57-7.51 (m, 2H, $H^{1,6}$), 7.40 (t, ^3J= 8.2 Hz, 1H, H^{14}), 7.21 (d_d, ^3J= 8.2 Hz, ^4J= 1.0 Hz 1H, H^{15}), 7.02 (d, ^3J= 8.3 Hz, 1H, H^{13}), 4.75 (s, 1H, H^{17}).

^{13}C{^{1}H} NMR ($CDCl_3$, 151 MHz, 295 K): δ(ppm) = 191.5 (C^{18}), 154.8 (C^{12}), 137.4 (C^9), 136.5 (C^7), 135.2 (C^{16}), 132.2 (C^{10}), 131.5 (C^5), 130.9 (C^{14}), 129.9 (C^7), 129.4 (C^2), 128.6 (C^3), 127.8 ($C^{1/6}$), 126.0 ($C^{1/6}$), 122.5 (C^8), 121.9 (C^{15}), 120.7 (C^{11}), 114.3 (C^{13}).

IR: $\tilde{\nu}$ = 3149, 1688, 1661, 1618, 1595, 1445, 1330, 1287, 1244, 1029, 976, 901, 820, 782, 671 cm^{-1}.

HR-MS (ESI$^+$, EtOAc): $[M-H_2O]^-$: $C_{13}H_9O-H^-$, calculated *m/z* 281.0375, found *m/z* 281.0375.

5*H*-Chromeno[3,4-b]pyridin-5-ol 78

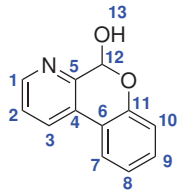

78

The reaction followed synthesis procedure B. 3-Chloropicolin-aldehyde (500 mg, 3.53 mmol), (2-hydroxyphenyl)boronic acid (731 mg, 5.30 mmol), sodium carbonate (3.18 g, 30.0 mmol) and tetrakis(triphenyl-phosphine)palladium(0) (364 mg, 353 μmol) were dissolved in DME (27 ml), EtOH (14 ml) and water (10 ml). Purification via column chromatography (silica, cyclo-Hex 1: EtOAc 1, R_f = 0.41) served 5*H*-chromeno[3,4-b]bipyridin-5-ol **78** (255 mg, 1.28 mmol, 36%) as a colorless solid.

^{1}H NMR ($CDCl_3$, 600 MHz, 295 K): δ(ppm) = 8.57 (d_d, ^{3}J= 4.9 Hz, ^{4}J= 1.5 Hz, 1H, H^3), 8.20 (d_d, ^{3}J= 8.0 Hz, ^{4}J= 1.4 Hz, 1H, H^1), 7.80 (d_d, ^{3}J= 7.8 Hz, ^{4}J= 1.5 Hz, 1H, H^7), 7.49 (d_d, ^{3}J= 8.0 Hz, ^{4}J= 4.8 Hz, 1H, H^2), 7.38 (t_d, ^{3}J= 8.1 Hz, ^{4}J= 7.3 Hz, 1H, H^9), 7.19 (m, 1H, H^{10}), 7.16 (m, 1H, H^8), 6.57 (s, 1H, H^{12}).

^{13}C{^{1}H} NMR ($CDCl_3$, 151 MHz, 295 K): δ(ppm) = 150.7 (C^{11}), 149.0 (C^5), 147.6 (C^3), 130.8 (C^9), 130.5 (C^1), 124.9 (C^4), 124.8 (C^2), 123.2 (C^7), 122.6 (C^{10}), 118.8 (2C, $C^{6,8}$), 92.1 (C^{12}).

IR: $\tilde{\nu}$ = 2705, 1609, 1572, 1455, 1418, 1302, 1248, 1206, 1196, 1108, 1054, 1042, 996, 886, 851, 819, 780, 738, 699 cm^{-1}.

HR-MS (ESI$^+$, EtOAc): $[M+H]^+$: $C_{12}H_9NO_2$+H^+, calculated *m/z* 200.0706, found *m/z* 200.0707.

5*H*-Chromeno[4,3-b]pyridin-5-ol 79

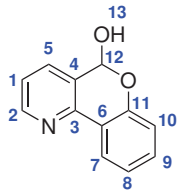

79

The reaction followed synthesis procedure B. 2-Chloronicotin-aldehyde (500 mg, 3.53 mmol), (2-hydroxyphenyl)boronic acid (731 mg, 5.30 mmol), sodium carbonate (3.18 g, 30.0 mmol) and tetrakis(triphenyl-phosphine)palladium(0) (364 mg, 353 μmol) were dissolved in DME (27 ml), EtOH (14 ml) and water (10 ml). Purification *via* column chromatography (silica, cyclo-Hex 1: EtOAc 1, R_f= 0.51) served 5*H*-chromeno[4,3-b]bipyridin-5-ol **79** (475 mg, 2.38 mmol, 68%) as a yellow solid.

^{1}H NMR (DMSO-d_6, 600 MHz, 295 K): δ(ppm) = 8.67 (d_d, ^{3}J= 4.7 Hz, ^{4}J= 1.6 Hz, 1H), 8.23 (d_d, ^{3}J= 7.7 Hz, ^{4}J= 1.7 Hz, 1H), 7.81 (d_d, ^{3}J= 7.6 Hz, ^{4}J= 1.7 Hz, 1H), 7.59 (d, ^{3}J= 6.2 Hz, 1H), 7.42-7.38 (m, 2H), 7.14 (t, ^{3}J= 7.5 Hz, 1H), 7.07 (d_d, ^{3}J= 8.1 Hz, ^{4}J= 1.3 Hz, 1H), 6.46 (d, ^{3}J= 6.1 Hz, 1H).

^{13}C{^{1}H} NMR (DMSO-d_6, 200 MHz, 293.15 K): δ(ppm) = 152.8, 150.0, 146.1, 134.2, 131.1, 126.9, 123.9, 123.9, 123.0, 121.8, 121.5, 117.8, 92.07.

IR: $\tilde{\nu}$ = 2696, 1611, 1594, 1495, 1471, 1452, 1430, 1305, 1242, 1198, 1157, 1130, 1102, 1039, 991, 971, 883, 807, 792, 758, 722 cm^{-1}.

HR-MS (ESI^{+}, EtOAc): [M+H]$^{+}$: $C_{12}H_9NO_2$+H^{+}, calculated *m/z* 200.0706, found *m/z* 200.0707.

8-(Trifluoromethyl)-5*H*-Chromeno[4,3-b]pyridin-5-ol 83

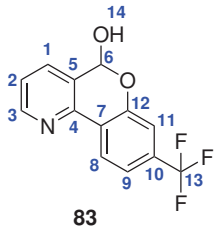

83

The reaction followed synthesis procedure B. 2-Chloronicotin-aldehyde (225 mg, 1.59 mmol), (2-hydroxy-4-(trifluoromethyl)-phenyl)boronic acid (491 mg, 2.38 mmol), sodium carbonate (656 mg, 6.2 mmol) and tetrakis(triphenyl-phosphine)palladium(II) dichloride (164 mg, 159 μmol) were dissolved in DME (14 ml), EtOH (7 ml) and water (7 ml). Purification *via* column chromatography (silica, cyclo-hexane 1: EtOAc 1, R_f= 0.48) served 8-(trifluoromethyl)-5*H*-chromeno[4,3-b]bipyridin-5-ol **83** (260 mg, 973 μmol, 61%) as a light brown solid.

^{1}H NMR ($CDCl_3$, 600 MHz, 295 K): δ(ppm) = 8.74 (d_d, ^{3}J= 4.8 Hz, ^{4}J= 1.6 Hz, 1H,

H^3), 8.46 (d, ^3J= 8.1 Hz, 1H, H^1), 7.75 (d_d, ^3J= 7.7 Hz, ^4J= 1.7 Hz, 1H, H^1), 7.41 (d, ^3J= 8.1 Hz, 1H, H^9), 7.38-7.35 (m, 2H, $H^{2,\ 11}$), 6.56 (s, 1H, H^6).

$^{13}C\{^1H\}$ NMR ($CDCl_3$, 151 MHz, 295 K): δ(ppm) = 152.2 (C^{12}), 150.8 (C^3), 145.5 (C^4), 134.6 (C^1), 126.2 (C^5), 125.3 (C^8), 124.5 ($C^{7/10}$), 123.7 (C^2), 122.7 ($C^{7/10}$), 119.2 (C^9), 115.3 (C^{11}), 92.8 (C^6).

IR: $\tilde{v}$ = 3060, 1600, 1512, 1446, 1422, 1327, 1279, 1246, 1194, 1158, 1138, 1126, 1109, 1053, 968, 948, 874, 838, 786, 725, 663 cm^{-1}.

MS (APCI$^+$, 2-propanol): $[M+H]^+$: $C_{13}H_8F_3NO_2$+H^+, calculated *m/z* 268.7, found *m/z* 268.1.

6.4 Chapter 2

6.4.1 General Procedure to methylated β-Amino alcohols 111-113(WI5)

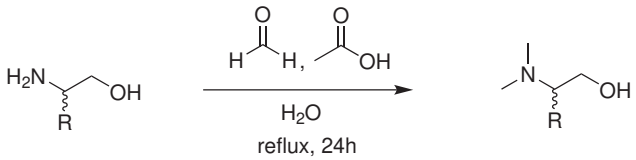

R/S- **111-113**

All Eschweiler-Clarke methylation reactions were performed according to A. T. Davidson et al.[171]. A two neck flask (100 ml) was charged with β-amino alcohol (1.00 equiv.) and formic acid (88%) dissolved in H_2O. Subsequently, formaldehyde (37%, 4.20 equiv.) was added dropwise over a time of 10 min. to the reaction mixture. The reaction was refluxed at 100°C for 24 h. After cooling to room temperature, NaOH (5M) was added and the mixture was extracted three times with Et_2O. The combined organic layers were washed with NaOH (5M), Brine, and H_2O. Subsequently, the combined organic layers were dried over Na_2SO_4. The solvent was removed *in vacuo*. The resulting methylated β- amino alcohols **111-113** were obtained as yellow oils without further purification.

R-2-(Dimethylamino)-4-methylpentan-1-ol 111

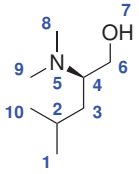

R-**111**

R-Leucinol (1.09 ml, 8.53 mmol), formic acid (88%, 1.45 ml), H_2O (2.5 ml), formaldehyde (37%, 2.68 ml, 35.8 mmol), NaOH (5M, 8.5 ml), Et_2O (3·9 ml). Compound **111** was obtained as a yellow oil (1.01 g, 6.95 mmol, 82%).

^{1}H NMR ($CDCl_3$, 600 MHz, 295 K): δ(ppm) = 3.57 (s, 1H, H^7), 3.24 (d_d, ^2J= 10.5 Hz, ^3J= 4.9 Hz, 1H, $H^{6a/b}$), 3.21 (d_d, ^2J= 10.5 Hz, ^3J= 4.9 Hz, 1H, $H^{6a/b}$), 2.63-2.67 (m, 1H, H^4), 2.23 (s, 6H, $H^{8,9}$), 1.53-1.44 (m, 1H, H^2), 1.29 (d_d, ^2J= 13.2 Hz, ^3J= 9.2 Hz, 1H,

$H^{3a/b}$), 1.85-1.90 (m, 1H, H^2), 1.00-0.93 (m, 1H, $H^{3a/b}$), 0.89 (d_d, ^2J= 22.7 Hz, ^3J= 15.0 Hz, 6H, $H^{1,10}$).

$^{13}C\{^1H\}$ NMR ($CDCl_3$, 151 MHz, 295 K): δ(ppm) = 62.47 (C^4), 62.44 (C^6), 39.90 (2C, $C^{8,9}$), 32.93 (C^3), 24.15 (C^2), 22.13 (2C, $C^{1,10}$).

IR: $\tilde{v}$ = 3404, 2954, 2929, 2868, 2828, 1602, 1458, 1410, 1384, 1367, 1286, 1170, 1052, 1024, 950, 851, 762 cm^{-1}.

HR-MS (ESI^+, 2-propanol): $[M+H]^+$: $C_8H_{19}NO+H^+$, calculated *m/z* 146.1539, found *m/z* 146.1540.

S-2-(Dimethylamino)-4-methylpentan-1-ol 111

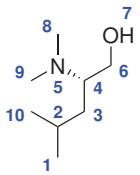

S-**111**

S-Leucinol (3.90 ml, 30.5 mmol), formic acid (88%, 5.25 ml), H_2O (9 ml), formaldehyde (37%, 9.200 ml, 128.2 mmol), NaOH (5M, 30 ml), Et_2O (3·30 ml). Compound **111** was obtained as yellow oil (3.81 g, 26.3 mmol, 86%).

^1H NMR ($CDCl_3$, 600 MHz, 295 K): δ(ppm) = 3.57 (s, 1H, H^7), 3.24 (d_d, ^2J= 10.5 Hz, ^3J= 4.9 Hz, 1H, $H^{6a/b}$), 3.21 (d_d, ^2J= 10.5 Hz, ^3J= 4.9 Hz, 1H, $H^{6a/b}$), 2.63-2.67 (m, 1H, H^4), 2.23 (s, 6H, $H^{8,9}$), 1.53-1.44 (m, 1H, H^2), 1.29 (d_d, ^2J= 13.2 Hz, ^3J= 9.2 Hz, 1H, $H^{3a/b}$), 1.85-1.90 (m, 1H, H^2), 1.00-0.93 (m, 1H, $H^{3a/b}$), 0.89 (d_d, ^2J= 22.7 Hz, ^3J= 15.0 Hz, 6H, $H^{1,10}$).

$^{13}C\{^{1}H\}$ NMR ($CDCl_3$, 151 MHz, 295 K): δ(ppm) = 62.47 (C^4), 62.44 (C^6), 39.90 (2C, $C^{8,9}$), 32.93 (C^3), 24.15 (C^2), 22.13 (2C, $C^{1,10}$).

IR: $\tilde{\nu}$ = 3404, 2954, 2929, 2868, 2828, 1602, 1458, 1410, 1384, 1367, 1286, 1170, 1052, 1024, 950, 851, 762 cm^{-1}.

HR-MS (ESI^+, 2-propanol): $[M+H]^+$: $C_8H_{19}NO+H^+$, calculated *m/z* 146.1539, found *m/z* 146.1540.

R-2-(Dimethylamino)-3-methylbutan-1-ol 112

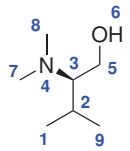

R-**112**

R-Valinol (3.40 ml, 30.5 mmol), formic acid (88%, 5.25 ml), H_2O (9 ml), formaldehyde (37%, 9.200 ml, 128.2 mmol), NaOH (5M, 30 ml), Et_2O (3·30 ml). Compound **112** was obtained as yellow oil (3.35 g, 25.5 mmol, 84%).

^{1}H NMR ($CDCl_3$, 800 MHz, 295 K): δ(ppm) = 3.58 (m, 1H, $H^{5a/b}$), 3.24 (m, 1H, $H^{5a/b)}$), 2.50-2.41 (m, 6H, $H^{7,8}$), 2.37-2.31 (m, 1H, H^3), 1.90-1.85 (m, 1H, H^2), 1.05-0.97 (m, 3H, $H^{1/9}$)), 0.90-0.83 (m, 3H, $H^{1/9}$).

$^{13}C\{^{1}H\}$ NMR ($CDCl_3$, 200 MHz, 293.15 K): δ(ppm) = 70.56 (C^3), 59.15 (C^5), 40.97 (2C, $C^{7,8}$), 27.54 (C^2), 19.62 (2C, $C^{1,9}$).

IR: $\tilde{\nu}$ = 3388, 2957, 2872, 2826, 2784, 1456, 1412, 1386, 1366, 1278, 1192, 1155, 1133, 1097, 1044, 1012, 936, 840, 752, 661 cm^{-1}.

HR-MS (ESI$^+$, 2-propanol): $[M+H]^+$: $C_7H_{17}NO+H^+$, calculated m/z 132.1383, found m/z 132.1385.

S-2-(Dimethylamino)-4-methylbutan-1-ol 112

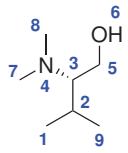

S-**112**

S-Valinol (3.40 ml, 30.5 mmol), formic acid (88%, 5.25 ml), H_2O (9 ml), formaldehyde (37%, 9.200 ml, 128.2 mmol), NaOH (5M, 30 ml), Et_2O (3·30 ml). Compound **112** was obtained as yellow oil (3.24 g, 24.5 mmol, 81%).

^{1}H NMR ($CDCl_3$, 800 MHz, 295 K): δ(ppm) = 3.58 (m, 1H, $H^{5a/b}$), 3.24 (m, 1H, $H^{5a/b)}$), 2.50-2.41 (m, 6H, $H^{7,8}$), 2.37-2.31 (m, 1H, H^3), 1.90-1.85 (m, 1H, H^2), 1.05-0.97 (m, 3H, $H^{1/9}$)), 0.90-0.83 (m, 3H, $H^{1/9}$).

^{13}C{^{1}H} NMR ($CDCl_3$, 200 MHz, 293.15 K): δ(ppm) = 70.56 (C^3), 59.15 (C^5), 40.97 (2C, $C^{7,8}$), 27.54 (C^2), 19.62 (2C, $C^{1,9}$).

IR: $\tilde{\nu}$ = 3388, 2957, 2872, 2826, 2784, 1456, 1412, 1386, 1366, 1278, 1192, 1155, 1133, 1097, 1044, 1012, 936, 840, 752, 661 cm^{-1}.

HR-MS (ESI$^+$, 2-propanol): $[M+H]^+$: $C_7H_{17}NO+H^+$, calculated m/z 132.1383, found m/z 132.1385.

R-2-(Dimethylamino)-3-phenylpropan-1-ol 113

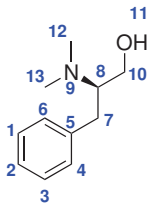

R-**113**

R-Phenylalaninol (4.61 g, 30.5 mmol), formic acid (88%, 5.25 ml), H_2O (9 ml), formaldehyde (37%, 9.200 ml, 128.2 mmol), NaOH (5M, 30 ml), Et_2O (3·30 ml). Compound **113** was obtained as yellow oil (4.90 g, 27.5 mmol, 90%).

^{1}H NMR (chloroform-d, 800 MHz, 295 K): δ(ppm) = 7.32-7.25 (m, 2H, $H^{4,6}$), 7.24-7.18 (m, 1H, H^2), 7.18-7.11 (m, 2H, $H^{1,3}$), 3.43 (m, 1H, H^{10a}), 3.38-3.33 (m, 1H, H^{10b}), 2.93 (m, 2H, $H^{8,11}$), 2.41-2.34 (m, 2H, $H^{7a,b}$), 2.40 (s_d, ^3J= 2.2 Hz, 6H, $H^{12,13}$).

^{13}C{^{1}H} NMR ($CDCl_3$, 200 MHz, 293.15 K): δ(ppm) = 128.96 (2C, $C^{4,6}$), 128.92 (2C, $C^{1,3}$), 126.31 (C^2), 67.01 (C^8), 60.26 (C^{10}), 40.16 (2C, $C^{12,13}$), 30.58 (C^7).

IR: $\tilde{\nu}$ = 3215, 3020, 2936, 2864, 2828, 2781, 1942, 1668, 1597, 1582, 1494, 1453, 1444, 1409, 1383, 1373, 1296, 1254, 1166, 1104, 1089, 1076, 1062, 1046, 1030, 1003, 951, 906, 852, 778, 740 cm^{-1}.

HR-MS (ESI$^+$, 2-propanol): $[M+H]^+$: $C_{11}H_{17}NO+H^+$, calculated *m/z* 180.1383, found *m/z* 180.1384.

S-2-(Dimethylamino)-3-phenylpropan-1-ol 113

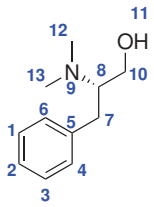

S-**113**

S-Phenylalaninol (4.61 g, 30.5 mmol), formic acid (88%, 5.25 ml), H_2O (9 ml), formaldehyde (37%, 9.200 ml, 128.2 mmol), NaOH (5M, 30 ml), Et_2O (3·30 ml). Compound **113** was obtained as yellow oil (4.7 g, 26.2 mmol, 86%).

^{1}H NMR ($CDCl_3$, 800 MHz, 295 K): δ(ppm) = 7.32-7.25 (m, 2H, $H^{4,6}$), 7.24-7.18 (m, 1H, H^2), 7.18-7.11 (m, 2H, $H^{1,3}$), 3.43 (m, 1H, H^{10a}), 3.38-3.33 (m, 1H, H^{10b}), 2.93 (m, 2H, $H^{8,11}$), 2.41-2.34 (m, 2H, $H^{7a,b}$), 2.40 (s_d, ^3J= 2.2 Hz, 6H, $H^{12,13}$).

$^{13}C\{^1H\}$ NMR ($CDCl_3$, 200 MHz, 293.15 K): δ(ppm) = 128.96 (2C, $C^{4,6}$), 128.92 (2C, $C^{1,3}$), 126.31 (C^2), 67.01 (C^8), 60.26 (C^{10}), 40.16 (2C, $C^{12,13}$), 30.58 (C^7).

IR: $\tilde{\nu}$ = 3215, 3020, 2936, 2864, 2828, 2781, 1942, 1668, 1597, 1582, 1494, 1453, 1444, 1409, 1383, 1373, 1296, 1254, 1166, 1104, 1089, 1076, 1062, 1046, 1030, 1003, 951, 906, 852, 778, 740 cm^{-1}.

HR-MS (ESI^+, 2-propanol): $[M+H]^+$: $C_{11}H_{17}NO+H^+$, calculated *m/z* 180.1383, found *m/z* 180.1384.

6.4.2 General Procedure to benzylated β-Amino alcohols 115-118 (WI6)

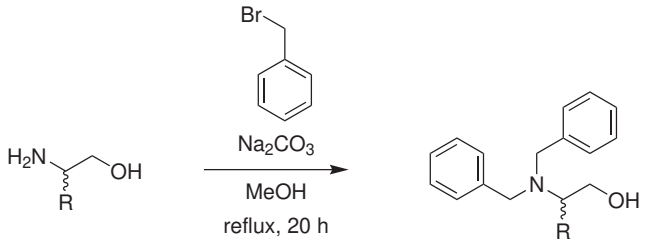

R/S- **114-118**

β-amino alcohol (500 mg, 1.00 equiv.) and Na_2CO_3 (1.50 equiv.) were dissolved in methanol (5.0 ml) in a flask. An excess of benzyl bromide (1.50-2.00 equiv.) was added to the reaction mixture. The mixture was refluxed and stirred at 80°C for 20 h. The reaction mixture was quenched with dist. water (5.0 ml). The organic layer was separated and the aqueous layer was extracted with ethyl acetate(3·10.0 ml). The combined organic layers were dried over anhydrous $MgSO_4$. The solvent was removed *in vacuo*. The product was purified by column chromatography (Silica, PE: EtOAc).

S-2-(Dibenzylamino)-2-phenylethan-1-ol 115

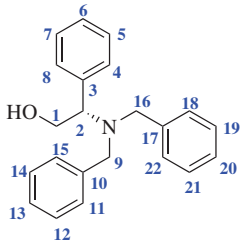

S-**115**

Synthesis was performed according to the General procedure (WI6). *S*-Phenylglycinol (500.0 mg, 3.64 mmol), benzyl bromide (0.87 ml, 7.29 mmol), Na_2CO_3 (579.5 mg, 5.47 mmol) and methanol (5.0 ml). The crude product was purified by column chromatography (PE: EtOAc; gradient 15:1 to 5:1; R_f (PE 10: EtOAc 1) = 0.24). Compound **115** was yielded as a colorless oil (780 mg, 2.46 mmol, 73%).

^{1}H NMR ($CDCl_3$, 800 MHz, 295 K): δ(ppm) = 7.40 (d_d,^{3}J= 4.8 Hz, ^{4}J= 4.8 Hz, 2H, $H^{5,7}$), 7.36 (t, ^{3}J= 4.9 Hz, 1H, H^{6}), 7.32 (d, ^{3}J= 3.0 Hz, 8H, $H^{11,12,14,15,18,19,21,22}$), 7.27-7.23 (m, 4H, $H^{4,8,13,20}$), 4.11 (d_d,^{2}J= 12.9 Hz, ^{3}J= 5.9 Hz, 1H, H^{1}), 3.93-3.90 (m, 1H, H^{2}), 3.91 (d, ^{2}J= 9.0 Hz, 2H, $H^{9,16}$), 3.58 (d_d, ^{2}J= 7.2 Hz, ^{3}J= 3.5 Hz, 1H, H^{1}), 3.12 (d, ^{2}J= 9.0 Hz, 2H, $H^{9,16}$), 3.03 (br s, 1H, OH).

^{13}C{^{1}H} NMR ($CDCl_3$, 200 MHz, 293.15 K): δ(ppm) = 139.22 (2C, $C^{10,17}$), 135.14 (C^{3}),129.45 (2C, $C^{4,8}$), 129.13 (4C, $C^{11,15,18,22}$), 128.72 (4C, $C^{12,14,19,21}$), 128.53 (2C, $C^{5,7}$), 128.19 (C^{6}), 127.42 (2C, $C^{13,20}$), 63.10 (C^{2}), 60.53 (C^{1}), 53.61 (2C, $C^{9,16}$).

IR: $\tilde{v}$ = 3455, 3028, 1736, 1602, 1494, 1453, 1409, 1372, 1242, 1217, 1113, 1073, 1026, 1002, 970, 911, 871, 760, 744 cm^{-1}.

HR-MS (ESI^{+}, EtOAc): $[M+H]^{+}$: $C_{22}H_{23}NO+H^{+}$, calculated *m/z* 318.1852, found *m/z* 318.1851.

R-2-(Dibenzylamino)-2-phenylethan-1-ol 115

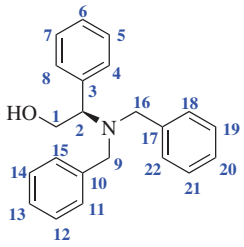

R-**115**

Synthesis was performed according to the General procedure (WI6). *R*-Phenylglycinol (500.0 mg, 3.64 mmol), benzyl bromide (0.87 ml, 7.29 mmol), Na_2CO_3 (579.5 mg, 5.47 mmol) and methanol (5.0 ml). The crude product was purified by column chromatography (PE: EtOAc; gradient 15:1 to 5:1; R_f (PE 10: EtOAC 1) = 0.24). Compound **115** was yielded as a colorless oil (780 mg, 2.46 mmol, 73%).

^{1}H NMR ($CDCl_3$, 800 MHz, 295 K): δ(ppm) = 7.41 (d_d,^{3}J= 4.9 Hz, ^{4}J= 4.9 Hz, 2H, $H^{5,7}$), 7.36 (t, ^{3}J= 4.7 Hz, 1H, H^{6}), 7.32 (d, ^{3}J= 3.0 Hz, 8H, $H^{11,12,14,15,18,19,21,22}$), 7.27-7.23 (m, 4H, $H^{4,8,13,20}$), 4.15-4.09 (m, 1H, H^{1}), 3.93-3.90 (m, 1H, H^{2}), 3.91 (d, ^{2}J= 8.9 Hz, 2H, $H^{9,16}$), 3.59 (d_d, ^{2}J= 7.2 Hz, ^{3}J= 3.5 Hz, 1H, H^{1}), 3.13 (d, ^{2}J= 9.0 Hz, 2H, $H^{9,16}$), 3.03 (br s, 1H, OH).

^{13}C{^{1}H} NMR ($CDCl_3$, 200 MHz, 293.15 K): δ(ppm) = 139.21 (2C, $C^{10,17}$), 135.13 (C^{3}),129.44 (2C, $C^{4,8}$), 129.13 (4C, $C^{11,15,18,22}$), 128.71 (4C, $C^{12,14,19,21}$), 128.52 (2C, $C^{5,7}$), 128.19 (C^{6}), 127.42 (2C, $C^{13,20}$), 63.08 (C^{2}), 60.51 (C^{1}), 53.60 (2C, $C^{9,16}$).

IR: $\tilde{v}$ = 3455, 3028, 1736, 1602, 1494, 1453, 1409, 1372, 1242, 1217, 1113, 1073, 1026, 1002, 970, 911, 871, 760, 744 cm^{-1}.

HR-MS (ESI^{+}, EtOAc): $[M+H]^{+}$: $C_{22}H_{23}NO+H^{+}$, calculated *m/z* 318.1852, found *m/z* 318.1852.

R-2-(Dibenzylamino)-3-methylbutan-1-ol 114

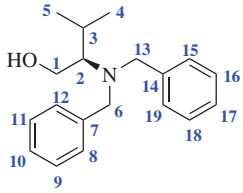

R-**114**

Synthesis was performed according to the General procedure (WI6). *R*-Valinol (500.0 mg, 4.85 mmol), benzyl bromide (1.15 ml, 9.69 mmol), Na_2CO_3 (770.5 mg, 7.26 mmol) and methanol (5.0 ml). The crude product was purified by column chromatography (PE: EtOAc; gradient 20:1 to 2:1; R_f (PE 5: EtOAC 1) = 0.58). Compound **114** was yielded as a colorless oil (661 mg, 2.33 mmol, 64%).

^{1}H NMR ($CDCl_3$, 800 MHz, 295 K): δ(ppm) = 7.31 (t,^{3}J= 5.0 Hz, 4H, $H^{9,11,16,18}$), 7.27-7.23 (m, 1H, $H^{8,10,12,15,17,19}$), 3.89 (d, ^{2}J= 9.3 Hz, 2H, $H^{6,13}$), 3.68 (d, ^{2}J= 8.8 Hz, 2H, $H^{6,13}$), 3.57 (d_d, ^{2}J= 6.6 Hz, ^{3}J= 2.8 Hz, 1H, H^{1}), 3.43 (d_d, ^{2}J= 6.6 Hz, ^{3}J= 2.8 Hz, 1H, H^{1}), 3.03 (s, 1H, OH), 2.56-2.52 (m, 1H, H^{2}), 2.07 (d_q, ^{2}J= 4.8 Hz, ^{3}J= 4.8 Hz, 1H, H^{3}), 1.14 (d, ^{3}J= 4.5 Hz, 3H, $H^{4/5}$), 0.89 (d, ^{3}J= 4.5 Hz, 3H, $H^{4/5}$).

^{13}C{^{1}H} NMR ($CDCl_3$, 200 MHz, 293.15 K): δ(ppm) = 139.79 (2C, $C^{7,14}$), 129.36 (4C, $C^{8,12,15,19}$), 128.60 (4C, $C^{9,11,16,18}$), 127.32 (2C, $C^{10,17}$), 64.75 (4C, C^{2}), 59.31 (C^{1}), 54.30 (2C, $C^{6,13}$), 27.72 (C^{3}), 22.91 ($C^{4/5}$), 20.23 ($C^{4/5}$).

IR: $\tilde{\nu}$ = 3404, 2956, 1494, 1453, 1362, 1245, 1207, 1137, 1098, 1064, 1028, 1009, 910, 857, 786, 745, 728 cm^{-1}.

HR-MS (ESI^{+}, EtOAc): $[M+H]^{+}$: $C_{19}H_{25}NO_0$+H^{+}, calculated *m/z* 284.2009, found *m/z* 284.2007.

S-2-(Dibenzylamino)-3-methylbutan-1-ol 114

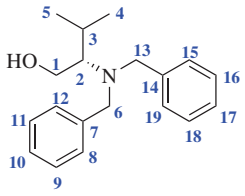

S-**114**

Synthesis was performed according to the general procedure (WI6). *S*-Valinol (500.0 mg, 4.85 mmol), benzyl bromide (1.15 ml, 9.69 mmol), Na_2CO_3 (770.5 mg, 7.26 mmol) and methanol (5.0 ml). The crude product was purified by column chromatography (PE: EtOAc; gradient 20:1 to 2:1; R_f (PE 5: EtOAc 1) = 0.58). Compound **114** was yielded as

a colorless oil (595 mg, 2.10 mmol, 58%).

^{1}H NMR ($CDCl_3$, 800 MHz, 295 K): δ(ppm) = 7.31 (t, ^{3}J= 5.0 Hz, 8H, $H^{9,11,16,18}$), 7.27-7.23 (m, 2H, $H^{8/10/12/15/17/19}$), 3.89 (d, ^{2}J= 9.1 Hz, 2H, $H^{6,13}$), 3.68 (d, ^{2}J= 8.8 Hz, 2H, $H^{6,13}$), 3.57 (d_d, ^{2}J= 6.6 Hz, ^{3}J= 2.8 Hz, 1H, H^{1a}), 3.43 (d_d, ^{2}J= 6.6 Hz, ^{3}J= 2.8 Hz, 1H, H^{1b}), 3.03 (s, 1H, OH), 2.56-2.52 (m, 1H, H^{2}), 2.07 (d_q, ^{2}J= 4.7 Hz, ^{3}J= 4.7 Hz, 1H, H^{3}), 1.14 (d, ^{3}J= 4.6 Hz, 3H, $H^{4/5}$), 0.89 (d, ^{3}J= 4.8 Hz, 3H, $H^{4/5}$).

^{13}C{^{1}H} NMR ($CDCl_3$, 200 MHz, 293.15 K): δ(ppm) = 139.79 (2C, $C^{7,14}$), 129.35 (4C, $C^{8,12,15,19}$), 128.60 (4C, $C^{9,11,16,18}$), 127.31 (2C, $C^{10,17}$), 64.74 (4C, C^{2}), 59.32 (C^{1}), 54.30 (2C, $C^{6,13}$), 27.73 (C^{3}), 22.91 ($C^{4/5}$), 20.24 ($C^{4/5}$).

IR: $\tilde{v}$ = 3432, 2956, 1494, 1453, 1362, 1245, 1207, 1137, 1098, 1064, 1028, 1009, 910, 857, 786, 745, 728 cm^{-1}.

HR-MS (ESI^{+}, EtOAc): $[M+H]^{+}$: $C_{19}H_{25}NO_0$+H^{+}, calculated *m/z* 284.2009, found *m/z* 284.2007.

S-2-(Dibenzylamino)-3-phenylpropan-1-ol 116

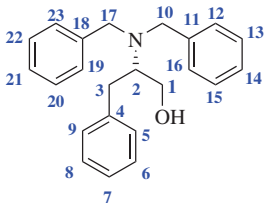

S-116

Synthesis was performed according to the general procedure (WI6). *S*-Phenyl alaninol (500.0 mg, 3.31 mmol), benzyl bromide (0.59 ml, 4.96 mmol) and Na_2CO_3 (525.7 mg, 4.96 mmol) were charged in a flask with methanol (5.0 ml). The crude product was purified by column chromatography (PE: EtOAc; gradient 15:1 to 5:1; R_f (PE 10: EtOAc 1)=

0.25). Compound **116** was yielded as a colorless solid (852 mg, 2.57 mmol, 78%).

^{1}H NMR ($CDCl_3$, 800 MHz, 295 K): δ(ppm) = 7.33-7.23 (m, 12H, $H^{6,8,12,13,14,15,16,19,20,21,22,23}$), 7.20-7.18 (m, 1H, H^{7}), 7.09 (d, ^{3}J= 5.0 Hz, 2H, $H^{5,9}$), 3.92 (d, ^{2}J= 8.9 Hz, 2H, $H^{10,17}$), 3.51-3.47 (m, 1H, H^{1}), 3.48 (d, ^{2}J= 8.9 Hz, 2H, $H^{10,17}$), 3.32 (d_d, ^{2}J= 7.12 Hz, ^{3}J= 3.24 Hz, 1H, H^{1}), 3.13-3.04 (m, 2H, $H^{2,3}$), 3.01 (s, 1H, OH), 2.43 (d_d, ^{2}J = 8.8 Hz, ^{3}J= 6.4 Hz, H^{3}).

^{13}C{^{1}H} NMR ($CDCl_3$, 200 MHz, 293.15 K): δ(ppm) = 139.28 (C^{4}), 139.08 ($C^{11,18}$), 129.16 (2C, $C^{5,9}$), 129.13 (4C, $C^{12,16,19,23}$), 128.70 (6C, $C^{13,14,15,20,21,22}$), 127.47 (2C, $C^{6,8}$), 126.39 (C^{7}), 60.99 (C^{2}), 60.49 (C^{1}), 53.35 (2C, $C^{10,17}$), 31.84 (C^{3}).

IR: $\tilde{\nu}$ = 3388, 3026, 2924, 1494, 1453, 1411, 1382, 1364, 1260, 1128, 1103, 1064, 1042, 1018, 997, 971, 909, 793, 751, 743, 720 cm^{-1}.

HR-MS (ESI^{+}, EtOAc): $[M+H]^{+}$: $C_{19}H_{25}NO_0$+H^{+}, calculated *m/z* 332.2009, found *m/z* 332.2007.

R-2-(Dibenzylamino)-3-phenylpropan-1-ol 116

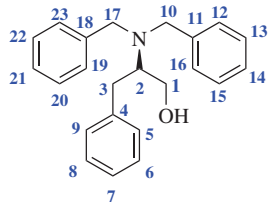

R-**116**

Synthesis was performed according to the general procedure (WI6). *S*-Phenyl alaninol (500.0 mg, 3.31 mmol), benzyl bromide (0.59 ml, 4.96 mmol) and Na_2CO_3 (526 mg, 4.96 mmol) were charged in a flask with methanol (5.0 ml). The crude product was purified by column chromatography (PE: EtOAc; gradient 15:1 to 5:1; R_f (PE 10: EtOAc 1)=

0.25). Compound **116** was yielded as a colorless solid (852 mg, 2.57 mmol, 78%).

^{1}H NMR ($CDCl_3$, 800 MHz, 295 K): δ(ppm) = 7.34-7.23 (m, 12H, $H^{6,8,12,13,14,15,16,19,20,21,22,23}$), 7.20-7.18 (m, 1H, H^{7}), 7.09 (d, ^{3}J= 5.0 Hz, 2H, $H^{5,9}$), 3.92 (d, ^{2}J= 8.9 Hz, 2H, $H^{10,17}$), 3.51-3.47 (m, 1H, H^{1}), 3.48 (d, ^{2}J= 8.9 Hz, 2H, $H^{10,17}$), 3.32 (d_d, ^{2}J= 7.12 Hz, ^{3}J= 3.24 Hz, 1H, H^{1}), 3.13-3.04 (m, 2H, $H^{2,3}$), 3.01 (s, 1H, OH), 2.43 (d_d, ^{2}J = 8.8 Hz, ^{3}J= 6.4 Hz, H^{3}).

^{13}C{^{1}H} NMR ($CDCl_3$, 200 MHz, 293.15 K): δ(ppm) = 139.28 (C^{4}), 139.08 ($C^{11,18}$), 129.16 (2C, $C^{5,9}$), 129.13 (4C, $C^{12,16,19,23}$), 128.70 (6C, $C^{13,14,15,20,21,22}$), 127.47 (2C, $C^{6,8}$), 126.39 (C^{7}), 60.99 (C^{2}), 60.49 (C^{1}), 53.35 (2C, $C^{10,17}$), 31.84 (C^{3}).

IR: $\tilde{v}$ = 3389, 3026, 2924, 1494, 1453, 1411, 1382, 1364, 1260, 1127, 1103, 1064, 1042, 1018, 997, 971, 909, 793, 751, 744, 720 cm^{-1}.

HR-MS (ESI^{+}, EtOAc): $[M+H]^{+}$: $C_{19}H_{25}NO+H^{+}$, calculated *m/z* 332.2009, found *m/z* 332.2007.

R-(1-Benzylpyrrolidin-2-yl)methanol 110

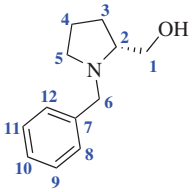

R-**110**

According to the General procedure (WI6) *R*-prolinol (0.49 ml, 4.94 mmol), benzyl bromide (0.88 ml, 7.41 mmol) and Na_2CO_3 (786 mg, 7.41 mmol) were charged in a flask with methanol (5.0 ml). The product **110** was yielded as a yellow liquid (83%).

^{1}H NMR ($CDCl_3$, 800 MHz, 295 K): δ(ppm) = 7.29-7.24 (m, 4H, $H^{8,9,11,12}$), 7.22-7.19 (m,

1H, H^{10}), 3.93 (d, ^2J=8.7 Hz, 1H, $H^{6a/b}$), 3.61 (d_d, ^2J= 2.3 Hz, ^3J= 7.2 Hz, 1H, H^1), 3.39 (d_d, ^2J= 1.58 Hz, $^{3a/b}J$= 7.26 Hz, 1H, H^1), 3.33 (d, ^2J= 8.8 Hz, 1H, $H^{6a/b}$), 2.95-2.92 (m, 1H, $H^{5a/b}$), 2.77 (br s, 1H, OH), 2.73-2.69 (m, 1H, H^2), 2.26 (d_d, ^2J= 11.2 Hz, ^3J= 6.4 Hz, 1H, $H^{5a/b}$), 1.92-1.85 (m, 1H, $H^{3a/b}$), 1.82-1.76 (m, 1H, $H^{3a/b}$), 1.68-1.62(m, 2H, $H^{4a,b}$).

$^{13}C\{^1H\}$ NMR ($CDCl_3$, 200 MHz, 293.15 K): δ(ppm) = 139.10 (C^7), 128.91 (2C, $C^{9,11}$), 128.49 (2C, $C^{8,12}$), 127.28 (1C, C^{10}), 64.50 (1C, C^2), 61.80 (1C, C^1), 58.66 (1C, C^6), 54.54 (1C, C^5), 27.84 (1C, C^3), 23.58 (1C, C^4).

IR: $\tilde{v}$ = 3404, 2971, 2873, 2800, 1495, 1454, 1381, 1154, 1115, 1078, 1041, 1028, 986, 912, 844, 737, 672 cm^{-1}.

HR-MS (ESI$^+$, EtOAc): $[M+H]^+$: $C_{12}H_{17}NO+H^+$, calculated *m/z* 192.1383, found *m/z* 192.1380.

S-1-Benzyl-2-(methoxymethyl)pyrrolidine 117

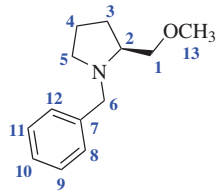

S-**117**

According to the General procedure (WI6) *S*-2-(methoxymethyl)pyrrolidine (0.54 ml, 4.34 mmol,), benzyl bromide (0.77 ml, 6.51 mmol) and Na_2CO_3 (690.2 mg, 6.51 mmol) were charged in a flask with methanol (5.0 ml). The crude product was purified by column chromatography (DCM: MeOH; gradient 60:1 to 30:1; R_f(DCM 30: MeOH 1)= 0.41). The product **117** was yielded as an orange liquid (445 mg, 2.17 mmol, 67%).

^{1}H NMR ($CDCl_3$, 400 MHz, 295 K): δ(ppm) = 7.34-7.29 (m, 4H, $H^{8,9,11,12}$), 7.24 (t, ^{3}J = 4.8 Hz, 1H, H^{10}), 4.10 (d, ^{2}J= 8.72 Hz, 1H, H^{6}), 3.49-3.38 (m, 2H, $H^{3,6}$), 3.36-3.31(m, 1H, H^{3}), 3.35 (s, 3H, H^{13}), 2.94 (t, ^{3}J= 4.74 Hz, 1H, H^{5}), 2.73 (s, 1H, H^{2}), 2.22 (d_t, ^{2}J= 5.2 Hz, ^{3}J= 5.2 Hz, 1H, H^{5}), 1.97-1.90 (m, 1H, H^{4}), 1.77-1.63 (m, 3H, $H^{1,4}$).

^{13}C{^{1}H} NMR ($CDCl_3$, 200 MHz, 293.15 K): δ(ppm) = 139.59 (C^{7}), 129.19 (2C, $C^{8,12}$), 128.29 (2C, $C^{9,11}$), 126.97 (C^{10}), 76.48 (C^{3}), 63.10 (C2), 59.71 (C^{6}), 59.26 (C^{13}), 54.66 (C^{5}), 28.63 (C^{4}),22.86 (C^{1}).

IR: $\tilde{v}$ = 2921, 2873, 2807, 1495, 1453, 1375, 1356, 1196, 1111, 1028, 976, 911, 845, 736 cm^{-1}.

HR-MS (ESI^{+}, EtOAc): $[M+H]^{+}$: $C_{13}H_{19}NO+H^{+}$, calculated *m/z* 206.1539, found *m/z* 206.1540.

S-2-(Dibenzylamino)-3,3-dimethylbutan-1-ol 118

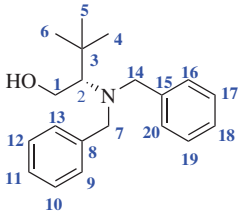

S-118

The synthesis was performed according to the general procedure (WI6). *S-tert*-Leucinol (500.0 mg, 3.81 mmol), benzyl bromide (0.68 ml, 5.72 mmol) and Na_2CO_3 (605.8 mg, 5.72 mmol) were charged in a flask with methanol (5.0 ml). The crude product was purified by column chromatography (PE: EtOAc; gradient 15:1 to 5:1; R_f (PE 5: EtOAc 1)= 0.54). The product **118** was yielded as a colorless oil (343 mg, 1.67 mmol, 58 %).

^{1}H NMR ($CDCl_3$, 400 MHz, 295 K): δ(ppm) = 7.31 (t, ^{3}J= 4.94 Hz, 4H, $H^{10,12,17,19}$),

7.25-7.23(m, 6H, $H^{9,11,13,16,18,20}$), 3.98 (d, ^2J= 8.8 Hz, 2H, $H^{7,14}$), 3.88 (d, ^2J= 8.8 Hz, 2H, $H^{7,14}$), 3.74 (d_d, ^2J= 6.9 Hz, ^3J= 6.9 Hz, 1H, H1), 3.67-3.65 (m, 1H, H^1), 2.65 (d_d, ^2J= 6.7 Hz, ^3J= 2.74 Hz, 1H, H^2), 2.28 (s, 1H, OH), 1.03 (s, 9H, $H^{4,5,6}$).

$^{13}C\{^1H\}$ NMR ($CDCl_3$, 200 MHz, 293.15 K): δ(ppm) = 140.20 (2C, $C^{8,15}$), 129.44 (4C, $C^{9,13,16,20}$), 128.52 (4C, $C^{10,12,17,19}$), 127.21 (2C, $C^{11,18}$), 66.94 (1C, C^2), 59.28 (1C, C^1), 55.27 (2C, $C^{7,14}$), 36.71 (1C, C^3), 29.30 (3C, $C^{4,5,6}$).

IR: $\tilde{v}$ = 3418, 2952, 1494, 1479, 1453, 1394, 1359, 1129, 1074, 1039, 1026, 999, 940, 911, 805, 745, 730 cm^{-1}.

HR-MS (ESI^+, EtOAc): $[M+H]^+$: $C_{20}H_{27}NO+H^+$, calculated *m/z* 298.2165, found *m/z* 298.2163.

6.4.3 General Procedure of Catalyst Screening in Alkylation Reactions with Zn-organyls (WI7)

The derivatized β-amino alcohols were prepared in 0.5M stock solutions in degassed anhydrous toluene. A flame-dried Schlenk-tube was charged with catalyst stock solution (0.05 equiv., 0.5M) and Zn-organyl (1.20 equiv., 1M in toluene or hexanes). The solution was stirred for 5-10 min. Subsequently, benzaldehyde (1.00 equiv.) was added. The reaction was stirred for a minimum of 6 h under Ar-atmosphere.

Sample Preparation for HPLC Analysis

A 0.2 ml sample was taken from the reaction and then subjected to a mini workup. This was carried out in a GC vial with 0.2 ml sample and 0.2 ml HCl (1M), well mixed by vortexing. After phase separation, the organic residue was collected with an Eppendorf pipette and transferred to a new GC vial with 200 μl inlet and septum. The organic solvent was removed at HV and the mass of the remaining residue was determined. Before HPLC analysis, the sample was resolved in 2-propanol (150-200 μl).

Yield Determination *via* Dilution Series

The yield was determined in the alkylations with dimethylzinc, diethylzinc, and diisopropylzinc by linear regression of a dilution series of four different product concentrations against the total area of both enantiomers. The concentrations were selected in the range of the product concentrations of the respective screening reactions. For the linear regression, there is a slight deviation due to a saturation effect, which was, however, neglected for an approximate yield, since the screening focus was on the potential enantiomeric excess (*ee*). The concentration of the resulting product in the catalyst screenings was determined by the remaining mass after solvent removal at the HV during sampling and the volume of 2-propanol added for resolution. The simpler method of using the sample volume was not always applicable due to the formation of solids by quenching with HCl during the workup, which complicated the recovery of the organic residue. The product concentration thus varied a bit due to the partly adapted sampling.

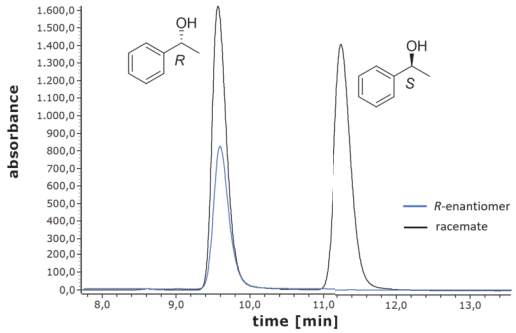

Figure 6.1: Enantiomeric separation of 1-phenylethan-1-ol.

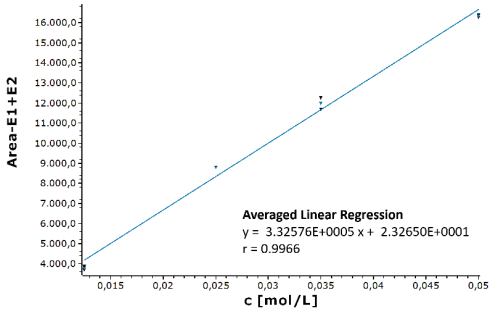

Figure 6.2: Linear regression of dilution series of 1-phenylethan-1-ol.

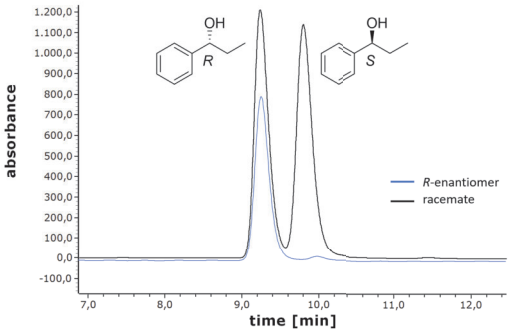

Figure 6.3: Enantiomeric separation of 1-phenylpropan-1-ol.

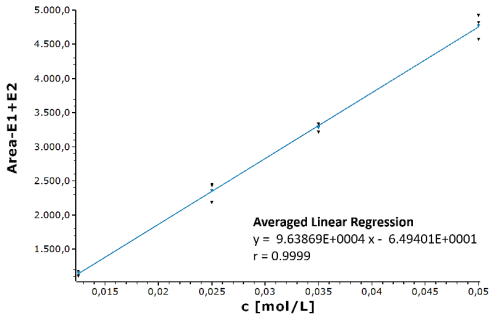

Figure 6.4: Linear regression of dilution series of 1-phenylpropan-1-ol.

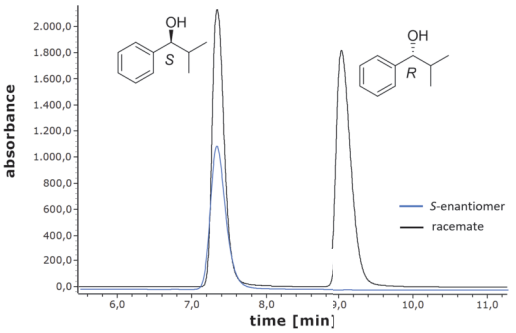

Figure 6.5: Enantiomeric separation of 2-methyl-1-phenylpropan-1-ol.

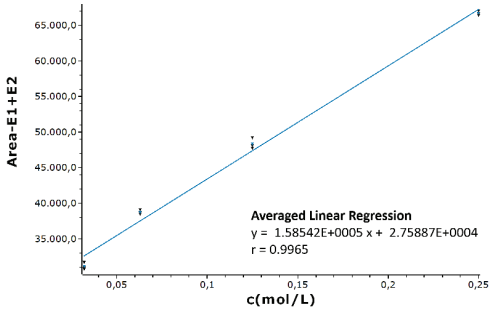

Figure 6.6: Linear regression of dilution series of 2-methyl-1-phenylpropan-1-ol.

Bibliography

[1] B. Feringa, R. A. Van Delden, *Angew. Chem. Int. Ed.* **1999**, *38*, 3418–3438.

[2] K. Soai, T. Kawasaki, *Chirality* **2006**, *18*, 469–478.

[3] T. Shibata, J. Yamamoto, N. Matsumoto, S. Yonekubo, S. Osanai, K. Soai, *J. Am. Chem. Soc.* **1998**, *120*, 12157–12158.

[4] T. Kawasaki, K. Jo, H. Igarashi, I. Sato, M. Nagano, H. Koshima, K. Soai, *Ange. Chem. Int. Ed.* **2005**, *44*, 2774–2777.

[5] T. Kawasaki, K. Hatase, Y. Fujii, K. Jo, K. Soai, S. Pizzarello, *Geochim. Cosmochim. Acta* **2006**, *70*, 5395–5402.

[6] V. Farina, J. T. Reeves, C. H. Senanayake, J. J. Song, *Chem. Rev.* **2006**, *106*, 2734–2793.

[7] M. Christmann, S. Bräse, *Asymmetric Synthesis - The Essentials*, *Vol. 2*, John Wiley, **2007**.

[8] Y. Izumi, *Angew. Chem. Int. Ed.* **1971**, *10 (12)*, 871–948.

[9] D. A. Evans, M. D. Ennis, D. J. Mathre, *J. Am. Chem. Soc.* **1982**, *104 (6)*, 1737–1739.

[10] K. Mikami, M. Lautens, *New Frontiers in Asymmetric Catalysis*, John Wiley, **2007**, p. 316.

[11] R. Noyori, *Asymmetric Catalysis in Organic Synthesis*, John Wiley, **1994**, pp. 1–3.

[12] R. S. A. of Science, Nobelprize in Chemistry 2001, **2001**, `https://www.nobelprize.org/prizes/chemistry/2001/9083-pressemitteilung-der-nobelpreis-in-chemie-2001/` (visited on 08/03/2023).

[13] M. J. Schweiter, K. B. Sharpless, *Tetrahedron Lett.* **1985**, *26 (21)*, 2543–2546.

[14] T. Katsuki, K. B. Sharpless, *J. Am. Chem. Soc.* **1980**, *102 (18)*, 5974–5976.

[15] R. Noyori, T. Ohkuma, M. Kitamura, H. Takaya, N. Sayo, H. Kumobayashi, S. Akutagawa, *J. Am. Chem. Soc.* **1987**, *109 (19)*, 5856–5858.

[16] A. Miyashita, A. Yasuda, H. Takaya, T. Ito, T. Souchi, R. Noyori, *J. Am. Chem. Soc.* **1980**, *102 (27)*, 7932–7934.

[17] N. Oguni, Y. Matsuda, T. Kaneko, *J. Am. Chem. Soc.* **1988**, *110*, 7877–7878.

[18] C. Puchot, O. Samuel, E. Dunach, S. Zhao, C. Agami, H. B. Kagan, *J. Am. Chem. Soc.* **1986**, *108*, 2353–2357.

[19] D. R. Fenwick, H. B. Kagan in *Topics in Stereochemistry*, John Wiley and Sons, **1999**, pp. 257–296.

[20] D. Guillaneux, S.-H. Zhao, O. Samuel, D. Rainford, H. B. Kagan, *J. Am. Chem. Soc.* **1994**, *116*, 9430–9439.

[21] T. Satyanarayana, S. Abraham, H. B. Kagan, *Ange. Chem. Int. Ed.* **2009**, *48*, 456–494.

[22] C. Girard, H. B. Kagan, *Ange. Chem. Int. Ed.* **1998**, *37*, 2922–2959.

[23] Y. Geiger, S. Bellemin-Laponnaz, *ChemCatChem* **2022**, *14*, e202200165.

[24] G. Storch, O. Trapp, *Nature Chem.* **2017**, *9*, 179–187.

[25] K. Soai, T. Shibata, H. Morioka, K. Choji, *Nature* **1995**, *378 (6559)*, 767–768.

[26] A. S., S. A., H. K.N., D. S.E., *Nature Chem.* **2020**, *12*, 412–423.

[27] L. F. Lindoy, I. M. Atkinson, *Self-assembly in Supramolecular Systems*, Royal Society of Chemistry, **2000**, pp. 1–7.

[28] M. H. Todd, *Chem. Soc. Rev.* **2002**, *31*, 211–222.

[29] M. G. Finn, K. B. Sharpless, *J. Am. Chem. Soc.* **1991**, *113*, 113–126.

[30] S. S. Woodard, M. G. Finn, K. B. Sharpless, *J. Am. Chem. Soc.* **1991**, *113*, 106–113.

[31] M. Kitamura, S. Okada, S. Suga, R. Noyori, *J. Am. Chem. Soc.* **1989**, *111*, 4028–4036.

[32] M. Yamakawa, R. Noyori, *J. Am. Chem. Soc.* **1995**, *117*, 6327–6335.

[33] F. Buono, P. J. Walsh, D. G. Blackmond, *J. Am. Chem. Soc.* **2002**, *124*, 13652–13653.

[34] W. A. Nugent, *Chem. Commun.* **1999**, 1369–1370.

[35] Y. K. Chen, A. M. Costa, P. J. Walsh, *J. Am. Chem. Soc.* **2001**, *123*, 5378–5379.

[36] T. Shibata, H. Morioka, T. Hayase, K. Choji, K. Soai, *J. Am. Chem. Soc.* **1996**, *118*, 471–472.

[37] T. Shibata, S. Yonekubo, K. Soai, *Angewandte Chemie* **1999**, *111*, 746–748.

[38] Z. Peng, K. Paschek, J. C. Xavier, *BioEssays* **2022**, *44*, 2200098.

[39] A. J. Bissette, S. P. Fletcher, *Ange. Chem. Int. Ed.* **2013**, *52*, 12800–12826.

[40] J. W. Szostak, *Nature* **2009**, *459*, 171–172.

[41] W. Ostwald, *Berichte über die Verhandlungen der Königlich Saechsischen Gesellschaft der Wissenschaften zu Leipzig Mathematisch-Physische Classe* **1890**, *42*, 189–191.

[42] W. Ostwald, *Z. f. Elektrochem.* **1901**, *7*, 995–1004.

[43] O. Markovitch, D. Lancet, *ALife* **2012**, *18*, 243–266.

[44] M. Eigen, P. Schuster, *Naturwissenschaften* **1977**, *64*, 541–565.

[45] A. I. Hanopolskyi, V. A. Smaliak, A. I. Novichkov, S. N. Semenov, *ChemSysChem* **2021**, *3*, e2000026.

[46] R. Breslow, *Tetrahedron Lett.* **1959**, *1*, 22–26.

[47] A. Butlerow, *CR Acad. Sci.* **1861**, *53*, 145–147.

[48] L. E. Orgel, *PLOS Biology* **2008**, *6*, 1–9.

[49] H. Rauchfuss, *Chemische Evolution und der Ursprung des Lebens*, Springer Berlin Heidelberg, Berlin, Heidelberg, **2005**, pp. 105–149.

[50] A. H. Weiss, R. B. LaPierre, J. Shapira, *J. Catal.* **1970**, *16*, 332–347.

[51] G. von Kiedrowski in *Bioorganic Chemistry Frontiers*, (Eds.: H. Dugas, F. P. Schmidtchen), Springer Berlin Heidelberg, Berlin, Heidelberg, **1993**, pp. 113–146.

[52] Z. Dadon, N. Wagner, G. Ashkenasy, *Ange. Chem. Int. Ed.* **2008**, *47*, 6128–6136.

[53] F. Frank, *Biochim. Biophys. Acta* **1953**, *11*, 459–463.

[54] K. Ichimura, *Chem. Rec.* **2002**, *2*, 46–55.

[55] K. J. Singh, A. C. Hoepker, D. B. Collum, *J. Am. Chem. Soc.* **2008**, *130*, 18008–18017.

[56] F. Barrios-Landeros, B. P. Carrow, J. F. Hartwig, *J. Am. Chem. Soc.* **2008**, *130*, 5842–5843.

[57] A. C. Hoepker, L. Gupta, Y. Ma, M. F. Faggin, D. B. Collum, *J. Am. Chem. Soc.* **2011**, *133*, 7135–7151.

[58] P. P. Neelakandan, A. Jiménez, J. D. Thoburn, J. R. Nitschke, *Ange. Chem. Int. Ed.* **2015**, *54*, 14378–14382.

[59] E. R. Thapaliya, S. Swaminathan, B. Captain, F. M. Raymo, *J. Am. Chem. Soc.* **2014**, *136*, 13798–13804.

[60] A. H. Alberts, H. Wynberg, *J. Am. Chem. Soc.* **1989**, *111*, 7265–7266.

[61] N. Chinkov, A. Warm, E. M. Carreira, *Ange. Chem. Int. Ed.* **2011**, *50*, 2957–2961.

[62] M. Mauksch, B. Tsogoeva, Svetlana, M. Martynova, Irina, S. Wei, *Ange. Chem. Int. Ed.* **2007**, *46*, 393–396.

[63] A. Blokhuis, D. Lacoste, P. Nghe, *Proc. Natl. Acad. Sci.* **2020**, *117*, 25230–25236.

[64] K. Soai, A. Matsumoto, T. Kawasaki in *Advances in Asymmetric Autocatalysis and Related Topics*, (Eds.: G. Palyi, R. Kurdi, C. Zucchi), Academic Press, **2017**, pp. 1–30.

[65] D. Blackmond, *Cold Spring Harb Perspect. Biol.* **2010**, 2:a002147.

[66] K. Soai, S. Niwa, H. Hori, *J. Chem. Soc.* **1990**, 982–983.

[67] T. Gehring, M. Busch, M. Schlageter, D. Weingand, *Chirality* **2010**, *22*, E173–E182.

[68] I. Sato, T. Yanagi, K. Soai, *Chirality* **2002**, *14*, 166–168.

[69] M. Busch, M. Schlageter, D. Weingand, T. Gehring, *Chem. Eur. J.* **2009**, *15*, 8251–8258.

[70] D. A. Singleton, L. K. Vo, *J. Am. Chem. Soc.* **2002**, *124*, 10010–10011.

[71] I. Sato, H. Urabe, S. Ishiguro, T. Shibata, K. Soai, *Angewandte Chemie* **2003**, *115*, 329–331.

[72] K. Soai, T. Shibata, I. Sato, *Bull. Chem. Soc. Jpn.* **2004**, *77*, 1063–1073.

[73] H. Wyneberg, *Chimia* **1989**, *43*, 150.

[74] M. Quack, *Ange. Chem. Int. Ed.* **2002**, *41*, 4618–4630.

[75] O. Trapp, *Frontiers in Chemistry* **2020**, *8*, DOI `10.3389/fchem.2020.615800`.

[76] O. Trapp, S. Lamour, F. Maier, A. F. Siegle, K. Zawatzky, B. F. Straub, *Chem. Eur. J.* **2020**, *26*, 15871–15880.

[77] N. Oguni, T. Omi, *Tetrahedron Lett.* **1984**, *25*, 2823–2824.

[78] I. Sato, D. Omiya, K. Tsukiyama, Y. Ogi, K. Soai, *Tetrahedron: Asymm.* **2001**, *12*, 1965–1969.

[79] D. G. Blackmond, C. R. McMillan, S. Ramdeehul, A. Schorm, J. M. Brown, *J. Am. Chem. Soc.* **2001**, *123*, 10103–10104.

[80] I. Sato, D. Omiya, H. Igarashi, K. Kato, Y. Ogi, K. Tsukiyama, K. Soai, *Tetrahedron: Asymm.* **2003**, *14*, 975–979.

[81] A. Matsumoto, T. Abe, A. Hara, T. Tobita, T. Sasagawa, T. Kawasaki, K. Soai, *Ange. Chem. Int. Ed.* **2015**, *54*, 15218–15221.

[82] D. Guillaneux, S.-H. Zhao, O. Samuel, D. Rainford, H. B. Kagan, *J. Am. Chem. Soc.* **1994**, *116*, 9430–9439.

[83] F. G. Buono, D. G. Blackmond, *J. Am. Chem. Soc.* **2003**, *125*, 8978–8979.

[84] D. G. Blackmond, *Tetrahedron: Asymm.* **2006**, *17*, 584–589.

[85] I. D. Gridnev, J. M. Serafimov, J. M. Brown, *Ange. Chem. Int. Ed.* **2004**, *43*, 4884–4887.

[86] J. Klankermayer, I. D. Gridnev, J. M. Brown, *Chem. Commun.* **2007**, 3151–3153.

[87] M. Quaranta, T. Gehring, B. Odell, J. M. Brown, D. G. Blackmond, *J. Am. Chem. Soc.* **2010**, *132*, 15104–15107.

[88] I. D. Gridnev, A. K. Vorobiev, *ACS Catalysis* **2012**, *2*, 2137–2149.

[89] T. Gehring, M. Quaranta, B. Odell, D. G. Blackmond, J. M. Brown, *Ange. Chem. Int. Ed.* **2012**, *51*, 9539–9542.

[90] Y. Geiger, *Chem. Soc. Rev.* **2022**, *51*, 1206–1211.

[91] S. V. Athavale, A. Simon, K. N. Houk, S. E. Denmark, *J. Am. Chem. Soc.* **2020**, *142*, 18387–18406.

[92] O. Trapp, *Ange. Chem. Int. Ed.* **2007**, *46*, 5609–5613.

[93] A. F. Siegle, O. Trapp, *Anal. Chem.* **2014**, *86*, 10828–10833.

[94] C. J. Welch, X. Gong, W. Schafer, E. C. Pratt, T. Brkovic, Z. Pirzada, J. F. Cuff, B. Kosjek, *Tetrahedron: Asymm.* **2010**, *21*, Henri Kagan: An 80th Birthday Celebration Special Issue - Part 3, 1674–1681.

[95] F. Maier, PhD thesis, Ruprecht-Karls-Universität Heidelberg, **2013**.

[96] D. Drahoovský, J.-M. Lehn, *J. Org. Chem.* **2009**, *74*, 8428–8432.

[97] Z. Li, L. Zhang, Y. Zhou, D. Zha, Y. Hai, L. You, *Eur. J. Org. Chem.* **2022**, *2022*, e202101461.

[98] J. Zhang, J. Qiu, C. Xiao, L. Yu, F. Yang, J. Tang, *Eur. J. Org. Chem.* **2016**, *2016*, 3380–3385.

[99] M. Lonar, M. Jakovljevi, D. ubari, M. Pavli, V. Buzjak Sluek, I. Cindri, M. Molnar, *Foods* **2020**, *9*, DOI `10.3390/foods9050645`.

[100] N. A. Khatune, M. E. Islam, M. E. Haque, P. Khondkar, M. M. Rahman, *Fitoterapia* **2004**, *75*, 228–230.

[101] D. R. Perrin, W. Bottomley, *Nature* **1961**, *191*, 76–77.

[102] N. Kaushik-Basu, A. Bopda-Waffo, T. T. Talele, A. Basu, P. R. R. Costa, A. J. M. da Silva, S. G. Sarafianos, F. Noel, *Nucleic Acids Res.* **2008**, *36*, 1482–1496.

[103] E. Bickoff, A. Livingston, A. Booth, *Arch. Biochem. Biophys.* **1960**, *88*, 262–266.

[104] L. Ruan, M. Shi, N. Li, X. Ding, F. Yang, J. Tang, *Org. Lett.* **2014**, *16*, 733–735.

[105] P. Mathew, D. Mathew, C. V. Asokan, *Synth. Commun.* **2007**, *37*, 661–665.

[106] T. W. G. Solomons, *Organic chemistry / T.W. Graham Solomons*, 4th ed., Wiley New York, **1988**, pp. 783–810.

[107] G. Gilli, F. Bellucci, V. Ferretti, V. Bertolasi, *J. Am. Chem. Soc.* **1989**, *111*, 1023–1028.

[108] D. E. Williams, W. L. Dunke, R. E. Rundle, *Acta Crystallogr.* **1962**, *15*, 627–635.

[109] M. N. C. Zarycz, C. Fonseca Guerra, *J. Phys. Chem. Lett.* **2018**, *9*, 3720–3724.

[110] P. R. Jones, *Chem. Rev.* **1963**, *63*, 461–487.

[111] F. Maier, O. Trapp, *Ange. Chem. Int. Ed.* **2012**, *51*, 2985–2988.

[112] G. Weseloh, C. Wolf, W. A. König, *Ange. Chem. Int. Ed.* **1995**, *34*, 1635–1636.

[113] P. U. Biedermann, V. Schurig, I. Agranat, *Chirality* **1997**, *9*, 350–353.

[114] S. Auras, O. Trapp, *Chirality* **2022**, *34*, 813–819.

[115] X. Xue, Z. Gu, *Org. Lett.* **2019**, *21*, 3942–3945.

[116] G. Bringmann, M. Heubes, M. Breuning, L. Göbel, M. Ochse, B. Schöner, O. Schupp, *J. Org. Chem.* **2000**, *65*, 722–728.

[117] G. Bringmann, T. Hartung, *Liebigs Annalen der Chemie* **1994**, *1994*, 313–316.

[118] G. Bringmann, D. Vitt, J. Kraus, M. Breuning, *Tetrahedron* **1998**, *54*, 10691–10698.

[119] G. Bringmann, M. Breuning, H. Endress, D. Vitt, K. Peters, E.-M. Peters, *Tetrahedron* **1998**, *54*, 10677–10690.

[120] S. Heitsch, L. C. Mayer, Y. L. Pignot, O. Trapp, *Chirality* **2023**, *n/a*, 1–13.

[121] R. A. Johnstone in *Comprehensive Organic Synthesis*, (Eds.: B. M. Trost, I. Fleming), Pergamon, Oxford, **1991**, pp. 259–281.

[122] X. Verdaguer, S. C. Berk, S. L. Buchwald, *J. Am. Chem. Soc.* **1995**, *117*, 12641–12642.

[123] E. Winterfeldt, *Synthesis* **1975**, *10*, 617–630.

[124] S. S. Moleele, J. P. Michael, C. B. de Koning, *Tetrahedron* **2006**, *62*, 2831–2844.

[125] A. A. Mikhaylov, A. D. Dilman, R. A. Novikov, Y. A. Khoroshutina, M. I. Struchkova, D. E. Arkhipov, Y. V. Nelyubina, A. A. Tabolin, S. L. Ioffe, *Tetrahedron Lett.* **2016**, *57*, 11–14.

[126] J. Yang, B. Chatelet, V. Dufaud, D. Hérault, M. Jean, N. Vanthuyne, J.-C. Mulatier, D. Pitrat, L. Guy, J.-P. Dutasta, A. Martinez, *Org. Lett.* **2020**, *22*, 891–895.

[127] A. Charette, M.-N. Roy in *Compr. Chiraltiy*, (Eds.: E. M. Carreira, H. Yamamoto), Elsevier, Amsterdam, **2012**, pp. 780–806.

[128] H. Shimizu, I. Nagasaki, K. Matsumura, N. Sayo, T. Saito, *Acc. Chem. Res.* **2007**, *40*, 1385–1393.

[129] T. Saito, T. Yokozawa, T. Ishizaki, T. Moroi, N. Sayo, T. Miura, H. Kumobayashi, *Adv. Synth. Catal.* **2001**, *343*, 264–267.

[130] N. Y. More, M. Jeganmohan, *Chem. Commun.* **2017**, *53*, 9616–9619.

[131] P. Ruzza, P. A. Serra, D. Fabbri, M. A. Dettori, G. Rocchitta, G. Delogu, *Eur. J. Med. Chem.* **2017**, *126*, 1034–1038.

[132] V. Schurig, *Chirality* **1998**, *10*, 140–146.

[133] O. Trapp, *Anal. Chem.* **2006**, *78*, 189–198.

[134] O. Trapp, *J. Chromatogr.* **2008**, *875*, 42–47.

[135] T. Ikai, Y. Okamoto, *Chem. Rev.* **2009**, *109*, 6077–6101.

[136] R. Noyori, M. Kitamura, *Ange. Chem. Int. Ed. in English* **1991**, *30*, 49–69.

[137] M. Kitamura, S. Suga, K. Kawai, R. Noyori, *J. Am. Chem. Soc.* **1986**, *108*, 6071–6072.

[138] M. Kitamura, H. Oka, R. Noyori, *Tetrahedron* **1999**, *55*, 3605–3614.

[139] T. Rasmussen, P.-O. Norrby, *J. Am. Chem. Soc.* **2001**, *123*, 2464–2465.

[140] T. Rasmussen, P.-O. Norrby, *J. Am. Chem. Soc.* **2003**, *125*, 5130–5138.

[141] B. Goldfuss, K. N. Houk, *J. Org. Chem.* **1998**, *63*, 8998–9006.

[142] B. Goldfuss, M. Steigelmann, S. I. Khan, K. N. Houk, *J. Org. Chem.* **2000**, *65*, 77–82.

[143] K. Soai, S. Niwa, *Chem. Rev.* **1992**, *92*, 833–856.

[144] K. Soai, A. Ookawa, T. Kaba, K. Ogawa, *J. Am. Chem. Soc.* **1987**, *109*, 7111–7115.

[145] A. Ookawa, K. Soai, *J. Chem. Soc. Perkin Trans. 1* **1987**, 1465–1471.

[146] K. Soai, A. Ookawa, K. Ogawa, T. Kaba, *J. Chem. Soc.* **1987**, 467–468.

[147] M. Asami, S. Inoue, *Chem. Lett.* **1991**, *20*, 685–688.

[148] P. Delair, C. Einhorn, J. Einhorn, J. Luche, *Tetrahedron* **1995**, *51*, 165–172.

[149] Y. Kawanami, T. Mitsuie, M. Miki, T. Sakamoto, K. Nishitani, *Tetrahedron* **2000**, *56*, 175–178.

[150] J. Beliczey, G. Giffels, U. Kragl, C. Wandrey, *Tetrahedron: Asymm.* **1997**, *8*, 1529–1530.

[151] P. A. Chaloner, S. Perera, *Tetrahedron Lett.* **1987**, *28*, 3013–3014.

[152] K. Soai, M. Nishi, Y. Ito, *Chem. Lett.* **1987**, *16*, 2405–2406.

[153] E. Corey, F. J. Hannon, *Tetrahedron Lett.* **1987**, *28*, 5233–5236.

[154] T. H. S. Yokoyama, K. Ebihara, K. Soai, *J. Chem. Soc. Chem. Commun.* **1987**, 1690–1691.

[155] K. Soai, S. Yokoyama, T. Hayasaka, *J. Org. Chem.* **1991**, *56*, 4264–4268.

[156] T. Katagiri, Y. Fujiwara, S. Takahashi, N. Ozaki, K. Uneyama, *Chem. Commun.* **2002**, 986–987.

[157] S. Lauzon, T. Ollevier, *Chem. Commun.* **2021**, *57*, 11025–11028.

[158] M. Yus, D. J. Ramón, O. Prieto, *Tetrahedron: Asymm.* **2003**, *14*, 1103–1114.

[159] I. Sato, T. Saito, K. Soai, *Chem. Commun.* **2000**, 2471–2472.

[160] S. Bastin, F. Agbossou-Niedercorn, J. Brocard, L. Pélinski, *Tetrahedron: Asymm.* **2001**, *12*, 2399–2408.

[161] J. M. Andrés, M. A. Martínez, R. Pedrosa, A. Pérez-Encabo, *Tetrahedron: Asymm.* **1994**, *5*, 67–72.

[162] C. Bolm, M. Zehnder, D. Bur, *Ange. Chem. Int. Ed.* **1990**, *29*, 205–207.

[163] P. A. Chaloner, E. Langadianou, S. A. R. Perera, *J. Chem. Soc. Perkin Trans. 1* **1991**, 2731–2735.

[164] C. Bolm, K. Muñiz, *Chem. Commun.* **1999**, 1295–1296.

[165] L. Huang W.-S., Pu, *J. Org. Chem.* **1999**, 4222–4223.

[166] K. Funabiki, A. Shibata, H. Iwata, K. Hatano, Y. Kubota, K. Komura, M. Ebihara, M. Matsui, *J. Org. Chem.* **2008**, *73*, 4694–4697.

[167] X. Wu, X. Li, M. McConville, O. Saidi, J. Xiao, *Journal of Molecular Catalysis A: Chemical* **2006**, *247*, 153–158.

[168] J. A. Forni, L. F. T. Novaes, R. Galaverna, J. C. Pastre, *Cat. Today* **2018**, *308*, 86–93.

[169] Z. Begum, H. Sannabe, C. Seki, Y. Okuyama, E. Kwon, K. Uwai, M. Tokiwa, S. Tokiwa, M. Takeshita, H. Nakano, *RSC Adv.* **2021**, *11*, 203–209.

[170] T. Hayase, T. Sugiyama, M. Suzuki, T. Shibata, K. Soai, *J. Fluor. Chem.* **1997**, *84*, 1–5.

[171] T. A. Davidson, K. Mondal, X. Yang, *J. Colloid Interface Sci.* **2004**, *276*, 498–502.

[172] L. Pu, *Acc. Chem. Res.* **2014**, *47*, 1523–1535.

[173] M.-C. Wang, Q.-J. Zhang, G.-W. Li, Z.-K. Liu, *Tetrahedron: Asymm.* **2009**, *20*, 288–292.

[174] G. Blay, I. Fernández, V. Hernández-Olmos, A. Marco-Aleixandre, J. R. Pedro, *Tetrahedron: Asymm.* **2005**, *16*, 1953–1958.

[175] Y. S. Sokeirik, H. Mori, M. Omote, K. Sato, A. Tarui, I. Kumadaki, A. Ando, *Org. Lett.* **2007**, *9*, 1927–1929.

[176] L. Schiaffino, G. Ercolani, *Ange. Chem. Int. Ed.* **2008**, *47*, 6832–6835.

[177] K. Soai, T. Hayase, K. Takai, T. Sugiyama, *J. Org. Chem.* **1994**, *59*, 7908–7909.

[178] K. Soai, I. Sato, *Comptes Rendus Chimie* **2003**, *6*, 1097–1104.

[179] G. R. Fulmer, A. J. M. Miller, N. H. Sherden, H. Gottlieb, A. Nudelman, B. M. Stoltz, J. E. Bercaw, K. I. Goldberg, *Organometallics* **2010**, *29*, 2176–2179.

[180] S. S. Moleele, J. P. Michael, C. B. de Koning, *Tetrahedron* **2006**, *62*, 2831–2844.

[181] A. A. Mikhaylov, A. D. Dilman, R. A. Novikov, Y. A. Khoroshutina, M. I. Struchkova, D. E. Arkhipov, Y. V. Nelyubina, A. A. Tabolin, S. L. Ioffe, *Tetrahedron Lett.* **2016**, *57*, 11–14.

7 Appendix

7.1 Supporting data for Chapter 1

7.1.1 Supporting NMR-data for Coumestan Compounds

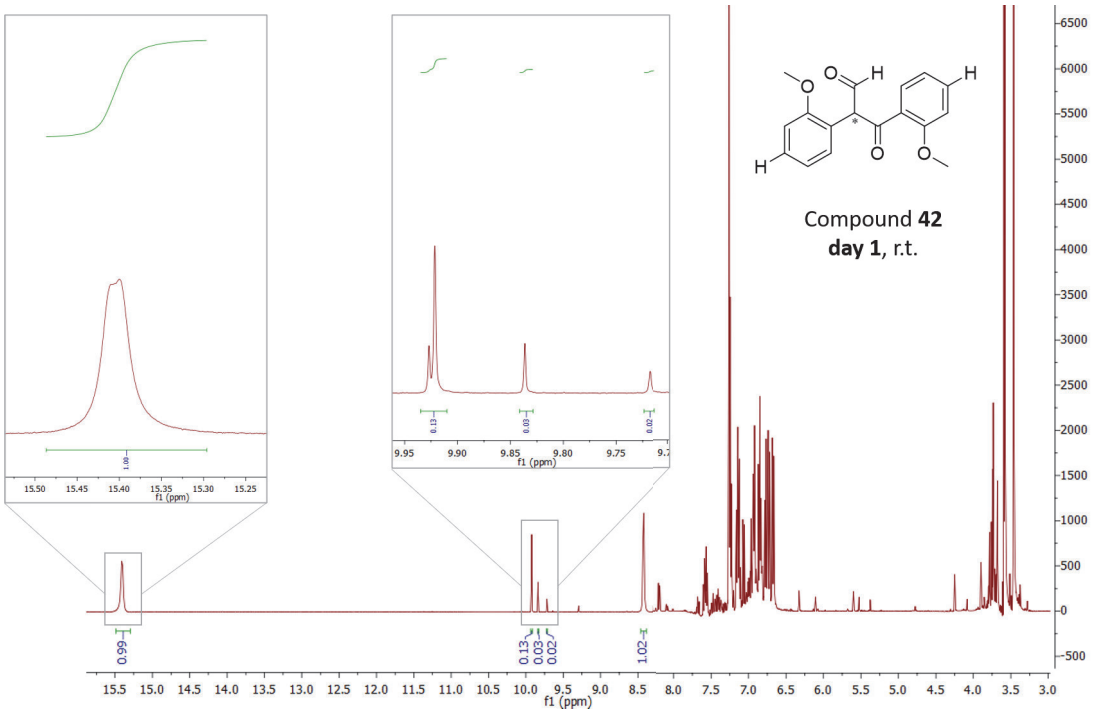

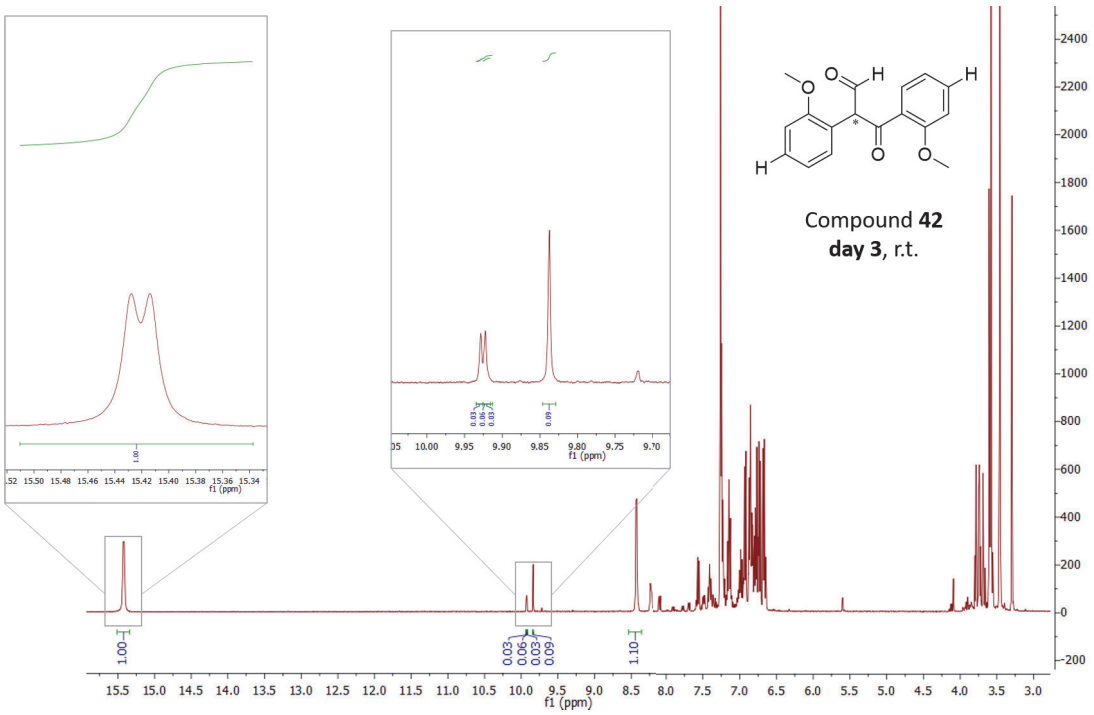
Compound **42**
day 3, r.t.
f1 (ppm)

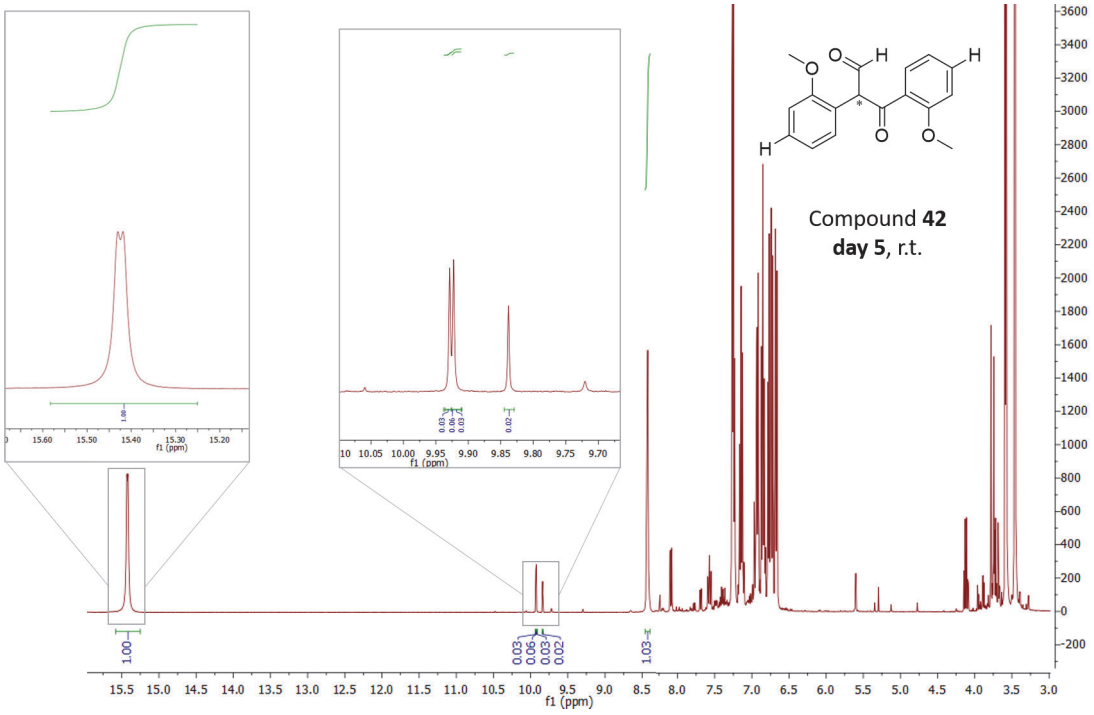
Compound **42**
day 5, r.t.
f1 (ppm)

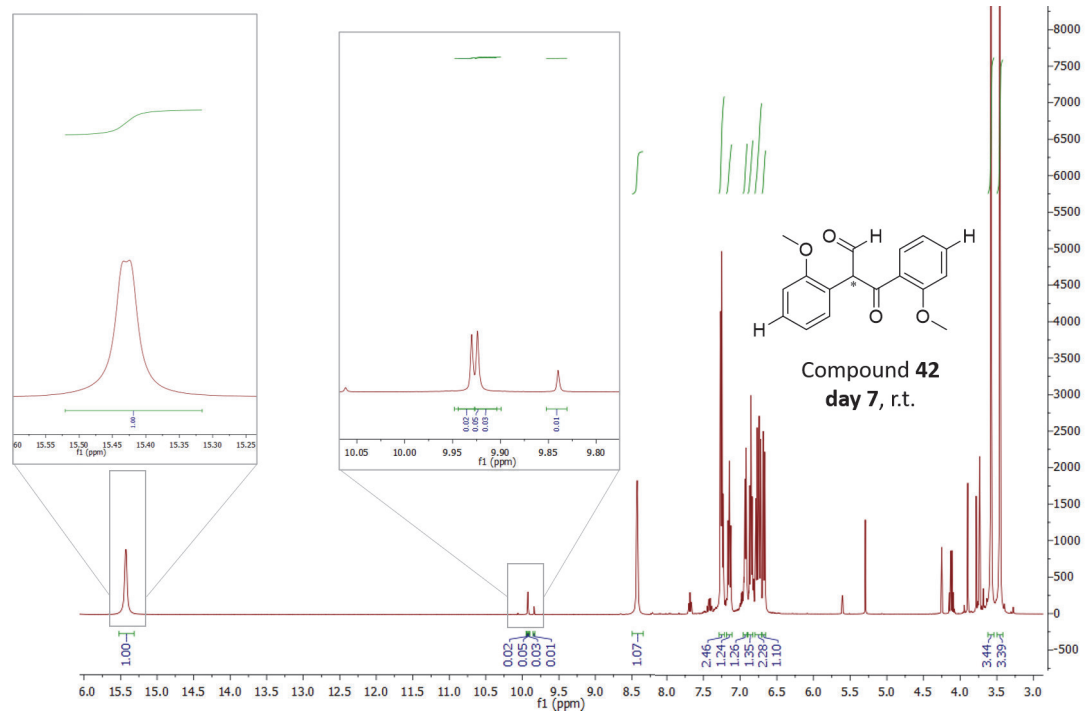
Compound **42**
day 7, r.t.
f1 (ppm)

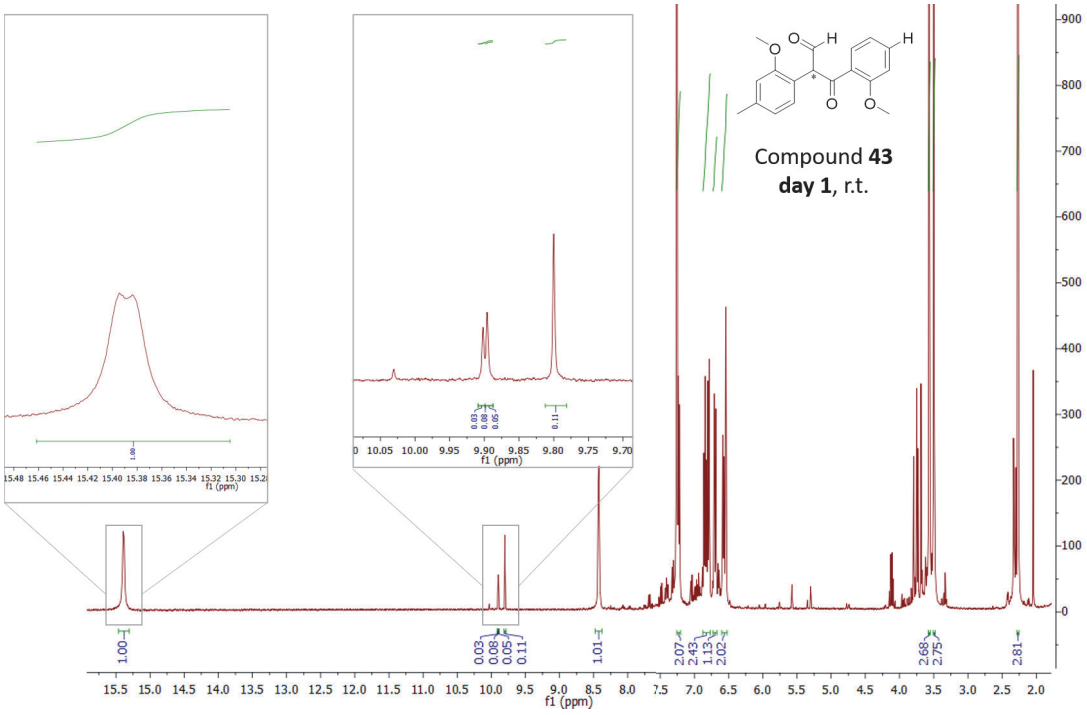
Compound **43**
day 1, r.t.
f1 (ppm)

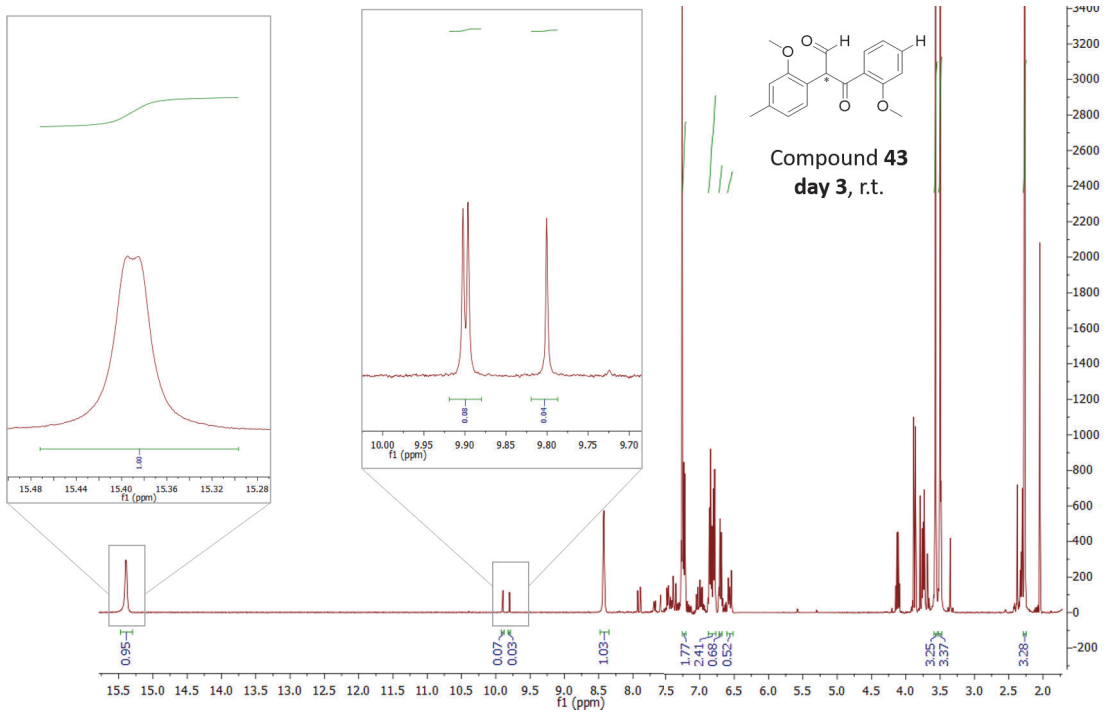
Compound **43**
day 3, r.t.
f1 (ppm)

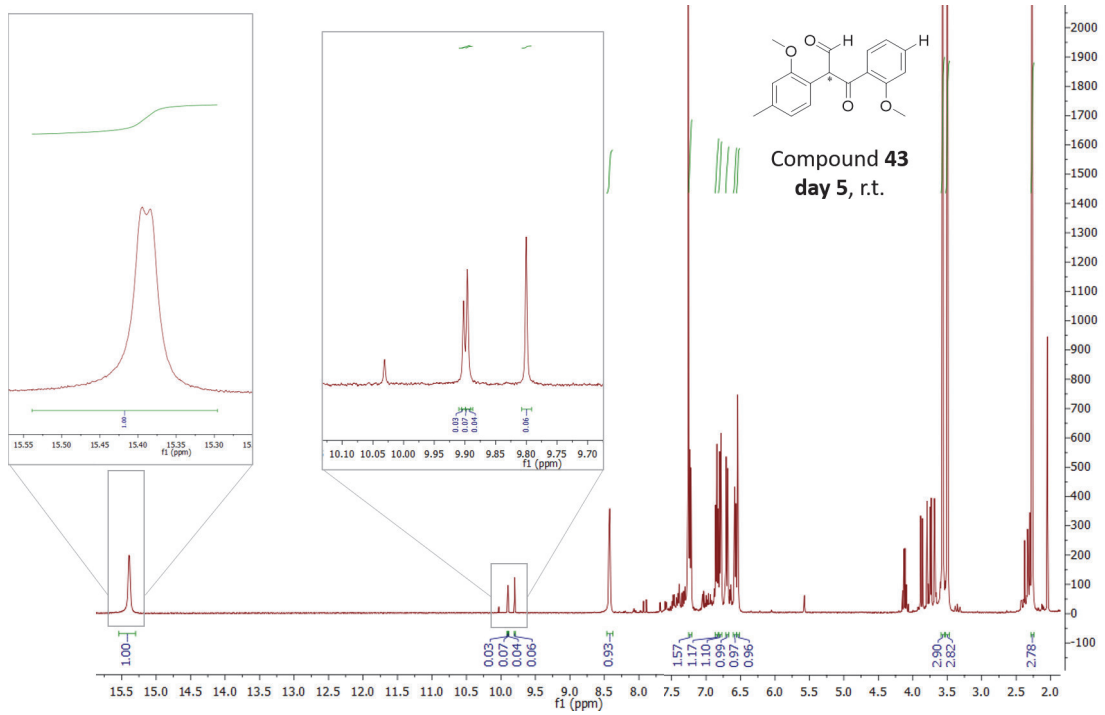
Compound **43**
day 5, r.t.
f1 (ppm)

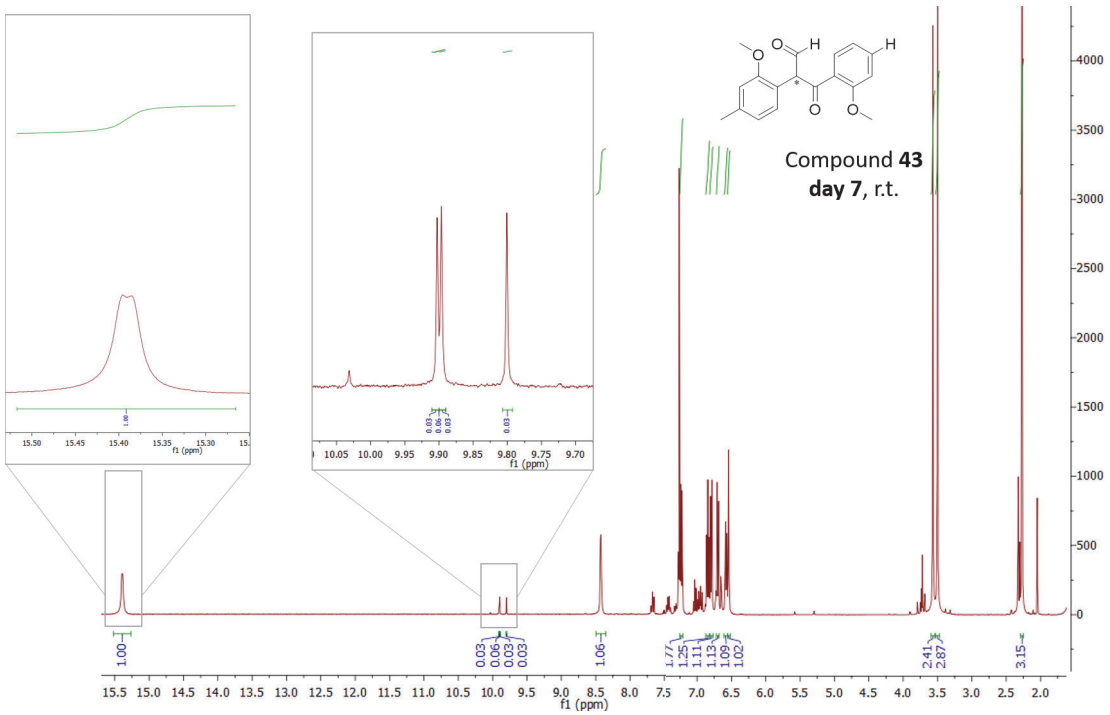
Compound **43**
day 7, r.t.
f1 (ppm)

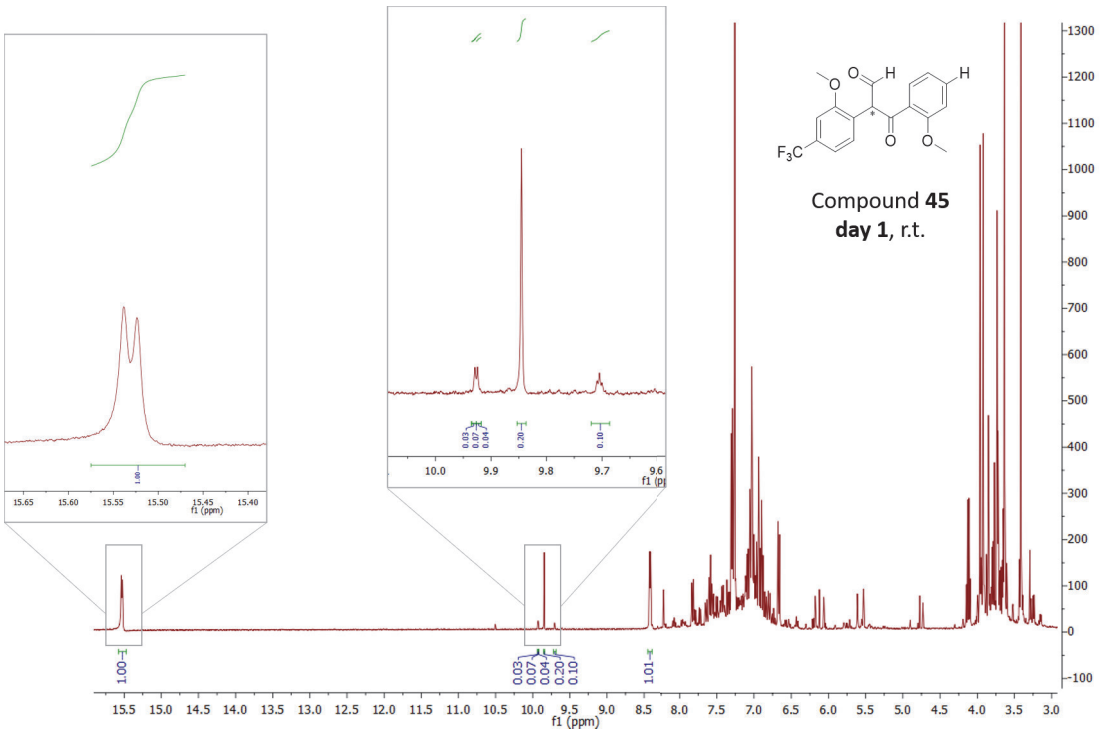
Compound **45**
day 1, r.t.
f1 (ppm)

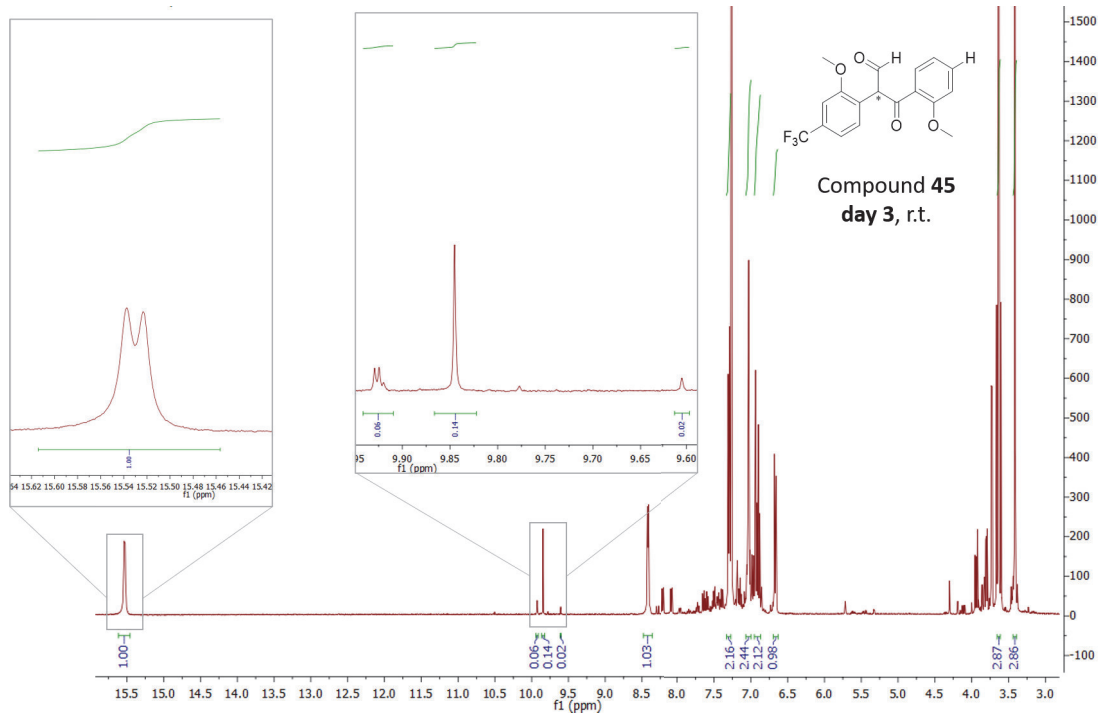
Compound **45**
day 3, r.t.
f1 (ppm)

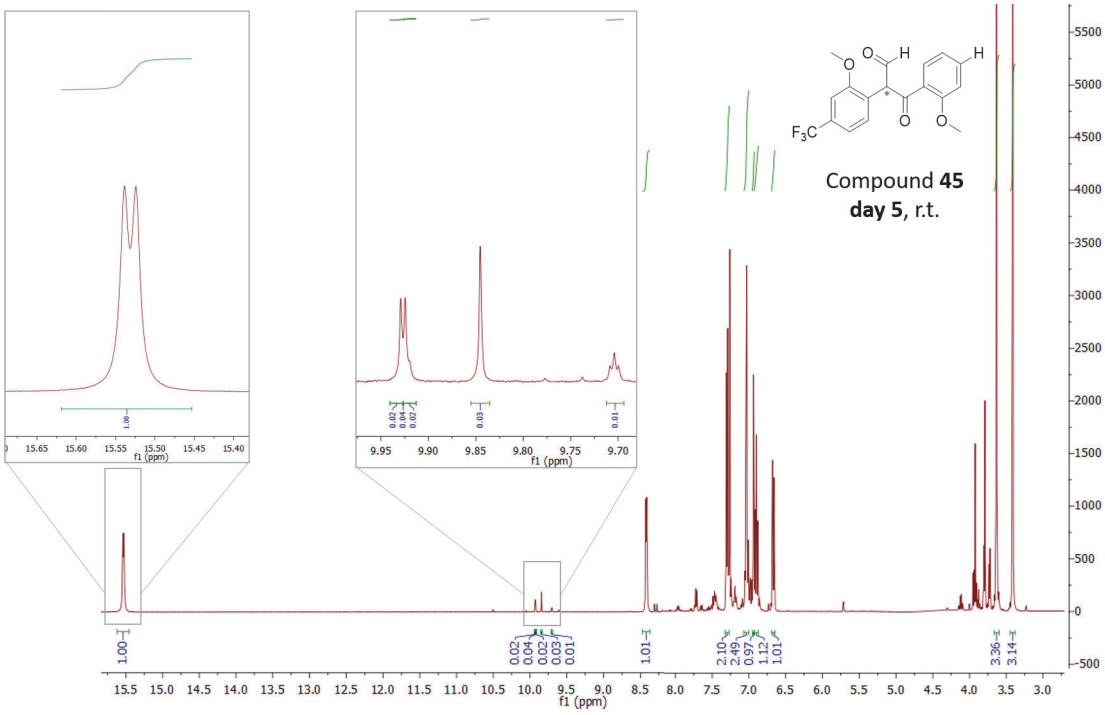
Compound **45**
day 5, r.t.
f1 (ppm)

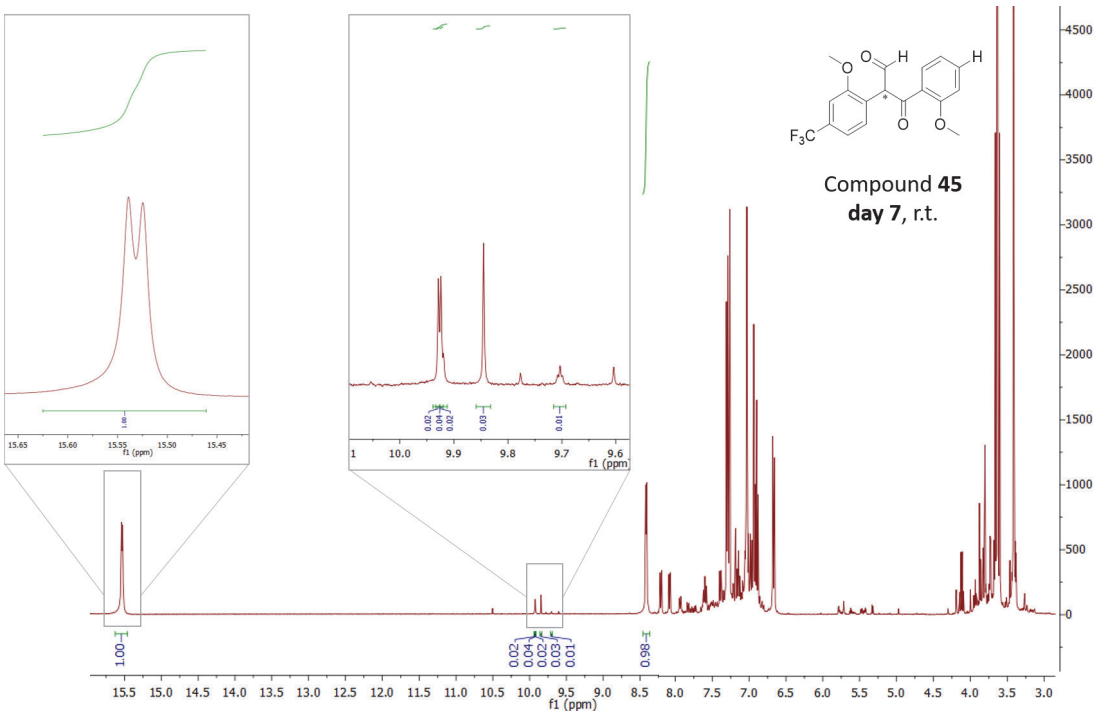
Compound **45**
day 7, r.t.
f1 (ppm)

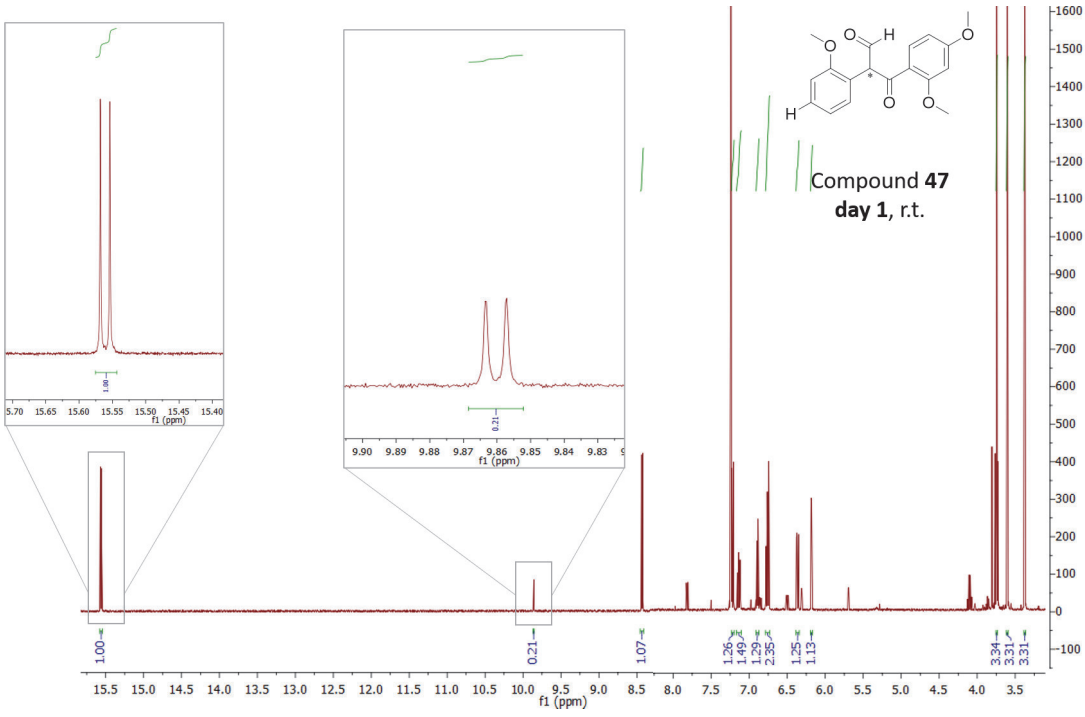
Compound **47**
day 1, r.t.
f1 (ppm)

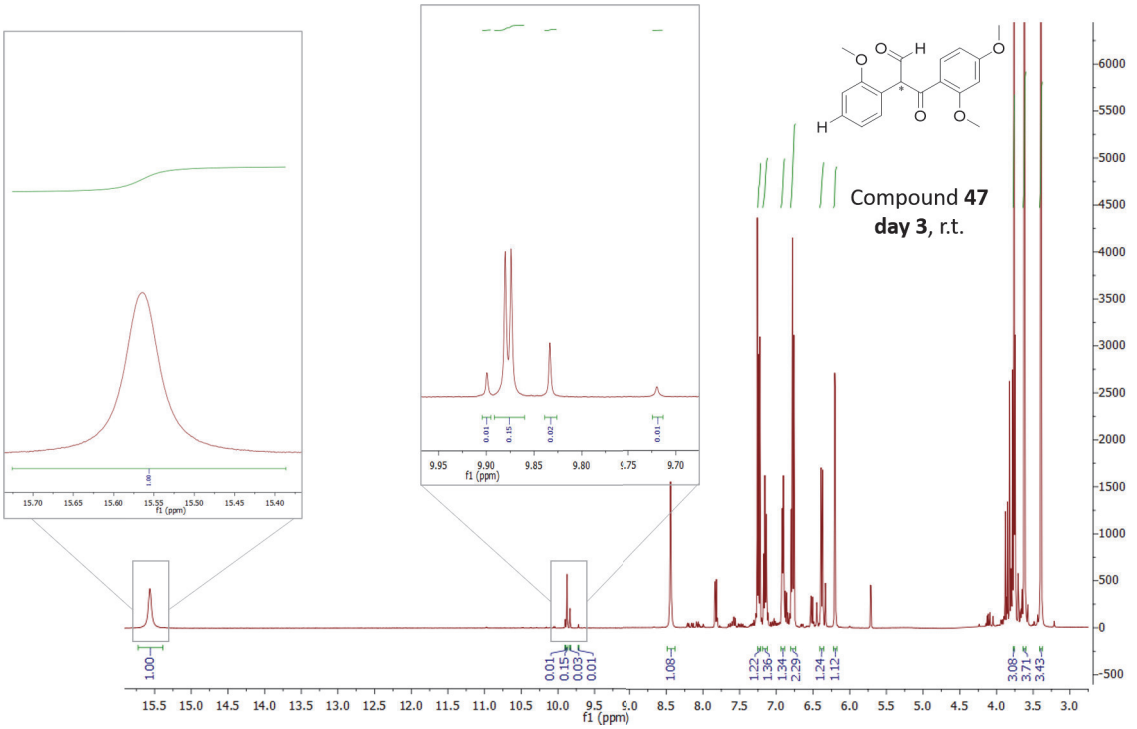
Compound **47**
day 3, r.t.
f1 (ppm)

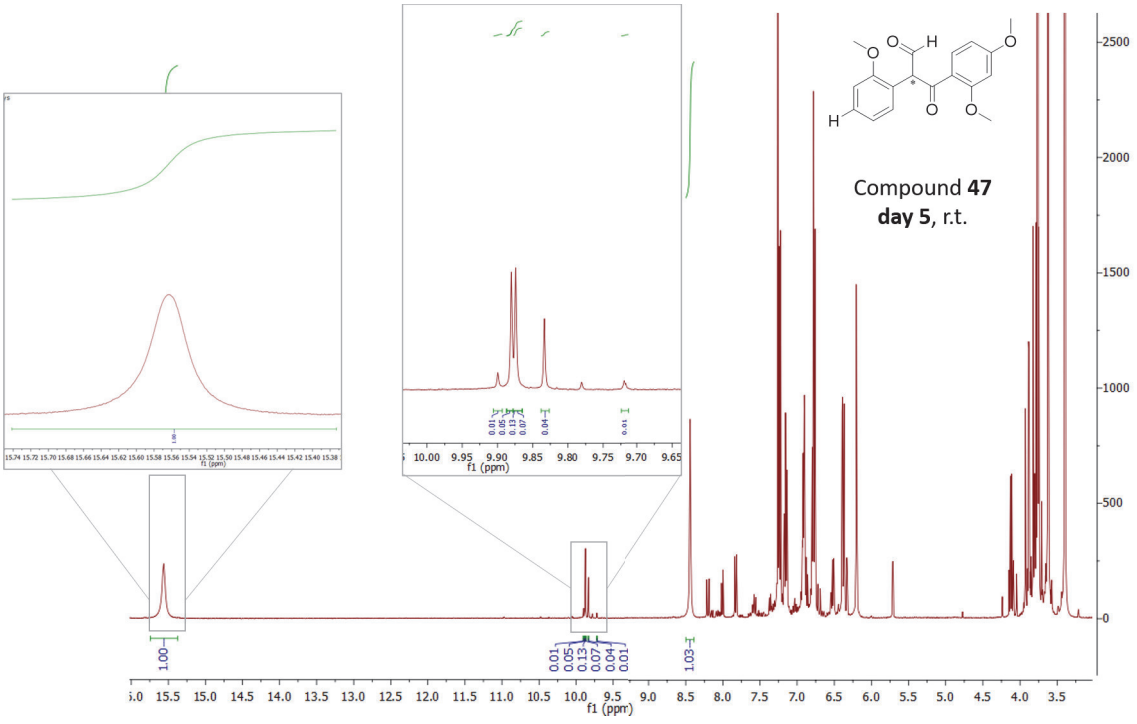
Compound **47**
day 5, r.t.
f1 (ppm)

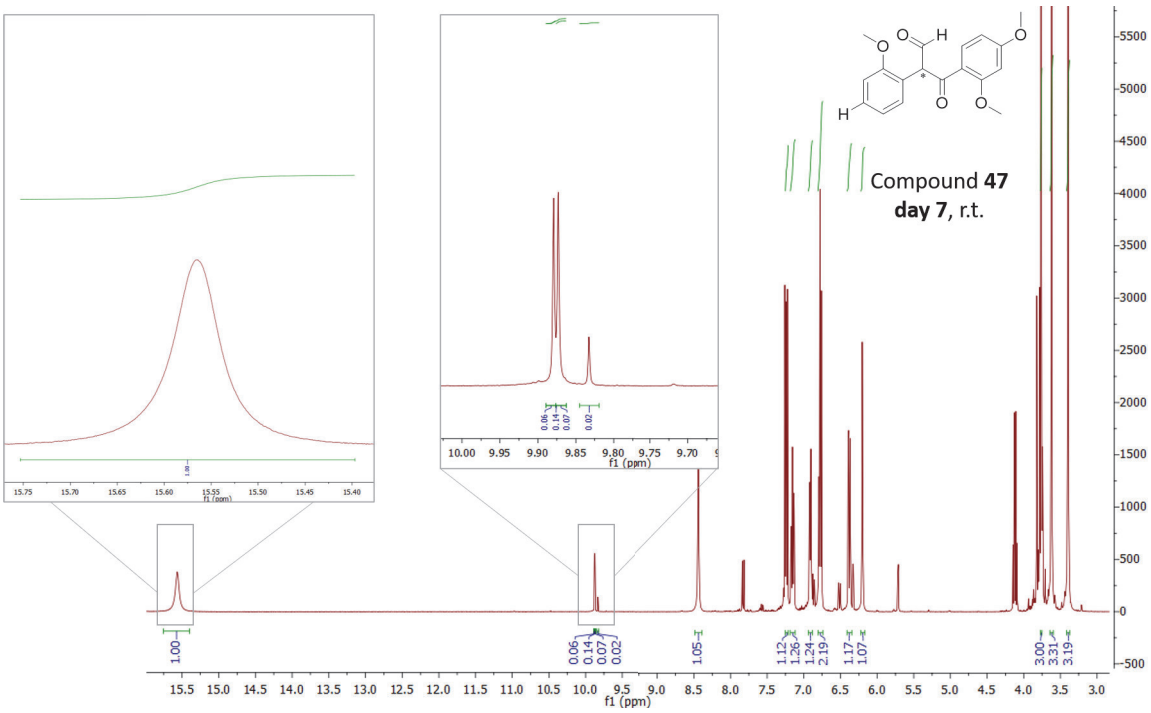
Compound **47**
day 7, r.t.
f1 (ppm)

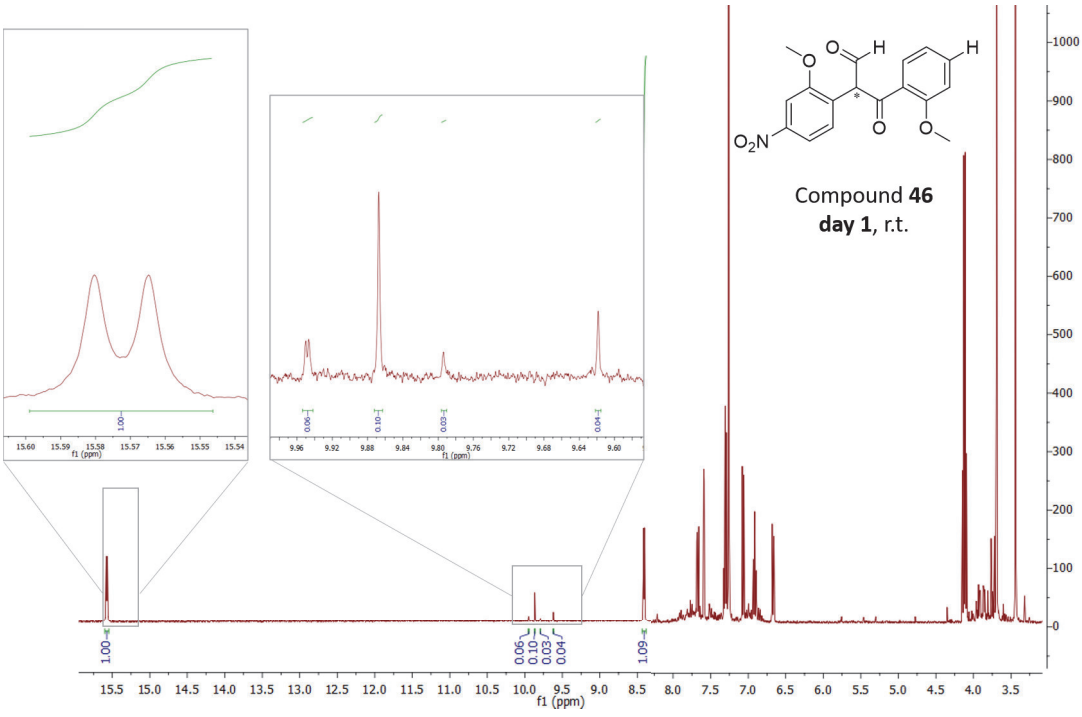
Compound **46**
day 1, r.t.
f1 (ppm)

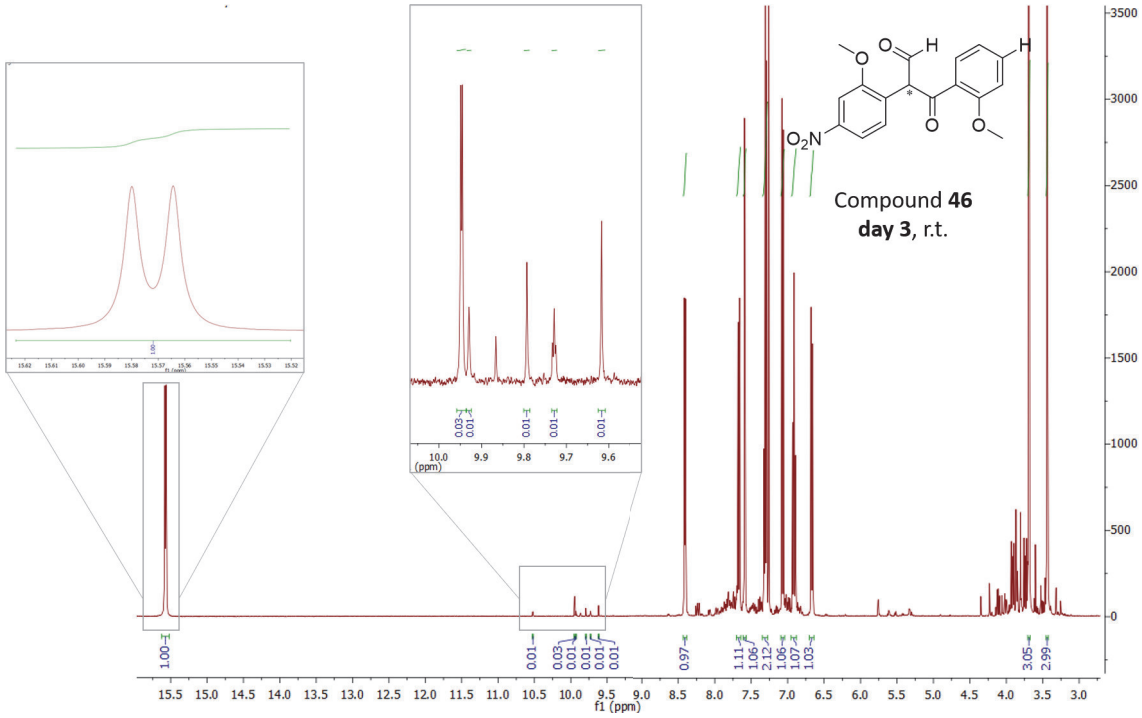
Compound 46
day 3, r.t.
f1 (ppm)

7.1.2 Supporting HPLC-data for Diorganozinc Alkylations with Hemiacetal Ligands

Dimethylzinc

#	Time	Area	Height	Width	Area%	Symmetry
1	9.43	760	57.6	0.22	51.860	0.748
2	11.217	705.5	47.1	0.2499	48.140	0.832

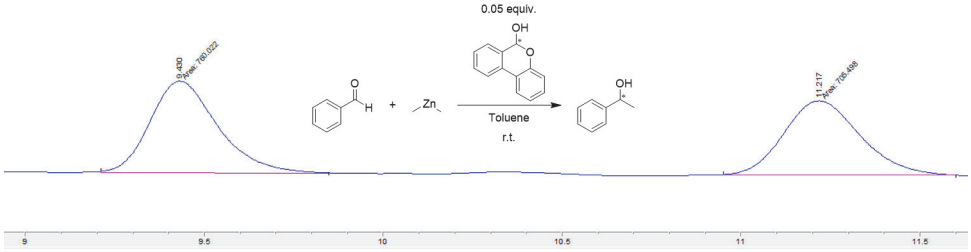

#	Time	Area	Height	Width	Area%	Symmetry
1	9.46	248	19.2	0.2156	49.745	0.778
2	11.198	250.6	16.2	0.2575	50.255	0.819

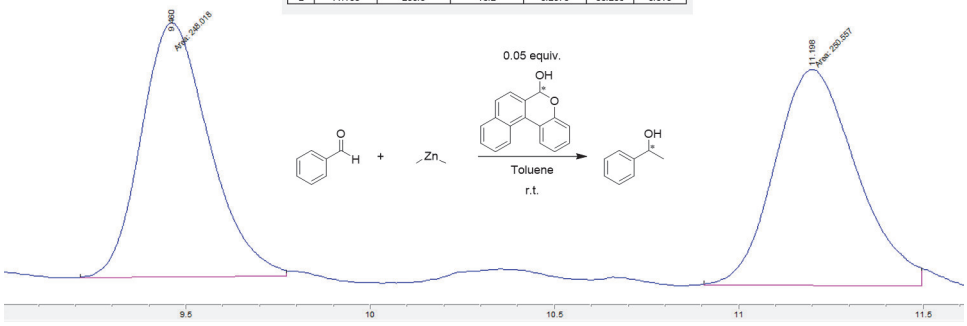

#	Time	Area	Height	Width	Area%	Symmetry
1	9.437	359.9	26.8	0.2234	49.994	0.749
2	11.174	359.9	22.7	0.2639	50.006	0.787

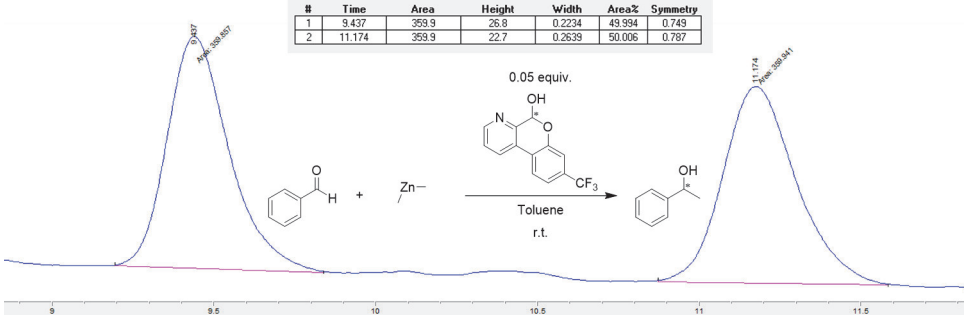

#	Time	Area	Height	Width	Area%	Symmetry
1	9.431	439.6	35.6	0.2056	48.499	0.814
2	11.189	466.8	30	0.259	51.501	0.766

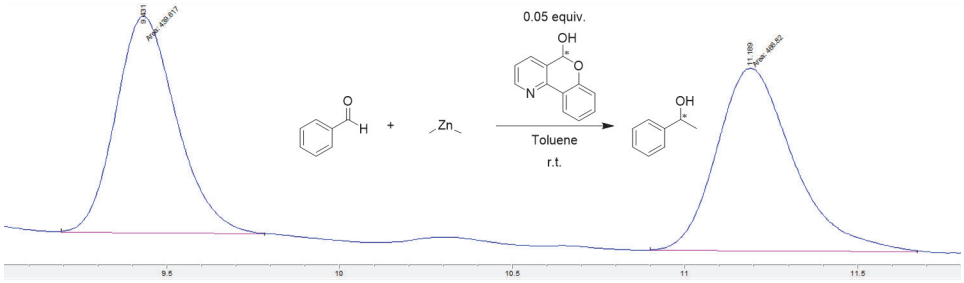

#	Time	Area	Height	Width	Area%	Symmetry
1	9.439	259.5	19.8	0.196	50.048	0.735
2	11.199	259	16.5	0.2355	49.952	0.784

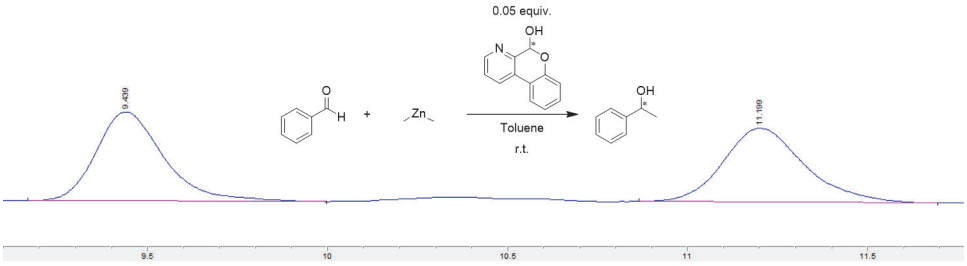

Diethylzinc

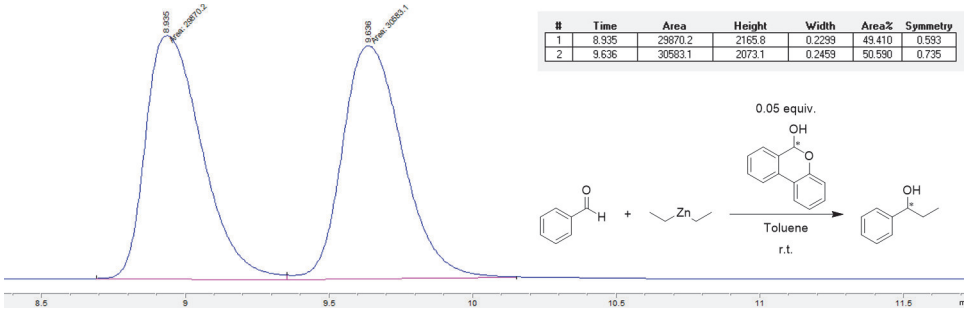

#	Time	Area	Height	Width	Area%	Symmetry
1	8.935	29870.2	2165.8	0.2299	49.410	0.593
2	9.636	30583.1	2073.1	0.2459	50.590	0.735

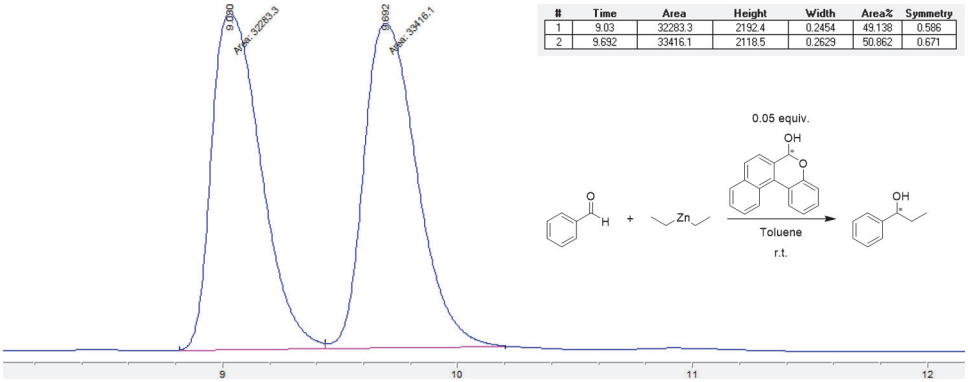

#	Time	Area	Height	Width	Area%	Symmetry
1	9.03	32283.3	2192.4	0.2454	49.138	0.586
2	9.692	33416.1	2118.5	0.2629	50.862	0.671

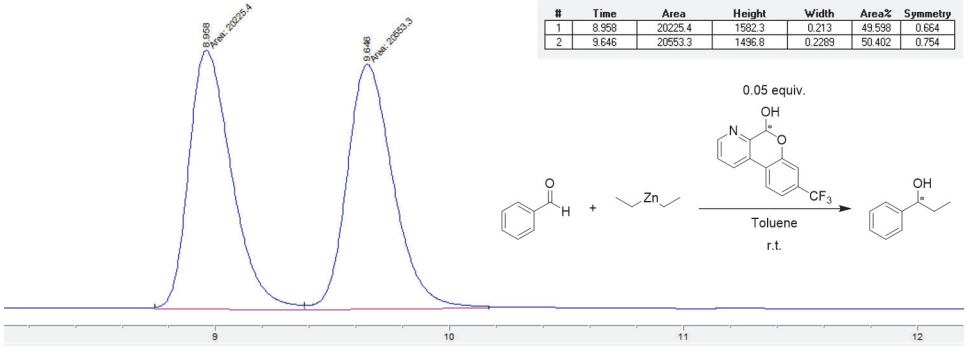

#	Time	Area	Height	Width	Area%	Symmetry
1	8.958	20225.4	1582.3	0.213	49.598	0.664
2	9.646	20553.3	1496.8	0.2289	50.402	0.754

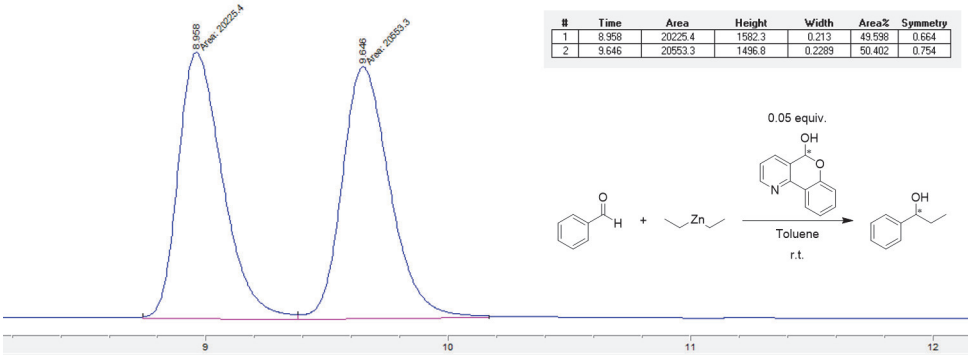

#	Time	Area	Height	Width	Area%	Symmetry
1	8.958	20225.4	1582.3	0.213	49.598	0.664
2	9.646	20553.3	1496.8	0.2289	50.402	0.754

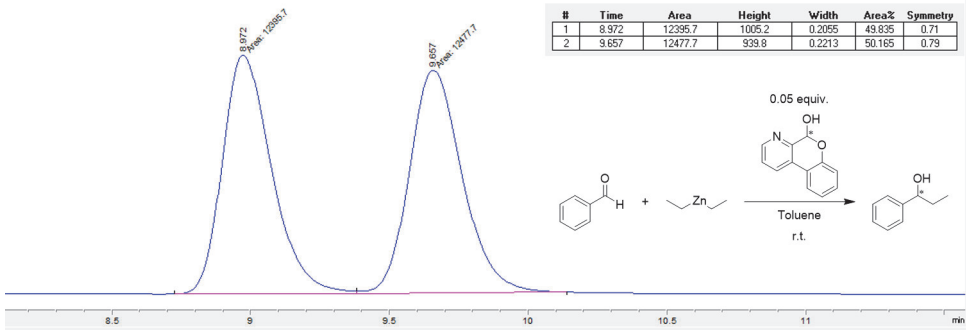

#	Time	Area	Height	Width	Area%	Symmetry
1	8.972	12395.7	1005.2	0.2055	49.835	0.71
2	9.657	12477.7	939.8	0.2213	50.165	0.79

Diisopropylylzinc

#	Time	Area	Height	Width	Area%	Symmetry
1	7.504	17751	1630.4	0.1815	50.053	0.726
2	8.99	17713.3	1332.7	0.2215	49.947	0.624

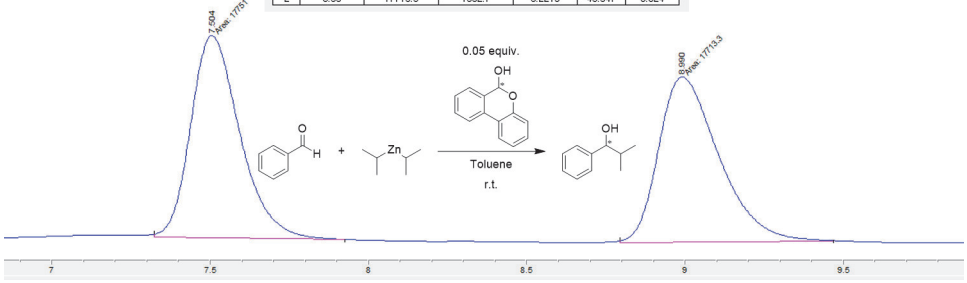

#	Time	Area	Height	Width	Area%	Symmetry
1	7.507	12174.7	1148.1	0.1767	49.402	0.734
2	9.005	12469.3	940.1	0.2211	50.598	0.665

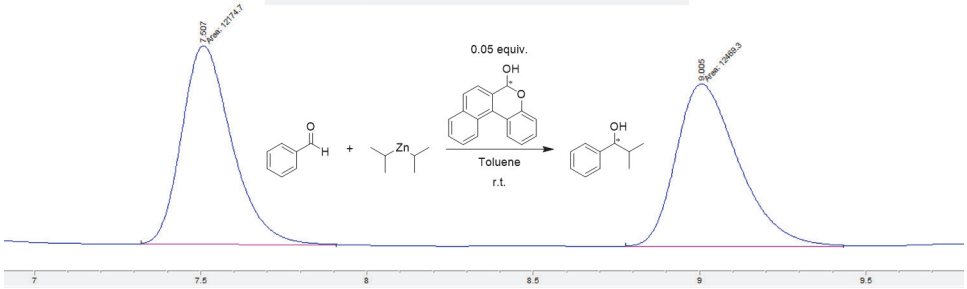

#	Time	Area	Height	Width	Area%	Symmetry
1	7.477	6776.5	621.3	0.1818	51.090	0.726
2	9.055	6487.5	506.5	0.2135	48.910	0.717

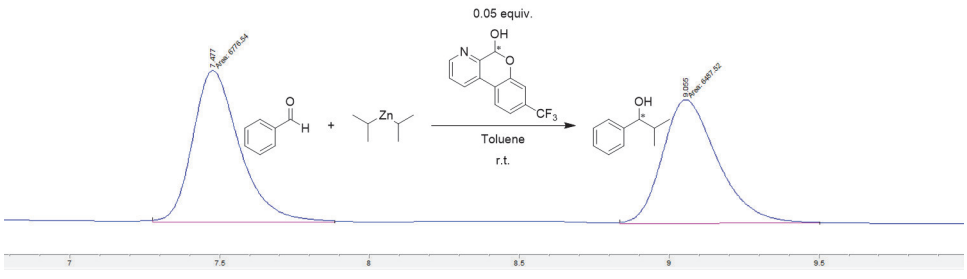

#	Time	Area	Height	Width	Area%	Symmetry
1	7.501	17585.8	1617	0.1813	49.388	0.721
2	8.995	18021.7	1352	0.2222	50.612	0.628

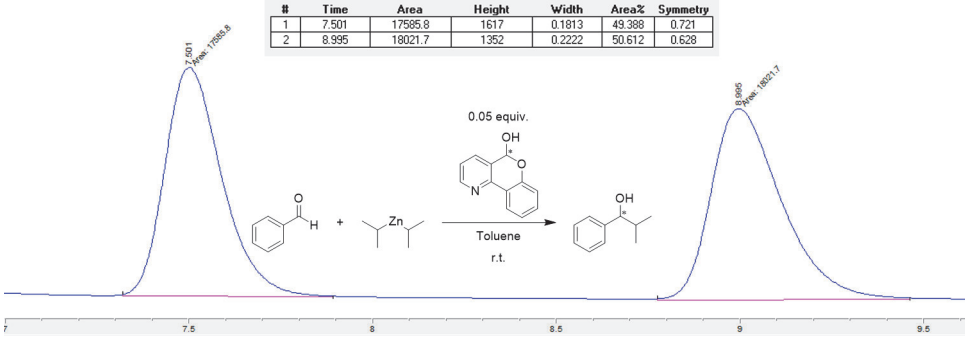

#	Time	Area	Height	Width	Area%	Symmetry
1	7.501	28425.1	2308.6	0.2052	48.242	0.683
2	8.971	30496.6	2077.7	0.2446	51.758	0.541

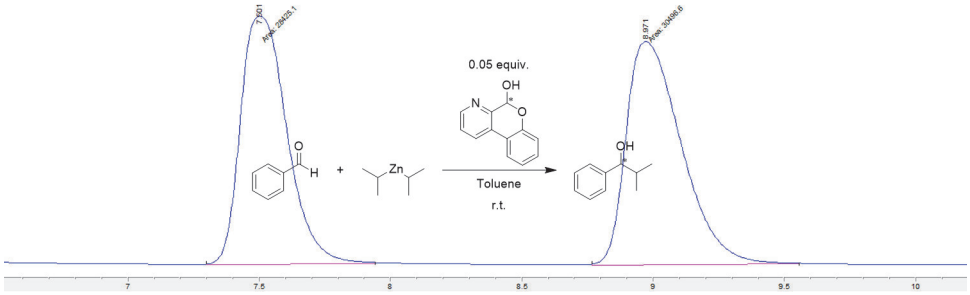

7.2 Supporting HPLC data for Chapter 2

7.2.1 Alkylation of Benzaldehyde with Dimethylzinc

All measurements shown below if not declared otherwise were performed on Chiralpak OD-H by Daicel Corporation at room temperature. The measurements were conducted using IPA: *n*-hexanes as eluent (5:95). Retention times may vary at least a bit due to different compositions (catalyst, remaining toluene and educt).

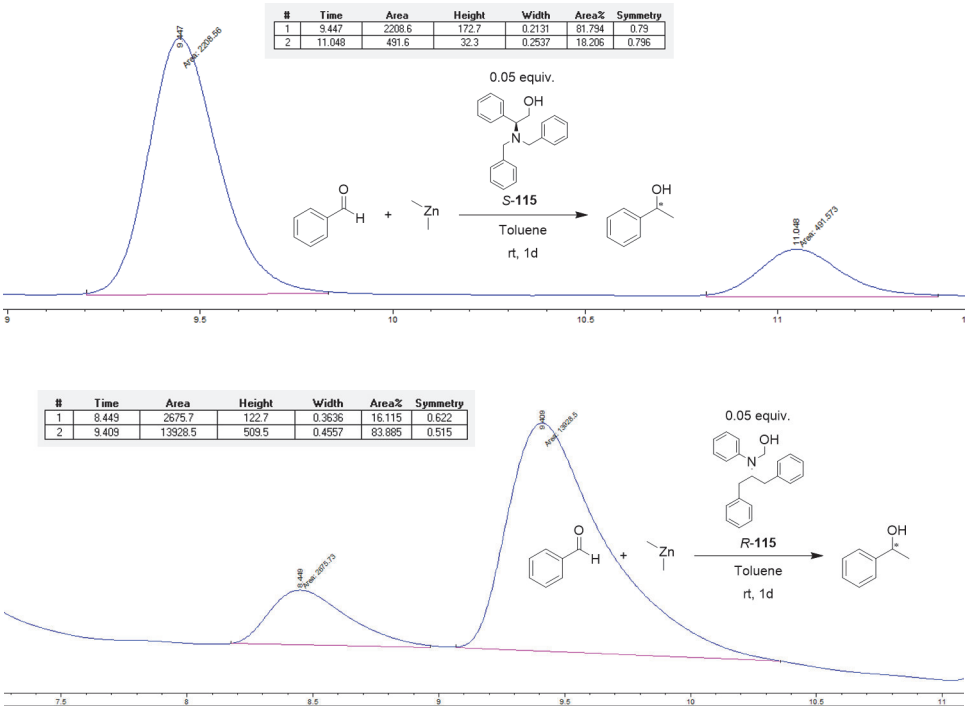

Figure 7.1: HPLC spectra below for compound *R*-**115** was measured on Chiralpak IF by Daicel Corporation (IPA 5: hexanes 95), due to catalyst overlaying with the product in the usual method used. The deviating retention times occur because of the different column and ratio of the eluent used.

#	Time	Area	Height	Width	Area%	Symmetry
1	9.376	4672.7	372.3	0.2092	67.111	0.782
2	10.997	2289.9	153.8	0.2481	32.889	0.841

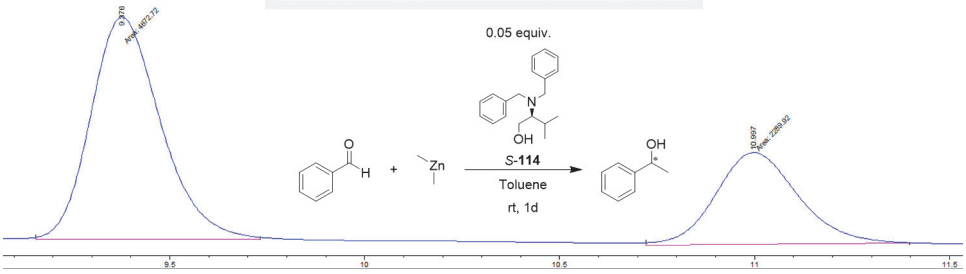

#	Time	Area	Height	Width	Area%	Symmetry
1	9.375	965	78.1	0.206	33.338	0.787
2	10.992	1929.5	136.1	0.2364	66.662	0.837

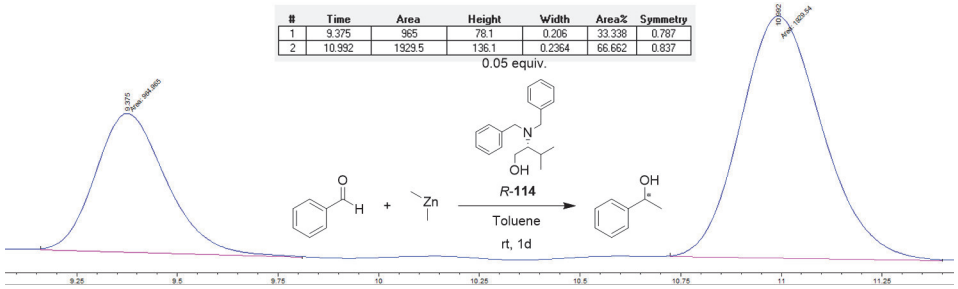

#	Time	Area	Height	Width	Area%	Symmetry
1	9.651	4627.6	338.6	0.2278	36.893	0.729
2	11.378	7915.6	483.8	0.2727	63.107	0.741

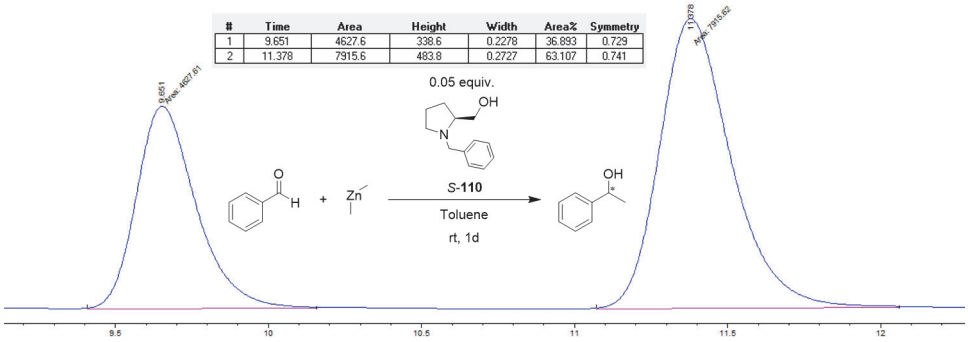

#	Time	Area	Height	Width	Area%	Symmetry
1	9.623	22314.6	1534.4	0.2424	44.199	0.598
2	11.362	28172.4	1601.5	0.2932	55.801	0.657

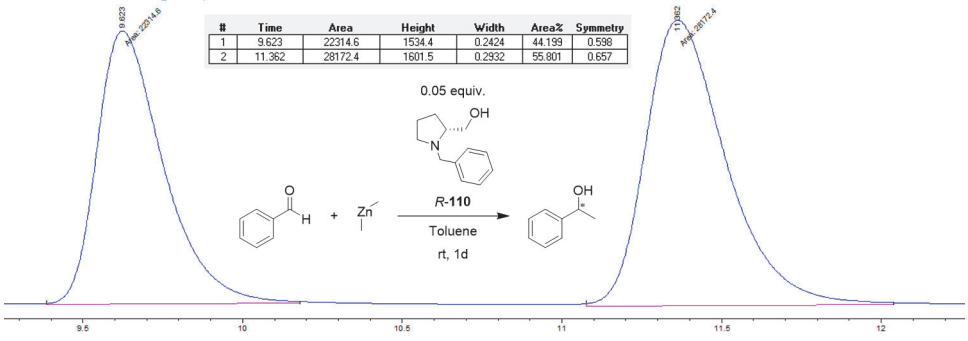

#	Time	Area	Height	Width	Area%	Symmetry
1	9.399	351	27.1	0.2156	71.664	0.897
2	11.054	138.8	10.4	0.2215	28.336	0.951

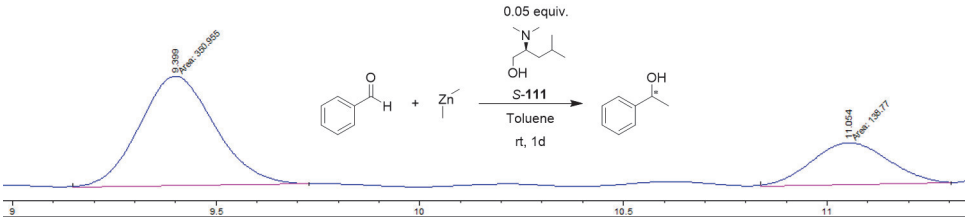

#	Time	Area	Height	Width	Area%	Symmetry
1	9.414	606.9	47.9	0.211	37.232	0.788
2	11.062	1023.1	71.5	0.2386	62.768	0.843

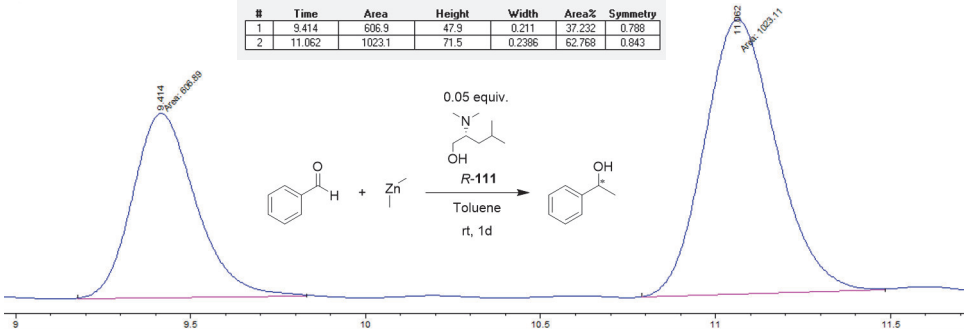

#	Time	Area	Height	Width	Area%	Symmetry
1	9.581	9159.8	696.5	0.2192	68.755	0.763
2	11.276	4162.6	278.3	0.2493	31.245	0.825

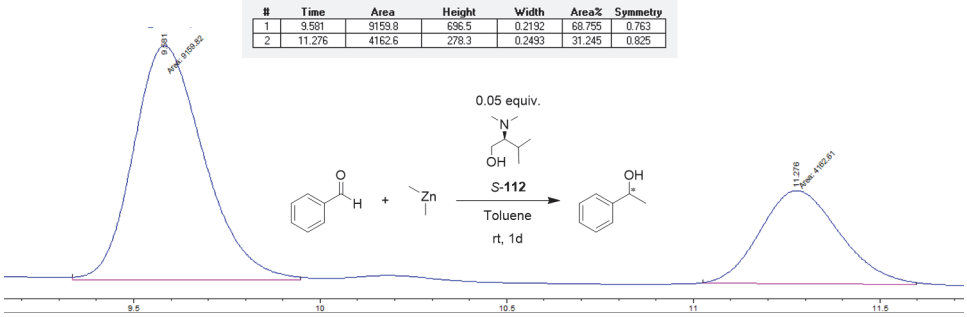

#	Time	Area	Height	Width	Area%	Symmetry
1	9.599	1741.3	136.4	0.2127	31.752	0.826
2	11.283	3742.8	249.4	0.2501	68.248	0.816

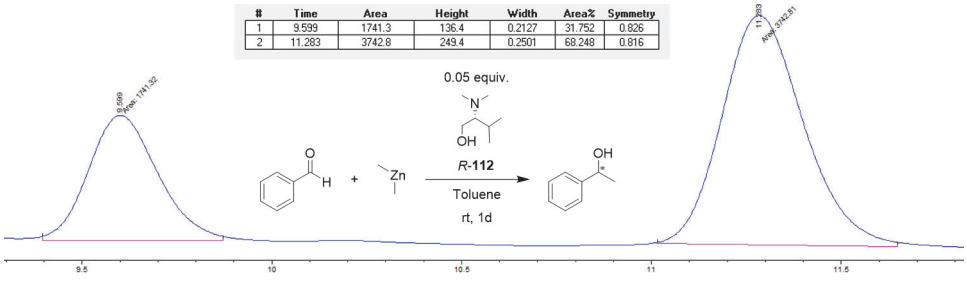

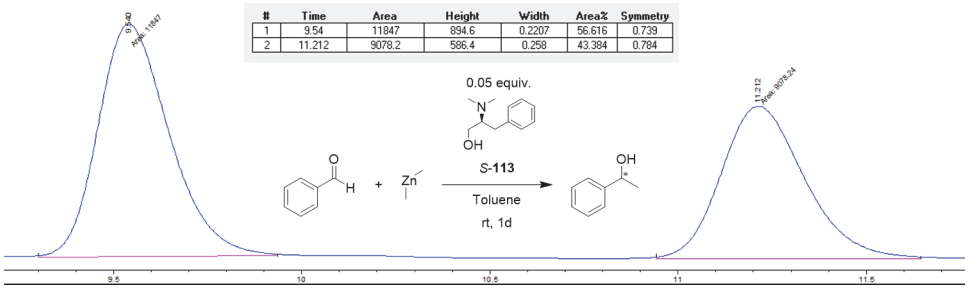

#	Time	Area	Height	Width	Area%	Symmetry
1	9.54	11847	894.6	0.2207	56.616	0.739
2	11.212	9078.2	586.4	0.258	43.384	0.784

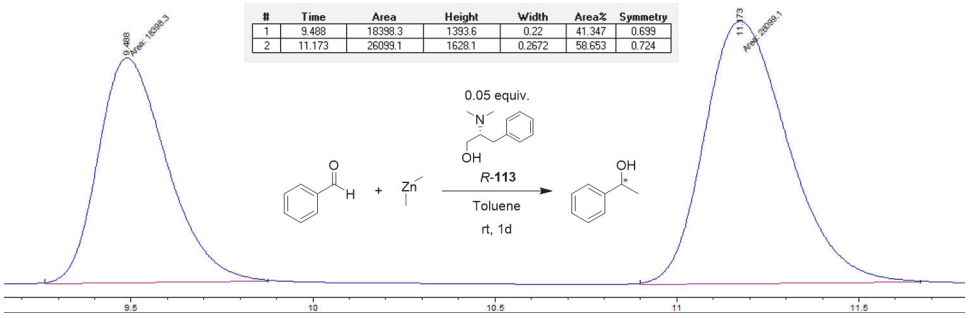

#	Time	Area	Height	Width	Area%	Symmetry
1	9.488	18398.3	1393.6	0.22	41.347	0.699
2	11.173	26099.1	1628.1	0.2672	58.653	0.724

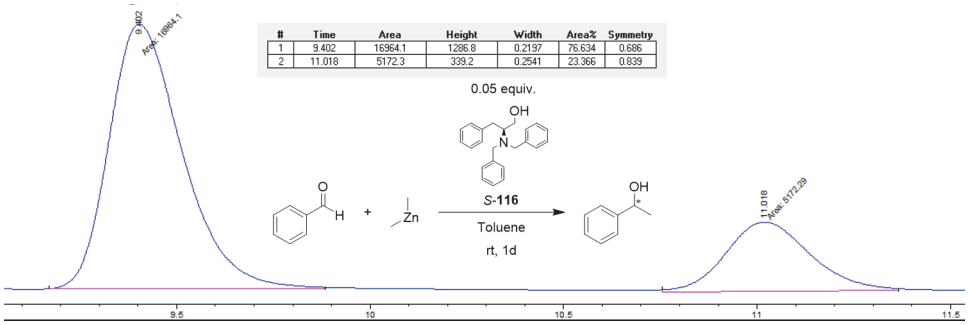

#	Time	Area	Height	Width	Area%	Symmetry
1	9.402	16964.1	1286.8	0.2197	76.634	0.686
2	11.018	5172.3	339.2	0.2541	23.366	0.839

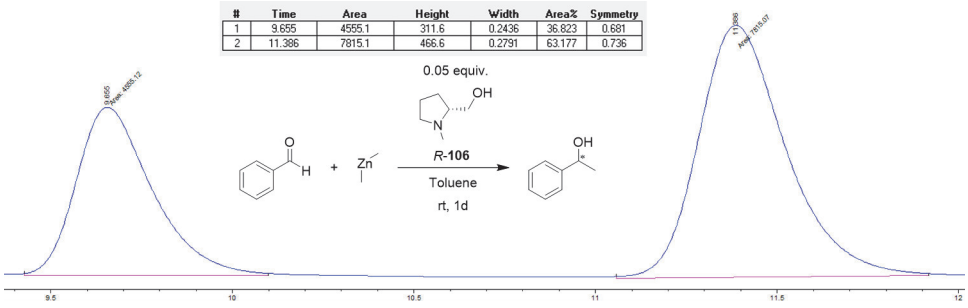

#	Time	Area	Height	Width	Area%	Symmetry
1	9.655	4555.1	311.6	0.2436	36.823	0.681
2	11.386	7815.1	466.6	0.2791	63.177	0.736

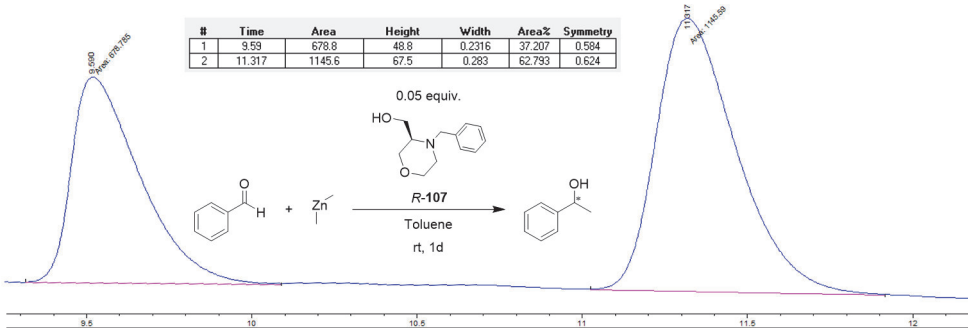

#	Time	Area	Height	Width	Area%	Symmetry
1	9.59	678.8	48.8	0.2316	37.207	0.584
2	11.317	1145.6	67.5	0.283	62.793	0.624

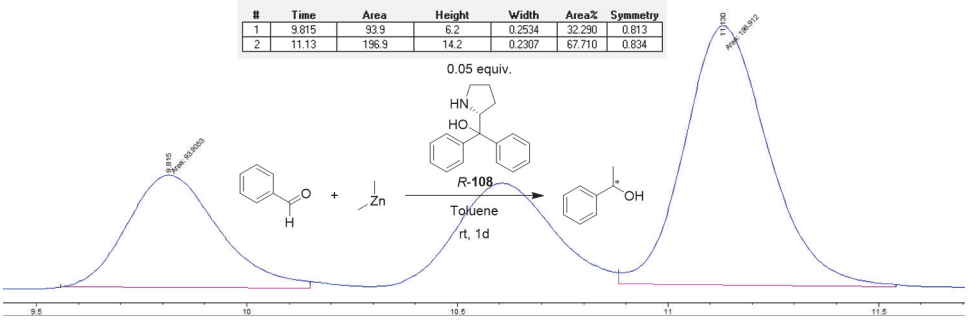

#	Time	Area	Height	Width	Area%	Symmetry
1	9.815	93.9	6.2	0.2534	32.290	0.813
2	11.13	196.9	14.2	0.2307	67.710	0.834

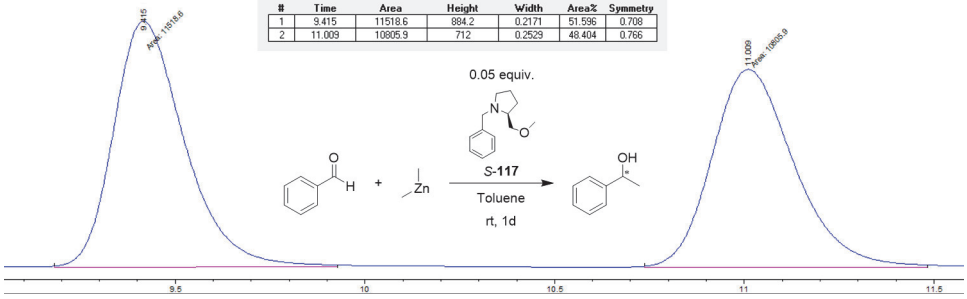

#	Time	Area	Height	Width	Area%	Symmetry
1	9.415	11518.6	884.2	0.2171	51.596	0.708
2	11.009	10805.9	712	0.2529	48.404	0.766

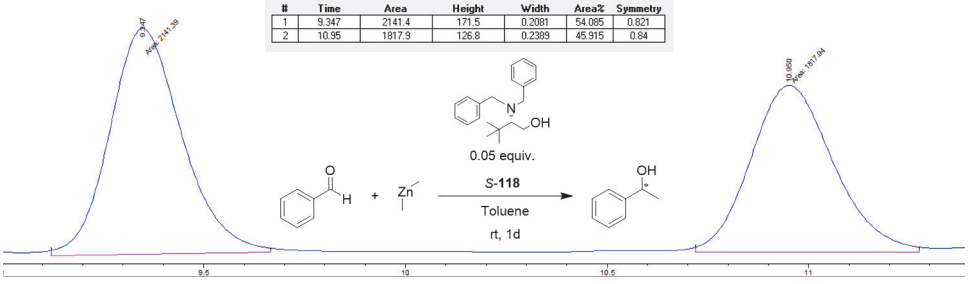

#	Time	Area	Height	Width	Area%	Symmetry
1	9.347	2141.4	171.5	0.2081	54.085	0.821
2	10.95	1817.9	126.8	0.2389	45.915	0.84

7.2.2 Alkylation of Benzaldehyde with Diethylzinc

All measurements shown below if not declared otherwise were performed on CHIRALPAK OD-H by DAICEL CORPORATION at room temperature. THe measurements were conducted using IPA: *n*-hexanes as eluent (5:95). Retention times may vary at least a bit due to different compositions (catalyst, remaining toluene and educt).

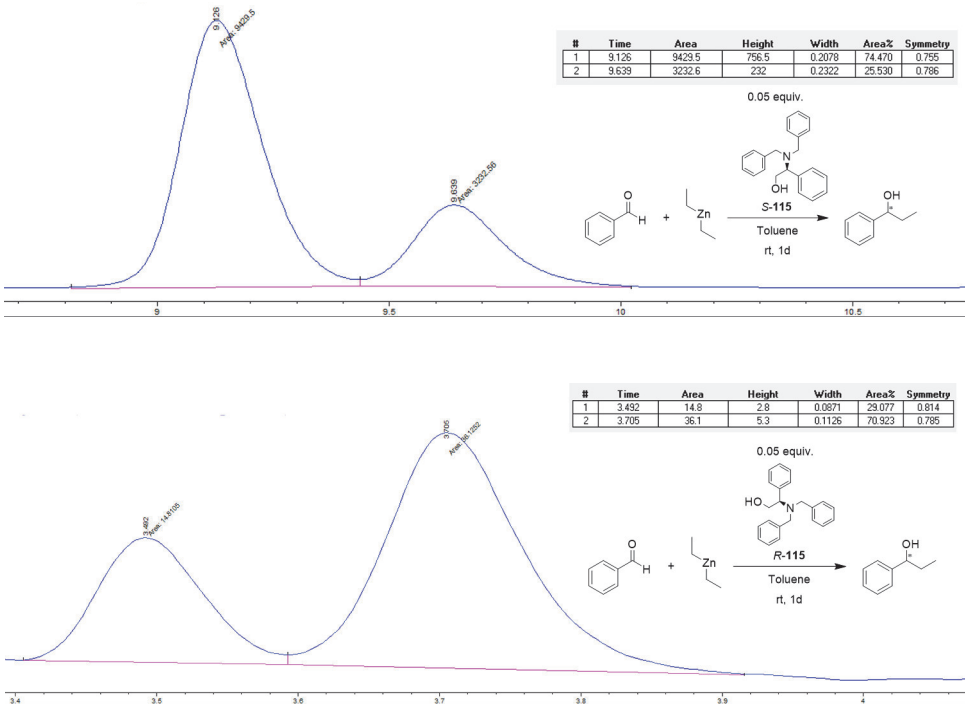

Figure 7.2: HPLC spectra below for compound *R*-**115** was measured on CHIRALPAK OD-RH by DAICEL CORPORATION (IPA 10: hexanes 90), due to catalyst overlaying with the product in the usual method used. The deviating retention times occur because of the different column and ratio of the eluent used.

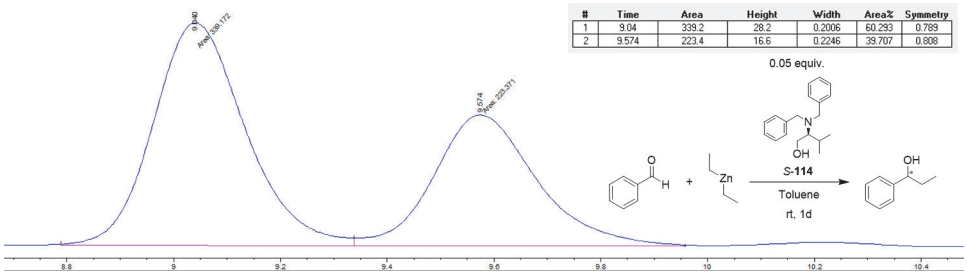

#	Time	Area	Height	Width	Area%	Symmetry
1	9.04	339.2	28.2	0.2006	60.293	0.789
2	9.574	223.4	16.6	0.2246	39.707	0.808

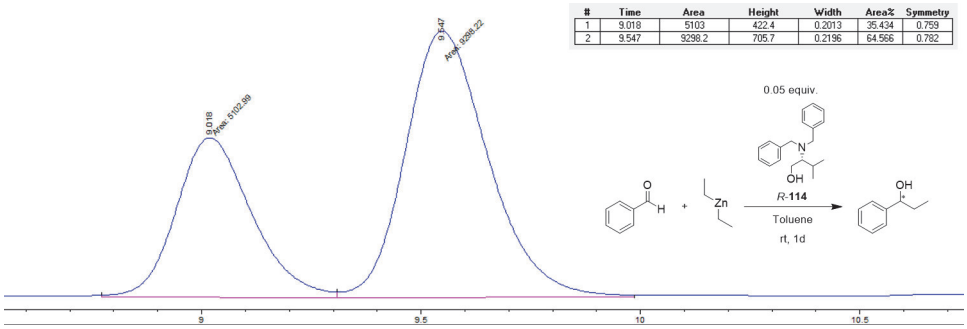

#	Time	Area	Height	Width	Area%	Symmetry
1	9.018	5103	422.4	0.2013	35.434	0.759
2	9.547	9298.2	705.7	0.2196	64.566	0.782

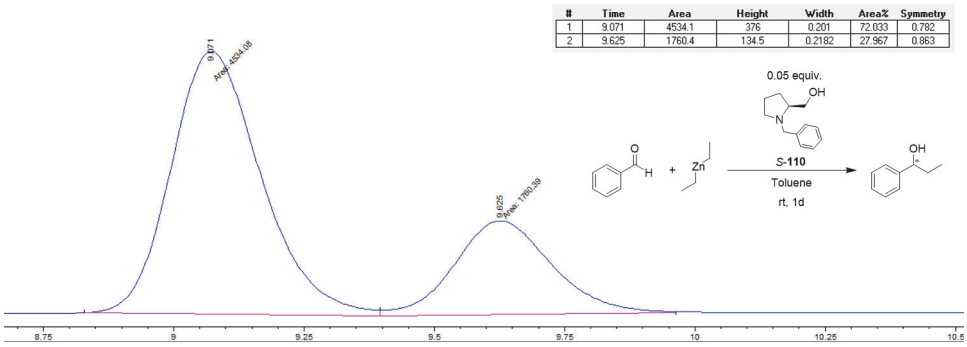

#	Time	Area	Height	Width	Area%	Symmetry
1	9.071	4534.1	376	0.201	72.033	0.782
2	9.625	1760.4	134.5	0.2182	27.967	0.863

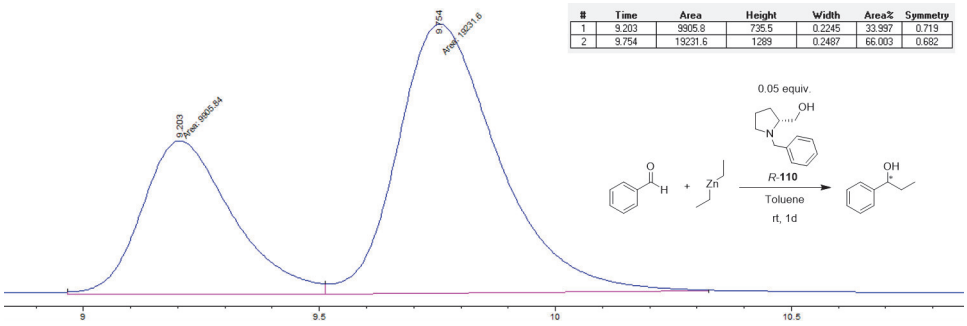

#	Time	Area	Height	Width	Area%	Symmetry
1	9.203	9905.8	735.5	0.2245	33.997	0.719
2	9.754	19231.6	1289	0.2487	66.003	0.682

#	Time	Area	Height	Width	Area%	Symmetry
1	9.09	4771.2	398.7	0.1995	64.104	0.781
2	9.632	2671.6	206.4	0.2157	35.896	0.826

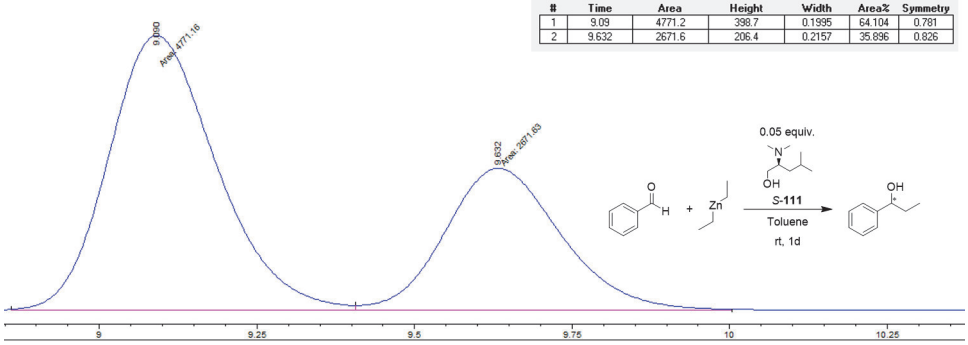

#	Time	Area	Height	Width	Area%	Symmetry
1	9.101	20825.4	1507.9	0.2302	37.677	0.608
2	9.735	34447.5	2114	0.2716	62.323	0.646

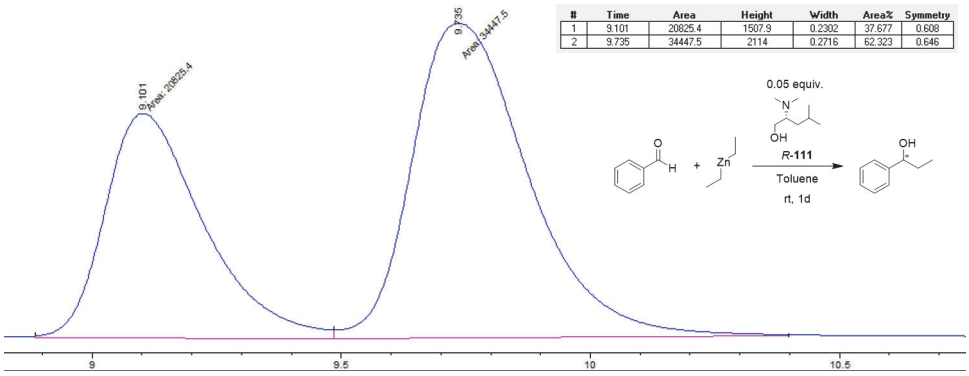

#	Time	Area	Height	Width	Area%	Symmetry
1	9.068	3442.9	283.4	0.2025	69.339	0.786
2	9.617	1522.4	116.4	0.218	30.661	0.866

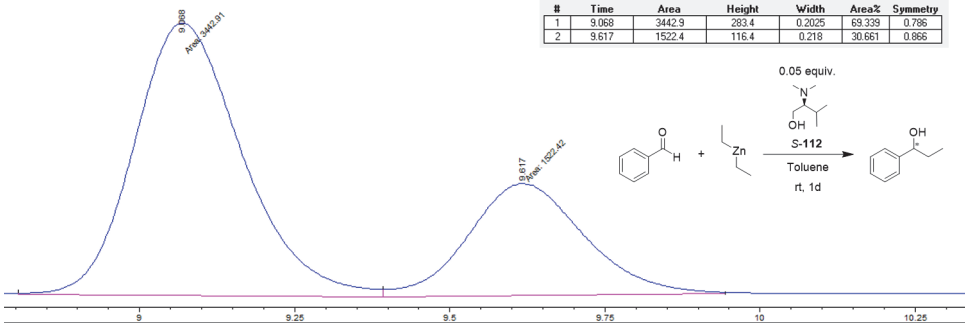

#	Time	Area	Height	Width	Area%	Symmetry
1	9.128	16426.6	1201.5	0.2279	31.973	0.625
2	9.749	34949.4	2118.7	0.2749	68.027	0.633

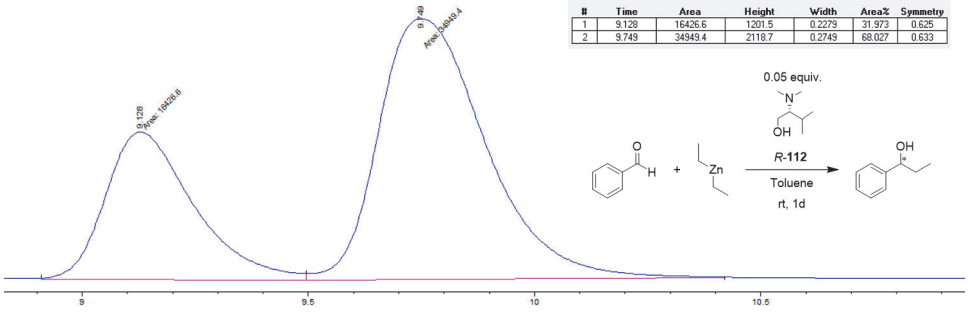

#	Time	Area	Height	Width	Area%	Symmetry
1	9.028	21183.1	1688.2	0.2091	57.385	0.664
2	9.594	15730.9	1193.5	0.2197	42.615	0.781

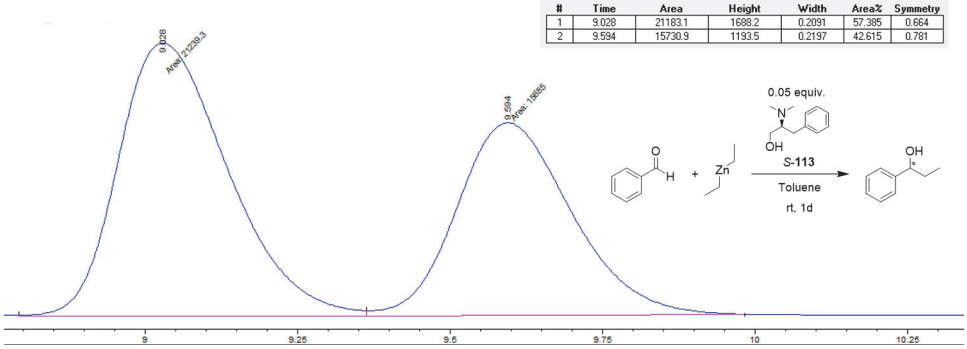

#	Time	Area	Height	Width	Area%	Symmetry
1	9.174	22810.8	1644.1	0.2312	37.141	0.643
2	9.738	38605.9	2261.7	0.2845	62.859	0.612

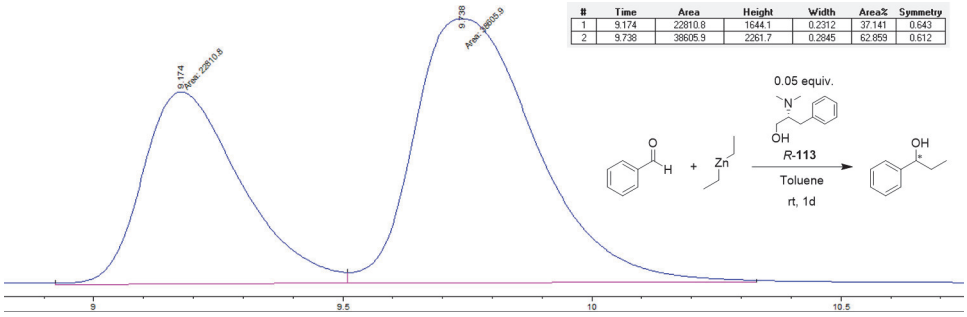

#	Time	Area	Height	Width	Area%	Symmetry
1	8.932	21742.1	1733.6	0.209	79.022	0.657
2	9.459	5772	434.1	0.2216	20.978	0.865

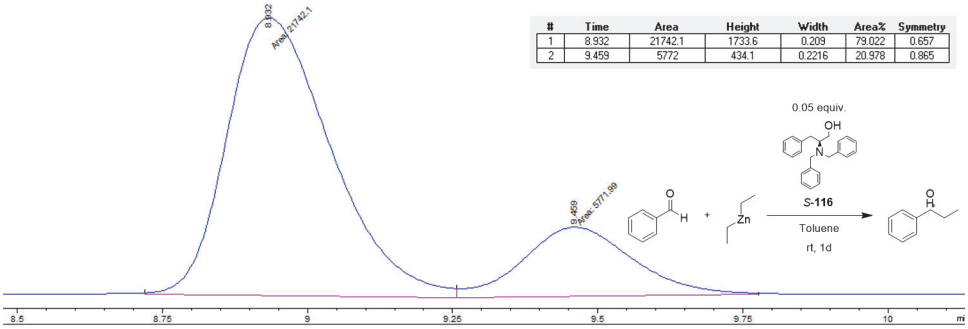

#	Time	Area	Height	Width	Area%	Symmetry
1	8.884	398	34.3	0.1931	28.169	0.673
2	9.369	1015	77.8	0.2173	71.831	0.626

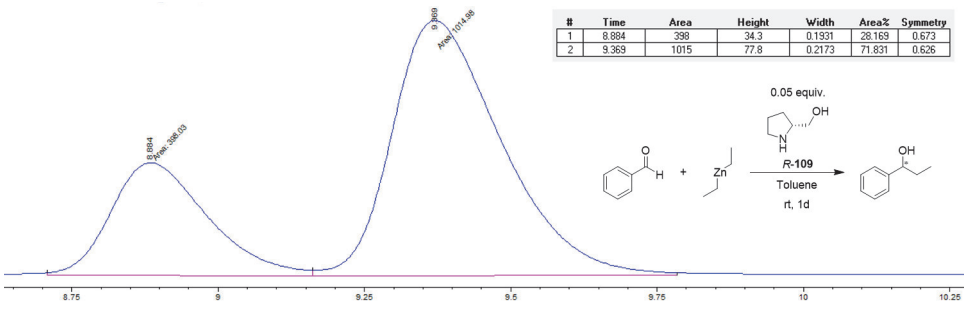

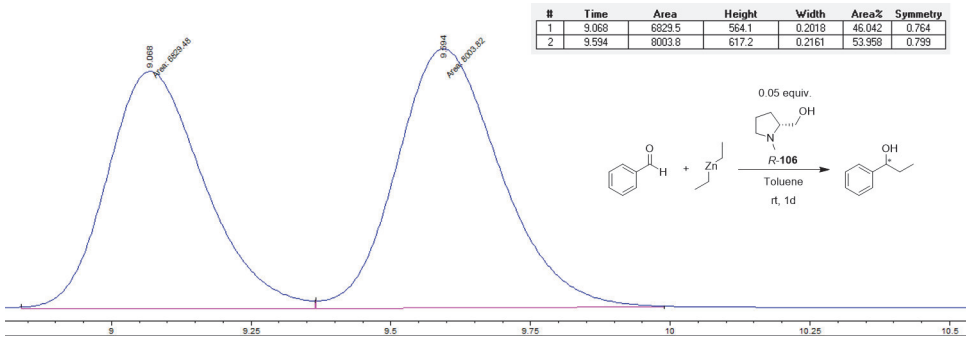

#	Time	Area	Height	Width	Area%	Symmetry
1	9.068	6829.5	564.1	0.2018	46.042	0.764
2	9.594	8003.8	617.2	0.2161	53.958	0.799

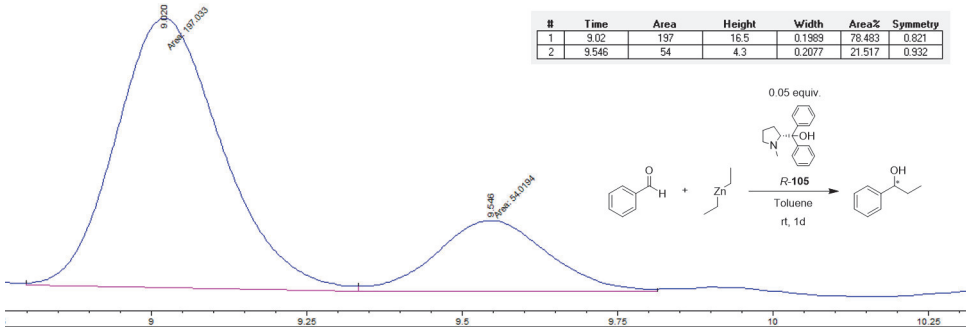

#	Time	Area	Height	Width	Area%	Symmetry
1	9.02	197	16.5	0.1989	78.483	0.821
2	9.546	54	4.3	0.2077	21.517	0.932

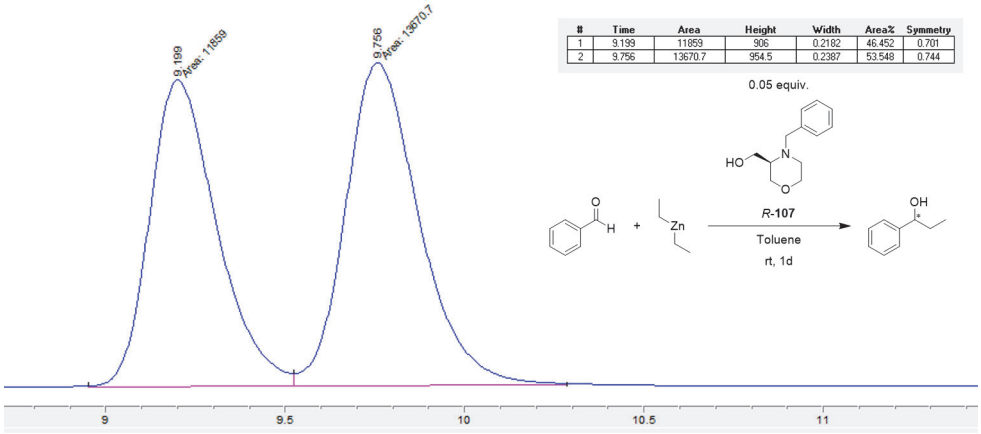

#	Time	Area	Height	Width	Area%	Symmetry
1	9.199	11859	906	0.2182	46.452	0.701
2	9.756	13670.7	954.5	0.2387	53.548	0.744

7.2.3 Alkylation of Benzaldehyde with Diisopropylzinc

All measurements shown below were performed on CHIRALPAK OD-H by DAICEL CORPORATION at room temperature if not declared otherwise (marked with *). The measurements were conducted using IPA: *n*-hexanes as eluent (5:95). Retention times may vary at least a bit due to different compositions (catalyst, remaining toluene and educt).

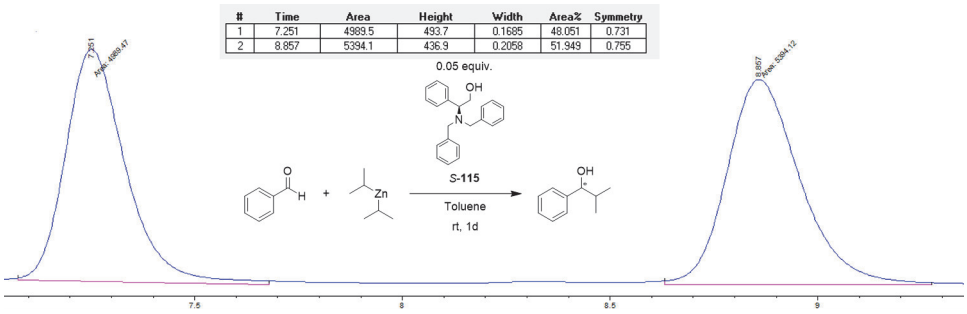

#	Time	Area	Height	Width	Area%	Symmetry
1	7.251	4989.5	493.7	0.1685	48.051	0.731
2	8.857	5394.1	436.9	0.2058	51.949	0.755

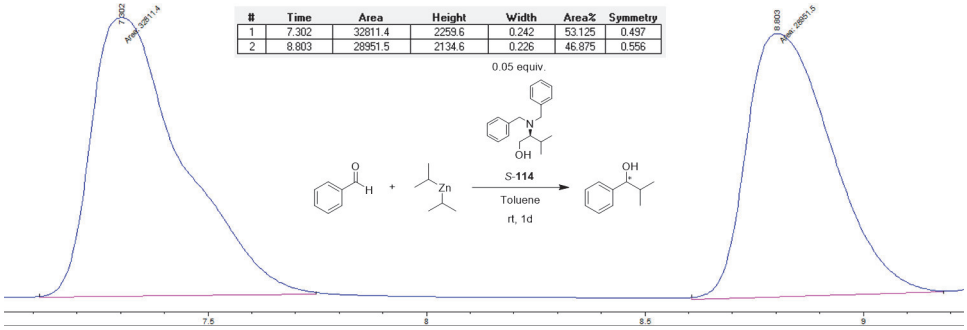

#	Time	Area	Height	Width	Area%	Symmetry
1	7.302	32811.4	2259.6	0.242	53.125	0.497
2	8.803	28951.5	2134.6	0.226	46.875	0.556

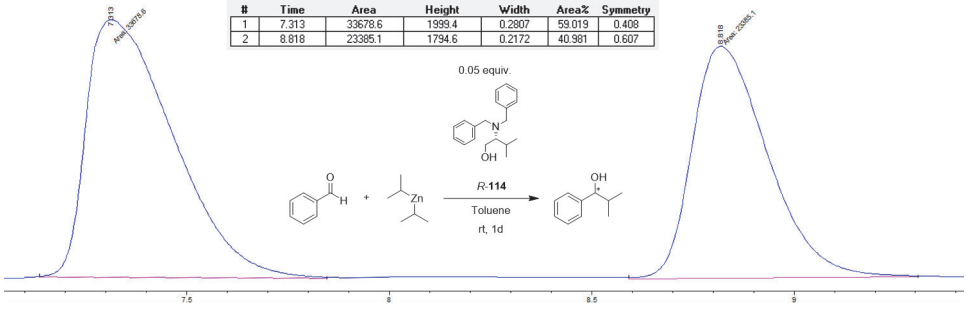

#	Time	Area	Height	Width	Area%	Symmetry
1	7.313	33678.6	1999.4	0.2807	59.019	0.408
2	8.818	23385.1	1794.6	0.2172	40.981	0.607

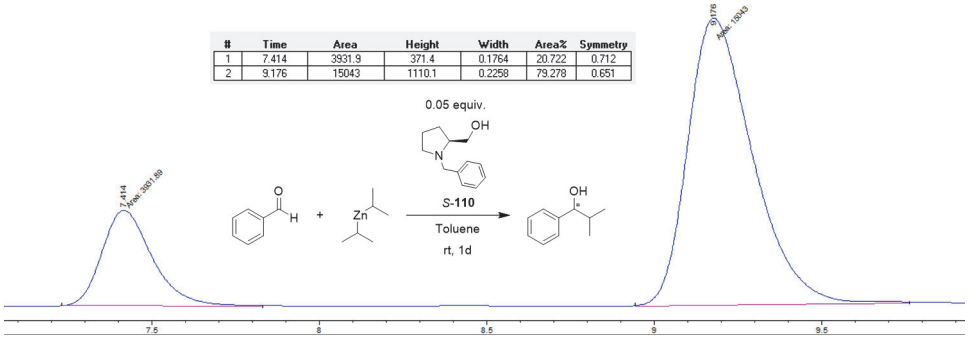

#	Time	Area	Height	Width	Area%	Symmetry
1	7.414	3931.9	371.4	0.1764	20.722	0.712
2	9.176	15043	1110.1	0.2258	79.278	0.651

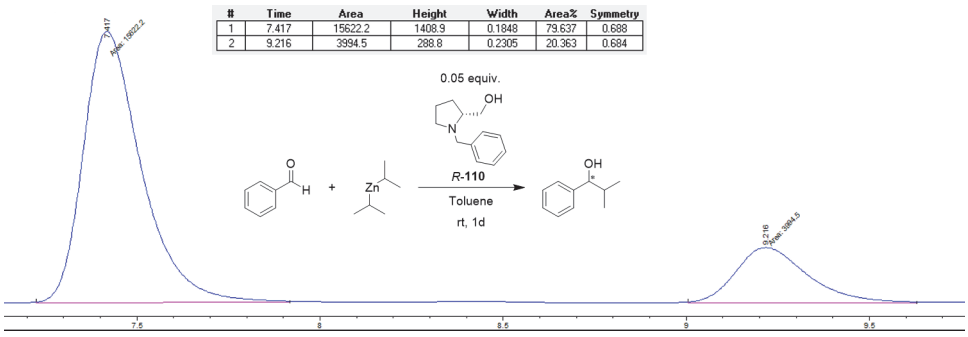

#	Time	Area	Height	Width	Area%	Symmetry
1	7.417	15622.2	1408.9	0.1848	79.637	0.688
2	9.216	3994.5	288.8	0.2305	20.363	0.684

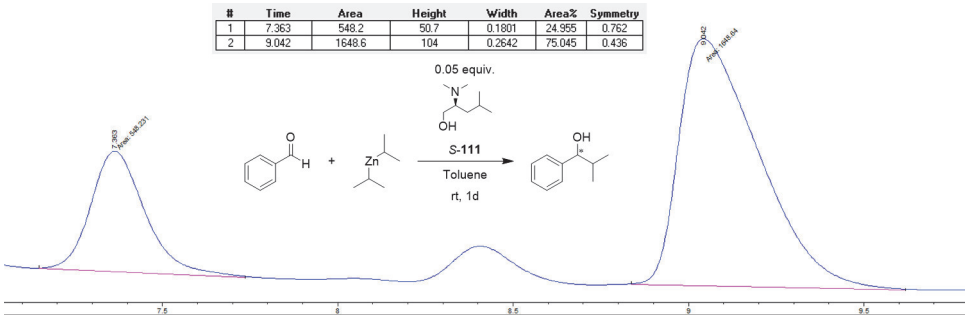

#	Time	Area	Height	Width	Area%	Symmetry
1	7.363	548.2	50.7	0.1801	24.955	0.762
2	9.042	1648.6	104	0.2642	75.045	0.436

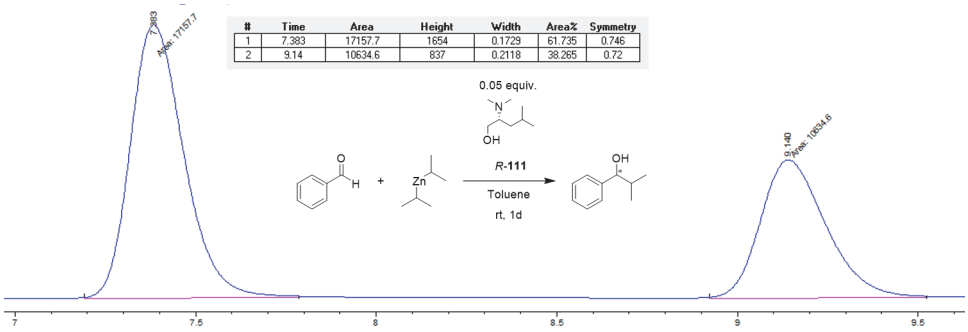

#	Time	Area	Height	Width	Area%	Symmetry
1	7.383	17157.7	1654	0.1729	61.735	0.746
2	9.14	10634.6	837	0.2118	38.265	0.72

#	Time	Area	Height	Width	Area%	Symmetry
1	7.341	4602.9	457.6	0.1676	13.873	0.765
2	8.861	28576.4	2047.5	0.2326	86.127	0.542

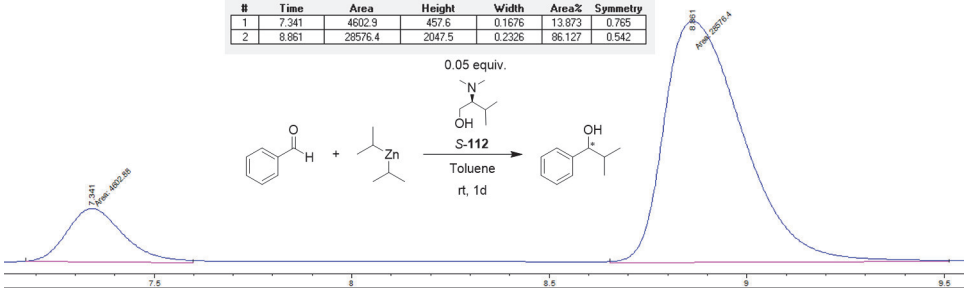

#	Time	Area	Height	Width	Area%	Symmetry
1	7.322	26297.5	2248.5	0.1949	84.310	0.687
2	8.9	4893.8	399.5	0.2042	15.690	0.788

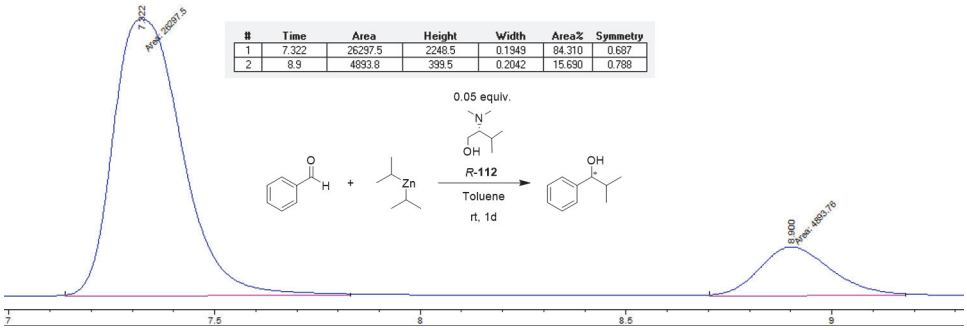

#	Time	Area	Height	Width	Area%	Symmetry
1	7.342	8644.7	854.3	0.1687	25.056	0.755
2	9.026	25857.4	1877.6	0.2295	74.944	0.571

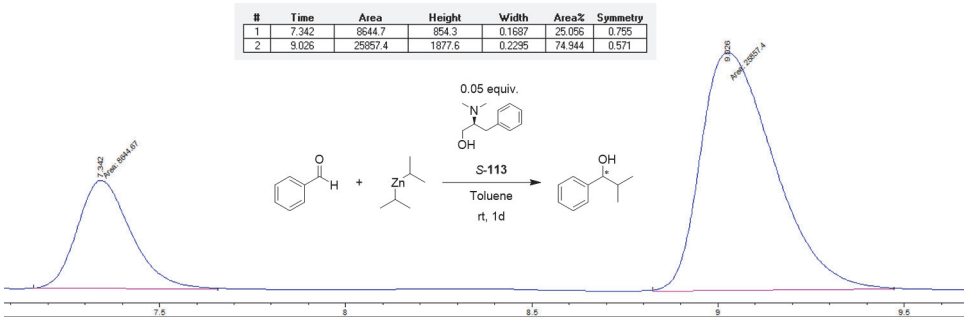

#	Time	Area	Height	Width	Area%	Symmetry
1	7.332	27232.6	2279.1	0.1992	78.560	0.666
2	9.074	7432	550.1	0.2252	21.440	0.695

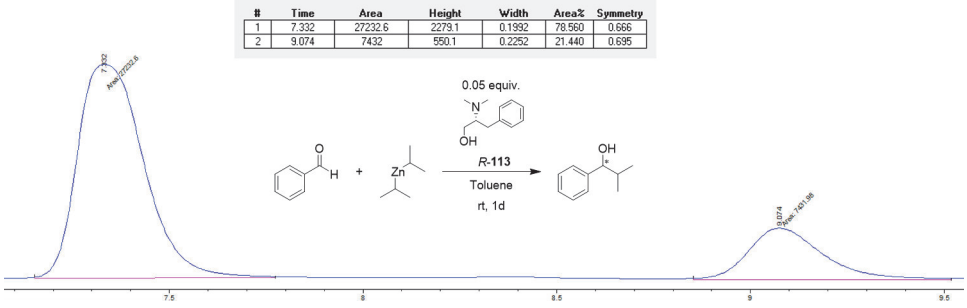

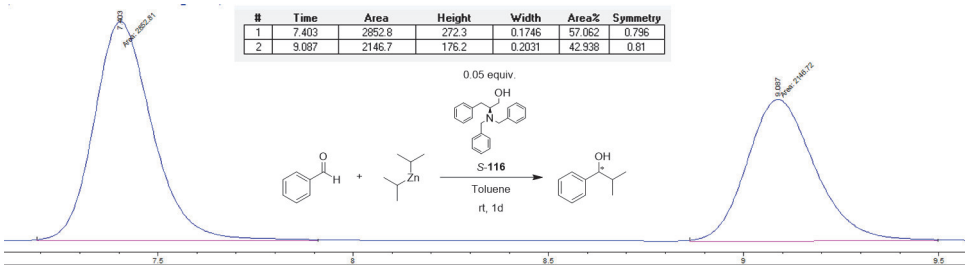

#	Time	Area	Height	Width	Area%	Symmetry
1	7.403	2852.8	272.3	0.1746	57.062	0.796
2	9.087	2146.7	176.2	0.2031	42.938	0.81

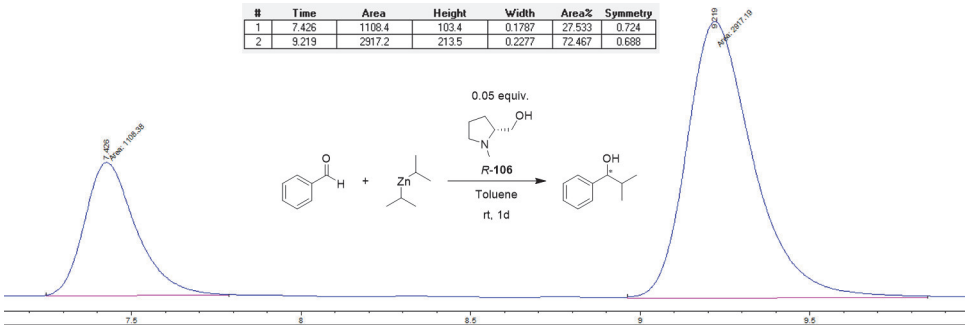

#	Time	Area	Height	Width	Area%	Symmetry
1	7.426	1108.4	103.4	0.1787	27.533	0.724
2	9.219	2917.2	213.5	0.2277	72.467	0.688

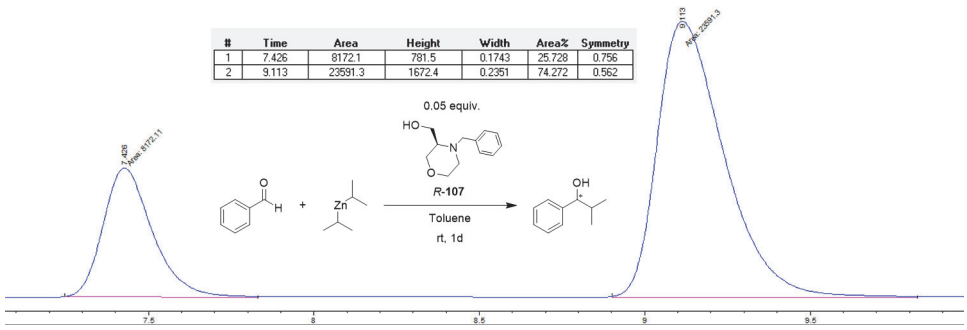

#	Time	Area	Height	Width	Area%	Symmetry
1	7.426	8172.1	781.5	0.1743	25.728	0.756
2	9.113	23591.3	1672.4	0.2351	74.272	0.562

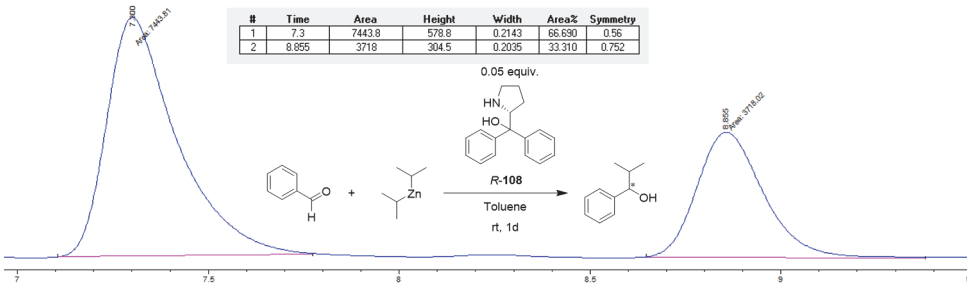

#	Time	Area	Height	Width	Area%	Symmetry
1	7.3	7443.8	578.8	0.2143	66.690	0.56
2	8.855	3718	304.5	0.2035	33.310	0.752

#	Time	Area	Height	Width	Area%	Symmetry
1	7.424	5611.7	550.4	0.1699	50.733	0.771
2	9.133	5449.5	429.1	0.2116	49.267	0.773

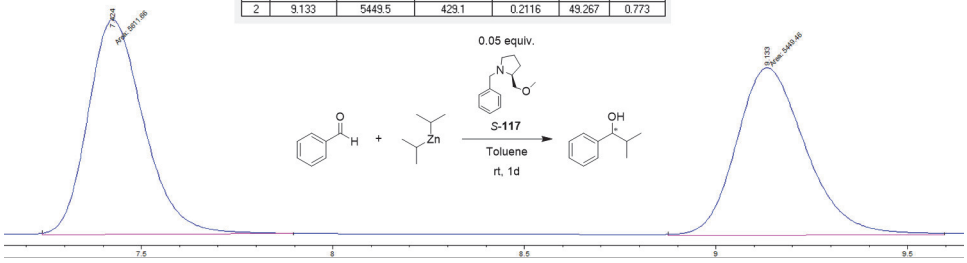

#	Time	Area	Height	Width	Area%	Symmetry
1	7.28	1210.6	121.8	0.1656	48.919	0.785
2	8.859	1264	99.8	0.2112	51.081	0.755

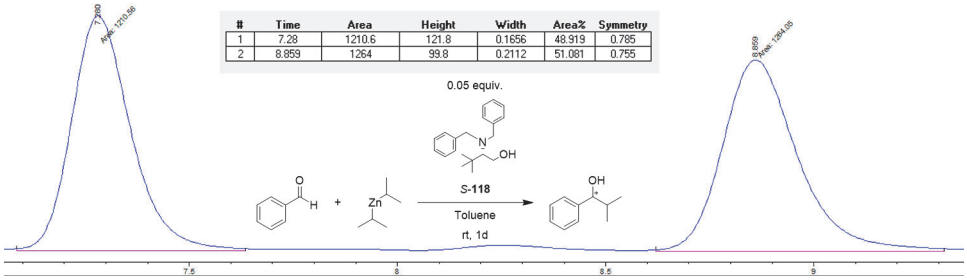

8 Danksagung

Im Rahmen meiner Dissertation möchte ich zu allererst meinem Doktorvater Prof. Dr. Oliver Trapp danken. Einerseits für die Ermutigung und den Zuspruch zu Beginn, als auch die Möglichkeit, die Arbeit sehr frei gestalten und erarbeiten zu können. Ohne Dich hätte ich mich vielleicht nicht zu diesem Schritt gewagt, ich konnte aus der Zeit unglaublich viel Wertvolles mitnehmen! Für die Übernahme des Zweitgutachtens möchte ich Prof. Dr. Anja Hoffmann-Röder meinen herzlichen Dank aussprechen. Desweiteren gilt mein Dank auch der gesamten weiteren Prüfungskommission: Prof. Karaghiosoff, Prof. Johrendt, Prof. Markic und Prof. Lotsch, die Zeit und Interesse für meine Arbeit mitgebracht haben.
Für die Unterstützung bei bürokratischen Themen, wie Dienstreiseanträge, finanzielle Angelegenheiten etc. möchte ich mich bei Dr. Claudia Meier und Heike Traub bedanken. Dass ich in schöner Erinnerung an meine Promotionszeit zurückdenken kann, ist vor allem Euch liebem gesamten AK Trapp zu verdanken. Brigitte und Carrie, ihr habt stets mit eurer fröhlichen Natur gute Laune versprüht und man konnte sich, egal ob bei Sonderbestellungen oder NMR Problematiken auf Euch verlassen.
Für chemischen Input möchte ich mich einmal bei MJ für meine Grundausbildung bedanken, ohne deine strenge Hand und gute Inhaltsvermittlung wäre das wahrscheinlich nichts geworden, sowie später bei Jan bzgl. synthetischer Fragestellungen als auch bei Alex, der nie die Geduld verloren hat mir analytische Geräte nach über einem Jahr Benutzung auch ein zweites mal zuerklären!
Ursprünglich angefangen hat mein Einstieg mit einem Forschungspraktikum in der Box von m^2. Danke, dass ihr mich gleich so herzlich aufgenommen habt und den Weg in den Arbeitskreis bereitet habt. Mit Euch bin ich schrittweise in die Otto-Lenghi Kochgruppe gerutscht, frecherweise ganz ohne Aufnahmeritual :) Ich erinner mich gerne an die schönen Koch-Freitage mit Flo, Jenny, Max, MJ und Anna, sowie die Erweiterung um meine Generation PhD-Jungspunde Lena, Christoph und Marian. Ich freue mich auf weitere,

mindestens einmal jährlich zirkulierende Otto-feste. Und wo wir grade bei Kulinarik sind, darf auch ein Dank an die Sushi-Sekt-Sekte nicht fehlen. Dabei sind sehr lustige Abende mit Jenny, Anna und Lena entstanden!
So, wer jetzt denkt in deisem Arbeitskreis wird nur getrunken und gegessen, hat falsch gedacht - ein gewisser physischer Ausgleich darf auch nicht fehlen. Zeitweise haben wir es sogar mal jeden Dienstag geschafft nach der Arbeit eine Runde auf unseren Rennrädern zu drehen, gipfelnd in einer belohnenden Eisdieleneinkehr in Gauting oder Neuried. Danke an Jan, Lena, Sabrina und Alex (AC) für diese schönen Ausfahrten und teilweise auch darüber hinaus für etwas größere Touren. Sogar fast einen Halbmarathon sind wir mal zusammen gelaufen, naja immerhin dafür zusammen trainiert in meinem Fall... danke trotzdem für den schönen Ausflug in Deine Heimat Max (PM) zusammen mit Fabi und Sabrina zum deutschen Weinstraßenmarathon.
Ein weiteres sehr schönes Erlebnis während der Promotion war die gemeinsame Konferenz und anschließender USA-Roadtrip mit Lena, Marian und Christoph. Ich erinnere mich gern mit Euch an Vierer-motelzimmer, Moskitofalls, sehenswerte Nationalparks mit und ohne Kraftwerk und mein persönliches Highlight: Ingrid und Al.
Eigentlich erst gegen Ende der Promotion zur schönen Regelmäßigkeit geworden, sind die Spaziergänge mit Laura durch unsere gemeinsame Nachbarschaft. Besser spät als nie - danke Dir für allerlei Gespräche, gegenseitige Schreibmotivation und Ausstausch!
Der wichtigste Begleiter meiner Promotion war natürlich täglicher Mayer-Heitsch-Content. Musikalische Ausschweifungen, neueste Memes, Geschichten aus dem Alltag, Diskussionen über Gott und die Welt, wilde Bestellungen bei Sportspar, ein Besuch im Schwabenländle und vieles mehr hab ich Lena zu verdanken! Mit Dir war es nie langweilig, ich glaube unter anderem, weil wir beide unterschiedlicher manchmal nicht sein könnten und trotzdem in jedem positive liebenswerte Seiten gefunden haben. Ich hoffe unsere Freundschaft begleitet uns auch über die Promotion hinaus und wir können noch ein paar Kontroversen austauschen :).
Größter Dank, gebührt natürlich auch meinen fleißigen Korrekturlesern Lena, Laura, Max und Christoph, die die Arbeit um ein paar Schreibfehler und Ähnlichem beraubt haben.
Zu guter Letzt möchte ich meinen Liebsten Danken! Allen vorran meinen Eltern Claudia und Frank, die mir stets alles erdenkliche in meiner gesamten Bildung ermöglicht haben. Darüber hinaus habe ich Euch zu verdanken, dass ich meine zahlreichen Hobbys ausüben konnte und Ihr mir, ob musikalisch oder sportlich, nie eine Förderung verweigert habt.

Danke, dass ihr immer da seid - nicht nur, wenn ich Euch brauch!
Ein weiterer großer Dank gilt meinem engsten langjährigen Freundeskeis. Wir kennen uns alle teils seit der ersten Klasse und haben schon auf dem Spielplatz zusammengespielt, der Rest kam dann im Gymnasium oder durch Bekanntschaften über Freunde dazu. Danke Euch für schöne Abende, Urlaube, offene Ohren und zahlreiche andere Erlebnisse in den letzten Jahren!
Zu guter letzt: Mein größter Dank gilt Christoph. Du bist immer für mich da, hast immer ein offenes Ohr, bist wahnsinnig gut in konstruktiven Lösungsvorschlägen und bist neben meinem Ruhepol generell der beste Teampartner den man sich vorstellen kann! Ich liebe es zusammen mit dir Quatsch zu machen, neue Dinge zu entdecken oder auch einfach nur zufrieden auf unserem Balkon zu liegen. Ich hoffe, dass uns das noch ganz viele Jahre begleitet!